Deposition of Oil Shale and Coal in China: the Eocene Fushun and Huadian Basins

Doctoral Thesis

Dipl.-Ing. Susanne Andrea Ingeborg Strobl, BSc

Supervisor:
Univ.-Prof. Mag.rer.nat. Dr.mont. Reinhard F. Sachsenhofer

Department of Applied Geosciences and Geophysics
Chair of Petroleum Geology
Montanuniversität Leoben

Leoben, 2014

Affidavit

I declare in lieu of oath, that I wrote this thesis and performed the associated research myself, using only literature cited in this volume.

(Dipl.-Ing. Susanne Andrea Ingeborg Strobl, BSc)

Danksagung

An dieser Stelle bedanke ich mich herzlich bei Herrn Professor Reinhard Sachsenhofer für die Betreuung dieser Arbeit. Seine stete Hilfe und Zeit trugen wesentlich zum Fortschritt dieser Arbeit bei. Bedanken möchte ich mich auch ganz besonders für die netten und unvergesslichen Reisen nach China und dafür, dass seine Tür jederzeit für mich offen stand, egal ob für wissenschaftliche oder nicht-wissenschaftliche Gespräche.

Professor Zhaojun Liu und seinem Forschungsteam rund um Qingtao Meng und Pingchang Sun von der Jilin University in Changchun, China, bin ich zu großem Dank verpflichtet. Sie organisierten die Geländearbeit in China und aufgrund ihrer Hilfe war es mir möglich, Proben aus den Fushun und Huadian Becken zu bekommen. Des Weiteren halfen sie mir oft mit Übersetzungen, da meistens nur chinesische Literatur vorhanden war. Ihr großes Fachwissen über die chinesischen Ölschiefervorkommen war eine wesentliche Grundlage für diese Arbeit.

Doris Groß gebührt großer Dank. Sie ist mir jederzeit mit Rat und Tat zur Seite gestanden, hat mich mehrmals geduldig motiviert und war mein wichtigster Diskussionspartner. Sie war und ist eine großartige Unterstützung in jeder Lebenslage. Danke für deine Freundschaft.

Besonders bedanke ich mich bei Sabine Feuchter und Gerd Rantitsch vom Lehrstuhl für Geologie und Lagerstättenlehre, sowie bei Thomas Meisel und Syed N.H. Bokhari vom Lehrstuhl für Allgemeine und Analytische Chemie an der Montanuniversität Leoben. Dank ihrer Hilfe war es mir möglich, Probenbearbeitungen und nötige Messungen an ihren Lehrstühlen durchzuführen. Sabine Feuchter danke ich an dieser Stelle für jedes aufbauende Wort während meiner Dissertationszeit.

Ich danke Achim Bechtel und Reinhard Gratzer für ihre Hilfe im Geochemie- und Isotopenlabor, sowie für ihre Ratschläge bei der Auswertung und Interpretation der geochemischen Daten.

Ich bedanke mich ganz herzlich bei Frau Ursula Schmid für ihre Unterstützung in allen administrativen Angelegenheiten. Sie macht oft Unmögliches möglich.

Meinen Freunden und Kollegen Jürgen Gusterhuber und Lorenz Scheucher danke ich für die lustige Zeit am Lehrstuhl. Ich freue mich über jedes Mail und Telefonat mit euch und auf viele Treffen mit euch – egal wo auf dieser Welt. Ich danke Jan Mayer für all die tollen Momente als Tutorenteam. Es war und ist immer ein Spaß mit ihm.

David Misch, Moritz Hellmayr, Anung Samsu, Bernhard Rupprecht, Marie-Louise Grundtner, Lukasz Pytlak, Martin Riedl und Stefan Neumeister danke ich für die gemeinsame Zeit am Lehrstuhl, für alle Kaffee- und Mittagspausen, sowie für viele aufbauende Worte. Es war eine unvergessliche Zeit mit euch.

Weiters bedanke ich mich an dieser Stelle bei all meinen Freunden und Bekannten, die in jeder Lebenslage zu mir stehen.

Andrea und Christian Reininger möchte ich für sämtliche gemeinsame Wochenenden in Wien danken, während denen ich so richtig abschalten und entspannen konnte. Danke für eure Unterstützung!

Meinen Geschwistern Franz, Maria und Ursula sowie ihren Familien danke ich für den familiären Halt, die freudigen Erlebnisse und Familienfeiern. Eine Bereicherung in meinem Leben sind seit jeher meine Nichten und Neffen Verena, Katja, Matthias, Annika, Jakob und Tim. Lieben Dank für eure Lebensfreude!

Meinen Eltern Senta und Franz gebührt größter Dank für die langjährige und liebevolle Unterstützung auf meinem Lebens- und Ausbildungsweg. Danke, dass ihr immer für mich da seid und ich mich, egal in welcher Lebenslage, auf euch verlassen kann!

Danke, Alexander! Danke, dass du mich immer aufrichtest, wenn es mal nicht nach Plan läuft. Danke für deine unendliche Geduld. Danke, dass du mich motivierst und mich zum Lachen bringst.

Abstract

The Fushun and Huadian basins, located along the DunMi fault zone (NE China), are filled with non-marine oil shale- and coal-bearing sediments of Eocene age. Despite similar tectonic setting and age, the habitat of oil shale and coal differs significantly in terms of thickness, distribution and quality. The Fushun Basin hosts world-class coal and oil shale deposits, which are mined in a huge open-pit mine. In contrast, the Huadian Basin hosts several relative thin oil shale and coal seams, which are mined underground.

During this study the depositional environment of coal and oil shale in both basins and factors controlling differences between them were investigated mainly based on detailed bulk geochemical, organic petrographical and organic geochemical data.

In the Fushun Basin, a single sub-bituminous coal seam, up to 120-m-thick (Guchengzi Formation), formed during the early transgressive stage of basin evolution. It is overlain by an up to 300-m-thick oil shale unit (Jijuntun Formation). During the deposition of oil shale, excellent preservation conditions of organic matter were established in a more than 100-m-deep lake with a stable stratified water column and photic zone anoxia. Especially in the upper unit of the Jijuntun Formation, the organic matter is dominated by algal and bacterial biomass. Relative high thermal maturity is due to high paleo-heat flow related to magmatic activity.

In the Huadian Basin 13 oil shale layers intercalated with fan delta sediments (Oil Shale Member) were deposited in a lake with relative low water depth (a few tens of meters) preventing stable water column stratification. Nevertheless, algal blooms and oxygen-depleted conditions resulted in high quality oil shale (e.g. oil shale layer 4). In contrast, strong input of terrestrial plants reduces the quality of the lower oil shale layers (e.g. oil shale layers 13-11). Thin coal layers accumulated during the late regressive stage of basin evolution (Carbonaceous Shale Member).

The main factor controlling differences in stratigraphic position, thickness and quality of oil shale and coal deposits in the Fushun and Huadian basins is tectonic subsidence. The subsidence rate was significantly higher in the Fushun Basin than in the Huadian Basin. This resulted in the formation of a thick coal seam during the transgressive phase of basin evolution. Similar coal is missing in the Huadian Basin. In addition, a

single thick high quality oil shale unit developed under deep lacustrine conditions in the Fushun Basin, whereas several thin oil shale layers were deposited in a relative shallow lake in the Huadian Basin. During the regressive stage of basin evolution, thin coal layers accumulated in the Huadian Basin, whereas equivalent coal is missing in the Fushun Basin. In general, the organic matter of the oil shale within the Fushun Basin mainly composed of algae and bacteria, whereas terrestrial organic matter is more abundant in the Huadian Basin. Moreover, differences in paleo-vegetation (gymnosperms prevail in Fushun; angiosperms prevail in Huadian) may indicate different climatic conditions.

Kurzfassung

Die nicht-marinen Fushun und Huadian Becken befinden sich entlang der DunMi-Störungszone in Nordostchina. Beide Becken beinhalten eozäne Ölschiefer- und Kohlevorkommen. Trotz ähnlicher tektonischer Position und Alter, weisen sowohl Ölschiefer als auch Kohle Unterschiede hinsichtlich ihrer Mächtigkeit, Verteilung und Qualität in beiden Becken auf. Im Fushun Becken werden sehr mächtige Kohle und Ölschiefer in einem riesigen Obertagebergbau gewonnen. Im Gegensatz dazu, werden relativ gering mächtige Ölschiefer- und Kohlelagen im Huadian Becken untertage abgebaut.

Ziele dieser Studie sind die Ablagerungsbedingungen organisch reicher Sedimente in den Fushun und Huadian Becken mittels detaillierter organisch geochemischer und petrographischer Daten zu rekonstruieren und miteinander zu vergleichen. Ein weiteres Ziel dieser Studie ist es, die kontrollierenden Faktoren, die für die Unterschiede in beiden Becken verantwortlich waren, herauszufinden.

Im Fushun Becken bildete sich ein bis zu 120-m-mächtiges Kohleflöz (Glanzbraunkohle, Guchengzi Formation) während der frühen transgressiven Phase der Beckenentwicklung. Dieses Flöz wird von einer bis zu 300-m-mächtigen Ölschiefereinheit (Jijuntun Formation) überlagert, welche in einem mehr als 100-m-tiefen See mit anoxischen Bedingungen, die bis in die photische Zone reichten, abgelagert wurde. Diese anoxischen Bedingungen sowie eine stabile Stratifizierung der Wassersäule trugen wesentlich zur hervorragenden Erhaltung des organischen Materials bei. Das organische Material der oberen Einheit der Jijuntun Formation besteht hauptsächlich aus Algen und Bakterien. Magmatische Aktivität und der damit einhergehende hohe Paläowärmefluss waren verantwortlich für die relativ hohe thermische Reife.

Im Huadian Becken wurden 13 dünne Ölschieferlagen mit zwischengelagerten Deltafächer-Sedimenten (Oil Shale Member) in einem seichten See abgelagert. Da die Wassertiefe nie mehr als ein paar Zehnermeter erreichte, konnte sich keine stabile Stratifizierung der Wassersäule bilden. Trotzdem konnten sich aufgrund von Algenblüten und sauerstoffreduzierten Bedingungen hoch-qualitative Ölschiefer (z.B. Ölschieferlage 4) ablagern. Die tieferen Ölschieferlagen (z.B. Ölschieferlagen 13 bis

11) sind wegen des Eintrags von Landpflanzen von schlechterer Qualität. Während der späten regressiven Phase der Beckenentwicklung wurden dünne Kohlelagen abgelagert (Carbonaceous Shale Member).

Die Unterschiede in stratigraphischer Position, Mächtigkeit und Qualität der Ölschiefer und Kohlen in den Fushun und Huadian Becken werden hauptsächlich von der Absenkungsgeschwindigkeit kontrolliert. Die Subsidenzrate war im Fushun Becken wesentlich höher als im Huadian Becken. Folglich lagerte sich ein sehr mächtiges Kohleflöz während der frühen transgressiven Phase der Beckenentwicklung im Fushun Becken ab, wohingegen im Huadian Becken eine ähnliche Kohle fehlt. Weiters wurde im Fushun Becken eine sehr mächtige hoch-qualitative Ölschiefereinheit in einem tiefen See gebildet. Im Huadian Becken hingegen, wurden mehrere dünne Ölschieferlagen in einem relativ seichten See abgelagert. Während der regressiven Phase der Beckenentwicklung bildeten sich im Huadian Becken dünne Kohlelagen; eine äquivalente Kohle tritt im Fushun Becken nicht auf. Generell besteht das organische Material des Ölschiefers im Fushun Becken aus Algen und Bakterien, wohingegen der Einfluss von Landpflanzen im Huadian Becken bedeutend ist. Zusätzlich könnten Unterschiede in der Paläovegetation (Gymnospermen dominieren in Fushun; Angiospermen in Huadian) ein Hinweis auf unterschiedliche klimatische Bedingungen sein.

Table of Contents

GENERAL PART OF DOCTORAL THESIS

PUBLICATIONS

APPENDIX

GENERAL PART OF DOCTORAL THESIS

1 General Introduction

1.1 Oil shales in general

Very fine-grained sedimentary rocks with high contents in thermally immature organic matter may be considered as oil shales, which are commonly defined as rocks containing organic matter that yields substantial oil and gas upon low temperature distillation (Dyni, 2006). Oil shale is a potential source rock that would have generated oil if it had been subjected to geologic burial at the requisite temperatures and pressures for sufficient time (Allix et al., 2011).

Methods for coaxing oil from shale to produce liquid fuels have existed for hundreds of years. The oldest method is to heat the mined oil shale in processing facilities on the surface to obtain shale oil. More recently, methods have been tested to heat the rock in situ and extract the shale oil through boreholes (Allix et al., 2011). The recovery methods are complicated and expensive, but high oil prices and predictions of future oil shortages, producing shale oil is becoming economically important nowadays. Fig. 1.1 shows that the tonnage of mined oil shale reached a peak in 1980, declined during the 1980s and 1990s and started to increase again since 1999.

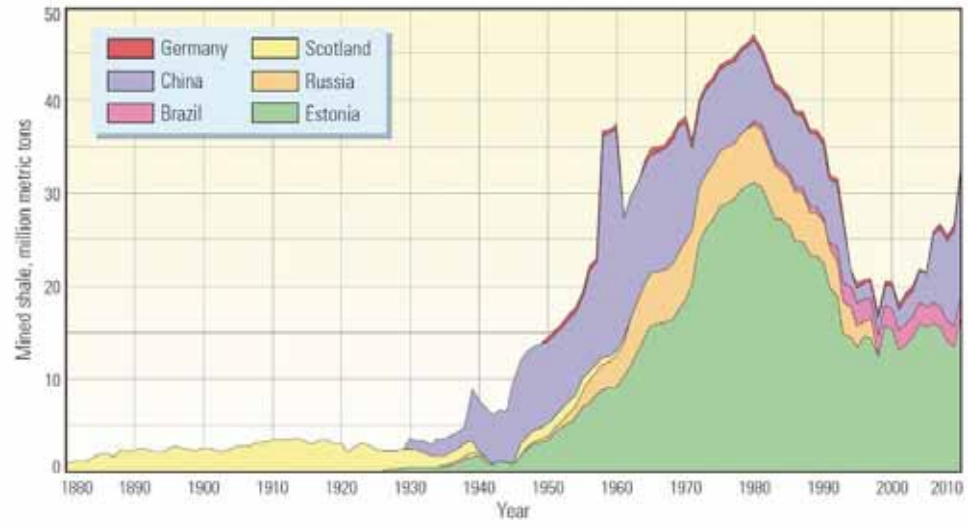

Fig. 1.1: Production of oil shale in millions of metric tons from 1880 to 2010 (Dyni, 2006; Allix et al., 2011).

The first known use of liquid petroleum derived from shale was in Austria (Tyrol) and dates to the mid-1300s, when medical practicioners touted its healing properties

(Allix et al., 2011). Whereas mining of these Upper Triassic (Norian) oil shales near Seefeld stopped in the second half of the 20th century (Köster et al., 1988), Lower Jurassic (Toarcian) oil shale is still mined in the Bächental (Neumeister et al., 2014). The produced oil is sold under the trade name "Tiroler Steinöl" for medical and cosmetic use.

The world´s greatest oil shale producer is Estonia, where Kukersite of Ordovician age is mined underground and in openpit mines since the 1920s (Aaloe et al., 2007). However, only a small part of the kukersite is used for shale oil production, whereas the main part is utilized in power plants (Aaloe et al., 2007).

Obviously, China also plays a significant role in the oil shale business and is responsible for the recent increase in mined shale. The most important commercial Chinese reserves are located in the Fushun Basin, where the total resource of oil shale is estimated at 3.6 x 10^9 tons (Liu et al., 2009).

Oil shale deposits are widespread thoughout the world. Hundreds of deposits occur in more than 30 countries, but high-quality shale oil resources are located in 14 countries (Fig. 1.2). World's shale oil resources are about 5.1 x 10^{11} m^3 (Allix et al., 2011).

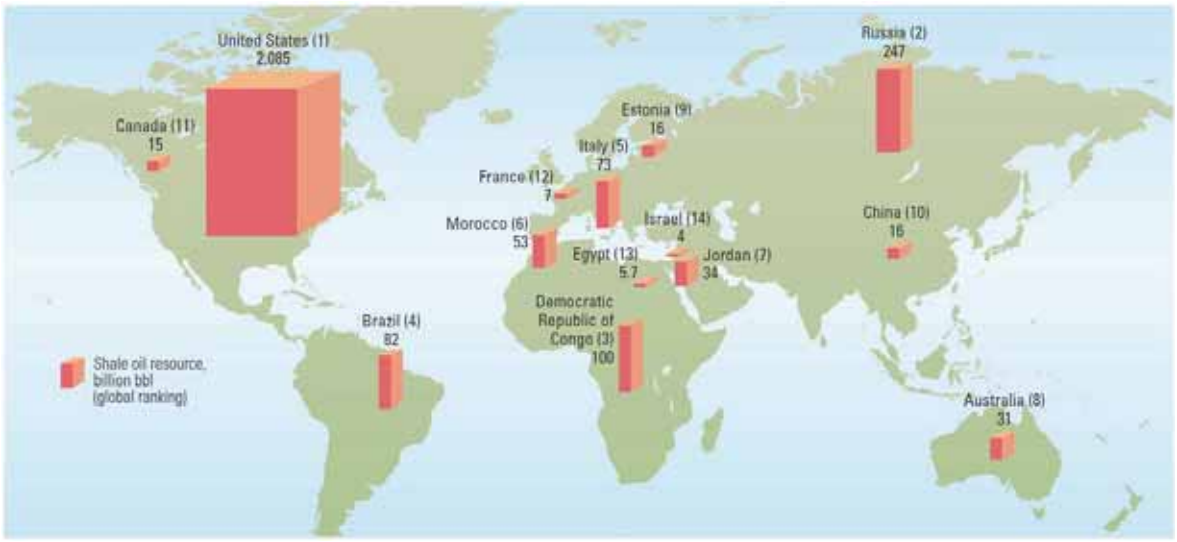

Fig. 1.2: World's most important oil shale deposits are located in 14 countries (Knaus et al., 2010; Allix et al., 2011).

Oil shale resources of different ages are distributed all over China. Many well-explored oil shale deposits are located in northeast China (Fig. 1.3). The non-marine

Songliao Basin, considered as a Mesozoic rift basin, is China's most oil-productive basin. The Upper Cretaceous Qingshankou and Nenjiang formations are the main source rocks within this basin and are also known as major oil shale resources (Liu et al., 2009; Bechtel et al., 2012). Furthermore, to the southeast of the Songliao Basin, several (Mesozoic and) Cenozoic oil shale- and coal-bearing basins are located along the Dunhua-Mishan ("DunMi") strike-slip fault, which was active during Mesozoic-Cenozoic time (Liu et al., 2009; Meng et al., 2012). The most prominent oil shale basins along this fault zone are the Eocene Fushun and Huadian basins hosting non-marine sediments with an Eocene age.

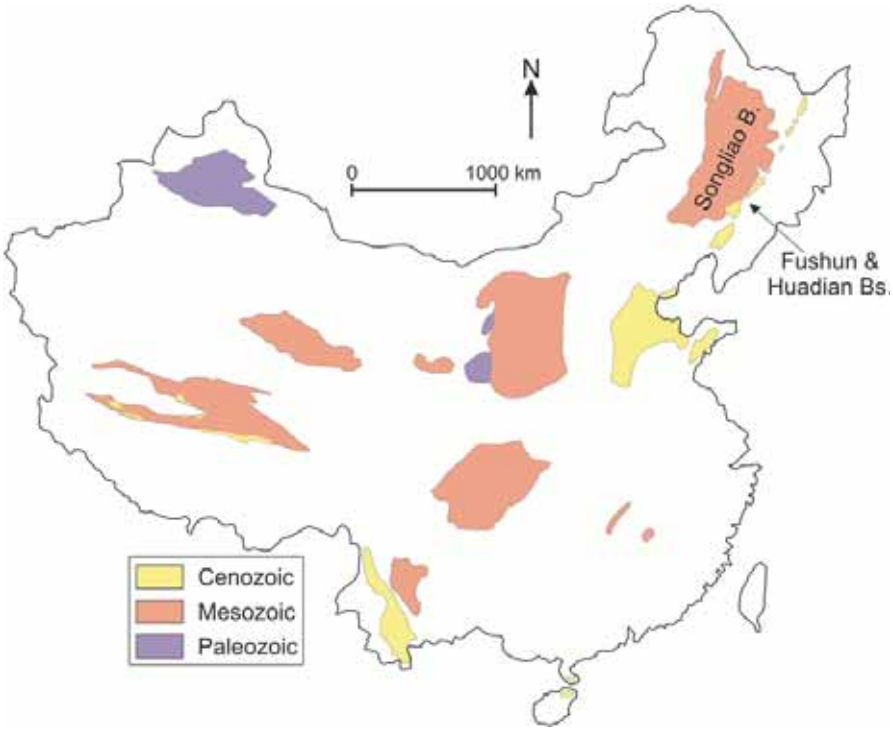

Fig. 1.3: Distribution of oil shale-bearing basins in China [modified according to Liu et al. (2009)].

Lacustrine oil shales with a Middle Eocene age are distributed all over the world and include i.a. the Parachute Creek Member of the Green River Formation (USA; Cumming et al., 2012), the Messel oil shale (Germany; Lenz et al., 2007), oil shales in Central Jordan (Alqudah et al., 2014), Turkey (Ocakoglu et al., 2012), and China (Fushun and Huadian basins; Quan et al., 2012; Sun et al., 2013). Although all of these basins include lacustrine rocks, the oil shales differ significantly in terms of organic richness, thickness, and vertical and lateral heterogeneity. For example both, the Fushun and Huadian basins host economic oil shale and coal deposits formed during

Eocene times and are located along the same fault zone, but show major differences in their basin evolution (Liu et al., 2009; Sun et al., 2013).

1.2 Previous research on oil shale and coal in the Fushun and Huadian basins

The economically most important oil shale deposit of China is located within the Fushun Basin, where a single, up to 120-m-thick coal seam (Guchengzi Formation) overlain by a world-class 300-m-thick oil shale (Jijuntun Formation) is exploited in a huge open pit mine. Compared to the Fushun Basin, a thick coal seam in the lower part (Pyrite Member) of the sedimentary succession is missing in the Huadian Basin. Instead, the basin hosts 13 commercial oil shale layers (Oil Shale Member), only a few meters thick, and several thin coal seams in the upper part (Carbonaceous Shale Member) of the stratigraphic column, which are mined underground (Liu et al., 2009; Sun et al., 2013).

Previous research related to the oil shale deposit in the Fushun Basin mainly focused on tectonic evolution (Wu et al., 2002), kinetics of pyrolysis (Li and Yue, 2003), shale oil reserves (Liu et al., 2009), and paleoclimatic evolution (Wang et al., 2010; Meng et al., 2012). The coal in the Fushun Basin was investigated regarding the geological setting of coal deposition (Johnson, 1990), coal metamorphism (Wu et al., 2000), tectonic (Wu et al., 2002) and paleoclimatic evolution (Wang et al., 2010; Quan et al., 2012), palynology and paleobotany (Ma et al., 2012; Su et al., 2014).

The oil shale and coal deposits of the Huadian Basin are hardly known in international publications. Only data on shale oil reserves (Liu et al., 2009), total organic carbon contents, hydrogen indices, oil yields (Sun et al., 2013) and petrography (Xie et al., 2014) are available.

1.3 Innovative aspects and importance of the expected results

Organic matter rich rocks including oil shale and coal deposits provide excellent archives for paleoenvironmental conditions. Bioproductivity, organic matter preservation, and dilution of organic matter by mineral matter are the main controls on the quality of lacustrine or marine organic matter rich rocks. Bioproductivity may be related to nutrient supply and climate, organic matter preservation is controlled by redox conditions (water-column stratification, global anoxic events, etc.), whereas the tectonic, paleogeographic and sequence stratigraphic settings strongly influence detrital input (e.g. Carroll and Bohacs, 1999, 2001; Liu et al., 2009; Passey et al., 2010; Bechtel et al., 2012). Excellent oil-prone source rocks form in lacustrine environments.

Tectonically controlled basins in humid environments are often characterized by a stratigraphic succession including from base to top fluvial sediments, a single thick coal seam and lacustrine deposits, which may be very high in organic matter contents (e.g. Sachsenhofer et al., 2003). This succession reflects the high subsidence rates characteristic for rift and strike-slip basins (Lambiase, 1990). When subsidence rates decrease the deep lake is filled by deltaic systems. Coal may form during the regressive filling stage of the basin, but is typically of lower quality than that formed during the transgressive stage (Sachsenhofer, 2000).

The thickness and distribution of coal and oil shale layers in the non-marine Fushun and Huadian basins show major differences, although both basins are located at the same strike-slip zone and were formed roughly contemporaneously. Therefore, this doctoral thesis has three major aims:

- to reconstruct the depositional environment of the coal and oil shale in the Fushun Basin,
- to reconstruct the depositional environment of the coal and oil shale in the Huadian Basin,
- and to investigate the factors controlling the differences between the Fushun and Huadian basins.

To reach the goals, key sections in the Fushun and Huadian basins were investigated. In the Fushun Basin a profile located in the West Open Pit mine south of Fushun City

was studied. The study of the Huadian Basin is based on core samples from well Hd3 drilled in the eastern part of the basin (Gonglangtou mining district).

The study on oil shale and coal deposition in these tectonically controlled basins is based on detailed bulk geochemical, organic petrographical and organic geochemical (biomarker) investigations. Mineralogical investigations have been performed in the Fushun Basin. In addition, the thermal history of the Fushun Basin was reconstructed using a 1D basin modeling approach.

The comparison of two basins with similar age and tectonic setting, but largely differing characteristics of coal and oil shale will provide important new insights into the evolution of strike-slip basins, the depositional environment and the architecture of coal and oil shale layers.

2 Geological setting

Several oil shale- and coal-bearing basins in northeast China are located along the Dunhua-Mishan ("DunMi") fault zone (Fig. 2.1), which was active during Mesozoic-Cenozoic time (Liu et al., 2009; Meng et al., 2012). This thesis deals with the most prominent ones:

- the Fushun Basin,
- and the Huadian Basin.

Both basins host Eocene non-marine organic-rich sediments. The geological setting of these basins is discussed separately in detail below.

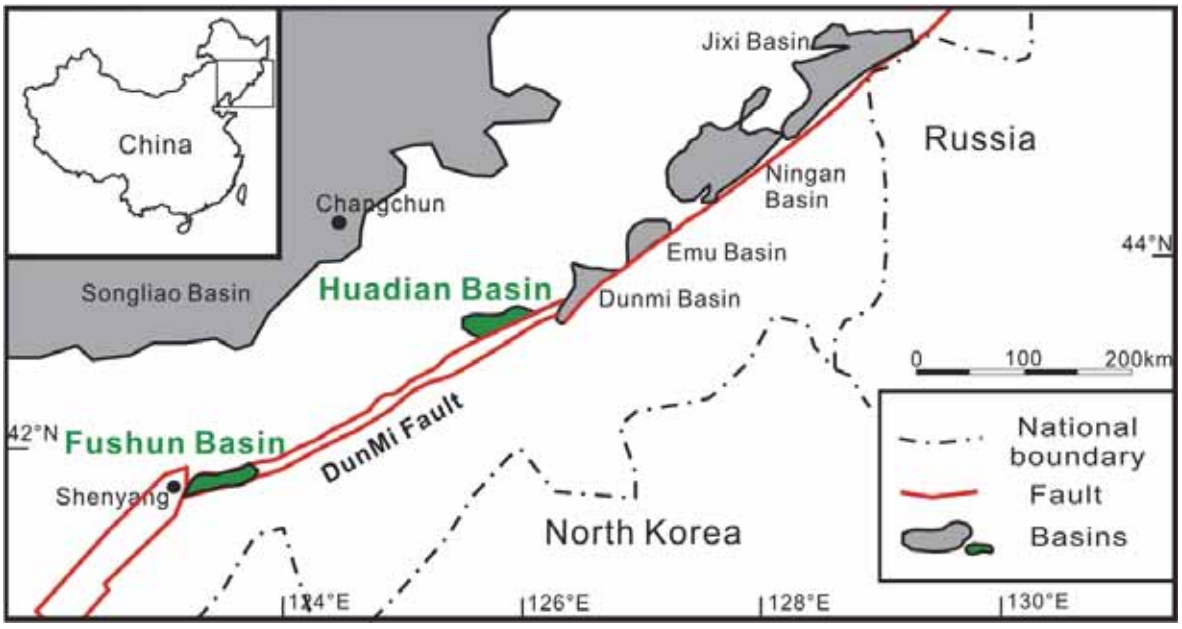

Fig. 2.1: Map showing the location of the DunMi fault zone and the Fushun and Huadian basins [modified according to Meng et al. (2012)].

2.1 Geological setting of the Fushun Basin

The Fushun Basin, considered as a strike-slip basin (Wu et al., 2002), is characterized by an east-west trending syncline, whose northern limb was removed by a large-scale thrust fault (Johnson, 1990; Fig. 2.2).

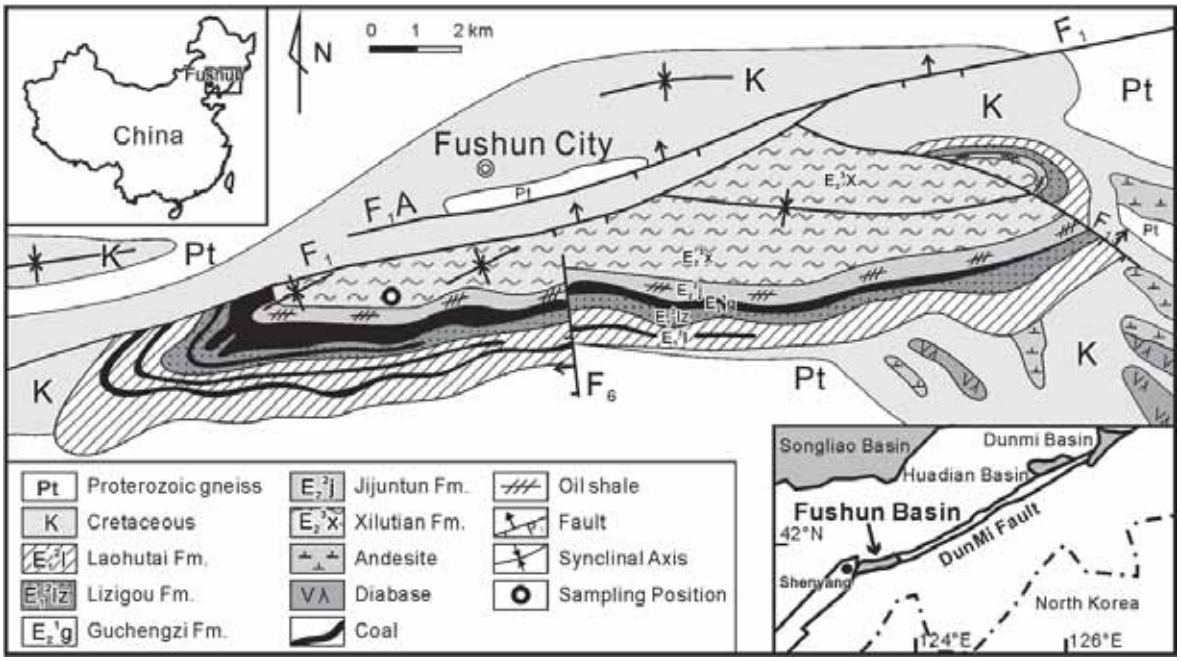

Fig. 2.2: Geological map of the Fushun Basin [modified according to Hong et al. (1980), Zhao et al. (1994), Wu et al. (2000), Hou et al. (2006), Meng et al. (2012)].

The basement of the Fushun Basin consists of Proterozoic gneiss and sediments of Cretaceous age. The basin fill contains from base to top: Laohutai and Lizigou formations (Paleocene), Guchengzi Formation (Lower Eocene), Jijuntun and Xilutian formations (Middle Eocene) and Gengjiajie Formation (Upper Eocene; Fig. 2.3). Special focus is taken on the Eocene Guchengzi and Jijuntun formations.

The coal seam within the Guchengzi Formation (Ypresian) is between 20 and 200 m thick including interseam sediments consisting of carbonaceous shale, mudstone and sandstone and conglomerate. Amber and siderite nodules occur thougout the coal seam (Johnson, 1990; Wu et al., 1998; Xu et al., 2012). The maturity of the coal seam increases from west to east from the sub-bituminous stage (~0.5%R_r) to the high volatile bituminous A stage (~0.9%R_r; Wu et al., 2000). According to Wu et al. (2000), the relatively high maturity is related to the Late Oligocene intrusion of diabase sills into the underlying Laohutai and Lizigou formations.

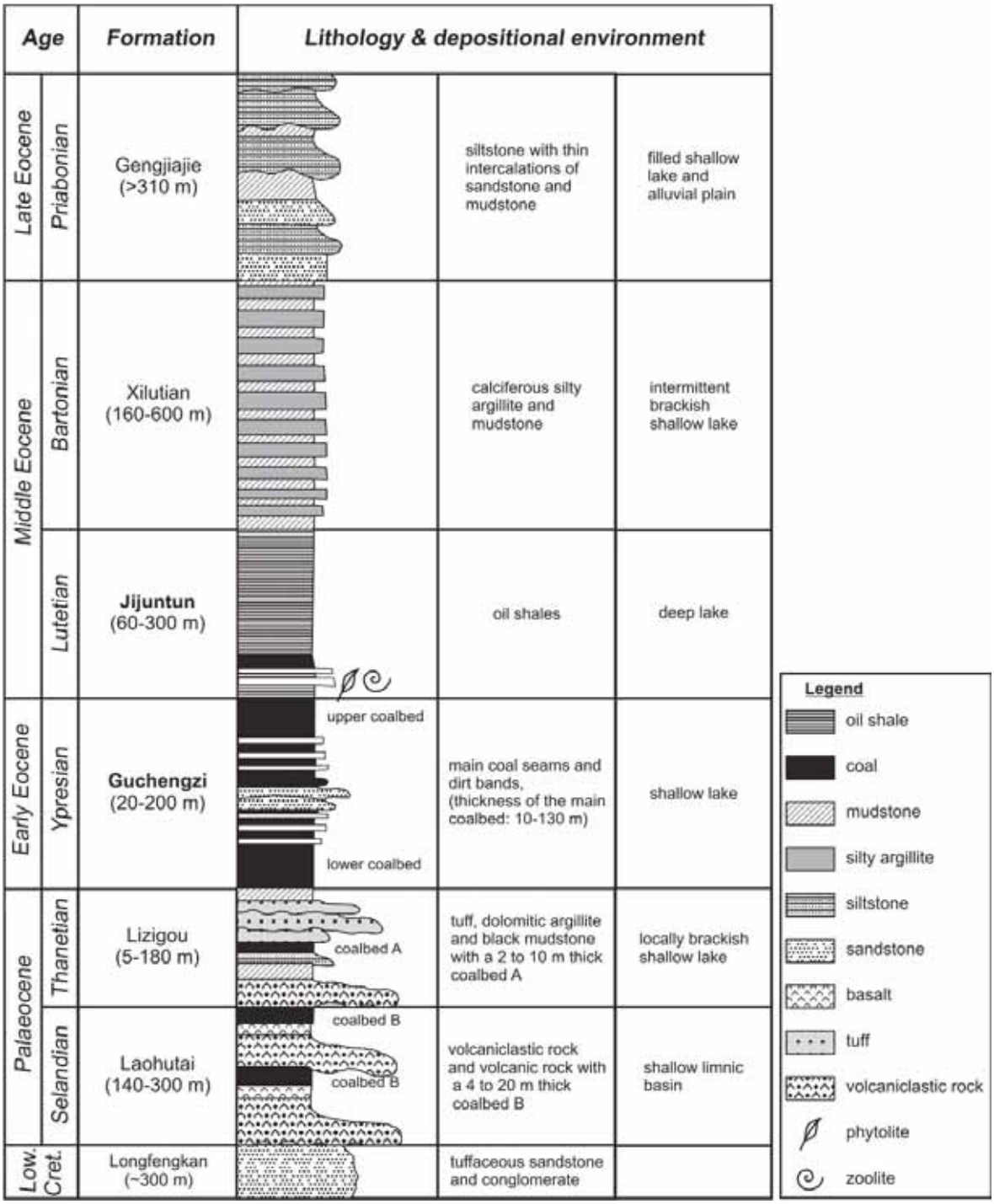

Fig. 2.3: Stratigraphic column of the Fushun Basin [modified according to Hong et al. (1980); Wu et al. (2000); Quan et al. (2012)]

The Jijuntun Formation (Lutetian), 60 to 300 m thick, is composed of thick oil shale intercalated by carbonaceous shale and mudstone (Wu et al., 2000; Meng et al., 2012). According to Liu et al. (2009), the depth of the lake increased during deposition of the oil shale-bearing succession. Low quality oil shale (oil yield <4.7 wt.%) was deposited in the lower part (shallow lake), whereas oil shale with high quality (oil yield >4.7 wt.%) was deposited in the upper part (deep lake; Liu et al. , 2009).

The Xilutian Formation (Bartonian), up to 600 m thick, comprises light green dolomitic mudstone intercalated by silty argillite deposited in a shallow lake environment (Wu et al., 2000; Meng et al., 2012).

Erosional remnants of mudstones and siltstones of the fluvial Gengjiajie Formation (Priabonian) appear only locally (Hong et al., 1980; Wu et al., 2000).

The climate during deposition of the basin fill was reconstructed by Quan et al. (2012) using the Coexistence Approach (Mosbrugger and Utescher, 1997). According to these investigations the coal seam of the Guchengzi Formation was deposited during the Early Eocene Climatic Optimum, whereas the mean annual temperature decreased during deposition of the oil shale-bearing Jijuntun Formation. The overlying Xilutian Formation represents a Mid-Eocene warming event. Huang et al. (1983) reconstructed a moist subtropical climate for the time of coal accumulation within the Guchengzi Formation. A warm and humid climate during deposition of the Jijuntun Formation and a hot and arid climate during deposition of the Xilutian Formation is postulated by Meng et al. (2012).

2.2 Geological setting of the Huadian Basin

The Huadian Basin is an east-west trending halfgraben basin (Fig. 2.4). Its Eocene basin fill (Huadian Formation) is up to 1500 m thick and overlies several basement units consisting of granite, Lower Paleozoic and Permo-Carboniferous rocks. The Quaternary cover is up to 15 m thick. The Huadian Formation consists from base to top of three members: Pyrite Member, Oil Shale Member and Carbonaceous Shale Member (Liu et al., 2009; Sun et al., 2011, 2013; Fig. 2.5).

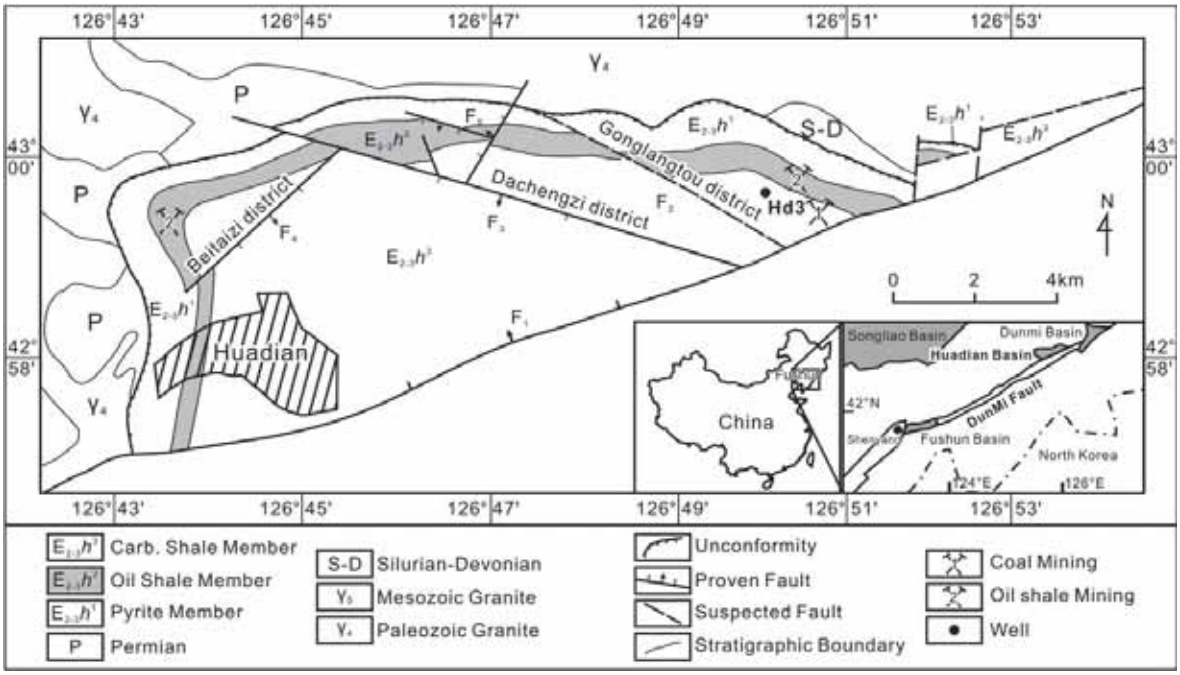

Fig. 2.4: Geological map of the Huadian Basin [modified according to Sun et al. (2013)].

The Pyrite Member represents the early, shallow stages of basin evolution. It comprises conglomerates and red mudstones near its base overlain by varicolored calcarenitic fine-grained sandstones, mudstones and coaly layers deposited in alluvial fan, fan delta, and shallow lake environments (Sun et al., 2011, 2013). The presence of pyrite crystals in fractures and pore spaces, interpreted to be hydrothermal in origin by Sun (2010), is eponymous for this member.

The Oil Shale Member was deposited during the expansion and deepening of the lake (Sun et al., 2013). It was dated as Middle Eocene based on a mammalian fauna (Zhang et al., 1986; Beard and Wang, 1991; Manchester et al., 2005). The total thickness of this member ranges from 65 to 244 m. The total number of oil shale layers varies from 6 to 26, but only 13 layers are suitable for shale oil exploitation (Wang et al., 2005). Significant differences exist between oil shale deposited in the lower, middle and upper parts of the Oil Shale Member: Oil shale with relative high thickness (up to 7 m), but low to moderate quality occurs in the lower part), whereas thin (<3 m) oil shales with high quality are found in the middle part. Low quality oil shale, less than 2 m thick, occurs in the upper part). The lateral extent of the oil shale layers increases upward within the lower part, reaches a maximum in the middle part and decreases upward in the upper part (Sun et al., 2013). The average TOC content of the Oil Shale

Member is 3.6 wt.%. The highest TOC value of a 1-m-thick interval occurs in the middle part (30.0 wt.%; Sun et al., 2013).

Shallow lacustrine conditions prevailed during deposition of the Carbonaceous Shale Member. It represents the final filling stage of basin evolution. Economic coal seams, about 2 m thick, accumulated along the lake margins and are accompanied by bituminous shale (Sun et al., 2013).

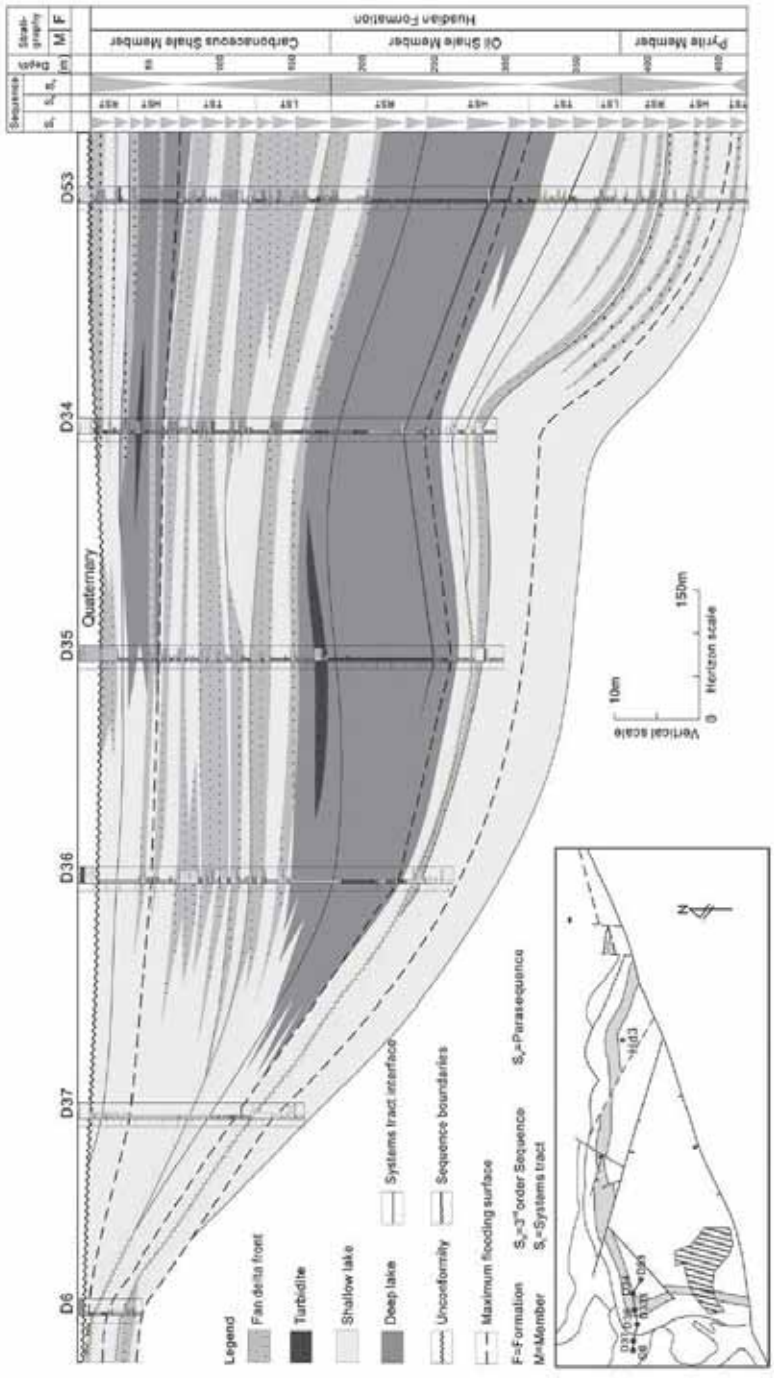

Fig. 2.5: Facies architecture and sequence stratigraphic framework of the Huadian Formation [modified according to Sun et al. (2011)].

3 Samples and methods

In the Fushun Basin, 79 samples have been taken along a vertical profile in the West Open Pit mine in the south of Fushun City representing an approximately 100-m-thick succession (Fig. 2.2). 29 samples represent the coal-bearing Guchengzi Formation, 48 samples represent the oil shale-bearing Jijuntun Formation and two samples were taken within the Xilutian Formation (Appendix).

In the Huadian Basin, a total of 96 core samples were taken from borehole Hd3 drilled in the eastern part of the basin (Gonglangtou mining district; Fig. 2.4) within the depth interval of 23.1 to 515.5 m. This interval represents the whole Huadian Formation consisting of Pyrite (14 samples), Oil Shale (73 samples), and Carbonaceous Shale (9 samples) members. Sample selection was based on the average TOC content of 1-m-thick intervals provided by Sun et al. (2013). Special focus has been taken on the oil shale and coaly layers. A complete photo documentation of core samples from borehole Hd3 is shown in the Appendix.

To reconstruct the depositional environment of oil shale and coal within the Fushun and Huadian basins, the following methods were applied.

Carbon and sulfur analyses

Carbon and sulfur analyses were performed on all samples from the Fushun and Huadian basins. Total carbon (TC) and sulfur (S) contents were determined using a Leco CS-230 elemental analyzer. Total organic carbon (TOC) content was determined with the same instrument on samples pre-treated with hydrochloric acid. Total inorganic carbon (TIC) contents were calculated by the difference between TC and TOC. The TIC is used to calculate calcite equivalent percentages ($Calc_{eq}$ = TIC x 8.333) of the samples.

Rock Eval pyrolysis

Pyrolysis analysis was performed on all samples from the Fushun and Huadian basins using a Rock Eval 2+ analyzer. Depending on the TOC content, 10 mg to 60 mg of each pulverized sample were heated gradually in an inert atmosphere. Within this method, the amount of pyrolyzate released from kerogen was normalized to TOC to give the

hydrogen index (HI). The temperature of maximum hydrocarbon generation (T_{max}) is defined at the maximum value of the S_2-peak (Espialié et al., 1985).

XRD

X-ray diffraction analyses were conducted on a Philips PW 1830/40 device using CuKα-radiation (1.54 Å, 35 kV, 35 mA) on selected samples from the Jijuntun Formation (Fushun Basin). Scans with a step size of 0.02 ° were run between 2 and 67 °2Θ in the air-dry state (random powder mount and oriented powder mount) and between 2 and 45 °2Θ in the ethylene-glycoliated state and after heating to 350 and 550°C. Qualitative processing was done using the dataset of Brindley and Brown (1980) and Moore and Reynolds (1997). Quantitative interpretation was carried out using the methods described by Schultz (1964).

XRF

The major element compound content was determined on selected samples from the Jijuntun Formation (Fushun Basin) using a wavelength dispersive X-ray fluorescence spectrometer (WD-XRF AXIOS from PANalytical) at the Department of General and Analytical Chemistry (Montanuniversitaet Leoben, Austria). Fine grained weighed amount of samples were subjected to platinum crucibles which were kept for three hours in muffle furnace at 1000°C for loss on ignition (LOI). Fused glass beads were formed through fusion of one gram of ignited sample mixed with 8 g of $Li_2B_4O_7$ with a Vulcan VAA2 instrument. The XRF was calibrated with more than 50 certified and non-certified geological reference materials and checked regularly through participation in the IAG proficiency testing program (GeoPT).

Organic petrography

Microscopic analysis on selected oil shale samples from the Fushun and Huadian basins was performed using polished blocks of whole-rocks cut perpendicular to bedding planes. For microscopic examination on coal samples from the Fushun Basin, samples were crushed to a maximum size of 1 mm. Maceral analysis was performed by a single-scan method (Taylor et al., 1998) with a Leica MPV microscope using reflected white light and blue-light excitation. An oil immersion objective (50x magnification) was used. 300 points (coal samples) and 500 points (oil shale

samples) per polished block were counted to provide composition at maceral level. The maceral abundances refer to volume percentages on a mineral matter-free basis (vol.% mmf).

To determine the maceral composition of the coal samples from the Fushun Basin (Guchengzi Formation), the maceral nomenclature for medium-rank coals was applied because of the sub-bituminous rank of the coal (ICCP, 1998; 2001; Sýkorová et al., 2005). There have been several suggestions to characterize coal facies from maceral ratios (von der Brelie and Wolf, 1981; Diessel, 1986, 1992). Maceral ratios developed by Calder et al. (1991) for Westphalian coals were applied. Using this method, the Groundwater Index (GWI) is the ratio of strongly gelified vitrinite plus detrital mineral matter to weakly gelified vitrinite. It shows the influence of rheotrophic swamp conditions.

$$\mathrm{GWI} = \frac{\text{gelovitrinite} + \text{mineral matter}}{\text{telovitrinite} + \text{detrovitrinite}}$$

The Vegetation Index (VI) contrasts macerals of forest affinity with those of herbaceous and aquatic affinity. Following Gruber and Sachsenhofer (2001), resinite was subdivided into *in-situ* resinite occurring within wood tissues and detrital resinite.

$$\mathrm{VI} = \frac{\text{telovitrinite} + \text{phlobaphinite} + \text{teloinertinite} + \text{suberinite} + \text{in situ resinite}}{\text{detrovitrinite} + \text{gelinite} + \text{inertodetrinite} + \text{sporinite} + \text{cutinite} + \text{liptodetrinite} + \text{bituminite} + \text{fluorinite} + \text{detrital resinite}}$$

The Tissue Preservation Index (TPI; Diessel, 1986) yields similar information than the VI. It has been calculated using the following equation.

$$\mathrm{TPI} = \frac{\text{telovitrinite} + \text{(semi)fusinite}}{\text{detrovitrinite} + \text{gelovitrinite} + \text{macrinite} + \text{inertodetrinite}}$$

Vitrinite reflectance was measured on selected samples from the Fushun and Huadian basins using a 100x objective in non-polarized light at a wavelength of 546 nm (Taylor et al., 1998). At least 50 points per sample were measured. Results are presented as mean random reflectance values ($\%R_r$).

Ash yield and moisture determinations of coal samples from the Fushun Basins (Guchengzi Formation) followed standard procedures (Deutsches Institut für Normung 51718, 1978, & 51719, 1980).

Organic geochemistry (biomarker analysis)

Organic geochemical analysis follows established procedures at the Chair of Petroleum Geology at the Montanuniversitaet Leoben, Austria (e.g. Bechtel et al., 2012). Portions of selected samples from the Fushun and Huadian basins were extracted for approximately 1 h using dichloromethane (DCM) in a Dionex ASE 200 accelerated solvent extractor. Asphaltenes were precipitated from a hexane-DCM solution (80:1) and separated by centrifugation. The hexane-soluble fractions were separated into NSO compounds, saturated and aromatic hydrocarbons using medium pressure liquid chromatography (MPLC) with a Köhnen-Willsch instrument (Radke et al., 1980). The saturated and aromatic hydrocarbon fractions were analyzed using a gas chromatograph equipped with a 30 m DB-5MS fused silica column (i.d. 0.25 mm; 0.25 µm film thickness) and coupled to a Thermo Fisher ISQ quadrupol mass spectrometer (GC-MS system). The oven temperature gradient was programmed from 70°C to 300°C at 4°C min^{-1}, followed by an isothermal period of 15 min. Helium was used as carrier gas. The sample was injected splitless, with the injector temperature at 275°C. The spectrometer was operated in the EI (electron ionization) mode over a scan range from *m/z* 50 to 650 (0.7 s total scan). Data were processed using an Xcalibur data system. Individual compounds were identified on the basis of retention time in the total ion current (TIC) chromatogram and by comparison of the mass spectra with published data. Relative percentages and absolute concentrations of different compound groups in the saturated and aromatic hydrocarbon fractions were calculated using peak areas from the gas chromatograms in relation to that of internal standards (deuteriated *n*-tetracosane and 1,1'binaphthyl, respectively). The concentrations were normalized to the TOC content.

Compound-specific stable isotope geochemistry

Carbon isotope determination of *n*-alkanes and acyclic isoprenoids was performed using a Trace GC instrument attached to a ThermoFisher DELTA-V isotope ratio mass spectrometer via a combustion interface (GC isolink, ThermoFisher) on selected samples from the Fushun and Huadian basins. For calibration, CO_2 was injected at the beginning and end of each analysis. The GC column and temperature program are the same as for GC-MS. Stable isotope ratios are reported in delta notation ($\delta^{13}C$; Coplen, 2011) relative to the Vienna-Pee Dee Belemnite (V-PDB) standard

($\delta^{13}C=[(^{13}C/^{12}C)_{sample}/(^{13}C/^{12}C)_{standard}-1]$). Delta notation is expressed in parts per thousand or per mil (‰). The analytical error was better than 0.2‰.

Thermal basin modeling

In the Fushun Basin, heat flows and erosional thicknesses were estimated using 1D basin modeling techniques (Yalcin et al., 1997) and PetroMod software. Calculation of vitrinite reflectance followed the "Easy%Ro" approach of Sweeney and Burnham (1990). Biomarker ratios (hopane isomerization) were calculated using kinetic data of Mackenzie and McKenzie (1983). Models were calibrated by modifying heat flow and the thickness of eroded sediments until a satisfactory fit between measured and calculated values was obtained. Input parameters include stratigraphic information about the sediments within the Fushun Basin.

4 Summary of publications and contribution to the field

4.1 Publication I – Depositional environment of oil shale within the Eocene Jijuntun Formation in the Fushun Basin (NE China)

Previous research related to the oil shale in the Fushun Basin mainly focused on tectonic evolution, kinetics of pyrolysis, oil reserves and paleoclimatic evolution. Very little research has been undertaken on the depositional environment and the factors controlling its variation through time. Hence, this paper presents the reconstruction of the depositional environment of the oil shale-bearing Jijuntun Formation in the Fushun Basin. This approach is based on mineralogy, inorganic and organic geochemistry, organic petrography, stable isotope geochemistry, and vitrinite reflectance measurements. In addition to the investigation of the depositional environment of the Jijuntun Formation, the oil shale potential and the thermal maturity were evaluated. Furthermore, the amount, type and origin of organic matter were investigated.

The oil shale-bearing Jijuntun Formation is characterized by low quality oil shale in the lower part and a high quality oil shale in the upper part, respectively. Study results show that this is due to significant input of landplants during deposition of the lower part, whereas aquatic organisms were the main contributors of the organic matter in the upper part. Very high TOC and HI values in the upper part are a result of high bioproductivity and excellent preservation conditions in a deep lake where photic zone anoxia were established. The detected clay mineral assemblages are in agreement with previous research on paleoclimatic conditions.

The Fushun Basin provides a textbook example for a fault-controlled basin, where gradual deepening of the depositional environment and the establishment of water column stratification resulted in a world-class oil shale deposit. The changes in depositional environment and oil shale quality are clearly reflected by biomarker proxies.

At the same time, the Fushun Basin provides excellent examples for biased proxies:

- The pristane/phytane ratio is a widely used redox parameter. However, in the case of the Jijuntun Formation a comparison with other redox parameters (e.g. aryl isoprenoids) shows that, pristane/phytane ratios yield erroneous results. Additional compound specific isotope investigations showed that this is due to different sources of pristane and phytane.
- RockEval parameter T_{max} is a widely used maturity parameter. However, in the Jijuntun Formation the observed T_{max} trend contradicts other maturity parameters (e.g. biomarker isomerization) and pretends an upward increase in thermal overprint ("overturning of the basin fill"). Results of maceral analysis show that the misleading T_{max} is due to vertical changes in kerogen type.

Thus, the Fushun Basin, impressively, provides evidence that single geochemical proxies have to be used with caution and that multiproxy studies are necessary to avoid misinterpretations.

4.2 Publication II – Paleoenvironment of the Eocene coal seam in the Fushun Basin (NE China): Implications from petrography and organic geochemistry

In this publication the depositional environment and the thermal history of the Guchengzi Formation are investigated based on macro- and micropetrographic data, bulk geochemical parameters, biomarker analysis, stable isotope geochemistry, and vitrinite reflectance measurements. This paper is the first study on factors controlling the depositional environment and coal facies in the Fushun Basin. It is also the first paper, which applies a combination of petrographical and organic geochemical techniques in a systematic way on Chinese coals.

The sub-bituminous coal seam in the Fushun Basin, famous for its high amber content, accumulated during the early transgressive stage of basin evolution. Peat accumulation was in equilibrium with basin subsidence for a long time. This resulted in a huge seam thickness (>100 m). Gymnosperms prevailed in the mire vegetation. The lower part of the thick coal seam represents deposition in a low-lying mire. High

ash yields in large areas of the basin indicate that low-lying mire conditions continued during deposition of the upper part of the seam. However, at the study site some geochemical proxies indicate coal accumulation in a raised mire. The uppermost part of the Guchengzi Formation reflects the drowning of the peat and the termination of coal deposition due to increased subsidence rates. A shallow lake was established after coal accumulation.

A 1D thermal model calibrated with hopane isomerization ratios and vitrinite reflectance data suggests that heat flow was very high (~200 mW/m^2) during maximum burial. Most probably, high heat flow was a result of Late Oligocene magmatic activity.

4.3 Publication III – Deposition of coal and oil shale in NE China: the Eocene Huadian Basin compared to the coeval Fushun Basin

This paper presents the depositional environment of the Huadian Basin and shows a comparison with the coeval Fushun Basin. Whereas the Fushun Basin is a worldwide known basin, the Huadian Basin is hardly found in international literature. Therefore, this study aims at the first reconstruction of the depositional environment of the Huadian Basin based on bulk geochemical proxies, maceral and biomarker data. The depositional environment of the Fushun Basin was investigated in publications I and II. Major differences in thickness, distribution and quality of coal and oil shale deposits exist between both basins, although both are located at the same fault zone and formed roughly contemporaneously. The comparison of these two basins provides important new insights into the evolution of tectonically controlled basins, the depositional environment and the architecture of coal and oil shale layers.

Early in the history of the Huadian Basin, thin coaly and bituminous mudstones accumulated in a shallow lake (Pyrite Member). Water depth increased during deposition of the Oil Shale Member, but did not exceed a few tens of meters preventing stable water column stratification. Algal blooms and oxygen-depleted conditions resulted in accumulation of 13 thin oil shale layers interrupted by the deposition of fan delta sediments. Oil shale quality varies between different layers

due to variable portions of terrestrial organic matter. Ash-rich coal layers mined in the Huadian Basin developed during the regressive late stage of basin evolution (Carbonaceous Shale Member). Biomarker data indicate a high portion of gymnosperms during deposition of the Carbonaceous Shale Member and a change from an angiosperm- to a gymnosperm-dominated vegetation.

High subsidence rates in the Fushun Basin favored deposition of thick coal (>100 m) during the transgressive stage and of high quality oil shale in a lake, where water depth probably exceeded 150 m. In contrast minor subsidence in the Huadian Basin resulted in a lake with moderate water depth (a few tens of meters) and deposition of several oil shale layers with varying quality. In the Huadian Basin economic coal developed only during the regressive stage.

The basin fill of tectonically controlled basins in humid environments often includes from base to top: fluvial sediments, a single thick coal seam and lacustrine deposits with high organic matter contents. This succession reflects the high subsidence rates characteristic for rift and strike-slip basins (Lambiase, 1990). When basin subsidence decreases, deltaic systems, occasionally with thin low-quality coal, fill the deep lake.

Although a coal seam deposited during the final regressive stage is missing in the Fushun Basin, its basin fill provides an excellent example for such a succession. A similar stratigraphic succession is not developed in the Huadian Basin. This is mainly due to minor subsidence rates causing relative low water depth and unstable conditions during deposition of the Oil Shale Member. The lack of a thick coal seam in the lower transgressive part of the basin fill (Pyrite Member), may also be caused by an arid climate.

Therefore, the main factor affecting stratigraphic position, thickness, distribution and quality of coal and oil shale deposits in the Fushun and Huadian basins are different subsidence rates. Furthermore, climatic conditions may have played a secondary role.

5 General Conclusions

The main results concerning the depositional environment of coal and oil shale within the Fushun Basin show that:

- The up to 120-m-thick coal seam of the Guchengzi Formation was deposited during the early transgressive stage of basin evolution. The sub-bituminous coal is generally hydrogen-rich, oil-prone and contains abundant amber. The lower part of the coal seam developed in a low-lying mire. At the study site, deposition of the upper part of the coal seam in a raised mire is indicated by low ash and sulfur contents. The uppermost part of the coal seam reflects the flooding of the mire due to increased subsidence rates. Paleo-vegetation was dominated by gymnosperms.
- The overlying oil-shale bearing Jijuntun Formation is up to 300 m thick and developed in a more than 100-m-deep freshwater lake. Photic zone anoxia and a stable stratified water column favored excellent preservation of organic matter. High quality oil shale was deposited in the upper unit of the Jijuntun Formation. Its organic matter is mainly composed of algae and bacteria.
- A 1D thermal model suggests that heat flow was high during maximum burial. High heat flow was a result of Late Oligocene magmatic activity.

The most important conclusions regarding the depositional environment of coal and oil shale within the Huadian Basin include:

- Thin coaly layers occur in all three members (Pyrite, Oil Shale and Carbonaceous Shale Member) of the Huadian Formation, but economic coal, developed during the regressive stage of basin evolution, is limited to the Carbonaceous Shale Member.
- 13 thin oil shale layers, intercalated by fan delta sediments, were deposited in the Oil Shale Member in a shallow lake. Water depth did not exceed a few tens of meters. Therefore, a stable stratified water column was not established. Moreover, the amount of terrestrial organic matter (prevailing angiosperms) is significant in the Huadian Basin, especially in oil shale from the lower part of the Oil Shale Member. The oil shale quality, therefore, varies significantly between different layers. Economic most important are layers 7 to 4.

A comparison of the depositional environments between the Eocene non-marine Fushun and Huadian basins show that:

- A single thick sub-bituminous coal seam was deposited in the early transgressive stage of basin evolution in the Fushun Basin, whereas equivalent coal is missing in the Huadian Basin, maybe due to a prevailing arid climate.
- After drowning of the mire, shallow and deep lacustrine conditions developed in the Fushun Basin due to increased subsidence rates. Photic zone anoxia established in the deep lake, suggesting high water depths. A stable stratified water column together with strictly anoxic conditions, high bioproductivity and excellent preservation conditions favored the accumulation of a very thick, high quality oil shale unit in the Fushun Basin. In comparison, the Huadian Basin is characterized by minor subsidence rates resulting in moderate water depths and the deposition of a high number of thin oil shale layers intercalated by fan delta sediments.
- The lower part of the oil shale unit in both basins is characterized by a strong terrestrial input. In the Fushun Basin gymnosperms prevail, whereas angiosperms are predominant in the Huadian Basin.
- Bacterial biomass is more abundant in the oil shale of the Fushun Basin than in the Huadian Basin. The input of bacteria and algae, forming kerogen type I to II, is highest in the upper part of the oil shale unit in both basins.
- During the regressive stage of basin evolution, thin coal layers accumulated in the Huadian Basin, whereas the deposition of a similar coal seam is missing in the Fushun Basin.

The sedimentary succession of the Fushun Basin is characteristic for many fault-controlled basins developed in humid environments. Such a characteristic stratigraphic succession could not develop in the Huadian Basin, maybe due to different climatic conditions and minor subsidence rates causing low water depth and unstable conditions during deposition of organic rich sediments.

Therefore, the main reason affecting quantity, quality and stratigraphic position of coal and oil shale deposits in the Fushun and Huadian basins are different subsidence rates. Furthermore, climatic conditions may have played a secondary role.

6 References

Aaloe, A., Bauert, H., Soesoo, A., 2007. Kukersite oil shale. MTÜ GEOGuide Baltoscandia. Tallinn, 31 pp.

Allix, P., Burnham, A., Fowler, T., Herron, M., Kleinberg, R., Symington, B., 2011. Coaxing Oil from Shale. Oilfield Review 22, 4-15.

Alqudah, M., Hussein, M.A., van den Boorn, S., Giraldo, V.M., Kolonic, S., Podlaha, O.G., Mutterlose, J., 2014. Eocene oil shales from Jordan – Paleoenvironmental implications from reworked microfossils. Marine and Petroleum Geology 52, 93-106.

Beard, K.C., Wang, B., 1991. Phylogenetic and biogeographic significance of the tarsiiform primate Asiomomys changbaicus from the Eocene of Jilin Province, Peoples Republic of China. American Journal of Physical Anthropology 85, 159-166.

Bechtel, A., Jia, J., Strobl, S.A.I., Sachsenhofer, R.F., Liu, Z., Gratzer, R., Püttmann, W., 2012. Palaeoenvironmental conditions during deposition of the Upper Cretaceous oil shale sequences in the Songliao Basin (NE China): Implications from geochemical analysis. Organic Geochemistry 46, 76-95.

Brindley, G.W., Brown, G., 1980. Crystal structures of clay minerals and their X-ray identification. Mineralogical Society, London.

Calder, J.H., Gibling, M.R., Mukhopadhyay, P.K., 1991. Peat formation in a Westphalian B piedmont setting, Cumberland basin, Nova Scotia: implications for the maceral-based interpretation of rheotrophic and raised paleomires. Bull. Soc. Geol. Fr. 162, 283-298.

Carroll, A.R., Bohacs, K.M., 1999. Stratigraphic classification of ancient lakes: balancing tectonic and climatic controls. Geology 27, 99–102.

Carroll, A.R., Bohacs, K.M., 2001. Lake-type controls on petroleum source rock potential in non-marine basins. AAPG Bulletin 85, 1033-1053.

Coplen, T.B., 2011. Guidelines and recommended terms for expression of stable-isotope-ratio and gas-ratio measurement results. Rapid Communications in Mass Spectrometry 25, 2538-2560.

Cumming, V.M., Selby, D., Lillis, P.G., 2012. Re-Os geochronology of the lacustrine Green River Formation: Insights into direct depositional dating of lacustrine successions, Re-Os systematic and paleocontinental weathering. Earth and Planetary Science Letters 359-360, 194-205.

Deutsches Institut für Normung (DIN) 51718, 1978. Feste Brennstoffe; Bestimmung des Wassergehaltes.

Deutsches Institut für Normung (DIN) 51719, 1980. Feste Brennstoffe; Bestimmung des Aschegehaltes.

Diessel, C.F.K., 1986. The correlation between coal facies and depositional environments. Proc. 20th Symp. Dep. Geol., Univ. Newcastle, Newcastle, NSW, 11-22.

Diessel, C.F.K., 1992. Coal- bearing Depositional Systems. Springer, Berlin, 721 pp.

Dyni, J.R., 2006. Geology and resources of some world oil-shale deposits. U.S. Geological Survey Scientific Investigations Report 2005-5294.

Espitalié, J., Deroo, G., Marquis, F., 1985. La pyrolyse Rock-Eval et ses applications (deuxième partie). Revue Institut Francais du Pétrole 40, 755-784.

Gruber, W., Sachsenhofer, R.F., 2001. Coal deposition in the Noric Depression (Eastern Alps): raised and low-lying mires in Miocene pull-apart basins. International Journal of Coal Geology 48, 89-114.

Hong, Y., Yang, Z., Wang, S., Sun, X., Du, N., Sun, M., Li, Y., 1980. A Research on the Strata and Paleontology of the Fushun Coal Field in Liaoning Province. Science Press, Beijing.

Hou, G., Dong, Q., Yu, W., Yan, L., Zhu, J., Miao, C., 2006. The geological characteristic and ore-forming process analysis of the oil shale in Fushun basin. Journal of Jilin University (Earth Science) 36, 991-1000.

Huang, Z., Liu, Z., Dai, H., Xu, S., 1983. On the sedimentary environment of the coal-bearing formation in the Fushun coal basin. Acta Geol. Sin. 57 (3), 261-269.

International Committee for Coal and Organic Petrology (ICCP), 1998. The new vitrinite classification (ICCP System 1994). Fuel 77, 349-358.

International Committee for Coal and Organic Petrology (ICCP), 2001. The new inertinite classification (ICCP System 1994). Fuel 80, 459-471.

Johnson, E.A., 1990. Geology of the Fushun coalfield, Liaoning Province, People's Republic of China. International Journal of Coal Geology 14, 217-236.

Knaus, E., Killen, J., Biglarbigi,K., Crawford, P., 2010. An Overview of Oil Shale Resources, in: Ogunsola, O.I., Hartstein, A.M., Ogunsola, O. (Eds.), Oil Shale: A Solution to the Liquid Fuel Dilemma. ACS Symposium Series 1032, 3-20.

Köster, J., Wehner, H., Hufnagel, H., 1988. Organic geochemistry and organic petrology of organic rich sediments within the „Hauptdolomit" formation (Triassic, Norian) of the Northern Calcareous Alps. Organic Geochemistry 13, 377-386.

Lambiase, J.J., 1990. A model for tectonic control of lacustrine stratigraphic sequences in continental rift basins, in: Katz, B.J. (Ed.), Lacustrine basin exploration: case studies and modern analogs. AAPG Memoir 50, 265-276.

Lenz, O.K., Wilde, V., Riegel, W., 2007. Recolonization of a Middle Eocene volcanic site: quantitative palynology of the initial phase of the maar lake of Messel (Germany). Review of Paleobotany and Palynology 145, 217-242.

Li, S., Yue, C., 2003. Study of pyrolysis kinetics of oil shale. Fuel 82, 337-342.

Liu, Z., Yang, H., Dong, Q., Zhu, J., Guo, W., Ye, S., Liu, R., Meng, Q., Zhang, H., Gan, S., 2009. Oil Shale in China. Petroleum Industry Press, Beijing.

Ma, X., Jiang, H., Cheng, J., Xu, H., 2012. Spatiotemporal evolution of Paleogene palynoflora in China and its implication for development of the extensional basins in East China. Review of Paleobotany and Palynology 184, 24-35.

Mackenzie, A.S., McKenzie, D.P., 1983. Aromatization and isomerization of hydrocarbons in sedimentary basins formed by extension. Geological Magazine 120, 417-470.

Manchester, S.R., Chen, Z., Geng, B., Tao, J., 2005. Middle Eocene flora of Huadian, Jilin Province, Northeastern China. Acta Paleobotanica 45, 3-26.

Meng, Q., Liu, Z., Bruch, A.A., Liu, R., Hu, F., 2012. Paleoclimatic evolution during Eocene and its influence on oil shale mineralisation, Fushun basin, China. Journal of Asian Earth Sciences 45, 95-105.

Moore, D.M., Reynolds, R.C., 1997. X-ray diffraction and the identification and analysis of clay minerals. Oxford University Press, New York.

Mosbrugger, V., Utescher, T., 1997. The coexistence approach – a method for quantitative reconstructions of Tertiary terrigenous paleoclimate data using plant fossils. Paleogeography, Paleoclimatology, Paleoecology 134, 61-86.

Neumeister, S., Algeo, T.J., Gratzer, R., Gawlick, H.-J., Newton, R.J., Sachsenhofer, R.F., 2014. Depositional environment of the Bächental bituminous marl: Evidence for local and global controls of Pliensbachian to Toarcian organic matter accumulation. Ber. Inst. Erdwiss. K.-F.-Univ. Graz, 20, 154.

Ocakoglu, F., Acikalin, S., Yilmaz, I.Ö., Safak, Ü., Gökceoglu, C., 2012. Evidence for orbital forcing in lake-level fluctuations in the Middle Eocene oil shale-bearing lacustrine successions in the Mudurnu Göynük Basin, NW Anatolia (Turkey). Journal of Asian Earth Sciences 56, 54-71.

Passey, Q.R., Bohacs, K.M., Esch, W.L., Klimentidis, R., Sinha, S., 2010. From Oil-Prone Source Rock to Gas-Producing Shale Reservoir-Geologic and Petrophysical Characterization of Unconventional Shale-Gas Reservoirs. SPE 131350.

Quan, C., Liu, Y., Utescher, T., 2012. Paleogene temperature gradient, seasonal variation and climate evolution of northeast China. Paleogeography, Paleoclimatology, Paleoecology 313-314, 150-161.

Radke, M., Willsch, H., Welte, D.H., 1980. Preparative hydrocarbon group type determination by automated medium pressure liquid chromatography. Analytical Chemistry 52, 406-411.

Sachsenhofer, R.F., 2000. Geodynamic controls on deposition and maturation of coal in the Eastern Alps, in: Neubauer, F., Höck, V. (Eds.), Aspects of Geology in Austria. Mitteilungen der Österreichischen Geologischen Gesellschaft 92, 185-194.

Sachsenhofer, R.F., Bechtel, A., Reischenbacher, D., Weiss, A., 2003. Evolution of lacustrine systems along the Miocene Mur-Mürz fault system (Eastern Alps, Austria) and implications on source rocks in pull-apart basins. Marine and Petroleum Geology 20, 83-110.

Schultz, L.G., 1964. Quantitative interpretation of mineralogical composition from X-ray and chemical data for the Pierre Shale. Geological Survey Professional Paper 391-C.

Su, K., Quan, C., Liu, Y., 2014. Cycas fushunensis sp. nov. (Cycadaceae) from the Eocene of northeast China. Review of Paleobotany and Palynology 204, 43-49.

Sun, P., 2010. Research on Sedimentary Characteristics of Huadian Formation of Paleogene in Huadian Basin. Thesis Jilin University.

Sun, P., Liu, Z., Meng, Q., Liu, R., Jia, J., Hu, X., 2011. Effect of the basin-fill features on oil shale formation in Paleogene, Huadian Basin. Journal of China Coal Society 36, 1110-1116.

Sun, P., Sachsenhofer, R.F., Liu, Z., Strobl, S.A.I., Meng, Q., Liu, R., Zhen, Z., 2013. Organic matter accumulation in the oil shale- and coal-bearing Huadian Basin (Eocene; NE China). International Journal of Coal Geology 105, 1-15.

Sweeney, J.J., Burnham, A.K., 1990. Evaluation of a simple model of vitrinite reflectance based on chemical kinetics. AAPG Bulletin 74, 1559-1570.

Sýkorová, I., Pickel, W., Christanis, K., Wolf, M., Taylor, G.H., Flores, D., 2005. Classification of huminite – ICCP System 1994. International Journal of Coal Geology 62, 85-106.

Taylor, H., Teichmüller, M., Davis, A., Diessel, C.F.K., Littke, R., Robert, P., 1998. Organic Petrology. Borntraeger. Berlin-Stuttgart.

von der Brelie, G., Wolf, M., 1981. Zur Petrographie und Palynologie heller und dunkler Schichten im rheinischen Hauptbraunkohlenflöz. Fortschr. Geol. Rheinl. Westfalen 29, 95-163.

Wang, Q., Bai, J., Sun, B., Sun, J., 2005. Strategy of Huadian oil shale comprehensive utilization. Oil Shale 22, 305-315.

Wang, Q., Ferguson, D.K., Feng, G., Ablaev, A.G., Wang, Y., Yang, J., Li, Y., Li, C., 2010. Climatic change during the Paleocene to Eocene based on fossil plants from Fushun, China. Paleogeography, Paleoclimatology, Paleoecology 295, 323-331.

Wu, C., Yuan, Y., Li, S., 1998. The synsedimentary structure framework and its control on the thickness of extra-thick coal bed and oil shale, Fushun Basin, China. Coal Geology and Exploration 6, 2-7.

Wu, C., Yang, Q., Zhu, Z., Liu, G., Li, X., 2000. Thermodynamic analysis and simulation of coal metamorphism in the Fushun Basin, China. International Journal of Coal Geology 44, 149-168.

Wu, C., Wang, X., Liu, G., Li, S., Mao, X., Li, X., 2002. Study on dynamics of tectonic evolution in the Fushun Basin, Northeast China. Science in China 45, 311-324.

Xie, X., Volkman, J.K., Qin, J., Borjigin, T., Bian, L., Zhen, L., 2014. Petrology and hydrocarbon potential of microalgal and macroalgal dominated oil shales from the Eocene Huadian Formation, NE China. International Journal of Coal Geology 124, 36-47.

Xu, S., Liu, Z., Dong, Q., Liu, S., Liu, R., Meng, Q., 2012. Eocene sedimentary evolution and its control over coal and oil shale development in Fushun Coalfield. Journal of China University of Petroleum 36, 45-67.

Yalcin, M.N., Littke, R., Sachsenhofer, R.F., 1997. Thermal History of Sedimentary Basins, in: Welte, D.H., Horsfield, B., Baker, D.R. (Eds.), Petroleum and Basin Evolution – Insights from Petroleum Geochemistry, Geology and Basin Modeling. Springer, Berlin, 71-167.

Zhang, P.L., Lu, B.C., Li, C.T., Sun, J.R., Liu, A., 1986. Discovery of the Huadian Fauna of the Early Tertiary and its geological significance. Jilin Geology 4, 1-14.

Zhao, C., Ye, D., Wei, D., Chen, B., Liu, D., 1994. Tertiary in Oil and Gas Province of China (III). Oil Industry Press, Beijing.

PUBLICATIONS

7 Depositional environment of oil shale within the Eocene Jijuntun Formation in the Fushun Basin (NE China)

Marine and Petroleum Geology 56 (2014), 166-183
DOI: 10.1016/j.marpetgeo.2014.04.011

Susanne A.I. Strobl[a], Reinhard F. Sachsenhofer[a], Achim Bechtel[a], Reinhard Gratzer[a], Doris Gross[a], Syed N.H. Bokhari[b], Rong Liu[c], Zhaojun Liu[c], Qingtao Meng[c], Pingchang Sun[c]

[a] Department of Applied Geosciences and Geophysics, Montanuniversitaet Leoben, Peter-Tunner-Straße 5, 8700 Leoben, Austria
[b] Department of General and Analytical Chemistry, Montanuniversitaet Leoben, Franz-Josef-Straße 18, 8700 Leoben, Austria
[c] College of Earth Sciences, Jilin University, Changchun 130061, China

Keywords

Jijuntun Formation; oil shale; biomarker; organic matter; mineralogical composition; oil shale potential

Abstract

The non-marine Fushun Basin in NE China is a fault-controlled basin filled with Eocene sediments. It hosts the largest opencast coal and oil shale mine in Asia. A single thick oil shale layer overlying sub-bituminous coal occurs within the Middle Eocene Jijuntun Formation. Based on mineralogy, inorganic and organic geochemistry, organic petrography, stable isotope geochemistry, and vitrinite reflectance measurements, the depositional environment and the oil shale potential of the oil shale-bearing succession were investigated. The Jijuntun Formation is subdivided into a lower and an upper unit characterized by a low and high quality oil shale, respectively. The thick oil shale layer of the Jijuntun Formation developed

under long-lasting stable conditions in a deep freshwater lake, after drowning of a swamp. The organic matter in the lower unit is characterized by landplant-derived macerals. The sediments containing a type II kerogen (HI: ~400 mgHC/gTOC) were deposited during warm and humid conditions. Lacustrine organisms predominant in the upper unit are forming kerogen type I (HI: ~700 mgHC/gTOC). High bioproductivity and excellent preservation conditions resulted in high TOC contents up to 23.6 wt.% in the upper unit. The organic matter preservation was controlled by photic zone anoxia originating in a temperature stratified water column in the deep lake, without significant changes in bottom water salinity. Mid-Eocene cooling during deposition of the upper unit of the Jijuntun Formation is reflected by clay mineral composition. A hot and arid climate favoring brackish conditions in a shallow lake prevailed during accumulation of the overlying carbonate-rich Xilutian Formation. Individual geochemical parameters in the Fushun Basin have to be used with caution, e.g. the maturity proxy T_{max} is affected by kerogen type, the redox proxy Pr/Ph ratio is probably biased by different sources of isoprenoids. This demonstrates the importance of multi-proxy studies.

7.1 Introduction

Rocks with very high organic matter contents often form an integral part of the fill of non-marine sedimentary basins (Carroll and Bohacs, 1999; Sachsenhofer et al., 2003). These sediments may represent excellent petroleum source rocks (e.g. Carroll and Bohacs, 2001) or even oil shales, which are commonly defined as thermally immature rocks yielding substantial oil and gas upon low temperature distillation (Dyni, 2006). In any case they are great archives of paleoenvironmental conditions.

Lacustrine oil shales with a Middle Eocene age are widespread throughout the world and include i.a. the Parachute Creek Member of the Green River Formation (USA; Cumming et al., 2012), the Messel oil shale (Germany; Lenz et al., 2007), oil shales in central Jordan (Alqudah et al., 2014), Turkey (Ocakoglu et al., 2012), and China (Fushun and Huadian basins; Quan et al., 2012; Sun et al., 2013a). Although all of these basins include lacustrine rocks, the oil shales differ significantly in terms of organic richness, thickness, and vertical and lateral heterogeneity. For example, both

the Fushun and Huadian basins are located at the same fault zone and formed at the same time. Nevertheless a single oil shale layer accumulated in the Fushun Basin, whereas a high number of relative thin layers occurs in the Huadian Basin (Sun et al., 2013a).

The present paper focuses on the world-class oil shale in the Eocene Fushun Basin in northeastern China (Fig. 7.1). In this basin oil shale, 50 to 300 m thick (Jijuntun Formation) overlying sub-bituminous coal, 20 to 200 m thick (Guchengzi Formation) is exploited in the largest opencast coal and oil shale mine in Asia (Meng et al., 2012). Whereas the oil shale, yielding 5 to 8 wt.% oil (max. 12 wt.%), is used to produce fuel, coal is used for heating purposes (Liu et al., 2009).

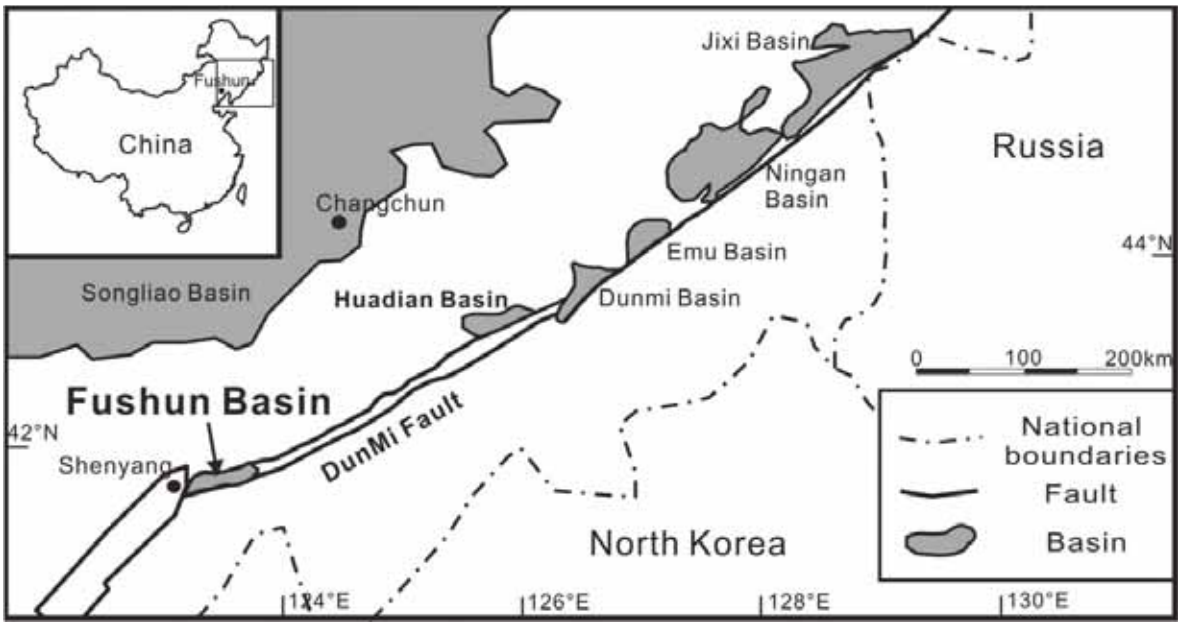

Fig. 7.1: Topographical map with special focus on the location of the Fushun Basin and the DunMi fault [modified according to Meng et al. (2012)].

Previous research related to the oil shale in the Fushun Basin mainly focused on tectonic evolution (Wu et al., 2002), kinetics of pyrolysis (Li and Yue, 2003), oil reserves (Liu et al., 2009), and paleoclimatic evolution (Wang et al., 2010; Meng et al., 2012). However, to date very little research has been undertaken on the depositional environment and the factors controlling its variation through time.

Hence, the main aim of our paper is to reconstruct the environmental conditions, which resulted in the deposition of the very thick oil shale layer of the Jijuntun Formation. To reach the goal, the depositional environment is characterized by

integrating lithological, mineralogical and maceral data with inorganic and organic geochemical proxies. Sun et al. (2013a) showed that the oil shale bearing unit (Oil Shale Member) in the Huadian Basin is of similar thickness than the Jijuntun Formation, but exhibits a cyclic structure with thirteen oil shale layers separated by organic lean rocks. Thus, an additional goal of the present paper is to investigate if a similar cyclicity appears in the more uniform Jijuntun Formation. In addition the maturity of the Jijuntun Formation and its oil shale potential are evaluated.

7.2 Geological setting

The Fushun Basin is a non-marine strike-slip basin located along the Dunhua-Mishan ("DunMi") fault zone (Wu et al., 2000; Fig. 7.1). The DunMi fault zone was active during Mesozoic-Cenozoic time (Liu et al., 2009; Meng et al., 2012). Several coal and oil shale-bearing basins are located along this fault zone. The most prominent ones are the Eocene Fushun and Huadian basins, which show major differences in their evolution although they have similar tectonic settings and ages (Liu et al., 2009; Sun et al., 2013a).

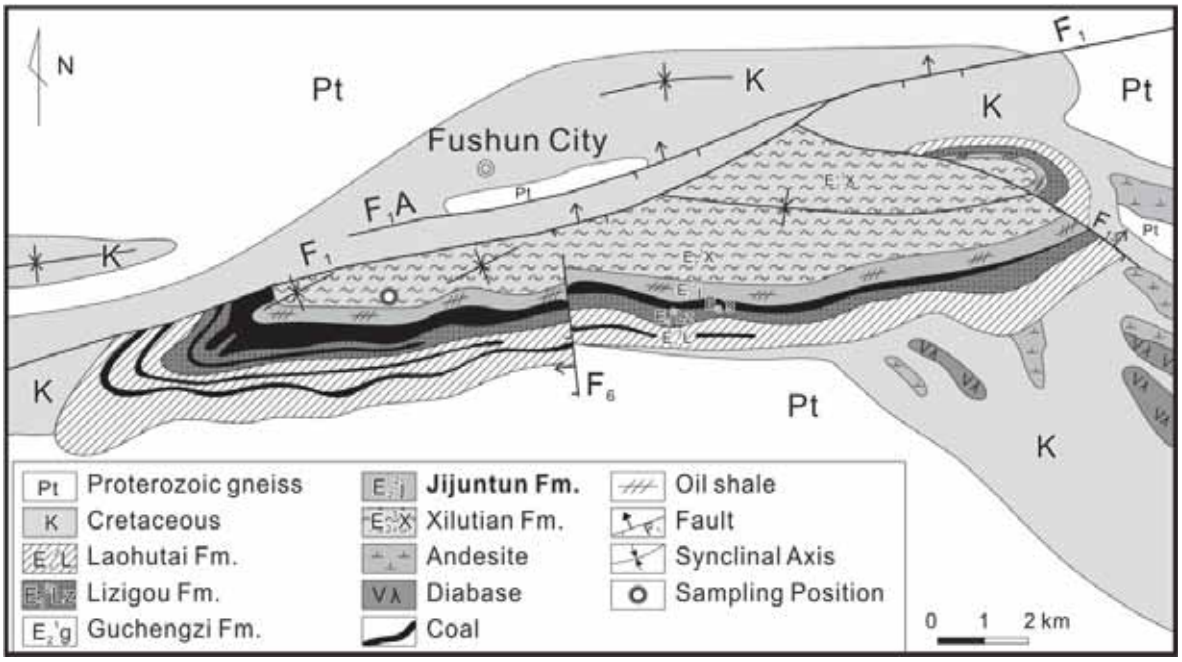

Fig. 7.2: Geological map of the Fushun Basin [modified according to Meng et al. (2012), Hou et al. (2006), Zhao et al. (1994)].

The Fushun Basin is characterized by an EW trending syncline, whose northern limb was removed by a large-scale thrust fault (Johnson, 1990; Fig. 7.2). The basement consists of Proterozoic gneiss and sediments of Cretaceous age. The basin fill contains from base to top: Laohutai and Lizigou formations (Paleocene), Guchengzi Formation (Lower Eocene), Jijuntun and Xilutian formations (Middle Eocene) and Gengjiajie Formation (Upper Eocene). A stratigraphic column of the Fushun Basin is provided together with a short description of depositional environment in Fig. 7.3.

The coal seam within the Guchengzi Formation (Ypresian) is between 20 m and 200 m thick. It accumulated in a freshwater swamp and reaches the sub-bituminous stage. Interseam sediments include carbonaceous shale, mudstone and sandstone. Amber and siderite nodules occur throughout the seam (Johnson, 1990).

The Jijuntun Formation (Lutetian), 50 m to 300 m thick, is composed of thick oil shale intercalated by carbonaceous shale and mudstone (Wu et al., 2000). Liu et al. (2009) assumed that the depth of the lake increased during deposition of the Jijuntun Formation. According to these authors, oil shale with low quality (about 10.0 wt.% TOC; oil yield <4.7 wt.%) was deposited in a relative shallow lake, whereas the high quality oil shale (up to 20.0 wt.% TOC; oil yield >4.7 wt.%) in the upper part of the Jijuntun Formation accumulated in a deep lake.

The Xilutian Formation (Bartonian), up to 600 m thick, comprises light green dolomitic mudstone intercalated by silty argillite deposited in a shallow lake environment (Wu et al., 2000).

Erosional remnants of mudstones and siltstones of the fluvial Gengjiajie Formation (Upper Eocene; Priabonian) appear only locally (Hong et al., 1980; Wu et al., 2000).

The climate during deposition of the basin fill was reconstructed by Quan et al. (2012) using the Coexistence Approach (Mosbrugger and Utescher, 1997). According to these investigations the upper part of the coal seam (Guchengzi Formation) was deposited during the Early Eocene Climatic Optimum, whereas the mean annual temperature decreased during deposition of the Jijuntun Formation. The overlying Xilutian Formation represents a Mid-Eocene warming event. Meng et al. (2012) used element ratios and clay mineral assemblages to reconstruct climatic conditions. These

authors argue for a warm and humid climate during deposition of the Jijuntun Formation and a hot and arid climate during deposition of the Xilutian Formation.

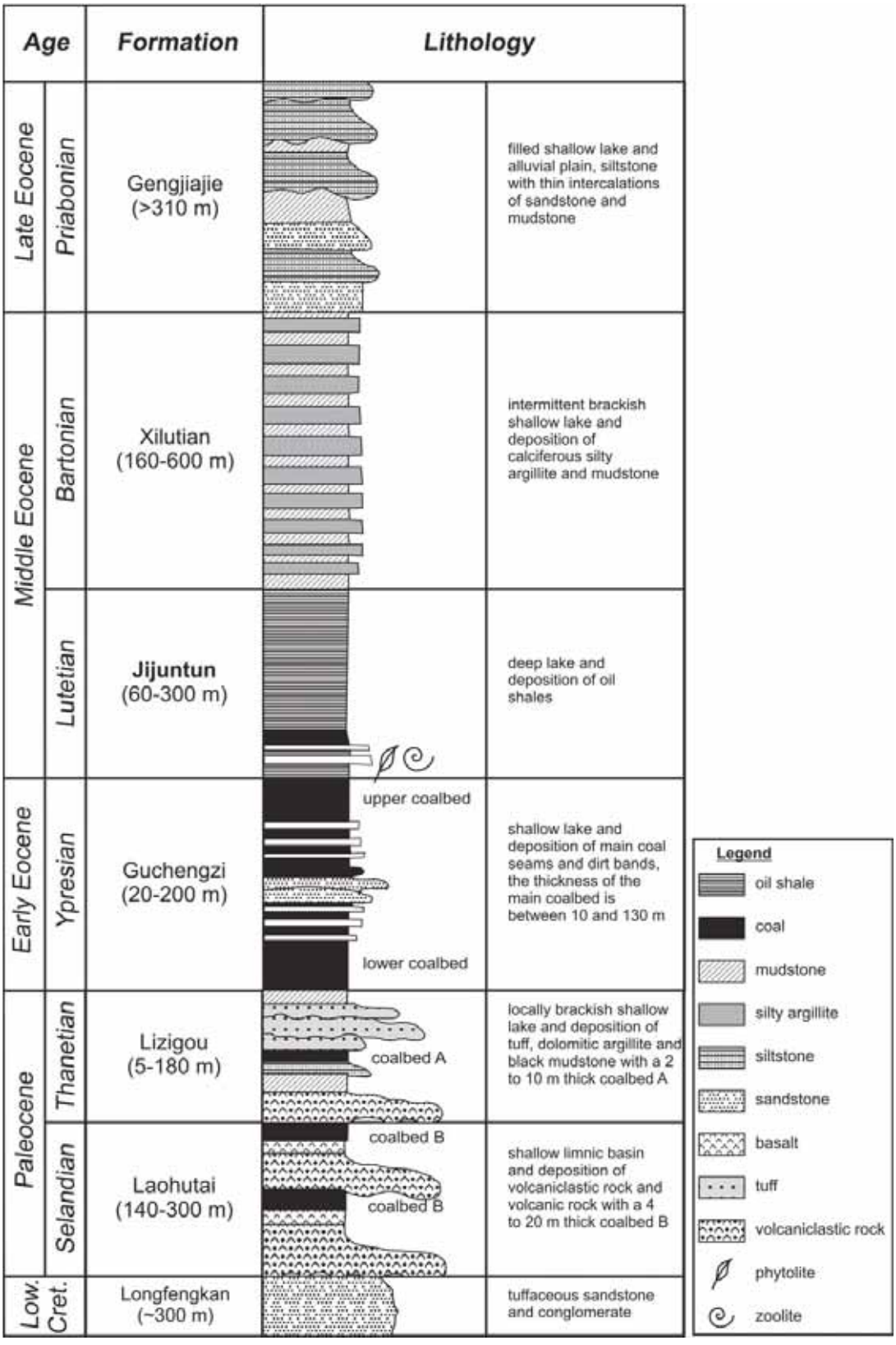

Fig. 7.3: Stratigraphic column of the Fushun Basin [modified according to Quan et al. (2012), Wu et al. (2000), Hong et al. (1980)].

7.3 Samples and methods

50 samples have been taken along a vertical profile in the eastern part of the West Open Pit mine in the south of Fushun City (41°50′33.4′′, 123°53′14.3′′). All samples are fresh, as they were taken from an active quarry face. Moreover microscopic inspection shows that pyrite is unweathered. 48 samples represent a 57-m-thick succession through the Jijuntun Formation. The uppermost two samples were taken within the Xilutian Formation.

7.3.1 Carbon and sulfur analyses

Total carbon (TC) and sulfur (S) contents of all samples were determined using a Leco CS-230 elemental analyzer. Total organic carbon (TOC) content was determined with the same instrument on samples pre-treated with hydrochloric acid. Total inorganic carbon (TIC) contents were calculated by the difference between TC and TOC.

7.3.2 Rock Eval pyrolysis

Pyrolysis analysis was performed using a Rock Eval 2+ analyzer. Depending on the TOC content, 10 mg to 50 mg of each pulverized sample were heated gradually in an inert atmosphere. Within this method, the amount of pyrolyzate released from kerogen was normalized to TOC to give the hydrogen index (HI). The temperature of maximum hydrocarbon generation (T_{max}) is defined at the maximum value of the S_2-peak.

Based on TOC and Rock Eval data, samples were selected for XRD and XRF measurements, maceral and biomarker analyses and compound-specific isotope analysis.

7.3.3 XRD

X-ray diffraction analyses were conducted on a Philips PW 1830/40 device using CuKα-radiation (1.54 Å, 35 kV, 35 mA). Scans with a step size of 0.02 ° were run between 2 and 67 °2Θ in the air-dry state (random powder mount and oriented powder mount) and between 2 and 45 °2Θ in the ethylene-glycoliated state and after heating to 350 and 550°C. Qualitative processing was done using the dataset of

Brindley and Brown (1980) and Moore and Reynolds (1997). Quantitative interpretation was carried out using the methods described by Schultz (1964).

7.3.4 XRF

The major element compound content was determined using a wavelength dispersive X-ray fluorescence spectrometer (WD-XRF AXIOS from PANalytical). Fine grained weighed amount of samples were subjected to platinum crucibles which were kept for three hours in muffle furnace at 1000°C for loss on ignition (LOI). Fused glass beads were formed through fusion of one gram of ignited sample mixed with 8 g of $Li_2B_4O_7$ with a Vulcan VAA2 instrument. The XRF was calibrated with more than 50 certified and non-certified geological reference materials and checked regularly through participation in the IAG proficiency testing program (GeoPT).

7.3.5 Organic petrography

Microscopic analysis was performed using polished blocks of whole-rocks cut perpendicular to bedding planes, a Leica MPV microscope and oil immersion objectives. Maceral analysis was performed using reflected white and fluorescent light and a 50x objective. 500 points per polished block were counted using the single scan method (Taylor et al., 1998). Vitrinite reflectance was measured using a 100x objective in non-polarized light at a wavelength of 546 nm (Taylor et al., 1998). Results are presented as mean random reflectance values (R_r). Because of the prevalence of very small vitrinite particles, vitrinite reflectance measurements of 50 points were possible only for two samples.

7.3.6 Organic geochemistry (biomarker analysis)

For organic geochemical analysis, portions of selected samples from the Jijuntun Formation were extracted for approximately 1 h using dichloromethane (DCM) in a Dionex ASE 200 accelerated solvent extractor. Asphaltenes were precipitated from a hexane-DCM solution (80:1) and separated by centrifugation. The hexane-soluble fractions were separated into NSO compounds, saturated and aromatic hydrocarbons using medium pressure liquid chromatography (MPLC) with a Köhnen-Willsch instrument (Radke et al., 1980). The saturated and aromatic hydrocarbon fractions

were analyzed using a gas chromatograph equipped with a 30 m DB-5MS fused silica column (i.d. 0.25 mm; 0.25 µm film thickness) and coupled to a Thermo Fisher ISQ quadrupol mass spectrometer (GC-MS system). The oven temperature gradient was programmed from 70°C to 300°C at 4°C min^{-1}, followed by an isothermal period of 15 min. Helium was used as carrier gas. The sample was injected splitless, with the injector temperature at 275°C. The spectrometer was operated in the EI (electron ionization) mode over a scan range from *m/z* 50 to 650 (0.7 s total scan). Data were processed using an Xcalibur data system. Individual compounds were identified on the basis of retention time in the total ion current (TIC) chromatogram and by comparison of the mass spectra with published data. Relative percentages and absolute concentrations of different compound groups in the saturated and aromatic hydrocarbon fractions were calculated using peak areas from the gas chromatograms in relation to that of internal standards (deuteriated *n*-tetracosane and 1,1'binaphthyl, respectively).The concentrations were normalized to the TOC content.

7.3.7 Compound-specific stable isotope geochemistry

Carbon isotope determination of *n*-alkanes and acyclic isoprenoids was performed using a Trace GC instrument attached to a ThermoFisher DELTA-V isotope ratio mass spectrometer via a combustion interface (GC isolink, ThermoFisher). For calibration, CO_2 was injected at the beginning and end of each analysis. The GC column and temperature program are the same as for GC-MS. Stable isotope ratios are reported in delta notation ($\delta^{13}C$; Coplen, 2011) relative to the Vienna-Pee Dee Belemnite (V-PDB) standard ($\delta^{13}C=[(^{13}C/^{12}C)_{sample}/(^{13}C/^{12}C)_{standard}-1]$). Delta notation is expressed in parts per thousand or per mil (‰). The analytical error was better than 0.2 ‰.

7.4 Results

7.4.1 Lithology and mineralogy

The studied profile of the Jijuntun Formation, 57 m thick, is shown in Fig. 7.4 together with mineralogical and bulk geochemical data.

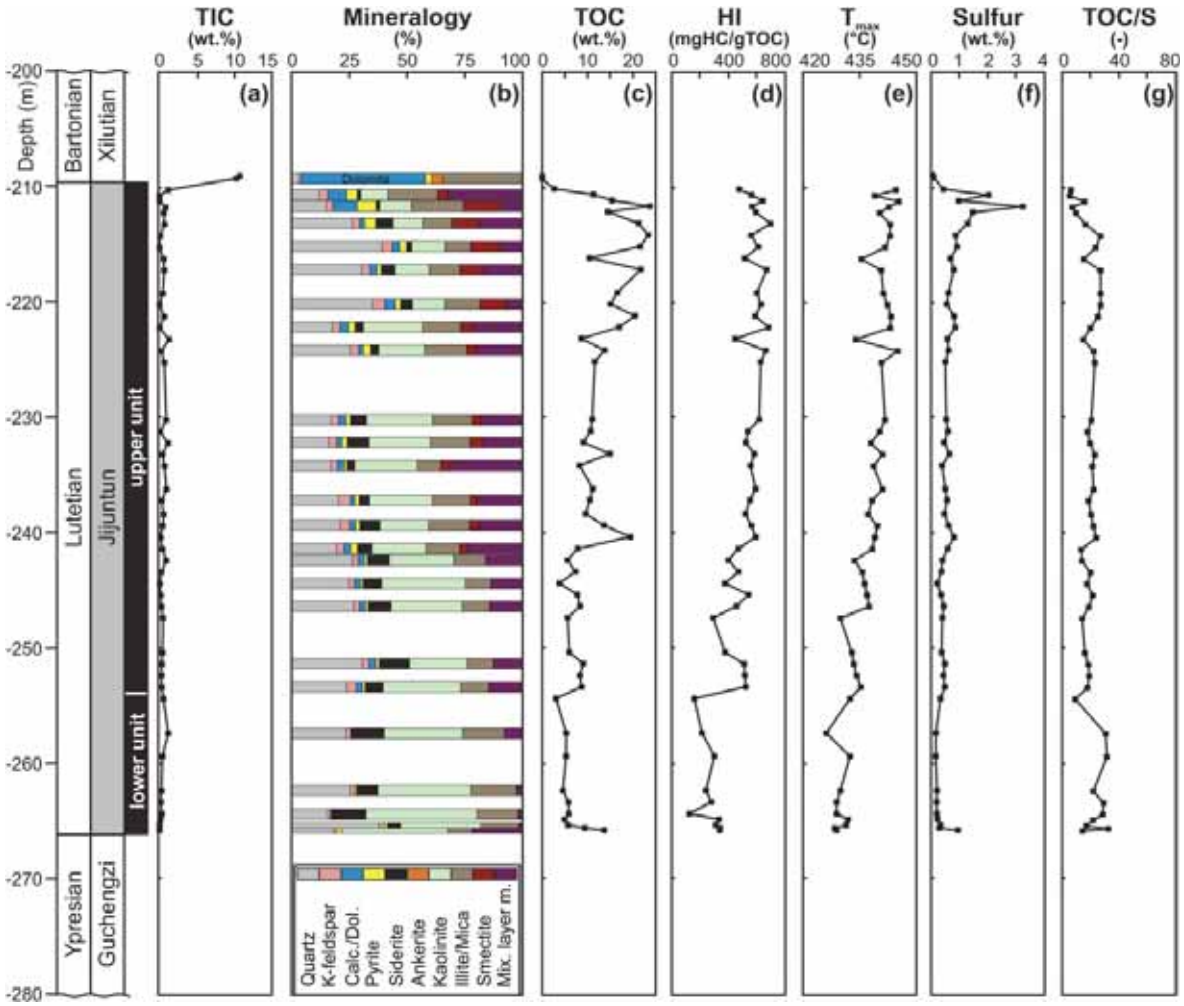

Fig. 7.4: Depth profiles of bulk geochemical proxies and mineralogical composition of the Jijuntun and the Xilutian Formations.

Based on TOC contents and HI data, the Jijuntun Formation is subdivided into a lower (-266 to -254 m) and an upper unit (-254 to -209 m).

The Jijuntun Formation overlies the coal seam of the Guchengzi Formation (~40 m thick) with a sharp contact, but several layers of shaly coal or coaly shale occur in the uppermost part of the seam. The Jijuntun Formation consists of carbonaceous shale, mudstones and thick oil shale layers. Low TIC percentages (Fig. 7.4a) reflect low carbonate contents. Plant remains occur frequently in the lowermost part of the Jijuntun Formation. The uppermost 1.5 m below the contact to the overlying Xilutian Formation is composed of brownish mudstone. In the studied section the base of the Xilutian Formation is formed by greenish dolostone with high TIC contents (Fig. 7.4a). The bulk of the Xilutian Formation consists of green mudstone beds intercalated by muddy carbonate rocks with frequent alternating, varicolored beds.

X-ray diffractograms of representative samples from the lower and the upper units of the Jijuntun Formation and from the Xilutian Formation are shown in Fig. 7.5.

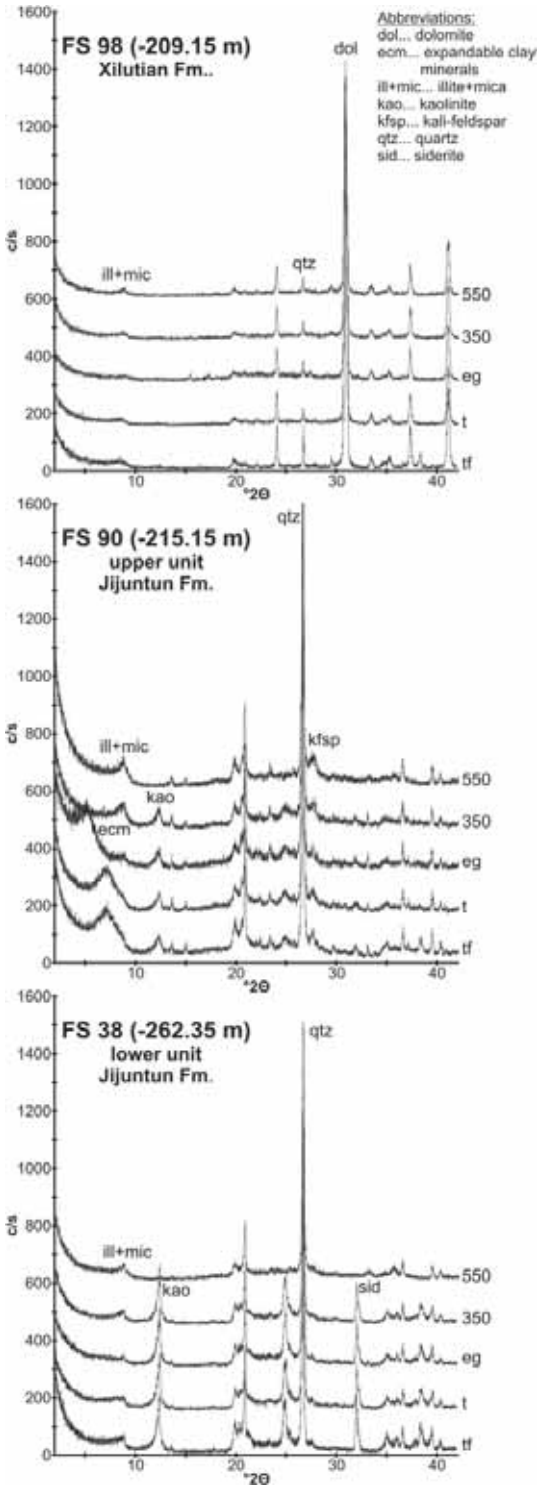

Fig. 7.5: X-ray diffractograms of representative samples from the lower and the upper units of the Jijuntun Formation and from the Xilutian Formation. Only the strongest reflection of each mineral is indicated. *Abbreviations:* tf, random powder mount; t, oriented powder mount; eg, ethylene-glycoliated state; 350, heat treated at 350°C; 550, heat treated at 550°C.

Tab. 7.1: Data from XRD and XRF measurements and organic petrography.

Sample	Depth	Quartz	K-fd/Algae	Calc./Dol.	Pyrite	Siderite	Ankerite	Kaolinite	Illite/Mica	Smectite	Mixed Layer	LOI	SiO_2	Al_2O_3	Fe_2O_3	CaO	MgO	Terrig. OM	Lamalg.	Telalg.
	(m)	(%)	(%)	(%)	(%)	(%)	(%)	(%)	(%)	(%)	(%)	(%)	(%)	(%)	(%)	(%)	(%)	(vol.%, mmf)	(vol.%, mmf)	(vol.%, mmf)
Ukturlak Formation																				
FS 98	-209.15	3	1	54	3		5	0	35	0	0	38.9	10.5	4.0	7.3	24.4	13.6			
Jiyunnat Formation - upper unit																				
FS 96	-210.65	12	4	8	5	1		12	22	4	33	23.7	44.0	15.6	6.5	3.5	1.7			
FS 94	-211.65	15	3	11	8	2		14	23	16	10	36.7	34.4	9.4	5.4	7.5	1.0	23	70	7
FS 92	-213.15	26	3	2	5	7		13	13	12	19	33.8	43.2	12.0	6.7	1.1	0.9			
FS 90	-215.15	39	4	3	3	2		14	11	13	10	32.4	48.9	11.7	3.5	0.4	0.7	14	85	0
FS 88	-217.15	30	4	3	2	6		15	13	10	17	33.1	45.9	11.8	5.7	0.6	0.8			
FS 86	-220.15	35	5	4	3	5		14	15	11	7	26.5	49.3	15.8	4.9	0.2	1.0	14	82	4
FS 84	-222.15	18	3	4	3	4		26	16	5	22	29.2	44.5	17.3	5.4	0.3	0.9			
FS 82	-224.15	25	4	2	3	4		20	18	4	20	25.1	49.0	17.0	4.5	0.2	0.9	16	84	0
FS 75	-230.15	17	3	3	2	7		29	17	4	18	24.5	44.2	17.6	8.8	1.0	1.2			
FS 73	-232.15	16	4	2	2	9		27	17	6	17	23.2	43.0	14.7	13.9	1.1	1.6	21	77	1
FS 71	-234.15	17	3	3	1	3		27	10	4	31	19.9	50.9	20.6	4.5	0.3	0.9			
FS 65	-237.15	20	5	2	2	4		27	16	3	20	22.7	49.0	18.8	5.3	0.4	0.9	28	71	1
FS 63	-239.35	21	4	2	2	9		21	18	4	19	25.6	48.0	14.2	8.0	0.8	1.2			
FS 61	-241.35	20	3	3	3	6		23	15	3	24	20.7	46.8	16.7	8.4	1.0	1.2	38	61	0
FS 46	-242.35	26	3	3	1	9		28	14	0	16	18.2	50.7	16.9	9.8	0.6	1.3	47	52	1
FS 44	-244.35	25	2	3	1	8		36	11	0	14	14.5	55.9	20.6	5.1	0.5	0.9			
FS 42	-246.35	27	2	2	1	10		31	12	0	14	20.2	50.4	16.1	9.5	0.6	1.0	31	66	2
FS 56	-251.35	31	3	3	1	13		25	11	0	13	20.5	51.4	14.2	10.1	0.5	1.1	39	60	10
FS 54	-253.35	24	4	3	1	8		34	12	0	15	20.2	51.9	17.9	6.7	0.4	0.8	37	61	2
Jiyunnat Formation - lower unit																				
FS 53	-254.35																	74	25	2
FS 52	-257.35	24	2	0	0	14		34	18	0	8	19.0	47.3	13.8	15.6	0.7	1.6			
FS 51	-259.35																	73	25	2
FS 38	-262.35	25	2	0	1	9		40	20	0	3	16.2	53.1	19.5	7.7	0.4	0.8	72	26	2
FS 36	-264.35	16	1	0	0	15		48	18	0	2	20.3	49.4	14.8	20.5	0.7	1.4	76	21	3
FS 34	-265.35	38	2	0	2	6		35	16	0	2	16.9	55.4	21.7	3.1	0.2	0.6			
FS 32	-265.80	18	1	0	2	0		46	11	0	22	26.3	47.8	20.6	2.4	0.1	0.5	88	11	1

Calc./Dol.: calcite and/or dolomite; Mixed Layer: mixed layer minerals; LOI: loss on ignition; Terrig. OM: terrigenous organic matter; Lamalg.: lamalginite; Telalg.: telalginite.

The mineralogical composition (Fig. 7.4b; Tab. 7.1) of sediments from the Jijuntun Formation is dominated by quartz (12-39%) and clay minerals (48-78%). Kaolinite, illite/mica, mixed layer minerals, and smectite occur in decreasing amounts. The kaolinite content decreases upward from 46 to 12%. Smectite is limited to the depth interval between -241 and -210 m and shows its highest abundance in the upper part of the Jijuntun Formation. Potassic feldspar occurs in low percentages. Calcite and dolomite are largely missing in the lower unit and occur in low amounts in the upper unit. Relative high percentages of calcite (9%) only occur in the uppermost part of the Jijuntun Formation. The percentage of siderite (up to 15%) varies throughout the profile, but, with the exception of the lowermost sample, shows a general upward decreasing trend. Pyrite displays an opposite trend. Its percentage is relatively high in the lowermost sample, low in the rest of the lower unit, and increases upward in the upper unit. Microscopical inspection reveals that pyrite occurs in all samples, both in the form of framboids or euhedras. Relative large framboids are more abundant in the lower part of the succession, relative small euhedras are more abundant in its upper part. We speculate that the euhedral crystals formed through re-crystallization of small framboids (Ostwald and England, 1979; Sawlowicz, 1993).

The studied sample from the Xilutian Formation contains mainly dolomite (54%) and illite/mica (35%), next to quartz, feldspar, pyrite and ankerite, which occur in low percentages.

The mineralogical composition is reflected by the contents of major element oxides (Tab. 7.1). Samples from the Jijuntun Formation contain high fractions of SiO_2 (34.4-55.9%) and Al_2O_3 (9.4-21.7%), but low percentages of CaO (0.1-7.5%) and MgO (0.5-1.7%). Fe_2O_3 (2.4-20.5%) and MnO (<0.3%) contents show a positive trend in the respective plots versus siderite content (r^2=0.70 and 0.67, respectively), showing that siderite is the main iron-bearing mineral. In contrast to samples from the Jijuntun Formation, the dolomitic sample from the Xilutian Formation contains high percentages of CaO (24.4%) and MgO (13.6%).

7.4.2 Bulk geochemical parameters

The bulk geochemical data are listed in Tab. 7.2.

Tab. 7.2: Data from LECO and Rock Eval measurements and compound specific stable isotope geochemistry.

Sample	Depth	TIC	TOC	S	TOC/S	S_1	S_2	S_1+S_2	PI	T_{max}	HI	α-C_{27}	Pristane	α-C_{29}	Phytane	α-C_{30}	α-C_{31}	α-C_{32}	α-C_{35}
	(m)	(wt%)	(wt%)	(wt%)		(mgHC/g)	(mgHC/g)	(mgHC/g)		(°C)	(mgHC/gTOC)	($\delta^{13}C$; ‰ PDB)	($\delta^{13}C$; ‰ PDB)	($\delta^{13}C$; ‰ PDB)	($\delta^{13}C$; ‰ PDB)	($\delta^{13}C$; ‰ PDB)	($\delta^{13}C$; ‰ PDB)	($\delta^{13}C$; ‰ PDB)	($\delta^{13}C$; ‰ PDB)
Tübelhorn Formation																			
PS 99	-208.95	11.5	0.0	0.1															
PS 98	-209.15	11.0	0.0	0.1															
Allgäu Formation - upper unit																			
PS 97	-210.15	1.1	2.8	0.4	6.3	0.1	13.2	13.3	0.01	445	477								
PS 96	-210.65	0.0	11.3	2.0	5.6	0.8	63.9	64.6	0.01	439	564								
PS 95	-211.15	0.0	15.3	1.0	15.8	1.0	98.7	99.7	0.01	445	643								
PS 94	-211.65	0.8	23.6	3.2	7.3	1.6	134.1	135.7	0.01	443	569								
PS 93	-212.15	0.5	14.4	1.5	9.9	1.1	85.8	86.8	0.01	440	595								
PS 92	-213.15	0.7	21.1	1.3	16.5	1.4	147.8	149.3	0.01	443	699	-25.9	-26.5	-27.0	-24.7	-26.8	-27.2	-27.1	-26.9
PS 91	-214.15	0.1	23.2	0.9	27.0	3.5	130.3	133.8	0.03	443	561								
PS 90	-215.15	0.0	21.4	0.9	23.5	2.9	131.3	134.2	0.02	442	613	-26.2	-26.3	-27.1	-25.1	-27.0	-27.5	-26.8	-27.2
PS 89	-216.15	0.5	10.5	0.7	15.3	1.5	34.1	35.6	0.03	436	516								
PS 88	-217.15	0.6	21.6	0.8	26.9	2.6	145.0	147.6	0.02	441	672	-26.0	-27.2	-26.8	-25.4	-27.3	-27.3	-26.7	-27.4
PS 87	-219.15	0.4	16.5	0.6	27.0	1.5	99.3	101.1	0.02	441	601								
PS 86	-220.15	0.0	15.9	0.6	27.0	1.9	94.8	96.7	0.02	442	632	-25.5	-26.8	-26.5	-24.6	-27.1	-27.1	-26.8	-27.1
PS 85	-221.15	0.6	20.3	0.8	25.1	1.5	119.9	121.5	0.01	443	591								
PS 84	-222.15	0.0	16.9	0.8	19.9	1.8	115.9	117.7	0.02	443	685	-25.4	-26.7	-26.9	-25.0	-27.0	-27.4	-27.3	-27.6
PS 83	-223.15	1.3	8.7	0.6	15.0	0.9	38.9	39.9	0.02	434	449								
PS 82	-224.15	0.2	13.7	0.6	22.2	1.2	91.3	92.4	0.01	445	665	-25.9	-26.1	-26.6	-24.3	-27.5	-27.5	-26.9	-27.3
PS 81	-225.15	0.6	11.6	0.5	23.0	1.1	73.0	74.1	0.02	441	629								
PS 75	-230.15	0.9	11.9	0.5	20.6	0.6	68.3	68.9	0.01	442	618								
PS 74	-231.15	0.1	10.7	0.6	18.0	1.1	57.7	58.8	0.02	440	540								
PS 73	-232.15	1.1	9.1	0.5	19.7	1.8	47.9	49.7	0.04	438	525	-26.0	-26.6	-26.4	-23.5	-27.1	-26.9	-27.8	-28.1
PS 72	-233.15	0.4	14.9	0.6	23.0	2.2	87.1	89.3	0.02	441	585								
PS 71	-234.15	0.6	8.3	0.4	21.2	1.0	46.1	47.2	0.02	439	558	-26.3	-27.0	-26.6	-25.7	-27.0	-27.2	-27.7	-27.9
PS 66	-236.15	0.9	11.2	0.5	22.2	1.3	66.2	67.5	0.02	441	593								
PS 65	-237.15	0.3	10.5	0.6	18.6	1.3	38.4	39.7	0.02	438	554	-26.0	-26.4	-26.5	-25.8	-26.8	-26.7	-28.4	-28.8
PS 64	-238.35	0.5	9.6	0.5	20.5	1.8	30.1	31.8	0.03	437	522								
PS 63	-239.35	0.4	13.6	0.6	22.1	2.2	76.5	78.8	0.03	440	563	-26.4	-26.5	-26.7	-26.0	-27.9	-27.1	-27.9	-28.5
PS 62	-240.35	0.1	19.3	0.8	23.9	2.9	114.7	117.6	0.02	439	594								
PS 61	-241.35	0.4	7.9	0.6	13.5	1.1	37.1	38.1	0.03	438	470	-26.6	-26.7	-27.3	-23.9	-27.1	-26.9	-28.8	-29.1
PS 46	-242.35	0.9	5.7	0.4	14.1	0.8	22.7	23.6	0.04	434	402	-27.3	-26.9	-27.8	-27.5	-28.1	-28.3	-30.7	-31.2
PS 45	-243.35	0.2	7.4	0.4	20.0	0.8	34.9	35.7	0.02	436	472								
PS 44	-244.35	0.0	3.9	0.2	17.7	0.5	14.7	15.2	0.03	436	376	-27.2	-27.2	-27.5	-27.7	-27.4	-27.9	-30.0	-30.4
PS 43	-245.35	0.1	7.8	0.4	21.6	0.8	42.2	43.0	0.02	437	543								
PS 42	-246.35	0.3	8.4	0.4	18.8	0.9	38.5	39.4	0.02	438	457	-27.4	-27.5	-27.7	-27.6	-27.5	-27.6	-30.2	-30.5
PS 41	-247.35	0.4	5.7	0.4	14.2	0.7	16.7	17.4	0.04	430	293								
PS 57	-250.35	0.4	6.0	0.4	16.1	0.8	22.9	23.7	0.03	433	378								
PS 56	-251.35	0.3	9.1	0.5	18.6	1.3	46.5	47.8	0.03	434	512	-26.5	-26.9	-27.0	-26.2	-27.3	-27.5	-29.2	-29.4
PS 55	-252.35	0.2	8.4	0.4	19.1	1.5	43.3	44.7	0.03	434	518								
PS 54	-253.35	0.3	8.7	0.5	17.8	0.6	45.7	46.4	0.01	435	524	-26.9	-27.3	-27.4	-26.7	-27.7	-28.0	-29.6	-29.7
Allgäu Formation - lower unit																			
PS 53	-254.35	0.5	3.2	0.3	9.4	0.2	5.1	5.2	0.04	433	160								
PS 52	-257.35	1.1	5.4	0.2	30.6	0.4	11.5	12.0	0.04	426	214	-27.6	-27.1	-28.3	-27.4	-28.1	-28.6	-30.3	-30.6
PS 51	-259.35	0.4	5.3	0.2	31.4	0.4	16.1	16.6	0.03	433	302								
PS 38	-262.35	0.3	4.7	0.2	21.9	0.4	11.3	11.8	0.03	430	242	-28.0	-27.8	-28.4	-27.8	-28.5	-28.6	-30.6	-30.9
PS 37	-263.35	0.1	5.9	0.2	29.1	0.4	16.4	16.9	0.03	429	280								
PS 36	-264.35	0.3	5.9	0.2	28.5	0.3	7.5	7.7	0.03	429	126	-28.2	-28.1	-28.3	-28.4	-28.6	-28.1	-30.3	-30.3
PS 35	-264.85	0.1	5.0	0.2	21.8	0.4	16.8	17.2	0.02	432	333								
PS 34	-265.35	0.0	5.8	0.3	17.1	0.5	18.0	18.5	0.03	432	312	-28.8	-28.4	-29.3	-28.1	-28.7	-28.7	-29.4	-29.6
PS 33	-265.69	0.0	9.4	0.3	32.4	1.0	32.3	33.3	0.03	429	343								
PS 32	-265.89	0.0	13.6	0.9	14.4	1.5	46.3	47.7	0.03	429	340	-26.6	-27.2	-27.3	-27.9	-27.6	-27.9	-29.7	-29.9

TIC: total inorganic carbon; TOC: total organic carbon; S: sulfur; S_1: free hydrocarbons; S_2: hydrocarbons generated during Rock Eval pyrolysis; S_1+S_2: generative potential; PI: production index; T_{max}: temperature with maximum hydrocarbon generation; HI: hydrogen index.

TOC contents in sediments overlying the coal seam are relatively high (up to 13.6 wt.%). The rest of the lower unit is characterized by moderate TOC contents varying between 3.2 and 5.9 wt.% (Fig. 7.4c). HI contents in the lower unit vary between 126 and 340 mgHC/gTOC and show a general upward decreasing trend (Fig. 7.4d). Samples from the lower unit plot inside the fields characteristic for type II and III kerogen in the HI versus T_{max} diagram (Fig. 7.6; Espitalié et al., 1984). The plot of S_2 versus TOC (Langford and Blanc-Valleron, 1990) suggests that the average "true" HI is about 400 mgHC/gTOC. This suggests the presence of kerogen type II in this unit (Fig. 7.6). T_{max} values are varying between 426 and 433°C in the lower unit (Fig. 7.4e). The observed values for the production index PI are generally low (<0.05). Sulfur contents are low as well (0.2-0.3 wt.%), with the exception of the lowermost sample (1.0 wt.%; Fig. 7.4f). These low sulfur contents result in high TOC/S ratios (9.4-32.4; Fig. 7.4g) despite of relative low TOC contents. High TOC/S ratios are typical for freshwater environments (Berner, 1984).

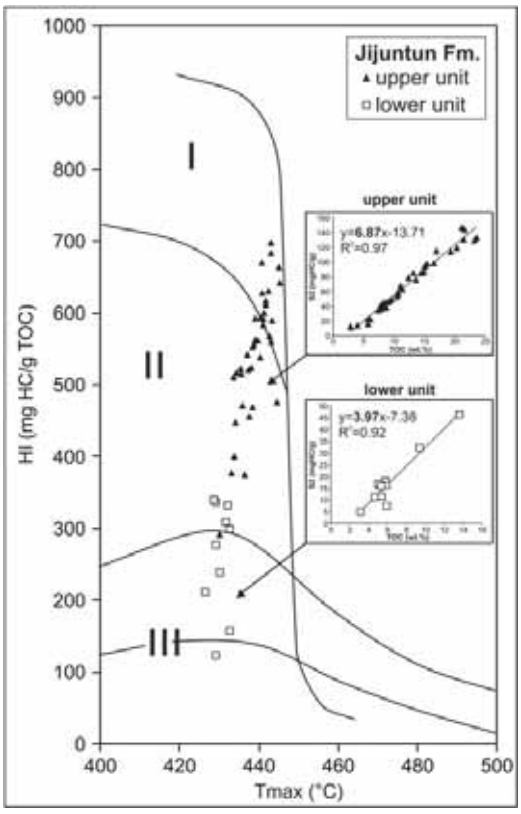

Fig. 7.6: Plot of HI vs. T_{max} [according to Espitalié et al. (1984)] outlining kerogen types of sediments from the Jijuntun Formation. S_2 vs. TOC correlations for the lower and upper unit of the Jijuntun Formation are shown as inserts [according to Langford and Blanc-Valleron (1990)]. The average "true" HI is indicated by the slope x 100 in the diagrams.

TOC contents in the upper unit vary between 2.8 and 23.6 wt.% and show an upward increasing trend, but decrease upward in the uppermost meter of the Jijuntun Formation (Fig. 7.4c). With the exception of a sample at -247 m depth (293 mgHC/gTOC), the HI is higher in the upper unit (378-699 mgHC/gTOC) than in the lower one and exhibits a general upward increasing trend (Fig. 7.4d). The dataset of the upper unit plots into the kerogen type I and II fields in Fig. 7.6. The average "true" HI of the upper unit is about 700 mgHC/gTOC suggesting the presence of kerogen type I (Fig. 7.6). T_{max} values between 430 and 445°C show a general upward increasing trend (Fig. 7.4e) suggesting that variations in type of organic matter rather than maturity affect the T_{max} versus depth trend (Peters, 1986). PI values are very low (0.01-0.04). Sulfur contents are generally below 1 wt.%, but increase near the top of the Jijuntun Formation to 3.2 wt.% at -212 m depth (Fig. 7.4f). Nevertheless TOC/S ratios remain high (5.6-27.0; Fig. 7.4g).

Sulfur contents show a good correlation (r^2=0.87) to the amount of pyrite within the whole Jijuntun Formation indicating that pyrite is the major source of sulfur. The position of the samples in the Fe-TOC-S ternary diagram (Dean and Arthur, 1989; Fig. 7.7) indicates sulfur limitation of pyrite formation due to freshwater conditions (Berner, 1984). As mentioned above, siderite is the main Fe source.

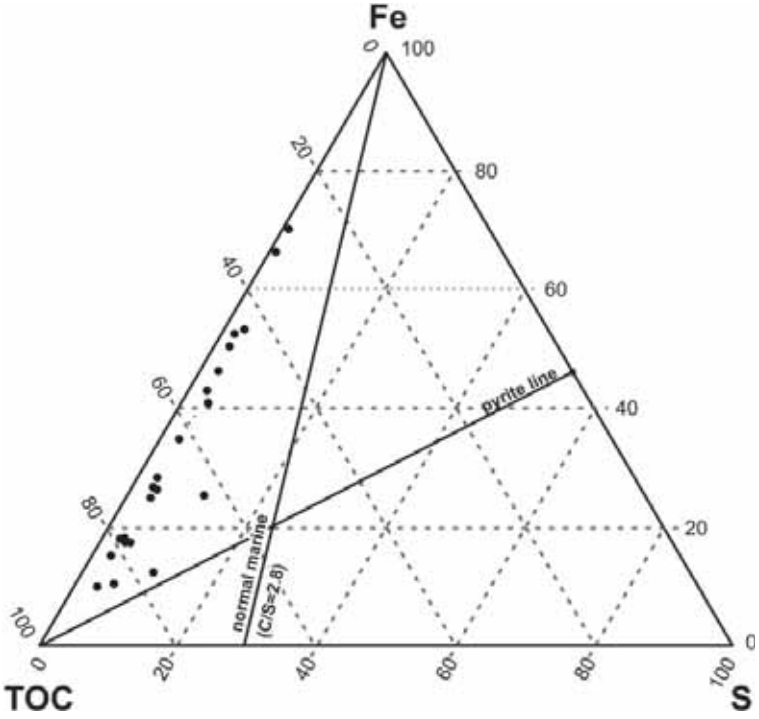

Fig. 7.7: Fe-TOC-S ternary diagram for sediments from the Jijuntun and Xilutian formations [according to Dean and Arthur (1989)].

In contrast to the samples from the Jijuntun Formation, the two samples from the overlying Xilutian Formation show very low TOC contents (<0.1 wt.%; Fig. 7.4c).

7.4.3 Organic petrography

The vertical variability of terrigenous organic matter, lamalginite and telalginite (in vol.%) on a mineral matter free (mmf) basis (Tab. 7.1) is plotted in Fig. 7.8a.

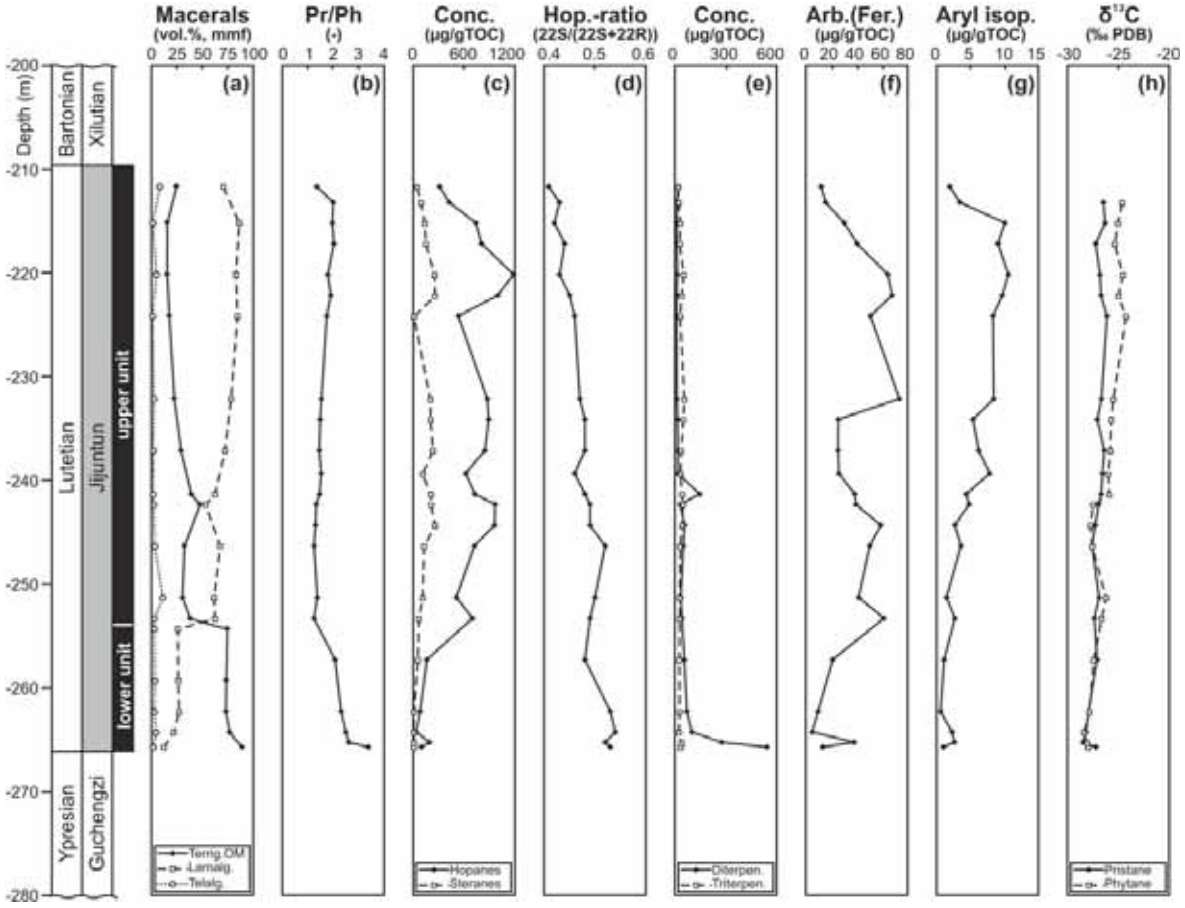

Fig. 7.8: Distribution of (a) macerals (terrigenous organic matter OM, lamalginite, telalginite), (b) pristane/phytane ratios, (c) hopane and sterane concentrations, (d) (22S/(22S+22R))-hopane ratios, (e) diterpenoid and triterpenoid concentrations, (f) arborane or fernane derivatives concentrations, (g) aryl isoprenoid concentrations, and (h) $\delta^{13}C$ for pristane and phytane within the Jijuntun Formation.

Significant amounts of terrigenous organic matter (OM) (73-88 vol.%; sum of vitrinite, inertinite, resinite and sporinite) occur in the lower unit of the Jijuntun Formation overlying the coal seam of the Guchengzi Formation (Fig. 7.9a and Fig. 7.9b). Vitrinite and sporinite are the predominant landplant derived macerals within this unit. Typically, vitrinite particles are small. The lowermost sample of the Jijuntun

Formation (-266 m) shows a vitrinite reflectance of 0.50%R_r (standard deviation: 0.0080), which fits well with values from the underlying coal seam (0.51%R_r; Strobl et al., 2013).

In the upper unit of the Jijuntun Formation, lamalginite is the most abundant maceral (52-85 vol.%). Lamalginite may originate from assemblages of algae and bacteria. Telalginite occurs in minor amounts (<10 vol.%) within the entire Jijuntun Formation (Fig. 7.9c, Fig. 7.9d, Fig. 7.9e and Fig. 7.9f). Typically, telalginite is characterized by a greenish flurorescence color, whereas lamalginite displays yellow to orange colors. The sample at -212 m depth yields a value of 0.34%R_r (standard deviation: 0.0141). However, vitrinite reflectance from this sample might be suppressed by bitumen impregnations (e.g. Carr, 2000).

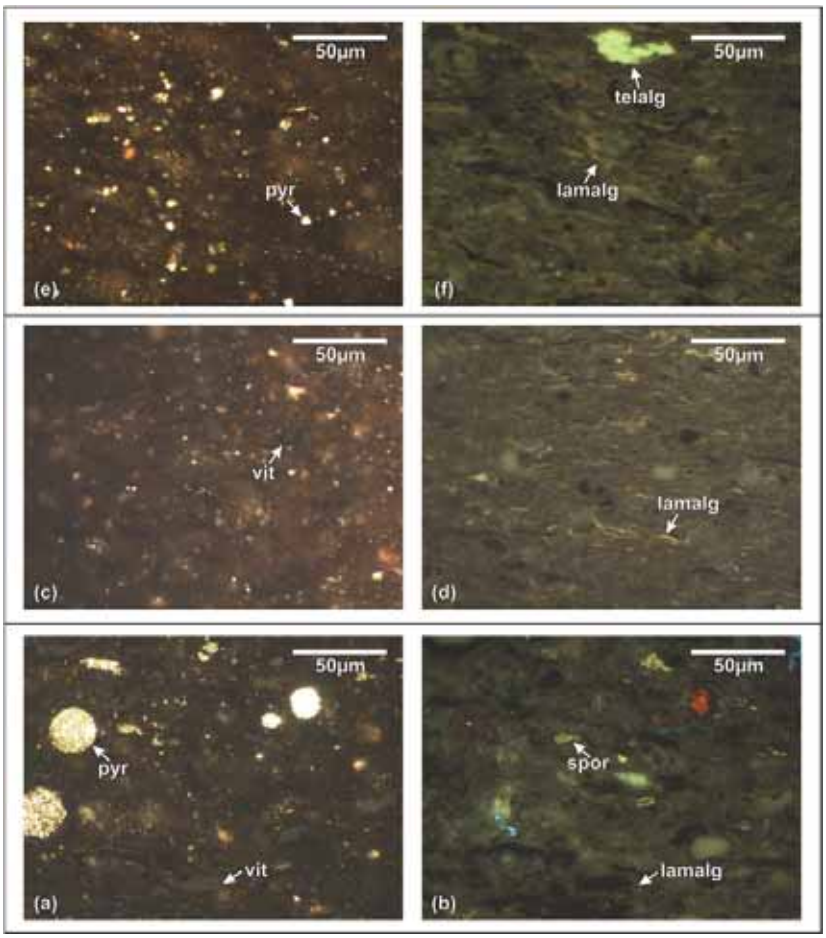

Fig. 7.9: Microphotographs of Jijuntun Formation (a) lower unit (FS 32) under white light, (b) lower unit (FS 32) under UV light, (c) upper unit (FS 65) under white light and (d) upper unit (FS 65) under UV light, (e) upper unit (FS 94) under white light and (f) upper unit (FS 94) under UV light. *Abbreviations:* vit, vitrinite; pyr, pyrite; spor, sporinite; lamalg, lamalginite; telalg, telalginite.

7.4.4 Organic geochemistry

Tab. 7.3: Data from biomarker analysis.

Sample	Depth	EOM	Sat. HC	Aro. HC	NSO	Asphalt.	α-C_{27}-n-alk.	α-C_{29}-n-alk.	α-C_{31}-n-alk.	CPI	Pr/Ph	Steranes	Hopanes	S/(S+R) hopanes	C_{30} Methyl-hopane	Steroid/ hopanoid	Diterpenoids	Triterpenoids	Benzo-hopanes	Ads/(Ads+Lam)-derriv.	Aryl-isoprenoids	MTTCs	MTTC ratio
	[m]	[mg/gTOC]	[%a]	[%a]	[%]	[%a]						[µg/gTOC]	[µg/gTOC]		[µg/gTOC]		[µg/gTOC]	[µg/gTOC]	[µg/gTOC]	[µg/gTOC]	[µg/gTOC]	[µg/gTOC]	
Ajamian Formation - upper unit																							
FK94	-211.65	11	21	13	37	9	0.00	0.05	0.03	1.87	1.4	34	307	0.48	24	0.1	9	4	13	12	2	2	0.74
FK92	-213.35	13	27	11	56	6	0.06	0.26	0.53	2.16	2.0	83	420	0.43	19	0.2	1	9	12	16	3	2	0.77
FK90	-215.15	25	35	12	44	9	0.23	0.30	0.34	2.03	2.0	129	737	0.42	30	0.2	6	18	20	39	10	5	0.83
FK88	-217.35	28	33	10	53	4	0.22	0.30	0.35	2.08	2.0	142	803	0.44	38	0.2	6	15	26	48	9	3	0.83
FK86	-220.15	31	39	14	39	8	0.16	0.25	0.42	2.14	1.8	245	1193	0.43	62	0.2	7	36	53	64	10	5	0.82
FK84	-222.15	32	37	9	50	4	0.14	0.27	0.44	2.13	1.9	249	996	0.45	45	0.2	6	26	38	67	10	5	0.84
FK82	-224.15	27	38	11	48	3	0.19	0.29	0.39	2.14	1.7	0	528	0.46	32	0.0	0	17	26	51	8	3	0.82
FK71	-232.15	56	37	10	49	4	0.16	0.24	0.45	2.08	1.5	194	871	0.47	44	0.2	6	41	52	73	8	4	0.81
FK71	-234.15	29	44	15	39	4	0.19	0.27	0.39	1.96	1.5	197	868	0.48	37	0.2	4	35	38	56	5	4	0.84
FK65	-237.15	27	51	13	32	5	0.17	0.27	0.42	1.96	1.5	224	844	0.49	42	0.3	5	22	31	45	6	5	0.86
FK63	-239.35	21	55	14	29	2	0.19	0.26	0.43	2.00	1.5	103	656	0.46	19	0.2	5	20	21	26	8	5	0.78
FK61	-241.35	21	56	16	25	3	0.14	0.25	0.47	2.06	1.5	202	724	0.48	24	0.3	134	29	34	38	4	4	0.79
FK48	-302.35	34	39	17	42	2	0.18	0.30	0.38	1.79	1.3	203	964	0.49	31	0.2	19	33	32	39	5	3	0.80
FK44	-304.35	26	43	18	37	3	0.15	0.30	0.40	1.84	1.3	250	958	0.49	37	0.3	44	30	32	59	4	4	0.84
FK42	-306.35	21	32	19	46	3	0.16	0.27	0.42	1.83	1.5	120	779	0.52	56	0.2	37	17	49	58	4	2	0.83
FK56	-251.35	18	40	17	42	2	0.21	0.30	0.35	1.83	1.4	103	585	0.50	30	0.2	25	15	33	42	2	2	0.84
FK54	-253.35	13	25	24	49	3	0.09	0.25	0.32	1.88	1.3	54	686	0.49	25	0.1	30	15	43	43	3	2	0.83
Ajamian Formation - lower unit																							
FK52	-257.35	8	36	29	33	3	0.19	0.31	0.36	2.06	2.1	45	196	0.49	7	0.3	44	15	36	21	1	1	0.56
FK50	-262.35	9	37	25	29	9	0.22	0.31	0.34	2.13	2.3	0	77	0.53	5	0.0	56	14	15	18	1	1	
FK36	-264.35	4	21	20	43	14	0.14	0.36	0.36	1.87	2.5	0	26	0.54	2	0.0	88	10	4	5	2		
FK34	-265.35	22	30	22	43	5	0.25	0.31	0.31	2.07	2.6	0	189	0.52	17	0.0	264	26	31	36	3		
FK32	-265.80	13	23	29	48	8	0.16	0.32	0.37	2.21	3.3	0	91	0.53	7	0.0	930	21	13	14	1		

EOM: extractable organic matter; Sat. HC: saturated hydrocarbons; Aro. HC: aromatic hydrocarbons; Asphalt.: asphaltenes; CPI: carbon preference index; Pr/Ph: pristane/phytane ratio; S/(S+R) hopanes: 22S/(22S+22R) C-31 hopane ratio; Ads/(Ads+Lam.)-derriv.: adriane or lupane derivatives; MTTCs: methyltrimethyltridecylchromans.

Within the Jijuntun Formation, the amount of the extractable organic matter (EOM) varies between 4 and 56 mg/g TOC (average 22 mg/gTOC). The proportion of hydrocarbons is high (34-72% of EOM). Saturated hydrocarbons (average 36% of EOM) are predominant over aromatic hydrocarbons (average 17% of EOM). The EOM is also composed of NSO compounds (average 42% of EOM) and asphaltenes (average 5% of EOM; Tab. 7.3).

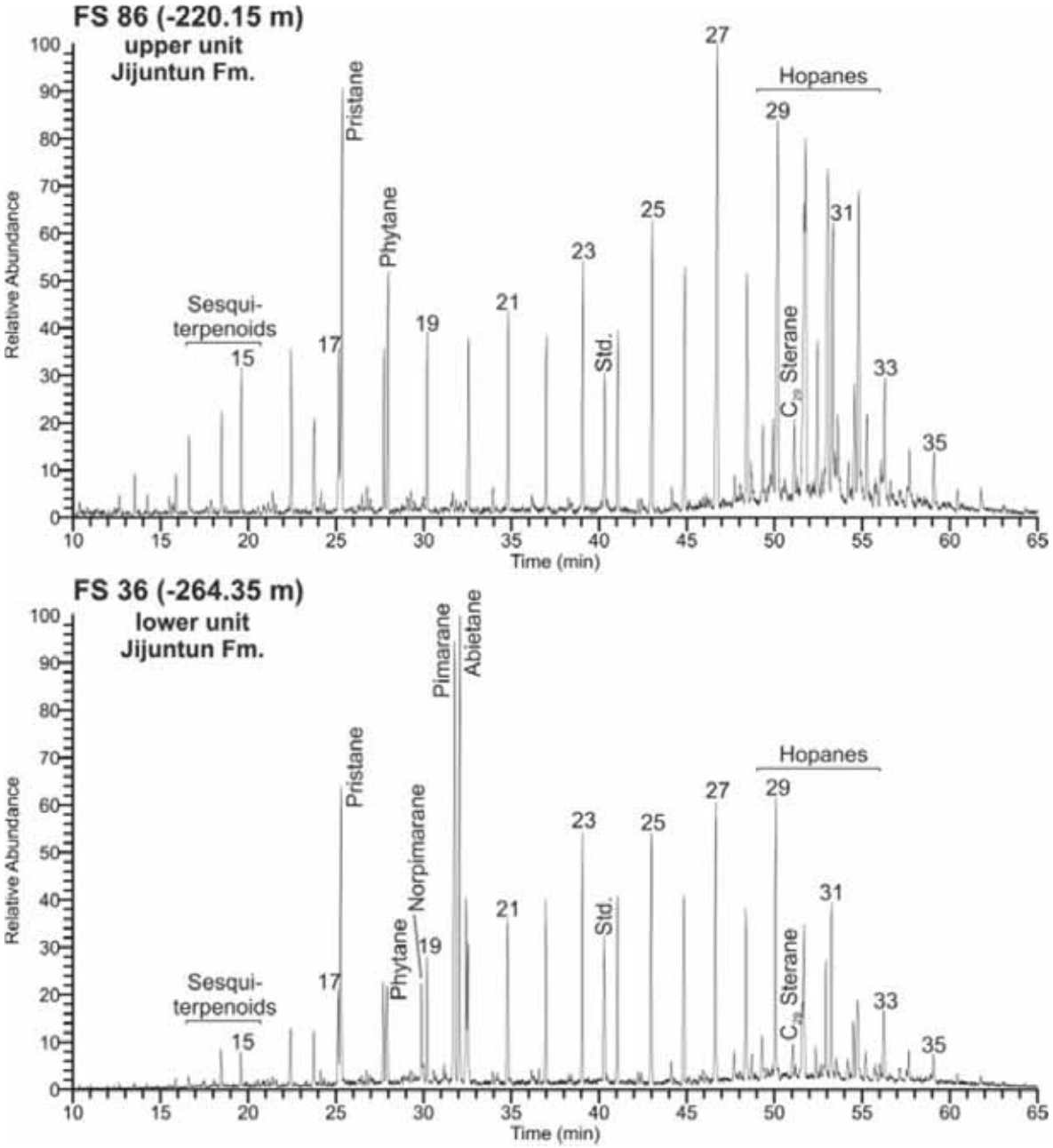

Fig. 7.10: Gas chromatograms (TICs) of saturated hydrocarbon fractions of samples from the lower and the upper unit of the Jijuntun Formation. *n*-Alkanes are labeled according to their carbon number. Std., standard (deuteriated *n*-tetracosane).

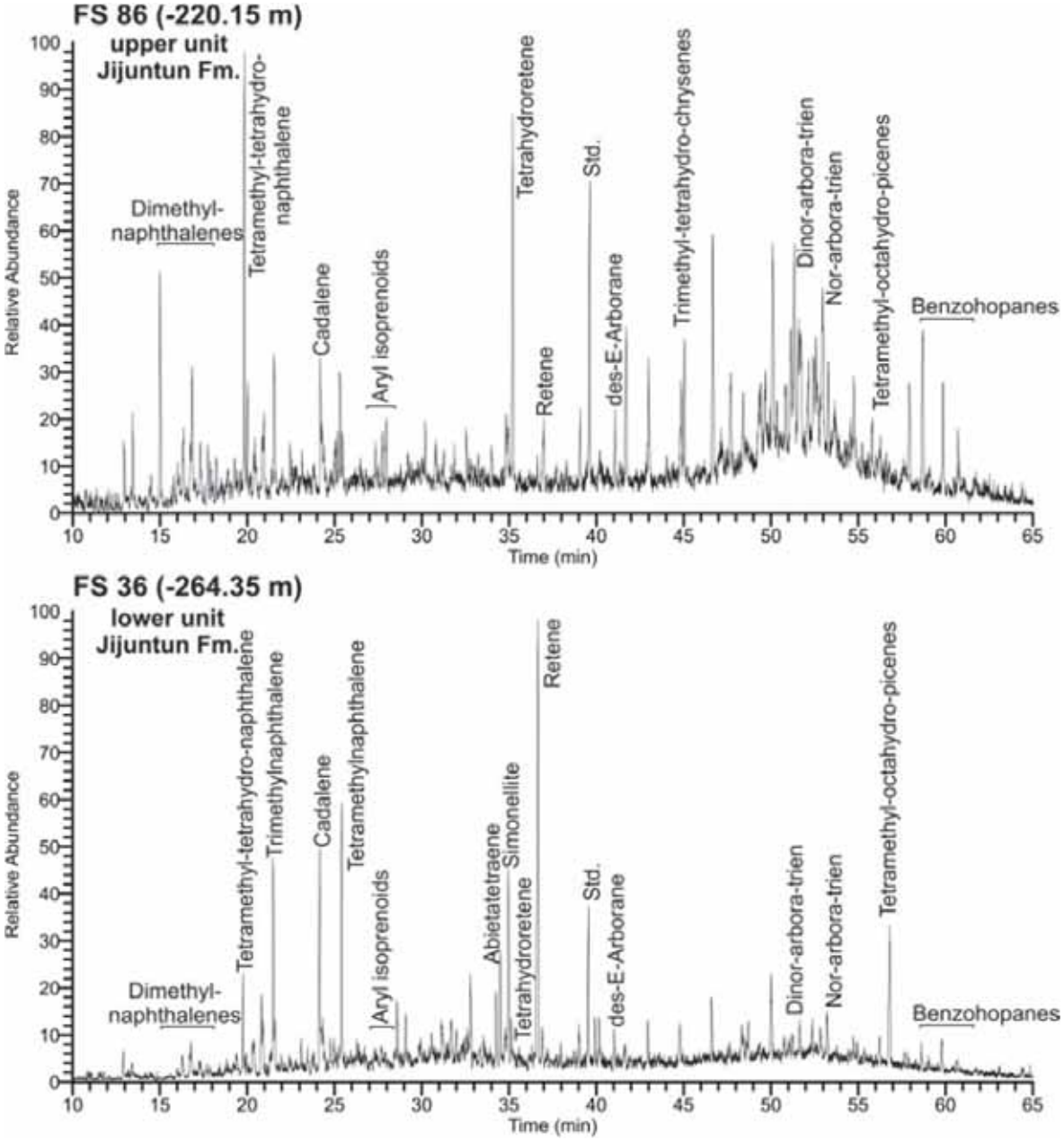

Fig. 7.11: Gas chromatograms (TICs) of aromatic hydrocarbon fractions of samples from the lower and the upper unit of the Jijuntun Formation. Std., standard (1,1´-binaphthyl).

Total ion chromatograms (TICs) of alkane and aromatic hydrocarbon fractions of representative samples from the lower and the upper units of the Jijuntun Formation are shown in Fig. 7.10 and Fig. 7.11, respectively. The concentrations and concentration ratios of compounds and compound groups in hydrocarbon fractions are listed in Tab. 7.3.

Sediments of both units are dominated by *n*-alkanes of intermediate (*n*-C_{21-25}) and long (*n*-C_{27-31}) chain length with an odd to even predominance. The carbon preference index (CPI; Bray and Evans, 1961) varies between 1.78 and 2.21.

The acyclic isoprenoids pristane (Pr) and phytane (Ph) are present in all samples. The Pr/Ph values are relative high (1.3-3.4) within the Jijuntun Formation. They decrease upward within the lower unit, reach a minimum at the boundary between the lower and upper units and, with exception of the uppermost sample, increase upward in the upper unit (Fig. 7.8b). The pristane/phytane (Pr/Ph) ratio is generally considered as a redox parameter (Didyk, 1978). Pr/Ph ratios between 1.0 and 3.0 have been proposed to indicate dysoxic conditions during early diagenesis. However, Pr/Ph ratios are known to be also affected by maturation (Tissot and Welte, 1984) and by differences in the precursors for acyclic isoprenoids (bacterial origin; Goossens et al., 1984; Volkman and Maxwell, 1986, ten Haven et al., 1987). In the present case, an influence of thermal stress on Pr/Ph ratios is unlikely, but different precursors for Pr and Ph have to be taken into account (see section 2.4.5).

Steranes are absent in the lowermost 5 m of the Jijuntun Formation (Fig. 7.8c) and are present in low amounts (45-250 µg/gTOC) above -257 m. C_{29} steranes, typically derived from vascular plants (Volkman, 1986) or freshwater microalgae (e.g. Volkman et al., 1999; Kodner et al. 2008), predominate. C_{29} steranes originate from algae rather than from vascular plants in the upper unit, because of their absence in the lowermost part of the Jijuntun Formation, which is overlying the coal seam and therefore influenced by terrigenous organic matter.

The hopanoid patterns are characterized by 17α, 21β and 17β, 21α hopanes from C_{27} to C_{32}, with C_{28} hopanes absent. The predominant hopanoid in all samples is the 17α, 21β-C_{30} hopane. The ratio of the 22S to 22S plus 22R isomers of the 17α, 21β-C_{31} hopanes increases downward from 0.41 to 0.54 (Fig. 7.8d) indicating vitrinite reflectance in the order of 0.4 to 0.5% (Peters et al., 2005). Hopanes occur in a relative low amount (28-156 µg/gTOC) in the lower unit and in a high amount (307-1183 µg/gTOC) in the upper unit of the Jijuntun Formation (Fig. 7.8c). The abundance of hopanes indicates an input from bacterial biomass (Ourisson et al., 1979; Rohmer et al., 1984). The occurrence of the 2α-methylhopane (2-62 µg/gTOC), derived from cyanobacteria (Summons et al., 1999; Farrimond et al., 2004), shows a parallel trend

to the hopane distribution. The 2α-methylhopane index (ratio of 2α-methylhopanes to sum of 2α-methylhopanes and hopanes) ranges between 0.03 and 0.08. These relative low values indicate low maturity (Summons and Jahnke, 1992; Tian et al., 2013) and a non-carbonate/evaporite environment (Summons et al., 1999). 3β-methylhopane, representing methanotrophic bacterial activity (Farrimond et al., 2004), was not detected.

The low sterane and the high hopane concentration result in a low steroid/hopanoid ratio (<0.3). According to Mackenzie (1984), a low value is typical for lacustrine or special bacteria-influenced facies.

Diterpenoids (e.g. pimarane, abietane, simonellite, retene) occur in relative high amounts (up to 530 µg/gTOC) within the lower unit of the Jijuntun Formation and show a decreasing upward trend. Within the upper unit they are generally rare (Fig. 7.8e). Sesquiterpenoids (e.g. eudesmane, homodrimane, cadalene) are present in all samples (1-381 µg/gTOC) and show their maximum concentration in the lowermost samples. Diterpenoids and sesquiterpenoids indicate a contribution of conifer species (e.g. Otto et al., 1997; Otto and Wilde, 2001). Aromatic non-hopanoid triterpenoids (trimethyl-tetrahydro-chrysenes, tetramethyl-octahydro-picenes) occur in relative low concentrations (6-41 µg/gTOC) throughout the whole Jijuntun Formation (Fig. 7.8e). These triterpenoids originate from angiosperms (Karrer et al., 1977; Dev, 1989).

Benzohopanes are abundant in all samples and vary between 4 and 53 µg/gTOC. These compounds are formed from bacterial precursors (Hussler et al., 1984).

The concentrations of arborane or fernane derivatives vary between 5 and 73 µg/gTOC (Fig. 7.8f). These derivatives originate either from higher landplants or bacteria (Hauke et al., 1992). A positive correlation between arborane or fernane derivatives and hopanoids (r^2=0.53) and low concentrations of arborane or fernane derivatives in the lower part dominated by terrigenous organic matter input support a bacterial origin.

C_{13} and C_{14} aryl isoprenoids were detected in all samples (1-10 µg/gTOC), but their concentration is significantly increased in the upper part of the Jijuntun Formation

(Fig. 7.8g). Aryl isoprenoids originate from photosynthetic green sulfur bacteria and, therefore, indicate photic zone anoxia (Summons and Powell, 1987).

Methylated 2-methyl-2-(trimethyltridecyl)chromans (MTTCs) occur in very low amounts (1-8 µg/gTOC) and are absent in the three lowermost samples. The trimethylated MTTC predominates over the dimethylated and the monomethylated MTTC. Methylated MTTCs have been widely used for paleosalinity reconstruction (Sinninghe Damsté et al., 1993; Barakat and Rullkötter, 1997). The MTTC ratio is defined as the concentration of trimethylated MTTC relative to the sum of methylated MTTCs (Sinninghe Damsté et al., 1987). The MTTC ratio varies in the narrow range between 0.74 and 0.86 consistent with a freshwater environment.

7.4.5 Compound-specific stable isotope geochemistry

The carbon isotopic composition of short-chain and long-chain *n*-alkanes, pristane and phytane of 10 selected samples from the Jijuntun Formation is plotted in Fig. 7.12. The measured data from all samples are listed in Tab. 7.2.

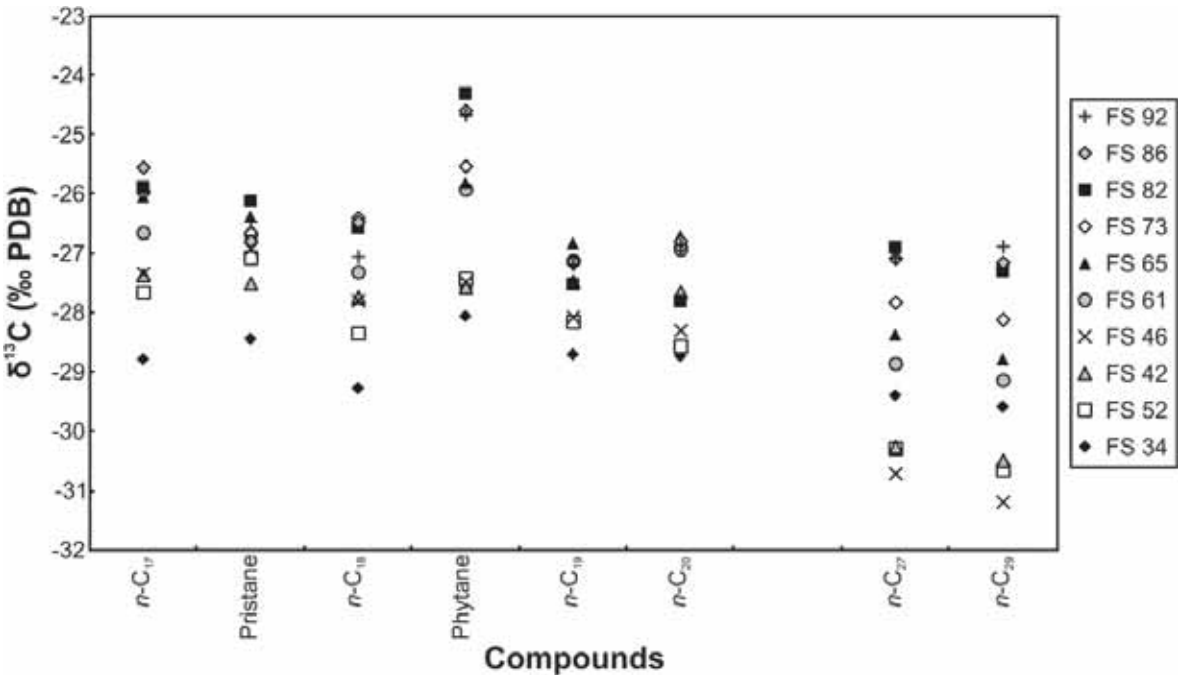

Fig. 7.12: Carbon isotopic composition of selected compounds in saturated hydrocarbon fractions of selected samples from the Jijuntun Formation.

The $\delta^{13}C$ values for the *n*-C_{17} to *n*-C_{20} alkanes (-25 to -29 ‰) show a decrease of about 1 ‰ with increasing chain length. Short-chain even *n*-alkanes are slightly

depleted in ^{13}C compared to the neighbouring odd *n*-alkanes. The *n*-C_{27} and *n*-C_{29} alkanes of samples below -242 m are more depleted in ^{13}C (ca. 2 ‰) than the short chain *n*-alkanes, whereas lower differences are obtained from the shallow samples. The results argue for a higher contribution of terrigenous organic matter in the deeper part of the succession (i.e. C_3 plants; O'Leary, 1988; Farquhar et al., 1989; Collister et al., 1994; Murray et al., 1994). The *n*-alkanes are more enriched in ^{13}C in shallow samples (above -242 m) than in deep samples.

Almost identical values of ^{13}C for the acyclic isoprenoids pristane and phytane are observed in the lower part (up to -242 m). This fact argues for a similar precursor (i.e. chlorophyll; Didyk et al., 1978; Goosens et al., 1984). Phytane is enriched in ^{13}C compared to pristane in the upper part (Fig. 7.8h). Hence, a second source for phytane is likely (Joachimsky et al., 2001) and the Pr/Ph ratio cannot be used as a redox proxy in the upper unit of the Jijuntun Formation. Archaea (fermentative and chemoautotrophic) can be excluded as sources for phytane, because of the lack of ^{13}C-depleted phytane (Thiel et al., 1999; Pancost and Sinninghe Damsté, 2003). Furthermore, recent studies provide evidence that phytol can be biosynthesized via two different pathways using different precursors, one of these pathways is thought to be widespread in bacteria (Schouten et al., 2008).

7.5 Discussion

7.5.1 Maturity

Although vitrinite reflectance from a sample from the upper unit of the Jijuntun Formation might be suppressed, vitrinite reflectance from the lower unit and from the underlying coal seam proves low maturity. This result fits well with low PI and T_{max} values in the Jijuntun Formation indicating that the sediments are immature. A continuous downward increase in maturity is reflected by the (22S/(22S+22R))-hopane ratio (Fig. 7.8d). In contrast, T_{max} values decrease downward (Fig. 7.4e). Whereas T_{max} is in the range of 430-445°C in the upper unit of the Jijuntun Formation dominated by type I kerogen, it is in the range of 426-433°C in the lower unit of the Jijuntun Formation dominated by type II kerogen. This shows that facies strongly

affects T_{max} and that T_{max} of type I kerogen in immature sediments is higher than that of kerogen type II and III (Espitalié et al., 1985).

7.5.2 Depositional environment and organic matter accumulation

Cartoons illustrating the depositional environment of the lower and upper unit of the Jijuntun Formation are shown in Fig. 7.13. A schematic sketch of the depositional environment of the upper part of the coal-bearing Guchengzi Formation in a low lying mire, indicated by high ash yields (Johnson, 1990), is added to show the initial stage before the onset of oil shale deposition.

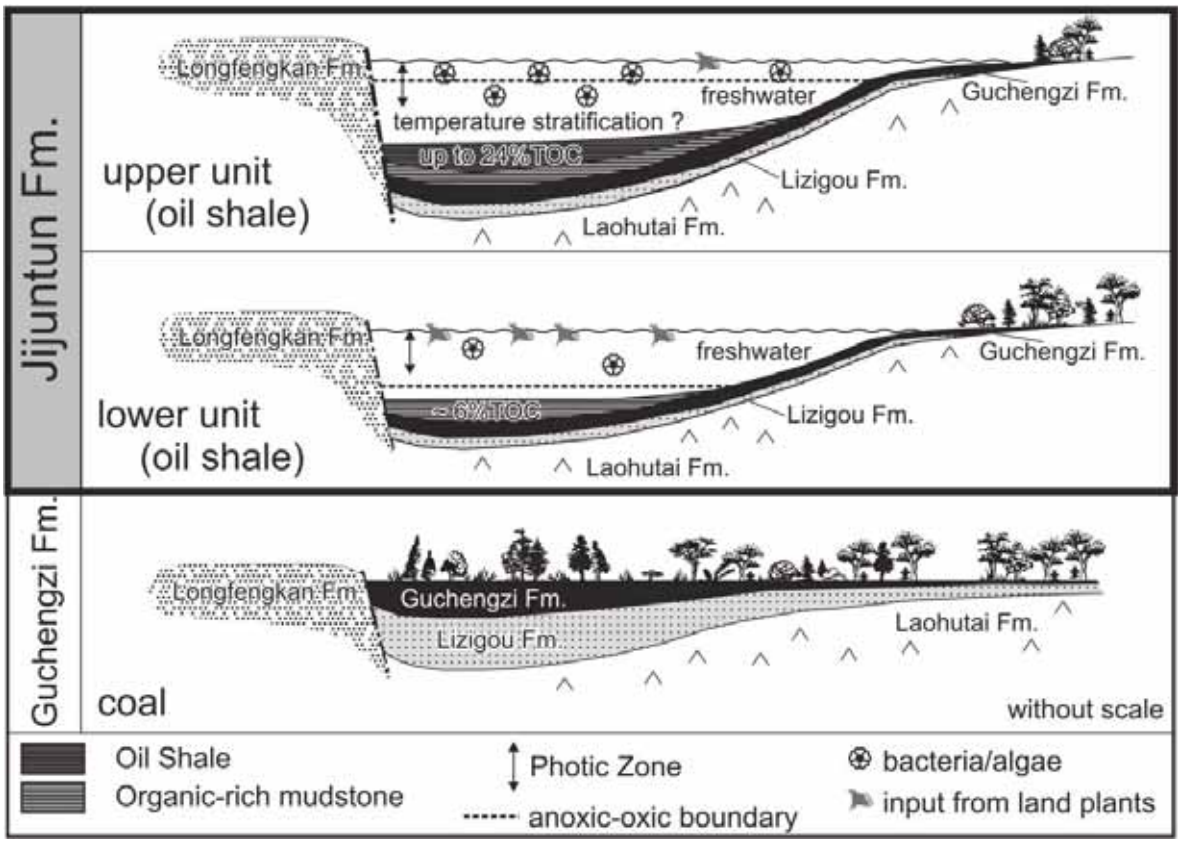

Fig. 7.13: Cartoon illustrating the depositional environment of the Jijuntun Formation and the underlying Guchengzi Formation.

7.5.2.1 Jijuntun Formation – Lower Unit

The onset of oil shale deposition reflects drowning of a low-lying mire, probably due to high subsidence rates, typical for fault-controlled basins (Gruber and Sachsenhofer, 2001). High TOC/S ratios indicate a freshwater environment during the deposition of the Jijuntun Formation (Fig. 7.4g). This interpretation is also supported by the

absence of gammacerane and the fact that MTTCs occur in very low amounts. Because of sulfur limitation in the freshwater environment, siderite is the main Fe-bearing mineral (Fig. 7.7). Pyrite, typically occurring as framboids, is rare.

The lower unit is characterized by high contents in kaolinite and low contents in mixed layer minerals (Fig. 7.4b). Following the argumentation of Meng et al. (2012), this indicates a humid warm climate. This interpretation agrees with Quan et al. (2012), who suggested that the upper part of the underlying coal seam (Guchengzi Formation) accumulated during the Early Eocene Climatic Optimum.

The high TOC contents in the lowermost part of the lower unit of the Jijuntun Formation and the upward decreasing trend reflect a decrease in input of landplant material after the deposition of the coal of the underlying Guchengzi Formation (Fig. 7.4c). The "true" HI of 400 mgHC/gTOC (Fig. 7.6) shows that – compared to the upper unit – the lower unit contains a relative hydrogen-poor type II kerogen, whereat abundant vitrinite may cause deviation towards lower HI. A high amount of landplant derived macerals (Fig. 7.8a; sporinite, resinite, vitrinite, inertinite) is reflected by the biomarker composition. The abundance of diterpenoids and sequiterpenoids (Fig. 7.8e) suggests that the terrigenous organic matter is dominated by conifers rather than by angiosperms. The upward decrease of Pr/Ph ratios reflects decreasing percentages of coaly material characterized by high Pr/Ph ratios (Fig. 7.8b).

Minor bacterial biomass is reflected by the presence of hopanes (Fig. 7.8c) and arborane or fernane derivatives (Fig. 7.8f).

7.5.2.2 Jijuntun Formation – Upper Unit

TOC/S ratios (Fig. 7.4g) and biomarker data (MTTCs, gammacerane) prove that freshwater conditions continued during deposition of the upper unit of the Jijuntun Formation. Partly high sulfur contents in the uppermost part of the Jijuntun Formation (Fig. 7.4f) and gradually decreasing TOC/S ratios in the uppermost 4 m (Fig. 7.4g) may reflect a trend towards slightly increased salinity. However, even the lowermost TOC/S ratios (5-7) prove that freshwater conditions prevailed (Fig. 7.4g). In general, siderite is the main Fe-bearing mineral, but pyrite occurs in slightly higher amounts in the upper than in the lower unit. Only in the uppermost samples pyrite

percentages exceed those of siderite (Fig. 7.4b) arguing for increased availability of sulfur. Pyrite typically occurs as euhedras, which are smaller than the framboids in the lower unit. We speculate that the euhedras represent re-crystallized small framboids, which formed in an anoxic water column (Wignall and Newton, 1998).

A continuous decrease in kaolinite and enhanced percentages of mixed layer minerals (Fig. 7.4b) may reflect a cooling trend following the Early Eocene Climatic Optimum (see also Quan et al., 2012).

Very high TOC contents (Fig. 7.4c) and a "true" HI of 700 mg/gTOC (Fig. 7.6) indicate the presence of kerogen type I, typical for lacustrine algal material. The most abundant maceral in the upper unit is lamalginite which is formed by algae and remains of bacteria. Terrigenous organic matter occurs very rarely (Fig. 7.8a). Bacterial biomass is also indicated by high amounts of hopanes (Fig. 7.8c), low steroid/hopanoid ratios, the occurrence of benzohopanes, and by arborane or fernane derivatives. It has been discussed above, that in the present case also C_{29} steranes are considered to originate from algae rather than from landplants.

The presence of C_{13} and C_{14} aryl isoprenoids points to photic zone anoxia. The concentration of aryl isoprenoids increases upward and reaches a maximum between -232 and -215 m depth. The amount of aryl isoprenoids (Fig. 7.8g) correlates with the amount of smectite (Fig. 7.4b). Middle Eocene volcanic events are well documented in NE China (Zhang et al., 2007; Wang et al., 2008). Because smectite (Fig. 7.4b) may reflect volcanic activity, we speculate that the volcanic activity may have fertilized the lake supporting bioproductivity. Thus Photic zone anoxia (Fig. 7.8g) may be a result of high bioproductivity and a stratified water body. In the absence of any indications for enhanced salinity, temperature stratification in a relative deep lake is likely. As discussed, the Pr/Ph ratio is not a reliable redox parameter in the upper unit of the Jijuntun Formation.

Photic zone anoxia (Fig. 7.8g) decreased during deposition of the uppermost part of the Jijuntun Formation. At the same time TOC (Fig. 7.4c) contents decrease drastically. HI values (Fig. 7.4d), which remain high (>450 mgHC/gTOC), suggest that this is primarily due to a decrease in productivity rather than due to enhanced degradation of organic matter.

7.5.2.3 Xilutian Formation

Dolomite layers in the Xilutian Formation (Fig. 7.4b) reflect the transition to a carbonate-rich shallow water environment. According to Meng et al. (2012), the Xilutian Formation has been deposited in a hot, arid climate resulting in a brackish water body. This interpretation agrees with deposition during an Eocene warming event, postulated by Quan et al. (2012).

7.5.3 Oil Shale Potential

Fushun Mining Group distinguishes a low quality oil shale (about 10.0 wt.% TOC; oil yield <4.7 wt.%) and a high quality oil shale (<20.0 wt.% TOC; oil yield >4.7 wt.%; Liu et al., 2009). This classification agrees with our subdivision of the Jijuntun Formation into a lower and an upper unit.

In the lower unit the oil shale is characterized by an average TOC content of 6.4 wt.%. Using the nomenclature of Peters (1986), the generative potential S_1+S_2 (5-48 mgHC/g) is good to very good (Fig. 7.14). Sediments within this unit contain the oil-prone kerogen type II ("true" HI 400 mgHC/gTOC). The Source Potential Index (SPI = $[S_1+S_2]*h*\rho/1000$, where h is thickness and ρ is bulk density; Demaison and Huizinga, 1994) has been calculated in order to quantify the amount of hydrocarbons, which can be generated from the lower unit beneath 1 m^2 surface area. The density has been defined using a correlation of density and TOC data for oil shales in NE China (e.g. Songliao and Huadian basins; Sun et al., 2013b). Considering a density of 2.2 t/m^3, the SPI in the lower unit is only 0.47 tHC/m^2.

The average TOC content in the upper unit is 12.2 wt.%, with the highest TOC content (23.6 wt.%) occurring in the uppermost part of the upper unit. The generative potential (13-149 mgHC/g) is very good to excellent in the upper unit (Fig. 7.14). The "true" HI of 700 mg/gTOC reflects the presence of the high-oil-prone kerogen type I. Considering a density of 2.1 t/m^3 for the upper unit, the SPI shows a significant higher value (6.51 tHC/m^2) than for the lower unit.

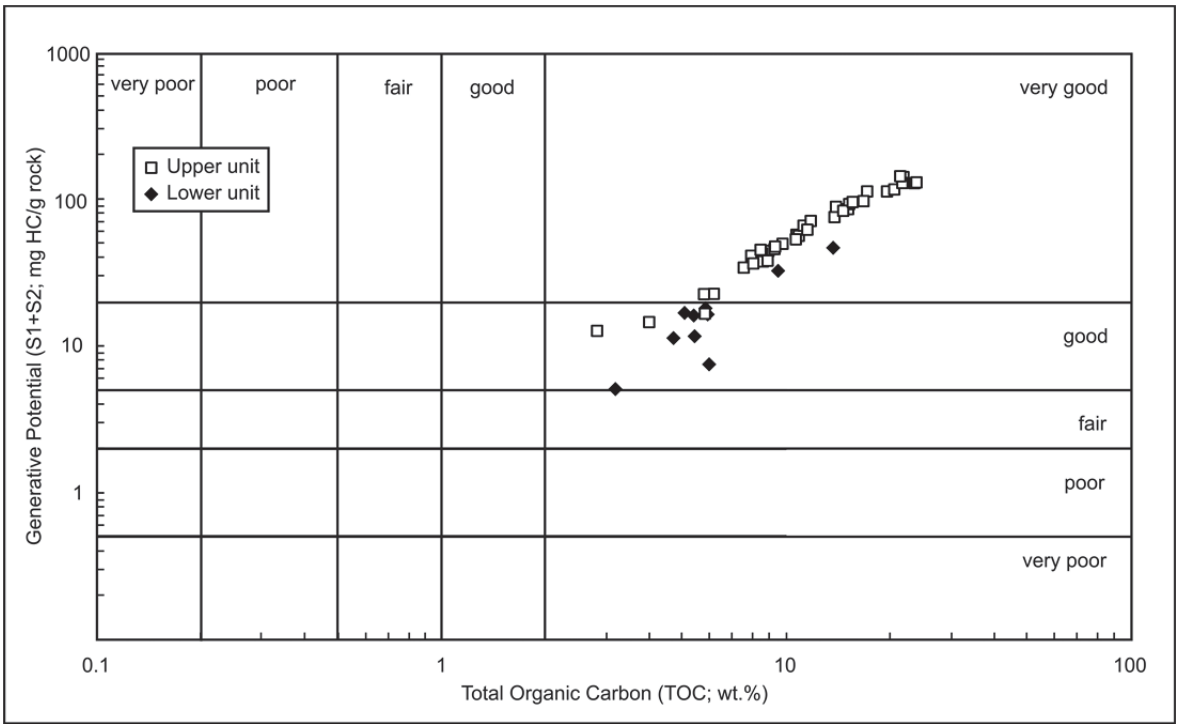

Fig. 7.14: Plot of Generative Potential (S_1+S_2) vs. Total Organic Carbon content (TOC) for the lower and upper unit of the Jijuntun Formation.

7.6 Summary

- The oil shale-bearing Eocene Jijuntun Formation in the Fushun Basin was deposited in a tectonically controlled freshwater lake, which originated after drowning of a swamp.
- A single thick oil shale layer is present in the Fushun Basin. In contrast, a high number of thin oil shale layers are present in the neighboring, coeval Huadian Basin (Sun et al., 2013a). This argues for long-lasting stable conditions during accumulation of the thick oil shale in the Fushun Basin, a result of high subsidence rates and a deep lacustrine environment, which avoided the development of a distinct cyclicity.
- Organic matter in the lower unit of the Jijuntun Formation originates from predominating landplants and minor aquatic organisms. Because of abundant landplant-derived liptinite macerals, the organic matter is formed by kerogen type II (average "true" HI 400 mgHC/gTOC). Low quality oil shale was

deposited within this unit. The detected clay mineral assemblage is in agreement with a warm and humid climate.

- The organic matter in the upper unit of the Jijuntun Formation is dominated by lacustrine organisms (e.g. bacteria, algae) forming kerogen type I (average "true" HI 700 mgHC/gTOC). TOC contents up to 23.6 wt.% and the presence of high quality oil shale are a result of high bioproductivity and excellent preservation conditions. Photic zone anoxia supported by temperature stratification in a deep lake controlled organic matter preservation. Vertical changes in clay mineral abundances reflect a cooling trend during deposition of the Jijuntun Formation postulated by Quan et al. (2012).
- The base of the overlying Xilutian Formation is formed by dolomitic rocks deposited during a hot and arid climate favoring brackish conditions in a shallow lake.
- The Fushun Basin provides an excellent example for the fact that geochemical proxies have to be used with caution and that multiproxy studies are necessary. In this basin, T_{max} is strongly affected by kerogen type and pretends upward increasing maturity, whereas Pr/Ph ratios are probably biased by different sources of the isoprenoids and do not reflect strictly anoxic conditions.

7.7 Acknowledgments

We would like to express our gratitude to Mr. Han Fang from the Fushun Mining Group Co., Ltd. who generously permitted us to take samples in the West Open Pit mine in Fushun, NE China. We also want to thank Mr. Jianliang Jia for his help during the fieldwork. Special thanks to Mr. Thomas C. Meisel from the Department of General and Analytical Chemistry at the Montanuniversitaet Leoben, who helped us with the XRF measurements. Mr. Hui Tian and Mr. Humberto Carvajal-Ortiz are thanked for helpful reviews of the manuscript. We are also grateful to Associate Editor Mr. Yongtai Yang for his editorial work.

7.8 References

Alqudah, M., Hussein, M.A., van den Boorn, S., Giraldo, V.M., Kolonic, S., Podlaha, O.G., Mutterlose, J., 2014. Eocene oil shales from Jordan – Paleoenvironmental implications from reworked microfossils. Marine and Petroleum Geology 52, 93-106.

Barakat, A.O., Rullkötter, J., 1997. A comparative study of molecular paleosalinity indicators: chromans, tocopherols and C20 isoprenoid thiophenes in Miocene lake sediments (Nördlinger Ries, Southern Germany). Aquatic Geochemistry 3, 169-190.

Berner, R.A., 1984. Sedimentary pyrite formation: An update. Geochimica et Cosmochimica Acta 48, 605-615.

Bray, E.E., Evans, E.D., 1961. Distribution of *n*-paraffins as a clue to recognition of source beds. Geochimica et Cosmochimca Acta 22, 2-15.

Brindley, G.W., Brown, G., 1980. Crystal structures of clay minerals and their X-ray identification. Mineralogical Society, London.

Carr, A.D., 2000. Suppression and retardation of vitrinite reflectance, part 1; Formation and significance for hydrocarbon generation. Journal of Petroleum Geology 23, 313-343.

Carroll, A.R., Bohacs, K.M., 1999. Stratigraphic classification of ancient lakes: balancing tectonic and climatic controls. Geology 27, 99–102.

Carroll, A.R., Bohacs, K.M., 2001. Lake-type controls on petroleum source rock potential in non-marine basins. AAPG Bulletin 85, 1033-1053.

Collister, J.W., Rieley, G., Stern, B., Eglinton, G., Fry, B., 1994. Compound-specific $\delta^{13}C$ analysis of leaf lipids from plants with differing carbon dioxide metabolism. Organic Geochemistry 21, 619-627.

Coplen, T.B., 2011. Guidelines and recommended terms for expression of stable-isotope-ratio and gas-ratio measurement results. Rapid Communications in Mass Spectrometry 25, 2538-2560.

Cumming, V.M., Selby, D., Lillis, P.G., 2012. Re-Os geochronology of the lacustrine Green River Formation: Insights into direct depositional dating of lacustrine successions, Re-Os systematic and paleocontinental weathering. Earth and Planetary Science Letters 359-360, 194-205.

Dean, W.E., Arthur, M.A., 1989. Iron-sulfur-carbon relationships in organic-rich sequences I: Cretaceous Western Interior Seaway. American Journal of Science 289, 708-743.

Demaison, G., Huizinga, B.J., 1994. Genetic Classification of Petroleum Systems using three factors: Charge, migration, and entrapment, in: Magoon, L.B., Dow, W.G. (Eds.), The Petroleum System – from Source to Trap. AAPG Memoir 60, pp.3-24.

Dev, S., 1989. Terpenoids; in: Rowe, J.W. (Ed.), Natural Products of Woody Plants. Springer, Berlin, pp. 691-807.

Didyk, B.M., Simoneit, B.R.T., Brassell, S.C., Eglinton, G., 1978. Organic geochemical indicators of paleoenvironmental conditions of sedimentation. Nature 272, 216-222.

Dyni, J.R., 2006. Geology and resources of some world oil-shale deposits. U.S. Geological Survey Scientific Investigations Report 2005-5294.

Espitalié, J., Marquis, F., Barsony, I., 1984. Geochemical logging, in: Voorhess, K.J. (Ed.), Analytical Pyrolysis. Butterworths, Boston, pp. 53-79.

Espitalié, J., Deroo, G., Marquis, F., 1985. La pyrolyse Rock-Eval et ses applications (deuxième partie). Revue Institut Francais du Pétrole 40, 755-784.

Farquhar, G.D., Ehleringer, J.R., Hubick, K.T., 1989. Carbon isotope discrimination and photosynthesis. Annual Review of Plant Physiology and Plant Molecular Biology 40, 503-537.

Farrimond, P., Talbot, H.M., Watson, D.F., Schulz, L.K., Wilhelms, A., 2004. Methylhopanoids: Molecular indicators of ancient bacteria and a petroleum correlation tool. Geochimica et Cosmochimica Acta 68, 3873-3882.

Goossens, H., de Leeuw, J.W., Schenck, P.A., Brassel, S.C., 1984. Tocopherols as likely precursors of pristane in ancient sediments and crude oils. Nature 312, 440-442.

Gruber, W., Sachsenhofer, R.F., 2001. Coal deposition in the Noric Depression (Eastern Alps): raised and low-lying mires in Miocene pull-apart basins. International Journal of Coal Geology 48, 89-114.

Hauke, V., Graff, R., Wehrung, P., Trendel, J.M., Albrecht, P., 1992. Novel triterpene-derives hydrocarbons of arborane/fernane series in sediments – Part I. Tetrahedron 48, 3915-3924.

Hong, Y., Yang, Z., Wang, S., Sun, X., Du, N., Sun, M., Li, Y., 1980. Study of Strata and Paleontology in Fushun Coalfield, Liaoning Province. Science Press.

Hou, G., Dong, Q., Yu, W., Yan, L., Zhu, J., Miao, C., 2006. The geological characteristic and ore-forming process analysis of the oil shale in Fushun basin. Journal of Jilin University (Earth Science) 36, 991-1000.

Hussler, G., Albrecht, P., Ourisson, G., 1984. Benzohopanes, a novel family of hexacyclic geomarkers in sediments and petroleums. Tetrahedron Letters 25, 1179-1182.

Joachimsky, M.M., Ostertag-Henning, C., Pancost, R.D., Strauss, H., Freeman, K.H., Littke, R., Sinninghe Damsté, J.S., Racki, G., 2001. Water column anoxia, enhanced productivity and concomitant changes in $\delta^{13}C$ and $\delta^{24}S$ across the Frasnian-Famennian boundary (Kowala-Holy Cross Mountains/Poland). Chemical Geology 175, 109-131.

Johnson, E.A., 1990. Geology of the Fushun coalfield, Liaoning Province, People's Republic of China. International Journal of Coal Geology 14, 217-236.

Karrer, W., Cherbuliez, E., Eugster, C.H., 1977. Konstitution und Vorkommen der organischen Pflanzenstoffe – Ergänzungsband 1. Birkhäuser, Basel – Stuttgart.

Kodner, R.B., Summons, R.E., Pearson, A., King, N., Knoll, A.H., 2008. Sterols in a unicellular relative to metazoans. Proceedings of the National Academy of Science of the USA 105, 9897-9902.

Langford, F.F., Blanc-Valleron, M.M., 1990. Interpreting Rock-Eval pyrolysis data using graphs of pyrolyzable hydrocarbons vs. total organic carbon. AAPG Bulletin 74, 799-804.

Lenz, O.K., Wilde, V., Riegel, W., 2007. Recolonization of a Middle Eocene volcanic site: quantitative palynology of the initial phase of the maar lake of Messel (Germany). Review of Paleobotany and Palynology 145, 217-242.

Li, S., Yue, C., 2003. Study of pyrolysis kinetics of oil shale. Fuel 82, 337-342.

Liu, Z., Yang, H., Dong, Q., Zhu, J., Guo, W., Ye, S., Liu, R., Meng, Q., Zhang, H., Gan, S., 2009. Oil Shale in China. Petroleum Industry Press, Beijing.

Mackenzie, A.S., 1984. Application of biological markers in petroleum geochemistry, in: Brooks, J., Welte, D.H. (Eds.), Advances in Petroleum Geochemistry. Academic Press, London, pp. 115-214.

Meng, Q., Liu, Z., Bruch, A.A., Liu, R., Hu, F., 2012. Paleoclimatic evolution during Eocene and its influence on oil shale mineralisation, Fushun basin, China. Journal of Asian Earth Sciences 45, 95-105.

Moore, D.M., Reynolds, R.C., 1997. X-ray diffraction and the identification and analysis of clay minerals. Oxford University Press, New York.

Mosbrugger, V., Utescher, T., 1997. The coexistence approach – a method for quantitative reconstructions of Tertiary terrigenous paleoclimate data using plant fossils. Paleogeography, Paleoclimatology, Paleoecology 134, 61-86.

Murray, A.P., Summons, R.E., Boreham, C.J., Dowling, L.M., 1994. Biomarker and *n*-alkane isotope profiles for Tertiary oils: relationship to source rock depositional setting. Organic Geochemistry 22, 521-542.

Ocakoglu, F., Acikalin, S., Yilmaz, I.Ö., Safak, Ü., Gökceoglu, C., 2012. Evidence for orbital forcing in lake-level fluctuations in the Middle Eocene oil shale-bearing lacustrine successions in the Mudurnu Göynük Basin, NW Anatolia (Turkey). Journal of Asian Earth Sciences 56, 54-71.

O'Leary, M.H., 1988. Carbon Isotopes in Photosynthesis – Fractionation techniques may reveal new aspects of carbon dynamics in plants. BioScience 38, 328-336.

Ostwald, J., England, B.M., 1979. The relationship between euhedral and framboidal pyrite in base-metal sulphide ores. Mineralogical Magazine 43, 297-300.

Otto, A., Walther, H., Püttmann, W., 1997. Sesqui- and diterpenoid biomarkers in Taxodium-rich Oligocene oxbow lake clays Weisselster basin, Germany. Organic Geochemistry 26, 105-115.

Otto, A., Wilde, V., 2001. Sesqui-, di-, and triterpenoids as chemosystematic markers in extant conifers – a review. Botanical Review 67, 141-238.

Ourisson, G., Albrecht, P., Rohmer, M., 1979. The hopanoids: paleo-chemistry and biochemistry of a group of natural products. Pure and Applied Chemistry 51, 709-729.

Pancost, R.D., Sinninghe Damsté, J.S., 2003. Carbon isotopic compositions of prokaryotic lipids as tracers of carbon cycling in diverse settings. Chemical Geology 195, 29-58.

Peters, K.E., 1986. Guidelines for evaluating petroleum source rocks using programmed pyrolysis. AAPG Bulletin 70, 318-329.

Peters, K.E., Walters, C.C., Moldowan, J.M., 2005. The Biomarker Guide – Biomarkers and Isotopes in Petroleum Exploration and Earth History. Cambridge University Press, New York.

Quan, C., Liu, Y., Utescher, T., 2012. Paleogene temperature gradient, seasonal variation and climate evolution of northeast China. Paleogeography, Paleoclimatology, Paleoecology 313-314, 150-161.

Radke, M., Willsch, H., Welte, D.H., 1980. Preparative hydrocarbon group type determination by automated medium pressure liquid chromatography. Analytical Chemistry 52, 406-411.

Rohmer, M., Bouvier-Nave, P., Ourisson, G., 1984. Distribution of hopanoid triterpenes in prokaryotes. Journal of General Microbiology 130, 1137-1150.

Sachsenhofer, R.F., Bechtel, A., Reischenbacher, D., Weiss, A., 2003. Evolution of lacustrine systems along the Miocene Mur-Mürz fault system (Eastern Alps, Austria) and implications on source rocks in pull apart basins. Marine and Petroleum Geology 20, 83-110.

Sawlowicz, Z., 1993. Pyrite framboids and their development: a new conceptual mechanism. Geologische Rundschau 82, 148-156.

Schouten, S., Özdirekcan, S., van der Meer, M.T.J., Blooker P., Baas, M., Hayes, J.M., Sinninghe Damsté, J.S., 2008. Evidence for substantial intramolecular heterogeneity in the stable carbon isotopic composition of phytol in photoautotrophic organisms. Organic Geochemistry 39, 135-146.

Schultz, L.G., 1964. Quantitative interpretation of mineralogical composition from X-ray and chemical data for the Pierre Shale. Geological Survey Professional Paper 391-C.

Sinninghe Damsté, J.S., Kock-Van Dalen, A.C., de Leeuw, J.W., Schenk, P.A., Guoying, S., Brassell, S.C., 1987. The identification of mono-, di-, and trimethyl 2-methyl-2-(4,8,12-trimethyltridecyl)chromans and their occurrence in geosphere. Geochimica et Cosmochimica Acta 51, 2393-2400.

Sinninghe Damsté, J.S., Keely, B.J., Betts, S.E., Baas, M., Maxwell, J.R., de Leeuw, J.W., 1993. Variations in abundances and distributions of isoprenoid chromans and long-chain alkylbenzenes in sediments of the Mulhouse Basin: a molecular sedimentary record of paleosalinity. Organic Geochemistry 20, 1201-1215.

Strobl, S.A.I., Bechtel, A., Sachsenhofer, R.F., Sun, P., Meng, Q., Liu, R., Liu, Z., 2013. Deposition of Oil Shale in the Fushun Basin, Eocene, NE China. 75th EAGE Conference & Exhibition incorporating SPE EUROPEC 2013, London. Poster presentation.

Summons, R.E., Powell, T.G., 1987. Identification of aryl isoprenoids in source rocks and crude oils: biological markers for the green sulphur bacteria. Geochimica et Cosmochimica Acta 51, 557-566.

Summons, R.E., Jahnke, L.L., 1992. Hopenes and hopanes methylated in ring-A: Correlation of the hopanoids from extant methylotrophic bacteria with their fossil analogues, in: Moldowan, J.M., Albrecht, P., Philp, R.P. (Eds.), Biological Markers in Sediments and Petroleum. Prentice-Hall, New Jersey, pp. 182-200.

Summons, R.E., Jahnke, L.L., Hope, J.M., Logan, G.A., 1999. 2-Methylhopanoids as biomarkers for cyanobacterial oxygenic photosynthesis. Nature 400, 554-557.

Sun, P., Sachsenhofer, R.F., Liu, Z., Strobl, S.A.I., Meng, Q., Liu, R., Zhen, Z., 2013a. Organic matter accumulation in the oil shale- and coal-bearing Huadian Basin (Eocene; NE China). International Journal of Coal Geology 105, 1-15.

Sun, P., Liu, Z., Gratzer, R., Xu, Y., Liu, R., Li, B., Meng, Q., Xu, J., 2013b. Oil yield and bulk geochemical parameters of oil shales from the Songliao and Huadian basins, China: A grade classification approach. Oil Shale 30, 402-418.

Taylor, H., Teichmüller, M., Davis, A., Diessel, C.F.K., Littke, R., Robert, P., 1998. Organic Petrology. Borntraeger. Berlin-Stuttgart.

ten Haven, H.L., de Leeuw, J.W., Rullkötter, J., Sinninghe Damsté, J.S., 1987. Restricted utility of the pristane/phytane ratio as a paleoenvironmental indicator. Nature 330, 641-643.

Thiel, V., Peckmann, J., Seifert, R., Wehrung, P., Reitner, J., Michaelis, W., 1999. Highly isotopically depleted isoprenoids: molecular markers for ancient methane venting. Geochimica et Cosmochimica Acta 63, 3959-3966.

Tian, H., Cheng, P., Zhou, Q., Xiao, X., Wilkins, R.W.T., 2013. Abnormal elevations of C_{34} 2α-methylhopane and C_{34} 2α-methylbenzohopane in a Lower Triassic mudstone sample, NW Sichuan Basin. Organic Geochemistry 63, 139-144.

Tissot, B.T., Welte, D.H., 1984. Petroleum Formation and Occurence, 2nd ed., Springer Verlag, Berlin.

Volkman, J.K., 1986. A review of sterol markers for marine and terrigenous organic matter. Organic Geochemistry 9, 83-99.

Volkman, J.K., Maxwell, J.R., 1986. Acyclic isoprenoids as biological markers, in: Johns, R.B. (Ed.), Biological Markers in the Sedimentary Record. Elsevier, Amsterdam, pp.1-42.

Volkman, J.K., Barrett, S.M., Blackburn, S.I., 1999. Eustigmatophyte microalgae are potential sources of C_{29} sterols, C_{22}-C_{28} *n*-alcohols and C_{28}-C_{32} *n*-alkyl diols in freshwater environments. Organic Geochemistry 30, 307-318.

Wang, K., Jia, H., Zhang, J., Peng, Y., 2008. The 44 Ma/42 Ma interval of volcanic events in northeast China and its significance in Geology and ore-searching. Geology and Resources 17, 161-165.

Wang, Q., Ferguson, D.K., Feng, G., Ablaev, A.G., Wang, Y., Yang, J., Li, Y., Li, C., 2010. Climatic change during the Paleocene to Eocene based on fossil plants from Fushun, China. Paleogeography, Paleoclimatology, Paleoecology 295, 323-331.

Wignall, P.B., Newton, R., 1998. Pyrite framboid diameter as a measure of oxygen deficiency in ancient mudrocks. American Journal of Science 298, 537-552.

Wu, C., Yang, Q., Zhu, Z., Liu, G., Li, X., 2000. Thermodynamic analysis and simulation of coal metamorphism in the Fushun Basin, China. International Journal of Coal Geology 44, 149-168.

Wu, C., Wang, X., Liu, G., Li, S., Mao, X., Li, X., 2002. Study on dynamics of tectonic evolution in the Fushun Basin, Northeast China. Science in China 45, 311-324.

Zhang, J., Peng, Y., Liu, J., 2007. An important discontinuity of the Paleogene volcanic incidents in northeast China and their prospecting significance. Jilin Geology 26, 1-7.

Zhao, C., Ye, D., Wei, D., Chen, B., Liu, D., 1994. Tertiary in Oil and Gas Province of China (III). Oil Industry Press, Beijing.

8 Paleoenvironment of the Eocene coal seam in the Fushun Basin (NE China): Implications from petrography and organic geochemistry

Accepted for publication in International Journal of Coal Geology
DOI: 10.1016/j.coal.2014.10.001

Susanne A.I. Strobl[a], Reinhard F. Sachsenhofer[a], Achim Bechtel[a], Qingtao Meng[b]

[a] Department of Applied Geosciences and Geophysics, Montanuniversitaet Leoben, Peter-Tunner-Straße 5, 8700 Leoben, Austria
[b] College of Earth Sciences, Jilin University, Changchun 130061, China

Keywords

Fushun Basin; Guchengzi Formation; coal petrography; mire facies; geochemistry

Abstract

The Fushun Basin in northeast China is a strike-slip basin filled with coal-bearing Eocene sediments. The basin fill includes from base to top volcaniclastic rocks, a 20 to 145 m thick coal seam (Lower Eocene Guchengzi Formation) and lacustrine oil shale, up to 300 m thick (Jijuntun Formation). The sub-bituminous coal of the Guchengzi Formation, famous for the amber inclusions, is exploited in the largest opencast coal and oil shale mine in Asia. In the present contribution the depositional environment and the thermal history of the Guchengzi Formation are investigated based on macro- and micropetrographic data, bulk geochemical parameters, biomarker analysis, stable isotope geochemistry, and vitrinite reflectance measurements. According to our interpretation, accumulation of the low-sulfur coal commenced in a low-lying mire near a shallow lake. Subsequently low-ash coal was deposited either in a low-lying mire protected from clastic influx or in a raised mire. Finally, high subsidence rates, typical for strike-slip basins, caused the flooding of the mire and terminated peat accumulation. Pristane/Phytane ratios suggest a gradual change from oxic to less oxic

conditions during the drowning phase of the seam. Organic-rich shales accumulated in the newly formed freshwater lake and resulted in the deposition of the overlying oil shale-bearing Jijuntun Formation. The coal is rich in liptinite macerals, especially sporinite. Gymnosperms dominated the paleovegetation of the mire, something that is also reflected by the frequent occurrence of resinite and amber and their biomarker composition. The coal reached the sub-bituminous or even the high volatile bituminous stage, despite the limited burial depth. Simple 1D models suggest that this is a result of high heat flow, rather than of deep burial and erosion. The hydrogen-rich coal is oil-prone.

8.1 Introduction

Strike-slip basins host some of the world's thickest coal seams, e.g. the Mongol-Altai and Kharkhiraa basins in Mongolia (Erdenetsogt et al., 2009), the Velenje Basin in Slovenia (Markic and Sachsenhofer, 1997), and the Fushun Basin in China (Johnson, 1990).

Strike-slip basins are often characterized by a stratigraphic succession including from base to top fluvial sediments, a single thick coal seam and lacustrine deposits, which may be very rich in organic matter (e.g. Lambiase, 1990; Sachsenhofer et al., 2003). This sequence indicates drowning of the peat due to high subsidence rates, which are characteristic for strike-slip basins. Coal may form during the regressive filling stage of the basin, but is typically of lower quality than that formed during the transgressive stage (Sachsenhofer, 2000).

The present paper focuses on the world-class coal deposit in the Eocene Fushun Basin in northeastern China. In this basin sub-bituminous coal (Guchengzi Formation) is exploited in the largest opencast coal mine in Asia (Meng et al., 2012), which is mainly used for heating purposes (Liu et al., 2009). The coal seam accumulated during the early transgressive stage of basin evolution (Wu et al., 2002). A very high amber content is a unique feature of the Fushun coal.

Previous research related to the coal in the Fushun Basin mainly focused on the geological setting of coal deposition (Johnson, 1990), coal metamorphism (Wu et al.,

2000), tectonic (Wu et al., 2002) and paleoclimatic evolution (Wang et al., 2010; Quan et al., 2012), palynology and paleobotany (Ma et al., 2012; Su et al., 2014). To our knowledge, to date no research has been undertaken on factors controlling the depositional environment and coal facies applying combined petrographical and organic geochemical techniques.

Hence, the main aim of our paper is to reconstruct the environmental conditions, which resulted in the deposition of the thick coal seam of the Guchengzi Formation. To reach the goal, biomarker data are interpreted together with bulk geochemical and maceral data. Compound-specific isotope analysis, vitrinite reflectance measurements and a one-dimensional thermal model are applied to provide further information on the evolution of the coal accumulation.

8.2 Geological setting

The Fushun Basin is a terrestrial strike-slip basin located along the Dunhua-Mishan ("DunMi") fault zone (Wu et al., 2000; Fig. 8.1). The DunMi fault zone was active during Mesozoic-Cenozoic times (Liu et al., 2009; Meng et al., 2012). Several coal and oil shale-bearing basins are located along this fault zone. The most prominent ones are the Eocene Fushun and Huadian basins (Liu et al., 2009; Sun et al., 2013).

The Fushun Basin is characterized by an EW trending syncline, which northern limb is removed by a large-scale thrust fault (Johnson, 1990; Fig. 8.1). The basement consists of Proterozoic gneiss and Cretaceous sedimentary rocks. The basin fill contains from base to top: Laohutai and Lizigou formations (Paleocene), Guchengzi Formation (Lower Eocene), Jijuntun and Xilutian formations (Middle Eocene) and Gengjiajie Formation (Upper Eocene). Coal was deposited in the Paleocene and Lower Eocene. The coal seams of the Laohutai and Lizigou formations are relative thin, compared to the major coal seam of the Guchengzi Formation. A stratigraphic column of the Fushun Basin along with a short description of depositional environment is provided in Fig. 8.3.

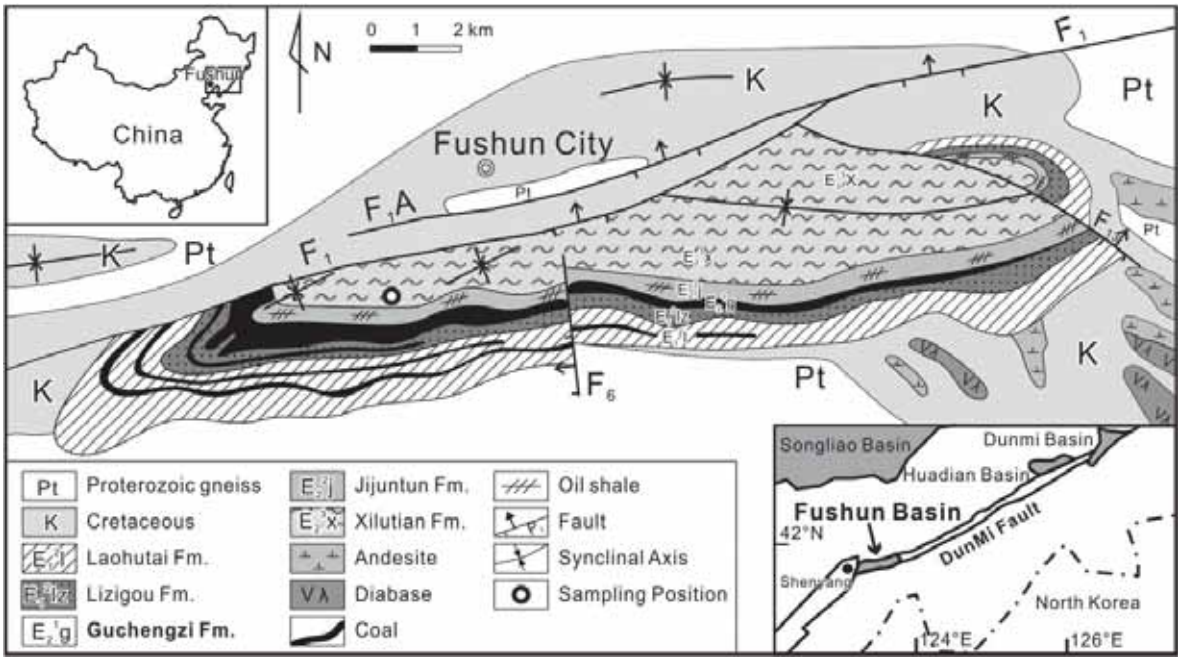

Fig. 8.1: Geological map of the Fushun Basin with location of the sampling site and a schematic map with special focus on the location of the Fushun Basin and the DunMi Fault is shown as insert [modified according to Hong et al. (1980), Wu et al. (2000), Meng et al. (2012), Strobl et al. (2014)].

The total thickness of the coal seam within the Guchengzi Formation (Ypresian) varies between 20 and 145 m (Fig. 8.2a) including interseam sediments consisting of carbonaceous shale, mudstone, sandstone and conglomerate (Johnson, 1990; Wu et al., 1998; Xu et al., 2012). Cross-sections shown by Wu et al. (1998; 2002) suggest that the high seam thicknesses are often due to very thick interseam sediments (Fig. 8.2b). Amber and siderite nodules occur throughout the coal seam (Johnson, 1990).

The maturity of the coal seam in the Guchengzi Formation increases from west to east from the sub-bituminous stage (~0.5%R_r) to the high volatile bituminous A stage (~0.9%R_r; Wu et al., 2000; Fig. 8.2a). According to Wu et al. (2000), the relatively high maturity is related to the Late Oligocene intrusion of diabase sills into the underlying Laohutai and Lizigou formations, which also resulted in coking of the coal in these formations.

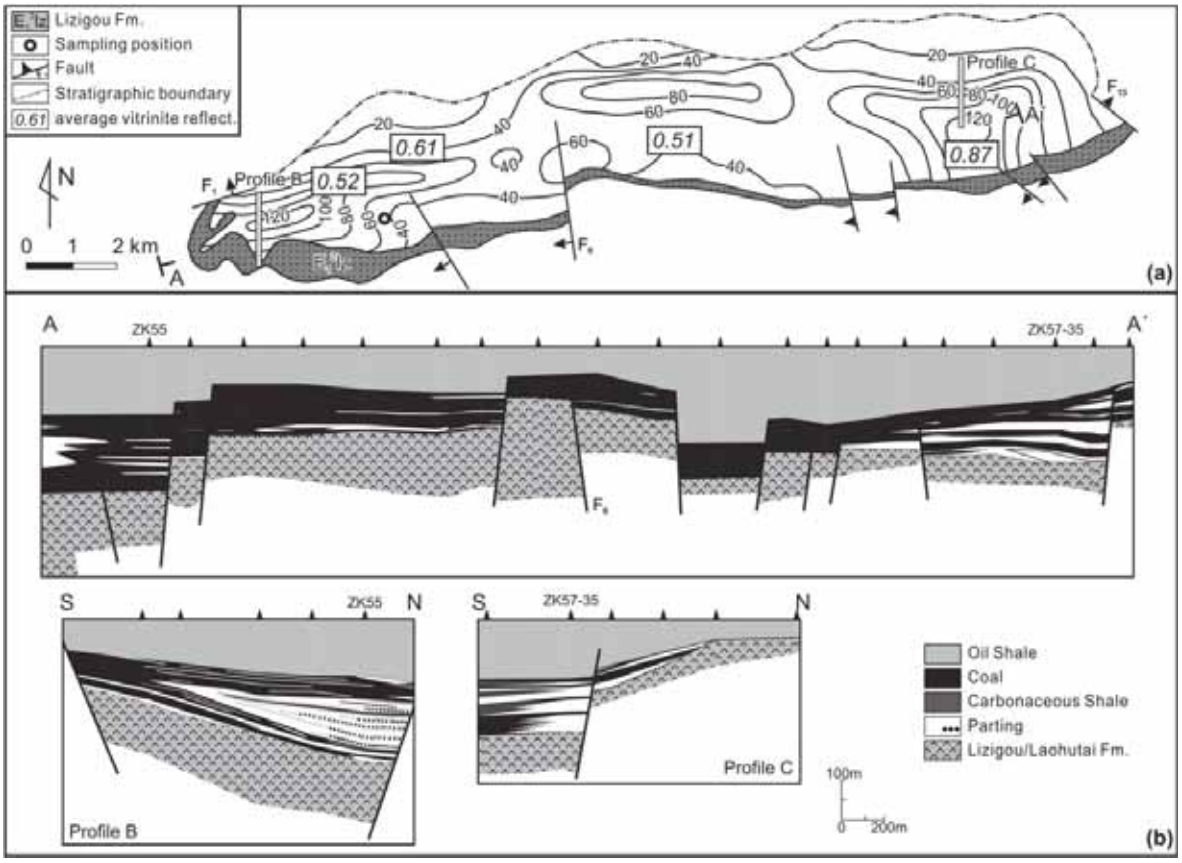

Fig. 8.2: (a) Lateral distribution of total thickness of the coal seam within the Guchengzi Formation [modified according to Liu et al. (2009), Xu et al. (2012)] and average vitrinite reflectance values according to Wu et al. (2000), and (b) profiles showing thicknesses of the coal seam and interseam sediments within the Fushun Basin [modified according to Wu et al. (1998), Wu et al. (2000)].

The Jijuntun Formation (Lutetian), 60 to 300 m thick, is composed of thick oil shale intercalated by carbonaceous shale and mudstone (Wu et al., 2000; Meng et al., 2012). The oil shale-bearing succession was deposited in a rapidly subsiding freshwater lake. Low quality oil shale (oil yield <4.7 wt.%) was deposited in the lower part (shallow lake), whereas oil shale with high quality (oil yield >4.7 wt.%) was deposited in the upper part (deep lake; Liu et al. , 2009; Strobl et al., 2014).

The Xilutian Formation (Bartonian), up to 600 m thick, comprises light green dolomitic mudstone intercalated by silty argillite deposited in a shallow lake environment (Wu et al., 2000; Meng et al., 2012).

Erosional remnants of mudstones and siltstones of the fluvial Gengjiajie Formation (Priabonian) appear only locally (Hong et al., 1980; Wu et al., 2000).

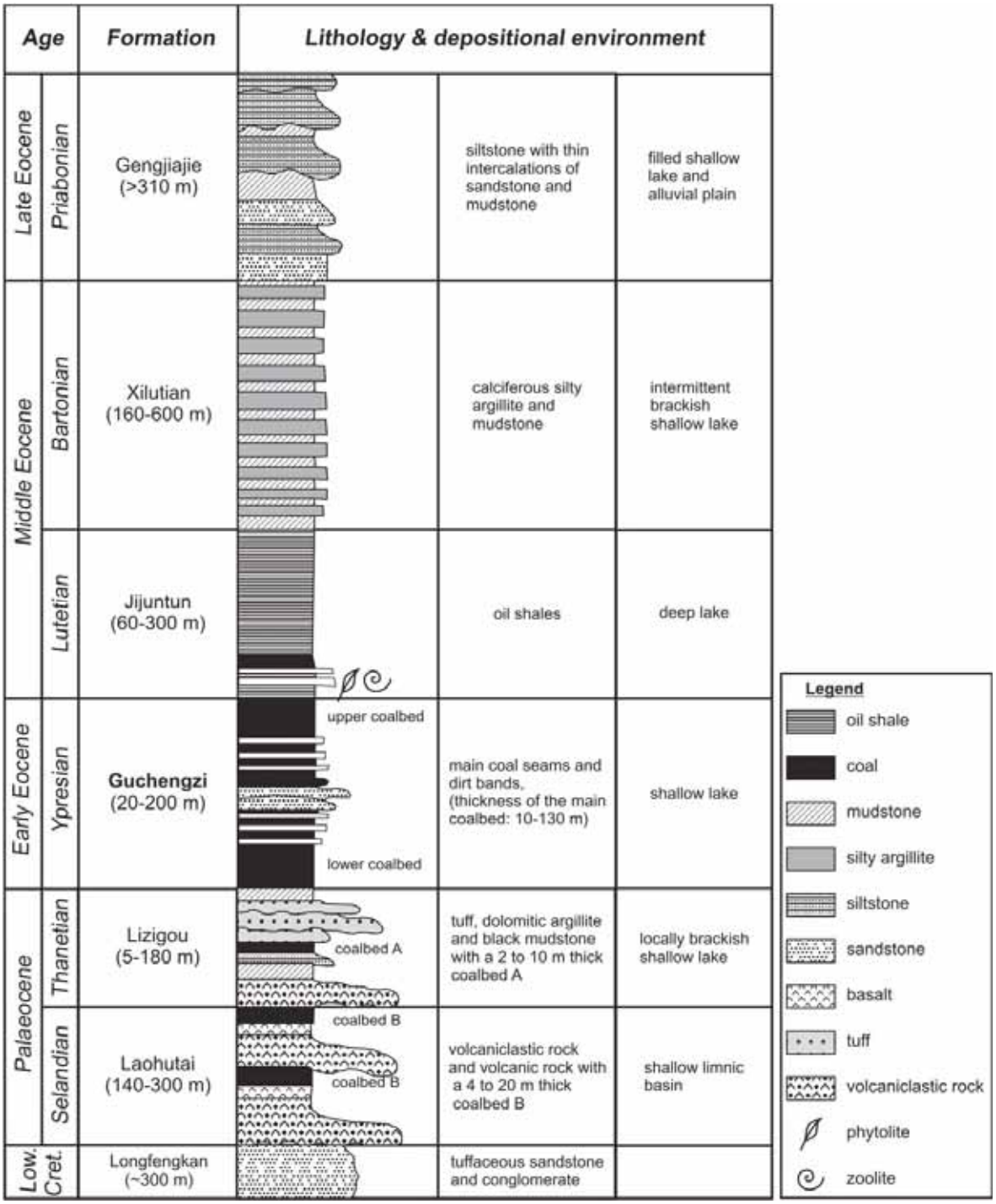

Fig. 8.3: Stratigraphic column of the Fushun Basin [modified according to Hong et al. (1980), Wu et al. (2000), Quan et al. (2012), Strobl et al. (2014)].

The climate during deposition of the basin fill was reconstructed by Quan et al. (2012) using the Coexistence Approach (Mosbrugger and Utescher, 1997). According to these investigations the coal seam (Guchengzi Formation) was deposited during the Early Eocene Climatic Optimum, whereas the mean annual temperature decreased during deposition of the Jijuntun Formation. The overlying Xilutian Formation represents a Mid-Eocene warming event. Huang et al. (1983)

reconstructed a moist subtropical climate for the time of coal accumulation within the Guchengzi Formation.

8.3 Samples and methods

Twenty nine samples have been taken along a vertical profile in the West Open Pit mine in the south of Fushun City (41°50'33.4''N, 123°53'14.3''E). The altitude of the top of the quarry is about 80 m. Sample depth is given in meters below sea level. The samples represent a 36-m-thick succession through the coal seam of the Guchengzi Formation in the western part of the Fushun Basin. In between, an eleven-meter-thick part was not exposed. Each sample comprises an interval of about 10 cm and is representative for a macroscopically homogenous layer, 0.1 to 2.0 m thick. In addition, pure amber has been isolated from the uppermost part of the seam.

Total organic carbon (TOC) and sulfur (S) contents were determined using a Leco CS-230 elemental analyzer. Samples were pre-treated with hydrochloric acid before determining TOC contents. Pyrolysis analysis was performed using a Rock Eval 2+ analyzer. Within this method the amount of pyrolyzate released from kerogen during gradual heating was normalized to TOC to give the hydrogen index (HI). As a maturation parameter, the temperature of maximum hydrocarbon generation (T_{max}) was determined. Ash yield and moisture determinations followed standard procedures (Deutsches Institut für Normung 51718, 1978, & 51719, 1980).

For microscopic examination, the samples were crushed to a maximum size of 1 mm. Maceral analysis was performed by a single-scan method (Taylor et al., 1998) with a Leica MPV microscope using reflected white light and blue-light excitation. An oil immersion objective (50x magnification) was used. At least 300 points per polished block were counted to provide composition at maceral level. The maceral nomenclature for medium-rank coals is applied because of the sub-bituminous rank of the coal (ICCP, 1998; 2001; Sýkorová et al., 2005). The maceral abundances refer to volume percentages on a mineral matter-free basis (vol.% mmf).

There have been several suggestions to characterize coal facies from maceral ratios (von der Brelie and Wolf, 1981; Diessel, 1986, 1992). Maceral ratios developed by

Calder et al. (1991) for Westphalian coals were applied. Using this method, the Groundwater Index (GWI) is the ratio of strongly gelified vitrinite plus detrital mineral matter to weakly gelified vitrinite. It shows the influence of rheotrophic swamp conditions.

$$\mathrm{GWI} = \frac{\text{gelovitrinite} + \text{mineral matter}}{\text{telovitrinite} + \text{detrovitrinite}}$$

The Vegetation Index (VI) contrasts macerals of forest affinity with those of herbaceous and aquatic affinity. Following Gruber and Sachsenhofer (2001), resinite was subdivided into *in-situ* resinite occurring within wood tissues and detrital resinite.

$$\mathrm{VI} = \frac{\text{telovitrinite} + \text{phlobaphinite} + \text{teloinertinite} + \text{suberinite} + \text{in situ resinite}}{\text{detrovitrinite} + \text{gelinite} + \text{inertodetrinite} + \text{sporinite} + \text{cutinite} + \text{liptodetrinite} + \text{bituminite} + \text{fluorinite} + \text{detrital resinite}}$$

The Tissue Preservation Index (TPI; Diessel, 1986) yields similar information than the VI. It has been calculated using the following equation.

$$\mathrm{TPI} = \frac{\text{telovitrinite} + \text{(semi)fusinite}}{\text{detrovitrinite} + \text{gelovitrinite} + \text{macrinite} + \text{inertodetrinite}}$$

The Gelification Index (GI; Diessel, 1986) is a useful facies indicator for lignite (e.g. Kalkreuth et al., 1991; Bechtel et al., 2003; 2007), but has a limited significance for sub-bituminous and higher-rank coals, in which it is difficult to distinguish between biochemical and geochemical gelification. Therefore, this parameter was not applied for the Fushun coal samples.

Three samples, one of the lower, and two of the upper parts of the coal seam, were selected for vitrinite reflectance measurements. Random vitrinite reflectance (%R_r) was measured using a 100x objective in non-polarized light at a wavelength of 546 nm (Taylor et al., 1998). At least 50 points per sample were measured.

Based on TOC, S, Rock Eval and maceral data, samples were selected for biomarker analyses and compound specific isotopic composition.

For organic geochemical analysis, portions of selected coal samples were extracted for approximately one hour using dichloromethane (DCM) in a Dionex ASE 200 accelerated solvent extractor. Asphaltenes were precipitated from a hexane-DCM

solution (80:1) and separated by centrifugation. The hexane-soluble fractions were separated into NSO compounds, saturated and aromatic hydrocarbons using medium pressure liquid chromatography (MPLC) with a Köhnen-Willsch instrument (Radke et al., 1980). The saturated and aromatic hydrocarbon fractions were analyzed using a gas chromatograph equipped with a 30 m DB-5MS fused silica column (i.d. 0.25 mm; 0.25 µm film thickness) and coupled to a Thermo Fisher ISQ quadrupole mass spectrometer (GC-MS system). The oven temperature gradient was programmed from 70° to 300°C at 4°C min^{-1}, followed by an isothermal period of 15 min. Helium was used as carrier gas. The sample was injected splitless, with the injector temperature at 275°C. The spectrometer was operated in the EI (electron ionization) mode over a scan range from *m/z* 50 to 650 (0.7 s total scan). Data were processed using an Xcalibur data system. Individual compounds were identified on the basis of retention time in the total ion current (TIC) chromatogram and by comparison of the mass spectra with published data. Relative percentages and absolute concentrations of different compound groups in the saturated and aromatic hydrocarbon fractions were calculated using peak areas from the gas chromatograms in relation to that of internal standards (deuteriated *n*-tetracosane and 1,1'binaphthyl, respectively). The concentrations were normalized to the TOC content.

Carbon isotope determination of *n*-alkanes and acyclic isoprenoids was performed using a Trace GC instrument attached to a ThermoFisher DELTA-V isotope ratio mass spectrometer via a combustion interface (GC isolink, ThermoFisher). For calibration, CO_2 was injected at the beginning and end of each analysis. The GC column and temperature program were the same as for GC-MS. Stable isotope ratios are reported in delta notation ($\delta^{13}C$; Coplen, 2011) relative to the Vienna-Pee Dee Belemnite (V-PDB) standard ($\delta^{13}C=[(^{13}C/^{12}C)_{sample}/(^{13}C/^{12}C)_{standard}-1]$). Delta notation is expressed in parts per thousand or per mil (‰). The analytical error was better than 0.2‰.

Heat flows and erosional thicknesses were estimated using 1D basin modeling techniques and PetroMod software. Calculation of vitrinite reflectance followed the "Easy%Ro" approach of Sweeney and Burnham (1990). Biomarker ratios (hopane isomerization) were calculated using kinetic data of Mackenzie and McKenzie (1983). Models were calibrated by modifying heat flow and the thickness of eroded sediments until a satisfactory fit between measured and calculated values was obtained. Vitrinite reflectance and hopane isomerization data from the overlying

Jijuntun Formation were adopted from Strobl et al. (2014). Input parameters include stratigraphic information about the sediments within the Fushun Basin.

8.4 Results

The lithological profile of the coal-bearing Guchengzi Formation is shown together with vertical variations of ash yields (dry basis, db), sulfur contents (db), hydrogen indices (HI), maceral group contents (vol.%, mineral matter free = mmf), and facies indices (groundwater index GWI and vegetation index VI) in Fig. 8.4. The studied coal seam is 36 m thick, but an eleven meter thick part in between was not exposed. Thus, the coal seam is divided by the non-exposed interval into a lower (-302.0 to -287.0 m) and an upper section (-276.0 to -265.9 m).

8.4.1 Macropetrography, ash yield and moisture

The coal seam consists of alternations of clean coal, shaly coal and coaly shale. The clean coal is characterized by amber inclusions. The lower section of the coal seam overlies a basaltic layer of the Lizigou Formation. It comprises clean coal in the lower and upper part and coaly shale in its middle part. The upper section consists mainly of clean coal. Shaly coal, coaly shale and thin layers of clean coal in the uppermost part indicate the transition zone between the Guchengzi Formation and the overlying Jijuntun Formation (Fig. 8.4).

Ash yields of clean coal layers vary between 2 and 16 wt.%, whereas ash yields of shaly coal layers vary between 24 and 32 wt.%. Coaly shale layers yield between 51 and 74 wt.% ash (Fig. 8.4a, Tab. 8.1). Moisture is low (< 4%) displaying a negative correlation with ash yield (r^2 = 0.67; Tab. 8.1).

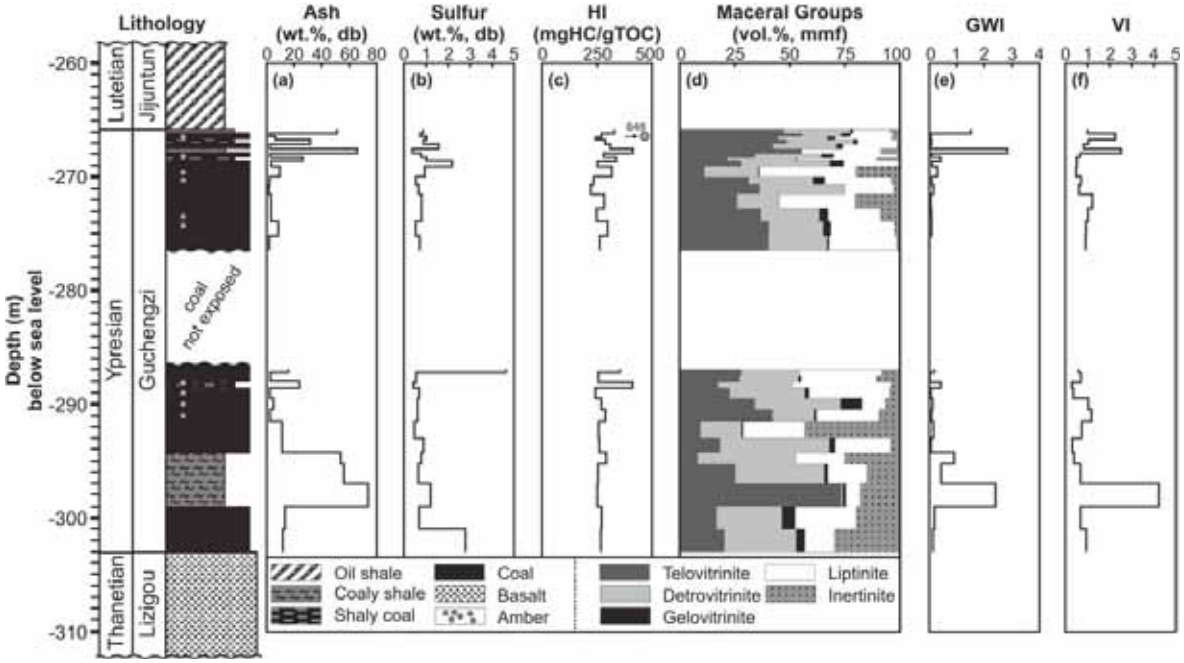

Fig. 8.4: Depth profiles of lithology combined with (a) ash yield, (b) sulfur content, (c) hydrogen index HI, (d) maceral-group and sub-group contents, (e) groundwater index GWI, and (f) vegetation index VI of the Guchengzi Formation.

8.4.2 Bulk geochemical parameters

Bulk geochemical data are listed in Tab. 8.1. Total organic carbon (TOC, as received = ar) contents are high within the clean coal layers (72-80 wt.%). TOC varies between 52 and 64 wt.% within the shaly coal layers, and between 14 and 40 wt.% within the coaly shale layers. As expected, the TOC content of pure amber is very high (83 wt.%).

Sulfur contents are generally low within the whole seam, but show elevated values at the base (2.8 wt.%) and top (4.7 wt.%) of the lower section, respectively (Fig. 8.4b).

The coals of the Guchengzi Formation are characterized by a relative high hydrogen index (HI = 222 to 415 mgHC/gTOC). T_{max} values in the range between 409 and 426°C agree with the sub-bituminous rank of the coal. Pure amber is characterized by a HI of 648 mgHC/gTOC (Fig. 8.4c) and a low T_{max} of 400°C. The HI versus T_{max} plot (Fig. 8.5) shows that the Fushun coals can be classified as mixed gas- and oil-prone to oil-prone (Peters and Moldowan, 1993). Considering the rank-related increase in HI of low-rank coals (Sykes and Snowdon, 2002), all coal samples exceed the minimum HI of 300 mgHC/gTOC required for oil generation (Pepper and Corvi, 1995) when their

thermal maturity reaches the onset of oil expulsion ("effective HI" of Sykes and Snowdon, 2002).

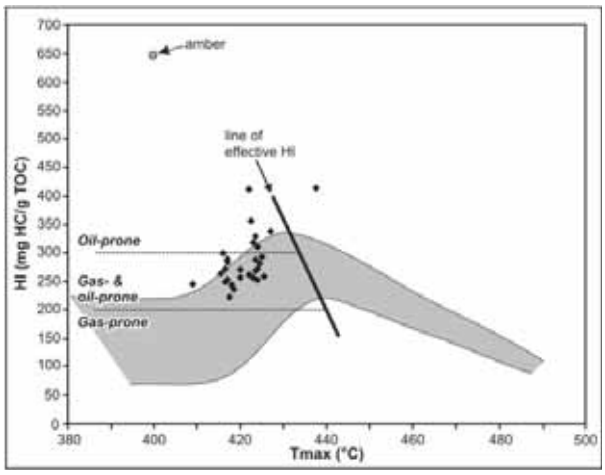

Fig. 8.5: Plot of HI vs. T_{max}, highlighting the increase in HI prior to the onset of oil expulsion [according to Sykes and Snowdon (2002)]. The classification of kerogen quality is according to Peters and Moldowan (1993).

Tab. 8.1: Ash yield, moisture, data from LECO and Rock Eval measurements.

Sample	Depth	Ash	Moisture	TOC[a]	S[b]	HI[c]	T_{max}[d]	S_2[e]
	(m)	(% db*)	(%)	(% ar*)	(% db*)	(mgHC/gTOC)	(°C)	(mgHC/g)
Guchengzi Formation - upper section								
FS 31	-265.90	51.2	2.3	40.2	0.9	330	424	133
FS 30	-266.40	2.0	4.0	77.6	0.7	272	417	211
FS 30a	-266.50	6.2	3.3	74.8	1.0	245	409	183
FS 29	-266.90	31.7	2.9	52.3	1.0	288	424	151
FS 28	-267.25	2.3	3.5	77.4	1.6	311	424	241
FS 27	-267.75	66.1	1.8	23.5	0.4	415	438	98
FS 26	-268.05	2.4	3.5	77.2	0.8	282	425	218
FS 25	-268.45	26.2	2.5	58.5	1.0	339	427	198
FS 24	-268.60	3.2	3.5	75.9	2.2	253	417	192
FS 23	-269.60	9.5	3.0	74.5	0.9	319	423	238
FS 22	-270.30	2.1	4.1	77.3	0.5	236	419	183
FS 21	-271.00	1.6	4.3	78.4	0.7	222	418	174
FS 16	-272.00	3.0	4.1	77.1	0.8	284	417	219
FS 17	-273.50	3.2	4.0	76.4	0.8	249	417	190
FS 17a	-274.30	8.4	3.5	72.3	0.5	300	416	217
FS 18	-276.00	1.8	4.2	78.4	0.7	264	416	207
Guchengzi Formation - lower section								
FS 15	-287.00	15.9	2.2	66.9	4.6	357	423	239
FS 14	-288.00	2.6	3.9	79.3	0.6	257	420	204
FS 14a	-288.15	23.8	1.6	64.2	0.4	413	422	265
FS 13	-289.00	2.3	3.8	78.5	0.7	244	418	192
FS 12	-290.00	5.0	3.1	77.3	0.6	271	420	210
FS 11	-291.00	2.4	3.2	79.7	0.6	289	417	231
FS 7	-292.00	11.2	2.6	74.6	0.5	259	426	193
FS 6	-294.00	11.3	2.5	71.9	0.9	262	422	188
FS 5	-294.50	53.9	1.4	33.3	0.8	294	425	98
FS 4	-296.00	56.3	1.4	32.0	0.6	256	423	82
FS 3	-298.00	73.9	0.9	13.8	1.2	253	424	35
FS 2	-300.00	13.3	1.9	71.7	0.7	272	424	195
FS 1	-302.00	11.8	2.3	72.6	2.8	269	424	195

[a]total organic carbon, [b]sulfur, [c]hydrogen index, [d]temperature with maximum hydrocarbon generation,
[e]hydrocarbons generated during Rock Eval pyrolysis.

8.4.3 Micropetrography, facies indicators and vitrinite reflectance

Representative photomicrographs of coal from the Guchengzi Formation are shown in Fig. 8.6. The vertical variability of maceral composition on a mineral matter free (mmf) basis (Tab. 8.2) is plotted in Fig. 8.4d.

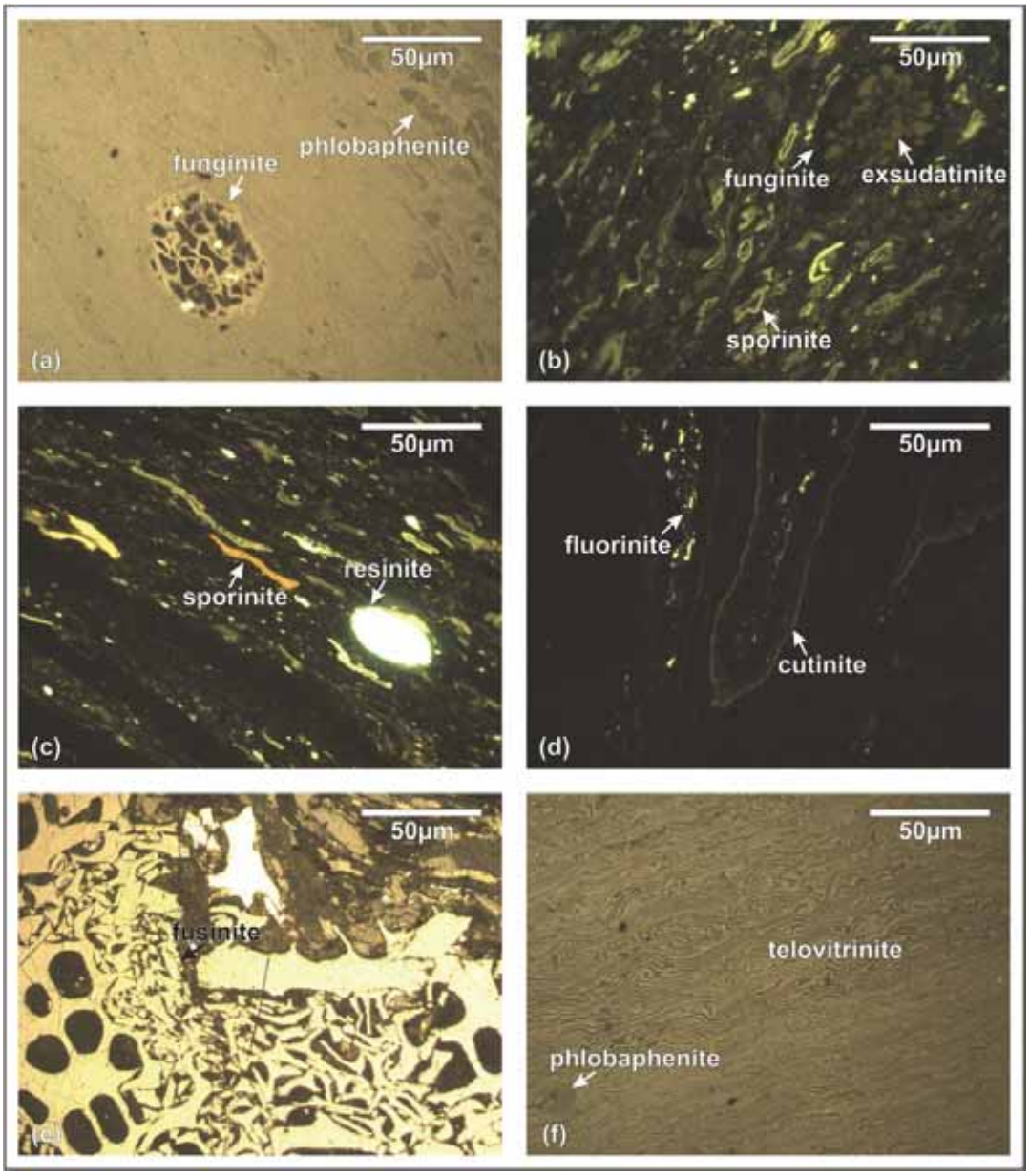

Fig. 8.6: Representative photomicrographs of coal from the Guchengzi Formation (oil immersion). (a) white light: detrovitrinite with phlobaphenite, and funginite. (b) blue-light excitation: detrovitrinite with sporinite, and funginite with exsudatinite. (c) blue-light excitation: detrovitrinite with sporinite, and detrital resinite. (d) blue-light excitation: detrovitrinite with a cross section through several leaves comprising cutinite, and fluorinite. (e) white light: fusinite. (f) white light: telovitrinite with phlobaphenite.

Tab. 8.2: Maceral composition and facies indices.

Sample	BS 1	BS 2	BS 3	BS 4	BS 5	BS 6	BS 7	BS 11	BS 12	BS 13	BS 14b	BS 14	BS 15	BS 18	BS 18a	BS 17	BS 16	BS 21	BS 22	BS 23	BS 24	BS 25	BS 26	BS 27	BS 28	BS 29	BS 30b	BS 30	BS 31
Depth (m)	302.00	300.00	299.00	296.00	294.50	294.00	292.60	291.00	290.00	289.00	288.15	288.09	287.00	276.00	274.30	273.50	272.00	271.60	270.30	269.60	268.60	268.45	268.05	267.75	267.25	266.90	266.60	266.40	265.90
(vol%, mmf)																													
Telinite	8	7	24	14	3	2	7	29	17	5	15	29	12	27	24	28	21	3	18	4	12	6	18	2	12	15	31	36	5
Collotelinite	12	18	50	12	6	16	3	84	18	18	3	19	16	17	17	16	6	35	18	3	23	17	29	64	35	35	14	20	43
Vitrodetrinite	29	26	9	39	43	67	16	85	35	34	32	23	25	20	24	13	17	37	22	28	28	27	24	8	28	30	22	17	39
Collodetrinite	3	3	1	1	0	3	2	3	3	0	1	4	1	3	0	4	4	1	2	0	7	3	2	0	0	0	0	1	0
Pseudinite	4	6	1	0	0	0	0	0	0	0	0	0	0	0	3	4	0	1	2	0	5	0	4	0	2	0	2	4	1
Gelinite	0	0	0	0	0	0	0	0	0	0	0	2	0	0	0	0	0	0	0	0	0	0	0	0	0	0	0	0	0
Phyllovitrinite	8	10	7	15	12	19	8	89	2	17	3	18	26	6	12	7	12	15	5	29	7	15	5	16	5	6	5	4	11
Sporinite	0	1	0	0	0	0	0	2	1	4	2	5	0	4	2	6	4	2	6	1	6	6	18	0	0	13	5	5	1
Cutinite	0	1	0	0	0	0	0	2	1	2	0	3	0	3	2	5	0	2	7	0	5	4	4	0	0	4	2	3	0
Fluorinite	1	1	0	0	0	0	0	1	0	2	0	4	0	4	2	1	0	2	6	0	6	4	0	0	0	0	0	1	0
Resinite-in situ	1	1	0	2	1	0	1	1	0	7	0	2	0	3	2	5	0	0	1	0	6	5	3	0	2	4	0	5	0
Resinite-detrital	3	3	0	1	0	0	1	7	0	9	2	4	1	7	7	4	4	0	1	0	3	5	5	0	2	6	1	4	4
Suberinite	0	0	0	0	0	0	0	0	0	0	0	2	0	0	0	0	0	0	0	0	0	0	0	0	0	0	0	0	0
Liptodetrinite	1	2	0	0	0	0	0	3	0	0	0	2	0	0	0	0	0	0	0	0	0	0	0	0	0	0	0	0	0
Lamalginite	0	0	0	0	0	0	0	0	0	0	0	0	0	0	0	0	0	0	0	0	0	0	0	0	0	0	0	0	0
Telalginite	0	0	0	0	0	0	0	0	0	0	0	0	0	0	0	0	0	0	0	0	0	0	0	0	0	0	0	0	0
Chlorophyllinite	0	0	0	0	0	0	0	0	0	0	0	0	0	0	0	0	0	0	0	0	0	0	0	0	0	0	0	0	0
Bituminite	3	1	0	0	0	0	0	0	0	0	0	0	0	0	0	0	0	0	0	0	0	0	0	0	0	0	0	0	0
Liptodetrinite	0	0	0	0	0	0	0	0	0	0	0	0	0	0	0	0	0	0	0	0	0	0	0	0	0	0	0	0	0
Exsudatinite	0	0	0	0	0	0	0	0	0	0	0	0	0	0	0	0	0	0	0	0	0	0	0	0	0	0	0	0	0
Pyritinite	16	8	4	5	9	0	0	0	0	0	0	0	0	0	0	0	0	0	0	0	0	0	0	0	0	0	0	0	0
Sclerotinite	0	0	0	0	0	0	0	0	0	0	0	0	0	0	0	0	0	0	0	0	0	0	0	0	0	0	0	0	0
Degradofusinite	4	3	1	0	3	0	21	0	0	0	0	0	0	0	0	0	0	0	0	0	0	0	0	0	0	0	0	0	0
Semifusinite	2	3	0	6	7	8	8	9	7	8	2	10	6	2	0	0	0	5	0	20	0	0	0	0	0	0	4	2	0
Fusinite	0	0	0	0	0	0	0	0	0	0	0	0	1	0	1	0	0	0	0	1	0	0	0	0	0	1	0	1	0
Macrinite	0	0	0	0	0	0	0	0	0	3	0	0	0	0	1	0	0	2	0	0	0	1	0	0	0	0	0	0	2
Inertodetrinite	7	3	11	5	6	2	14	1	0	1	1	0	0	0	1	1	0	1	0	0	0	1	0	4	0	0	0	0	0
GWI[1]	0.15	0.20	2.51	0.46	0.94	0.67	0.16	0.09	0.13	0.06	0.45	0.02	0.20	0.04	0.09	0.09	0.86	0.16	0.99	0.31	0.11	0.44	0.69	2.95	0.06	0.09	0.06	0.06	1.58
VI[2]	0.94	0.88	4.25	0.68	0.38	0.29	0.73	1.17	1.03	0.35	0.27	0.69	0.58	0.91	0.92	1.01	1.21	0.60	0.70	0.48	0.51	0.49	0.66	2.52	0.83	1.04	1.83	2.25	1.00
TPI[3]	1.16	1.20	6.54	0.89	0.55	0.42	1.24	2.64	1.27	0.62	0.61	1.42	1.29	1.62	1.67	1.78	2.38	0.88	1.34	1.30	0.79	0.97	1.34	3.60	1.56	1.60	2.31	3.49	1.38

[1]groundwater index, [2]vegetation index, [3]tissue preservation index.

Vitrinite is the major maceral group in the whole coal seam. The prevailing vitrinite macerals are telovitrinite (10-73%) and detrovitrinite (< 50%), whereas gelovitrinite is rare (< 9%). Liptinite is slightly more abundant in the upper section (< 45%) than in the lower one (< 44%). The main liptinite macerals are sporinite, cutinite, fluorinite, resinite and liptodetrinite. Lam- and telalginite appear in minor amounts in the upper section (< 14% and < 3%, respectively). Inertinite shows a general decreasing upward trend within the range of 43 to 1%. Fusinite and inertodetrinite are among the most abundant inertinite macerals. The amount of pyrofusinite predominates over degradofusinite in the lower part, whereas the upper part is characterized by a contrary distribution. Funginite is abundant in the upper part.

Samples with high liptinite contents are typically characterized by high hydrogen indices (Fig. 8.7). However, a better correlation between HI and liptinite was expected. Therefore, additional factors have to be taken into account. Within this context it is worth noting that the percentage of fluorescing, hydrogen-rich ("bituminized") vitrinite is negligible.

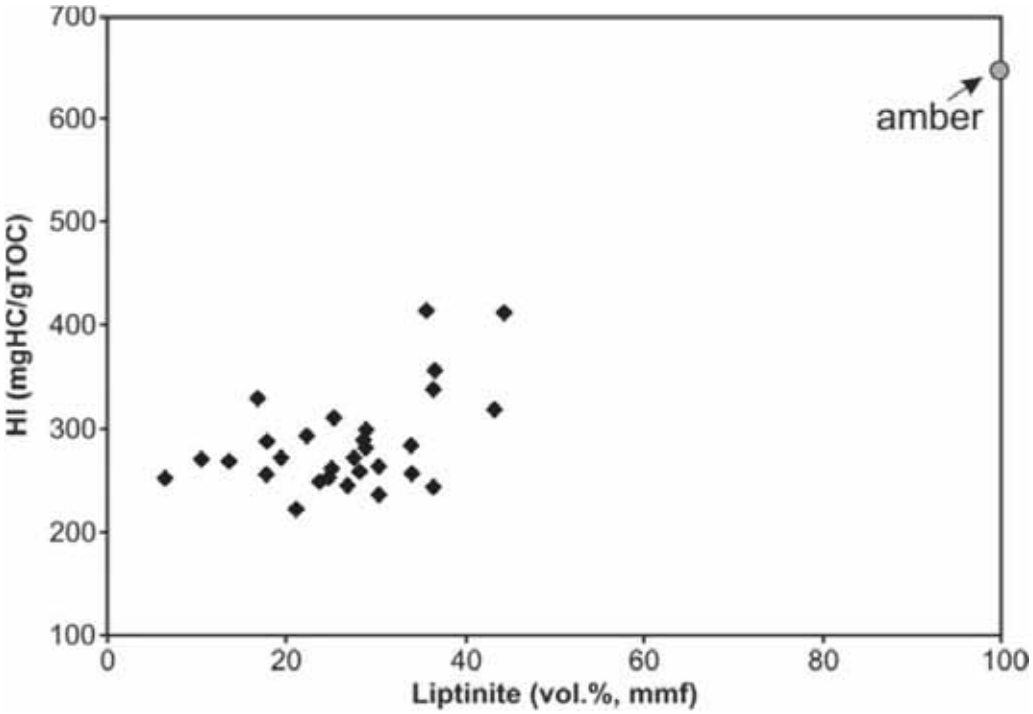

Fig. 8.7: Cross-correlation of HI vs. liptinite content in samples from the Guchengzi Formation.

The GWI typically ranges between 0.02 and 0.46 being higher only in coaly shale and shaly coal in the lower section and in the transition zone near the top of the seam

(Fig. 8.4e). VI and TPI show similar depth trends. Therefore, only VI is shown in Fig. 8.4. In general, VI (0.27 - 1.21) and TPI values (0.42 - 3.45) are low (Fig. 8.4f; Tab. 8.2). However, the coaly shale in the lower section (VI up to 4.25; TPI up to 6.54) and the transition zone near the top of the seam (VI up to 2.52; TPI up to 13.60) show elevated values.

Vitrinite reflectance of the lowermost sample of the Guchengzi Formation (-300.0 m) is 0.52%R_r. The two samples from the upper section have a vitrinite reflectance of 0.51%R_r (-270.3 m) and 0.50%R_r (-265.9 m), respectively.

8.4.4 Organic geochemistry

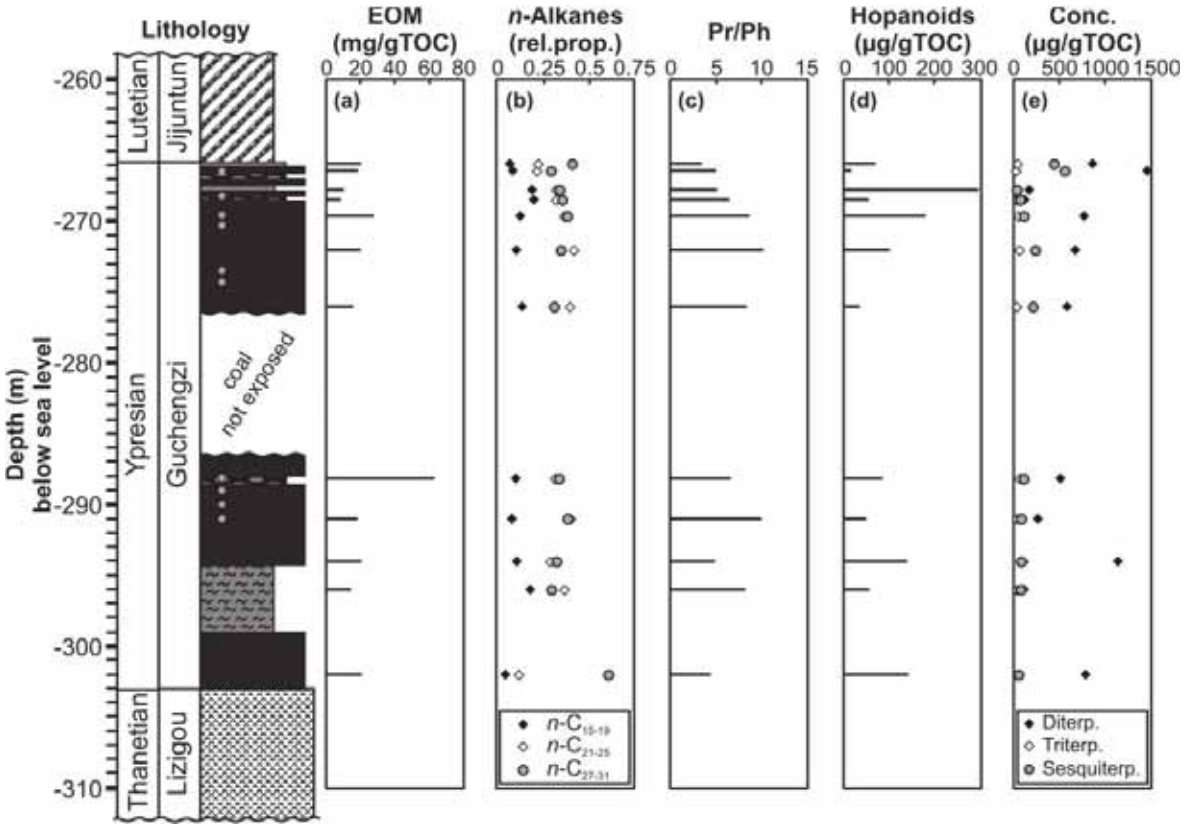

Fig. 8.8: Distribution of (a) extractable organic matter (EOM), (b) ratio of short (*n*-C_{15-19}), intermediate (*n*-C_{21-25}) and long chain (*n*-C_{27-31}) *n*-alkanes to sum of *n*-alkanes, (c) pristane/phytane ratio, (d) hopane concentration, (e) di-, tri- and sesquiterpenoid concentration within the Guchengzi Formation. For lithology see legend of Fig. 8.4.

Tab. 8.3: Results from biomarker analysis.

Sample	Depth (m)	EOM[a] (mg/gTOC)	Sat. HC[b] (%)	Aro. HC[c] (%)	NSO (%)	Asphalt[d] (%)	$n\text{-}C_{15,19}$/ n-alk.	$n\text{-}C_{21,25}$/ n-alk.	$n\text{-}C_{27,31}$/ n-alk.	CPI[e]	PrPh[f]	Hopanes (µg/gTOC)	S/(S+R) hopanes[g]	Benzo-hopanes (µg/gTOC)	Di-terpenoids (µg/gTOC)	Sesqui-terpenoids (µg/gTOC)	Tri-terpenoids (µg/gTOC)
Guchengzi Formation - upper section																	
FS 31	-265.90	20	12	19	55	15	0.06	0.22	0.41	2.1	3.4	79	0.59	12	868	435	24
FS 30	-266.40	19	22	28	35	15	0.08	0.21	0.29	2.1	5.0	16	0.61	2	1480	556	9
FS 27	-267.75	10	20	21	45	14	0.19	0.32	0.34	1.8	5.1	298	0.48	17	157	19	18
FS 25	-268.45	8	17	18	44	22	0.20	0.32	0.35	1.9	6.5	55	0.57	8	105	56	19
FS 23	-269.60	28	10	17	46	26	0.12	0.36	0.38	1.8	8.7	181	0.55	18	772	97	34
FS 16	-272.00	20	13	21	45	21	0.10	0.41	0.34	2.0	10.2	101	0.54	17	673	225	45
FS 18	-276.00	16	9	23	48	19	0.13	0.39	0.31	2.0	8.4	35	0.60	7	581	199	17
Guchengzi Formation - lower section																	
FS 14a	-288.15	63	2	5	22	70	0.10	0.31	0.33	1.8	6.6	86	0.55	14	507	95	49
FS 11	-291.00	18	10	12	57	21	0.08	0.40	0.38	1.9	9.9	49	0.57	7	255	67	23
FS 06	-294.00	20	18	29	40	12	0.10	0.29	0.32	1.7	4.9	140	0.59	15	1151	66	86
FS 04	-296.00	14	10	27	48	15	0.18	0.36	0.29	1.7	8.2	57	0.61	10	98	59	18
FS 01	-302.00	21	19	25	43	14	0.04	0.11	0.60	2.1	4.4	143	0.59	28	789	38	42

[a]extractable organic matter, [b]saturated hydrocarbons, [c]aromatic hydrocarbons, [d]asphaltenes, [e]carbon preference index, [f]pristane/phytane ratio, [g]22S/(22S+22R)-C31 hopane ratio.

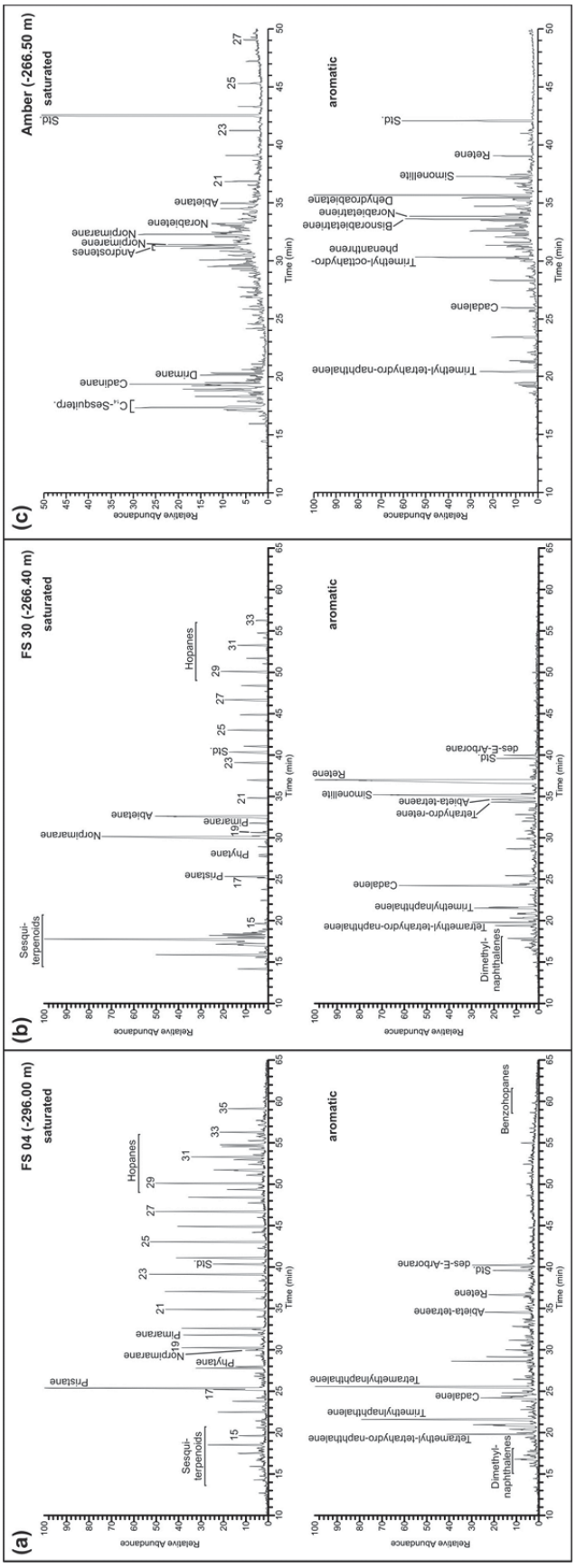

Fig. 8.9: Gas chromatograms (TICs) of saturated and aromatic hydrocarbon fractions of samples from (a) lower section, (b) upper section of the Guchengzi Formation, and (c) of pure amber. Std., standard.

Within the Guchengzi Formation, the amount of extractable organic matter (EOM) varies between 8 and 63 mg/gTOC (Fig. 8.8a). The proportion of hydrocarbons ranges between 8 and 50% of EOM. Aromatic hydrocarbons are predominant over saturated hydrocarbons. The EOM is also composed of NSO compounds and asphaltenes (Tab. 8.3).

Total ion chromatograms (TICs) of alkane and aromatic hydrocarbon fractions of representative samples from the lower and the upper sections of the Guchengzi Formation are shown in Fig. 8.9. The concentrations and concentration ratios of compounds and compound groups in hydrocarbon fractions are listed in Tab. 8.3.

Both sections are dominated by *n*-alkanes of intermediate (*n*-C_{21-25}) and long (*n*-C_{27-31}) chain length with and odd to even predominance (Fig. 8.8b). The carbon preference index (CPI; Bray and Evans, 1961) varies between 1.66 and 2.15. Short-chain *n*-alkanes show enhanced values in the coaly shale parts. Long-chain lipids are known as biomarkers for higher terrestrial plants (Gülz et al., 1992), whereas short-chain lipids are predominantly found in algae and micro-organisms (Cranwell, 1984).

The acyclic isoprenoids pristane (Pr) and phytane (Ph) are present in all samples. The Pr/Ph ratios are high (3.4-10.2) within the Guchengzi Formation. They show a general increasing upward trend within the lower section and decrease upward within the upper section (Fig. 8.8c). Didyk et al. (1978) considered the Pr/Ph ratio as a redox parameter. High Pr/Ph values (> 3.0) indicate the input of terrigenous organic matter under oxic conditions. Values between 1.0 and 3.0 were interpreted as reflecting dysoxic conditions during early diagenesis, and values below 1.0 have been proposed to indicate anoxic conditions.

The hopanoid patterns are characterized by 17α, 21β and 17β, 21α hopanes from C_{27} to C_{32}, with C_{28} hopanes absent. The predominant hopanoid in all samples is the 17α, 21β-C_{31} hopane. Hopanes are contained in a relative low amount (16-298 µg/gTOC; Fig. 8.8d). The most probable biological precursors of hopanoids found in coals are aerobic bacteria and fungi (Ourisson et al., 1979; Rohmer et al., 1992; Bechtel et al., 2001). The ratio of 22S to 22S plus 22R isomers of the 17α, 21β-C_{31} hopanes shows an increasing downward trend ranging from 0.48 to 0.61, which agrees with a downward increasing maturity. Benzohopanes occur in all samples in relatively low

amounts (2-28 µg/gTOC). These compounds are of bacterial derivation (Hussler et al., 1984).

Diterpenoids (e.g. norpimarane, pimarane, abietane, simonellite, retene) occur in relatively high amounts (98-1480 µg/gTOC) in all coal samples, showing their highest abundance near the top of the seam (Fig. 8.8e). Sesquiterpenoids (e.g. cadinane, drimane, eudesmane, homodrimane, cadalene) show a parallel trend to the distribution of diterpenoids, but sesquiterpenoids occur in relative lower amounts (19-556 µg/gTOC; Fig. 8.8e). Di- and sesquiterpenoids indicate that conifer species predominate the coal-forming flora (e.g. Otto et al., 1997; Otto and Wilde, 2001), suggesting a high contribution of resinous organic matter. The relative abundances of pimarane derivatives show a general decrease upward, whereas the contribution of abietane derivatives to the total diterpenoids increases towards the top of the seam. This change in terpenoid hydrocarbon composition may reflect changes in the paleovegetation. Aromatic non-hopanoid triterpenoids (e.g. trimethyl-tetrahydro-chrysenes, tetramethyl-octahydro-picenes) occur in relative low concentrations (9-86 µg/gTOC) through the whole Guchengzi Formation (Fig. 8.8e). These triterpenoids are known as biomarkers for angiosperms (Karrer et al., 1977; Dev, 1989).

Total ion chromatograms (TICs) of saturated and aromatic hydrocarbon fractions of pure amber at a depth of -266.50 m are shown in Fig. 8.9. The proportion of hydrocarbons is very low (< 5% of EOM), whereas the amount of NSO compounds is very high (> 90% of EOM). As expected, the pure amber consists mainly of diterpenoids of the abietane- and pimarane-type, and sesquiterpenoids of the cadinane- and drimane-type.

8.4.5 Compound-specific stable isotope geochemistry

The carbon isotopic composition of short and long chain *n*-alkanes, pristane and phytane, and sesqui- and diterpenoids of 12 samples from the Guchengzi Formation is plotted in Fig. 8.10. The results of the analyses are listed in Tab. 8.4.

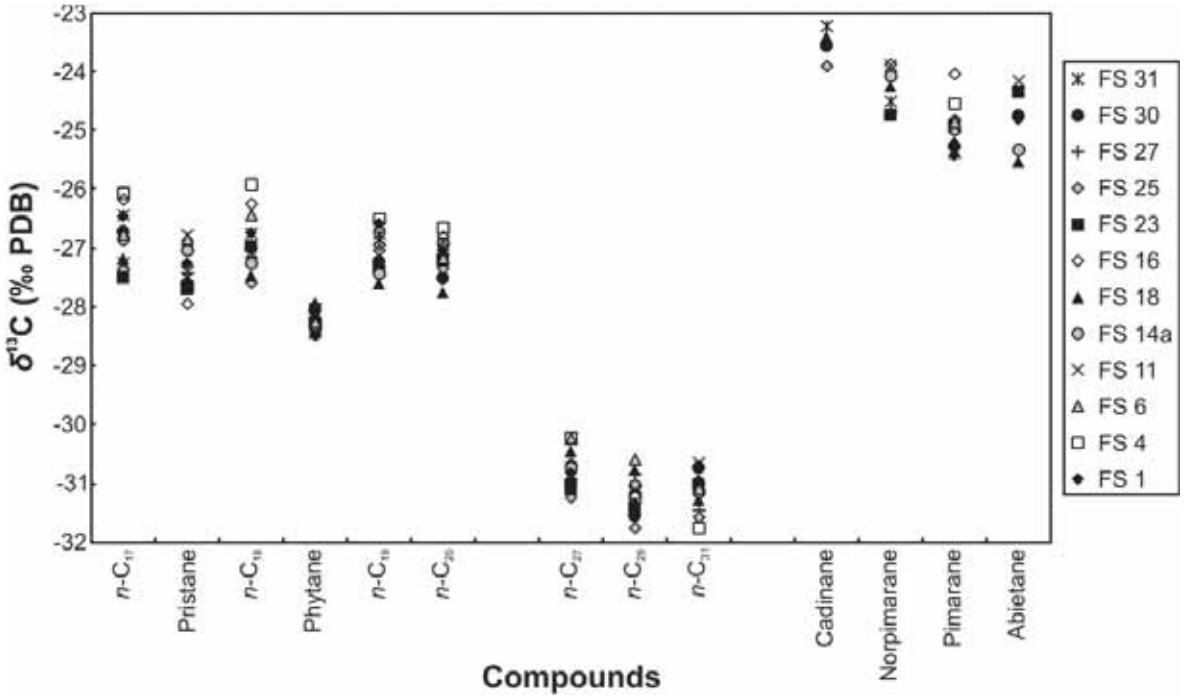

Fig. 8.10: Carbon isotopic composition of selected compounds in saturated hydrocarbon fractions of selected samples from the Guchengzi Formation.

The $\delta^{13}C$ values for the *n*-C_{17} to *n*-C_{20} alkanes vary between -26 and -28‰. The odd long chain *n*-alkanes (*n*-C_{27} to *n*-C_{31}) are more depleted in ^{13}C (ca. 4‰) than the short chain *n*-alkanes. This result argues for a contribution of terrigenous organic matter (i.e. C_3 plants; O'Leary, 1988; Farquhar et al., 1989; Collister et al., 1994; Murray et al., 1994).

The acyclic isoprenoids pristane and phytane are more depleted in ^{13}C than the short chain *n*-alkanes, whereas phytane is slightly more depleted (ca. 1‰) than pristane. This nearly equal $\delta^{13}C$ of both compounds argues for a similar precursor (i.e. chlorophyll; Didyk et al., 1978; Goossens et al., 1984).

Sesqui- and diterpenoids are enriched in ^{13}C and vary between -23 and -25‰, which is a range reported for such compounds in other coals (e.g. Schoell et al., 1994).

Tab. 8.4: Results from compound-specific stable isotope geochemistry.

Sample	Depth (m)	n-C_{17} ($\delta^{13}C$, ‰, PDB)	Pristane ($\delta^{13}C$, ‰, PDB)	n-C_{18} ($\delta^{13}C$, ‰, PDB)	Phytane ($\delta^{13}C$, ‰, PDB)	n-C_{19} ($\delta^{13}C$, ‰, PDB)	n-C_{20} ($\delta^{13}C$, ‰, PDB)	n-C_{27} ($\delta^{13}C$, ‰, PDB)	n-C_{29} ($\delta^{13}C$, ‰, PDB)	n-C_{31} ($\delta^{13}C$, ‰, PDB)	Cadinane ($\delta^{13}C$, ‰, PDB)	Norpimarane ($\delta^{13}C$, ‰, PDB)	Pimarane ($\delta^{13}C$, ‰, PDB)	Abietane ($\delta^{13}C$, ‰, PDB)
Guoluogzi Formation - upper section														
FS-31	-265.90	-26.4	-27.5	-26.7	-28.3	-26.8	-26.9		-31.5	-30.7	-23.2	-24.5	-25.4	
FS-30	-266.40	-26.7	-27.6	-27.0	-28.0	-27.2	-27.5	-31.0	-30.8	-31.1	-23.6		-25.3	-24.7
FS-27	-267.75	-26.8	-27.4	-27.1	-27.9	-27.3	-27.1	-30.9	-30.8	-31.4		-24.7		
FS-25	-268.45	-27.4	-27.3	-27.6	-28.5	-27.0	-27.3	-31.2	-31.7	-31.6	-23.9		-24.8	
FS-23	-269.60	-27.5	-27.7	-27.0	-28.3	-27.3	-27.2	-31.1	-31.4	-31.0		-24.7	-24.9	-24.3
FS-16	-272.00	-26.2	-27.9	-26.2	-28.4	-26.9	-26.8	-30.7	-31.2	-31.0		-23.9	-24.0	
Guoluogzi Formation - lower section														
FS-18	-276.00	-27.2	-27.6	-27.5	-28.4	-27.6	-27.7	-30.4	-30.8	-31.3	-23.4	-24.2	-25.2	-25.5
FS 14a	-288.15	-26.8	-27.0	-27.2	-28.3	-27.4	-26.9	-30.7	-31.0	-31.1		-24.1	-25.0	-25.3
FS-11	-291.00	-27.2	-26.8	-27.1	-28.1	-26.7	-26.9	-30.9	-31.1	-30.6		-23.9	-24.9	-24.1
FS-06	-294.00	-26.8	-26.8	-26.4	-28.2	-26.6	-27.2	-30.2	-30.6	-31.1			-24.8	
FS-04	-296.00	-26.1	-27.6	-25.9	-28.3	-26.5	-26.6	-30.2	-31.2	-31.7			-24.5	
FS-01	-302.00	-26.5	-27.3	-26.7	-28.0	-26.6	-27.0	-30.8	-31.3	-30.9			-25.4	-24.8

8.5 Discussion

8.5.1 Depositional environment

The thickness of coal seams is controlled by the interplay of subsidence and peat accumulation rates (e.g. McCabe, 1991). The total thickness of the coal seam in the Guchengzi Formation is very high. This shows that peat accumulation kept pace with basin subsidence for long time. However, in areas with the highest subsidence rate (hanging wall of syn-sedimentary normal faults), coal passes laterally into clastic facies (Fig. 8.2b) showing that at these sites subsidence exceeded peat accumulation rate.

Finally, subsidence rate increased in the entire basin and the mire was replaced by a basin-wide lacustrine system.

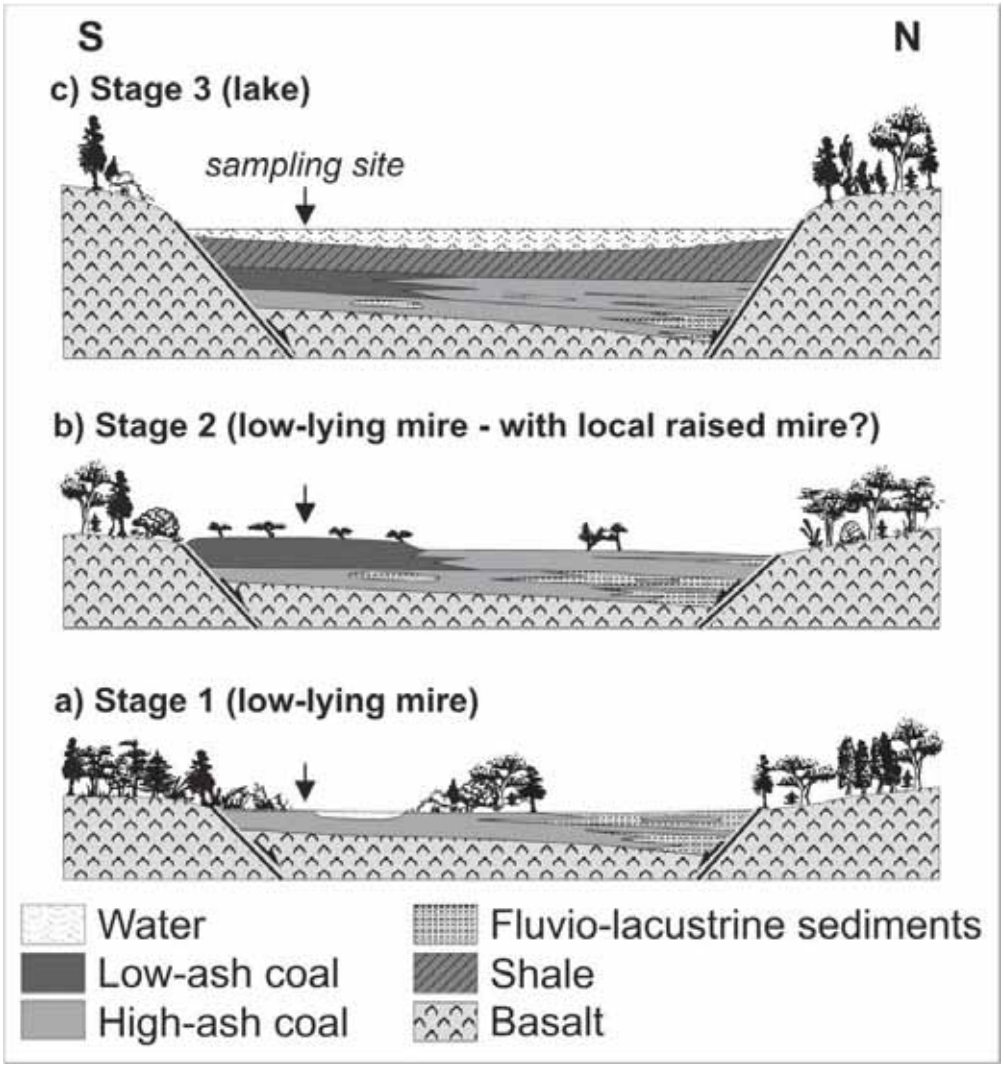

Fig. 8.11: Cartoon illustrating three stages of the evolution of the Fushun coal seam.

At the sampling site, the Fushun coal seam consists, from base to top, of (1) high-ash coal and coaly shale, (2) low-ash coal, and (3) a transition zone between coal and shale. These lithotypes reflect three different stages of peat accumulation (Fig. 8.11) discussed in detail below. Unfortunately the transition between the high- and low-ash coal is not exposed.

8.5.1.1 Stage 1 (low-lying mire)

Coals with relative high ash yields indicate that peat accumulation commenced in a low-lying (topogenous) mire (fen; see Fig. 8.11a). The coaly shale may be derived from a fluvio-lacustrine environment. This interpretation is supported by the lateral intercalating clastic layers (Johnson, 1990; Wu et al., 2000; Fig. 8.2b). The moderate to low sulfur content (Tab. 8.1) suggests mire development in a freshwater environment. The enrichment of sulfur at the impermeable base of the seam is probably a result of an increase in pH-value permitting sulfate-reducing bacteria to thrive (Casagrande, 1987). Apart from the base, sulfur content is enriched only in a thin layer with abundant framboidal pyrite near the top of the lower section. The cause of the sulfur-enrichment remains unclear, but may be related to a rise in water level resulting in more reducing and less acidic conditions.

A relative high GWI (Tab. 8.2) indicates that the topogenous mire was influenced by a relative high water-table. Nevertheless, high pristane/phytane ratios indicate oxic conditions.

High VI and TPI values reflect the abundance of decay-resistant plants (e.g. conifers). This is also supported by the predominance of conifer derived di- and sesquiterpenoids over angiosperm derived triterpenoids. The occurrence of resinite and amber also argues for a vegetation rich in conifers.

8.5.1.2 Stage 2 (low-lying mire with local raised mire?)

During stage 2, peat accumulation expanded northward. The number of seam partings is relatively low and increases northward (Fig. 8.2b; Fig. 8.11b). The partings suggest a northern sediment source and deposition in a low-lying mire.

At the sampling site in the southern portion of the basin, the lower part of the upper section of the coal seam is characterized by low ash coal with sulfur contents below 1%. Low-ash and low-sulfur coals are formed in freshwater topogenous mires, which are far from any detrital input, and in ombrogenous raised mires (bogs, see Fig. 8.11b; Diessel, 1992).

In the present case, petrography-based (telovitrinite percentages, VI, TPI) and biomarker-based (di-, sesqui-, triterpenoids) proxies, which do not show significant differences in the vegetation type (gymnosperm/angiosperm ratio) between the low-ash coal and the underlying ash-rich stage 1 coal, argue for deposition in a low-lying mire.

On the other hand, strike-slip basins, characterized by high subsidence rates, are traps for sediments. Within this frame, ash yields around 2% are extremely low. In addition, very low GWI values (Tab. 8.2) may be interpreted as an indicator for a dry depositional environment characteristic for raised mires, which are not affected by surficial waters. Strongly oxic conditions at the peat surface are indicated by very high pristane/phytane ratios (Tab. 8.3) and the abundance of (semi)degradofusinite as the main inertinite maceral. Thus, local and impermanent bog formation with limited peat accumulation cannot be excluded.

8.5.1.3 Stage 3 (transition zone between mire and lake)

The transition zone between coal and shale in the uppermost part of the upper section indicates flooding of the mire (Fig. 8.11c). Peat accumulation was ceased by rapid subsidence, resulting in a lacustrine environment in which organic-rich shales were deposited. Significant amounts of land-plant material were transported into the shallow lake after termination of peat accumulation (Strobl et al., 2014).

Highly variable ash yields, GWI and VI values (Tab. 8.2) point to unstable conditions during flooding. Sulfur contents also vary significantly between 0.4 and 2.2%. Nevertheless, they indicate deposition in a freshwater environment.

Conifers continued to predominate over angiosperms. Biomarker composition also proves the origin of amber from conifers. Apart from terrestrial plants, the presence

of aquatic organisms is indicated by alginite and elevated percentages of short-chain *n*-alkanes in two samples from the transition zone.

Pristane/phytane ratios (Tab. 8.3) are decreasing upward in the transition zone reflecting a trend from oxic to less oxic conditions.

8.5.2 Thermal history

A continuous maturity trend is reflected by downward increasing (22S/(22S+22R))-hopane ratios and T_{max} values within the Jijuntun and Guchengzi formations. The sub-bituminous rank of the Fushun coal is expressed by vitrinite reflectance values of 0.50 to 0.52%R_r.

Simple 1D thermal models calibrated with hopane isomerization ratios and vitrinite reflectance have been established to determine paleo-heat flow and thickness of eroded rocks. Input parameters include the lithology and present-day thickness of preserved rocks (Tab. 8.5). Petrophysical parameters pre-defined by the software (PetroMod 1D) have been considered. The thickness of eroded rocks, attributed to the Gengjiajie Formation, has been modified between 0 and 900 m. Absolute ages follow Quan et al. (2012). To keep the models simple, time-constant heat flows were applied.

Tab. 8.5: Input data for 1D thermal modeling.

Formation	Top (m)	Base (m)	Thickness (m)	Deposition (Ma)		Lithology
				From	To	
Gengjiajie	0	130	130	37.0	30.0	SILTsandy
Xilutian	130	411	281	40.5	37.0	LIMEshaly
Jijuntun	411	466	55	48.5	40.5	Shale (organic rich, 8% TOC)
Guchengzi	466	502	36	56.0	48.5	COALshaly
					56.0	

The models show the best fit applying a very high heat flow of 210 mW/m^2 and an erosional thickness of 0 m (Fig. 12; solid lines). Models with lower heat flows (133 and 100 mW/m^2) and higher amounts of erosion (450 and 900 m, respectively) overestimate vitrinite reflectance and produce a worse fit with the observed hopane isomerization trend. Thus, the models suggest minor erosion and very high heat flow during maximum burial. Heat flows exceeding 150 mW/m^2 are typically found in areas with magmatic heating. As suggested by Wu et al. (2000), intrusion of diabase

sills in the Laohutai and Lizigou formations after coal deposition may be responsible for the high Eocene heat flow.

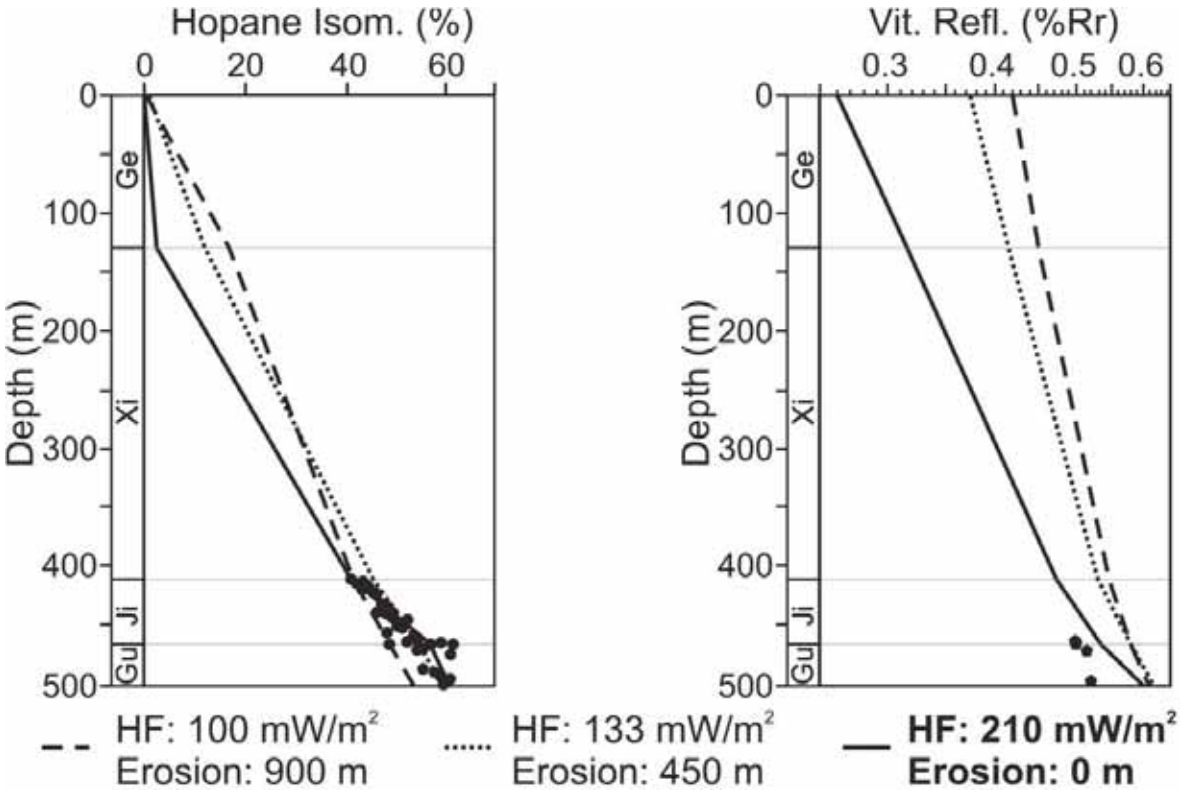

Fig. 8.12: 1D thermal models. Measured (dots) and calculated (lines) data plotted versus depth. Abbreviations: Gu, Guchengzi Formation; Ji, Jijuntun Formation; Xi, Xilutian Formation; Ge, Gengjiajie Formation; Hopane Isom., Hopane Isomerization; Vit. Refl., Vitrinite Reflectance; HF, Heat Flow.

8.6 Conclusions

The Eocene coal-bearing Guchengzi Formation in the Fushun Basin was deposited in a rapidly subsiding strike-slip basin. The coal being hydrogen-rich and oil-prone, is of sub-bituminous rank at the study site in the southwestern part of the basin, but reaches the high volatile bituminous rank in the eastern part of the basin.

The lower part of the coal seam is ash-rich and represents a low-lying mire environment, in which gymnosperms predominated over angiosperms. The middle part of the investigated profile is not exposed. At the study site, low-ash, low-sulfur coal predominates in the upper part of the seam. Petrography- and biomarker-based

proxies for vegetation types argue for accumulation in a low-lying mire. However, based on very low ash yields and proxies for eH conditions, deposition in a raised mire cannot be excluded. In any case, a topogenous mire existed in the northern part of the basin.

The uppermost part of the seam is characterized by a transition zone between coal and shale indicating the flooding of the freshwater mire and the termination of peat accumulation. Organic-rich shales of the overlying oil shale-bearing Jijuntun Formation were deposited in the newly formed lake.

A 1D thermal model suggests minor erosion and a high heat flow during maximum burial depth of the sub-bituminous coal. The high heat flow is likely due to Late Oligocene magmatic activity, indicated by diabase sills.

8.7 Acknowledgments

We would like to express our gratitude to Mr. Han Fang from the Fushun Mining Group Co., Ltd. who generously permitted us to take samples in the West Open Pit mine in Fushun (NE China) and to Prof. Zhaojun Liu from the Jilin University in Changchun (NE China) for his help and organization of the field trips. The authors also want to thank Mrs. Rong Liu, Mr. Pingchang Sun and Mr. Jianliang Jia for their help during the fieldwork. We are particularly grateful to two anonymous reviewers and the editor Prof. Shifeng Dai for their helpful comments.

8.8 References

Bechtel, A., Gruber, W., Sachsenhofer, R.F., Gratzer, R., Püttmann, W., 2001. Organic geochemical and stable isotopic investigation of coals formed in low-lying and raised mires within the Eastern Alps (Austria). Organic Geochemistry 32, 1289-1310.

Bechtel, A., Gruber, W., Sachsenhofer, R.F., Gratzer, R., Lücke, A., Püttmann, W., 2003. Depositional environment of the Late Miocene Hausruck lignite (Alpine Foreland

Basin): insights from petrography, organic geochemistry, and stable carbon isotopes. International Journal of Coal Geology 53, 153-180.

Bechtel, A., Reischenbacher, D., Sachsenhofer, R.F., Gratzer, R., Lücke, A., Püttmann, W., 2007. Relations of petrographical and geochemical parameters in the middle Miocene Lavanttal lignite (Austria). International Journal of Coal Geology 70, 325-349.

Bray, E.E., Evans, E.D., 1961. Distribution of *n*-paraffins as a clue to recognition of source beds. Geochimica et Cosmochimca Acta 22, 2-15.

Calder, J.H., Gibling, M.R., Mukhopadhyay, P.K., 1991. Peat formation in a Westphalian B piedmont setting, Cumberland basin, Nova Scotia: implications for the maceral-based interpretation of rheotrophic and raised paleomires. Bull. Soc. Geol. Fr. 162, 283-298.

Casagrande, D.J., 1987. Sulphur in peat and coal, in: Scott, A.C. (Ed.), Coal and Coal-Bearing Strata: Recent Advances. Geological Society Special Publication 32, London, pp. 87-105.

Collister, J.W., Rieley, G., Stern, B., Eglinton, G., Fry, B., 1994. Compound-specific $\delta^{13}C$ analysis of leaf lipids from plants with differing carbon dioxide metabolism. Organic Geochemistry 21, 619-627.

Coplen, T.B., 2011. Guidelines and recommended terms for expression of stable-isotope-ratio and gas-ratio measurement results. Rapid Communications in Mass Spectrometry 25, 2538-2560.

Cranwell, P.A., 1984. Lipid geochemistry of sediments from Upton Broad, a small productivity lake. Organic Geochemistry 7, 25-37.

Deutsches Institut für Normung (DIN) 51718, 1978. Feste Brennstoffe; Bestimmung des Wassergehaltes.

Deutsches Institut für Normung (DIN) 51719, 1980. Feste Brennstoffe; Bestimmung des Aschegehaltes.

Dev, S., 1989. Terpenoids; in: Rowe, J.W. (Ed.), Natural Products of Woody Plants. Springer, Berlin, pp. 691-807.

Didyk, B.M., Simoneit, B.R.T., Brassell, S.C., Eglinton, G., 1978. Organic geochemical indicators of paleoenvironmental conditions of sedimentation. Nature 272, 216-222.

Diessel, C.F.K., 1986. The correlation between coal facies and depositional environments. Proc. 20th Symp. Dep. Geol., Univ. Newcastle, Newcastle, NSW, 11-22.

Diessel, C.F.K., 1992. Coal- bearing Depositional Systems. Springer, Berlin, 721 pp.

Erdenetsogt, B.-O., Lee, I., Bat-Erdene, D., Jargal, L., 2009. Mongolian coal-bearing basins: Geological settings, coal characteristics, distribution, and resources. International Journal of Coal Geology 80, 87-104.

Farquhar, G.D., Ehleringer, J.R., Hubick, K.T., 1989. Carbon isotope discrimination and photosynthesis. Annual Review of Plant Physiology and Plant Molecular Biology 40, 503-537.

Goossens, H., de Leeuw, J.W., Schenck, P.A., Brassel, S.C., 1984. Tocopherols as likely precursors of pristane in ancient sediments and crude oils. Nature 312, 440-442.

Gruber, W., Sachsenhofer, R.F., 2001. Coal deposition in the Noric Depression (Eastern Alps): raised and low-lying mires in Miocene pull-apart basins. International Journal of Coal Geology 48, 89-114.

Gülz, P.-G., Müller, E., Herrmann, T., 1992 Chemical composition and surface structures of epicuticular leaf waxes from Castanea sativa and Asculus hippocastanum. Z. Naturforsch. C. 47, 661-666.

Hong, Y., Yang, Z., Wang, S., Sun, X., Du, N., Sun, M., Li, Y., 1980. A Research on the Strata and Paleontology of the Fushun Coal Field in Liaoning Province. Science Press, Beijing.

Huang, Z., Liu, Z., Dai, H., Xu, S., 1983. On the sedimentary environment of the coal-bearing formation in the Fushun coal basin. Acta Geol. Sin. 57 (3), 261-269.

Hussler, G., Albrecht, P., Ourisson, G., 1984. Benzohopanes, a novel family of hexacyclic geomarkers in sediments and petroleums. Tetrahedron Letters 25, 1179-1182.

International Committee for Coal and Organic Petrology (ICCP), 1998. The new vitrinite classification (ICCP System 1994). Fuel 77, 349-358.

International Committee for Coal and Organic Petrology (ICCP), 2001. The new inertinite classification (ICCP System 1994). Fuel 80, 459-471.

Johnson, E.A., 1990. Geology of the Fushun coalfield, Liaoning Province, People's Republic of China. International Journal of Coal Geology 14, 217-236.

Kalkreuth, W., Kotis, T., Papanicolaou, C., Kokkinakis, P., 1991. The geology and coal petrology of a Miocene lignite profile at Meliadi Mine Katerini, Greece. International Journal of Coal Geology 17, 51-67.

Karrer, W., Cherbuliez, E., Eugster, C.H., 1977. Konstitution und Vorkommen der organischen Pflanzenstoffe – Ergänzungsband 1. Birkhäuser, Basel – Stuttgart.

Lambiase, J.J., 1990. A model for tectonic control of lacustrine stratigraphic sequences in continental rift basins, in: Katz, B.J. (Ed.), Lacustrine basin exploration: case studies and modern analogs. AAPG Memoir 50, 265-276.

Liu, Z., Yang, H., Dong, Q., Zhu, J., Guo, W., Ye, S., Liu, R., Meng, Q., Zhang, H., Gan, S., 2009. Oil Shale in China. Petroleum Industry Press, Beijing.

Ma, X., Jiang, H., Cheng, J., Xu, H., 2012. Spatiotemporal evolution of Paleogene palynoflora in China and its implication for development of the extensional basins in East China. Review of Paleobotany and Palynology 184, 24-35.

Mackenzie, A.S., McKenzie, D.P., 1983. Aromatization and isomerization of hydrocarbons in sedimentary basins formed by extension. Geological Magazine 120, 417-470.

Markic, M., Sachsenhofer, R.F., 1997. Petrographic composition and depositional environments of the Pliocene Velenje lignite seam (Slovenia). International Journal of Coal Geology 33, 229-254.

McCabe, P.J., 1991. Tectonic controls on coal accumulation. Bulletin de la Société géologique de France 162, 277-282.

Meng, Q., Liu, Z., Bruch, A.A., Liu, R., Hu, F., 2012. Paleoclimatic evolution during Eocene and its influence on oil shale mineralisation, Fushun basin, China. Journal of Asian Earth Sciences 45, 95-105.

Mosbrugger, V., Utescher, T., 1997. The coexistence approach – a method for quantitative reconstructions of Tertiary terrigenous paleoclimate data using plant fossils. Paleogeography, Paleoclimatology, Paleoecology 134, 61-86.

Murray, A.P., Summons, R.E., Boreham, C.J., Dowling, L.M., 1994. Biomarker and *n*-alkane isotope profiles for Tertiary oils: relationship to source rock depositional setting. Organic Geochemistry 22, 521-542.

O'Leary, M.H., 1988. Carbon Isotopes in Photosynthesis – Fractionation techniques may reveal new aspects of carbon dynamics in plants. BioScience 38, 328-336.

Otto, A., Walther, H., Püttmann, W., 1997. Sesqui- and diterpenoid biomarkers in Taxodium-rich Oligocene oxbow lake clays Weisselster basin, Germany. Organic Geochemistry 26, 105-115.

Otto, A., Wilde, V., 2001. Sesqui-, di-, and triterpenoids as chemosystematic markers in extant conifers – a review. Botanical Review 67, 141-238.

Ourisson, G., Albrecht, P., Rohmer, M., 1979. The hopanoids: paleo-chemistry and biochemistry of a group of natural products. Pure and Applied Chemistry 51, 709-729.

Pepper, A.S., Corvi, P.J., 1995. Simple kinetic models of petroleum formation. Part III: modeling an open system. Marine and Petroleum Geology 12, 417-452.

Peters, K.E., Moldowan, J.M., 1993. The Biomarker Guide: Interpreting Molecular Fossils in Petroleum and Ancient Sediments. Prentice Hall, Englewood Cliffs.

Quan, C., Liu, Y., Utescher, T., 2012. Paleogene temperature gradient, seasonal variation and climate evolution of northeast China. Paleogeography, Paleoclimatology, Paleoecology 313-314, 150-161.

Radke, M., Willsch, H., Welte, D.H., 1980. Preparative hydrocarbon group type determination by automated medium pressure liquid chromatography. Analytical Chemistry 52, 406-411.

Rohmer, M., Bisseret, P., Neunlist, S., 1992. The hopanoids, prokaryotic triterpenoids and precursors of ubiquitous molecular fossils, in: Moldowan, J.M., Albrecht, P., Philp, R.P. (Eds.), Biological Markers in Sediments and Petroleum. Prentice Hall, New Jersey, 1-17.

Sachsenhofer, R.F., 2000. Geodynamic controls on deposition and maturation of coal in the Eastern Alps, in: Neubauer, F., Höck, V. (Eds.), Aspects of Geology in Austria. Mitteilungen der Österreichischen Geologischen Gesellschaft 92, 185-194.

Sachsenhofer, R.F., Bechtel, A., Reischenbacher, D., Weiss, A., 2003. Evolution of lacustrine systems along the Miocene Mur-Mürz fault system (Eastern Alps, Austria) and implications on source rocks in pull-apart basins. Marine and Petroleum Geology 20, 83-110.

Schoell, M., Simoneit, B.R.T., Wang, T.-G., 1994. Organic geochemistry and coal petrology of tertiary brown coal in the Zhoujing mine, Baise Basin, South China – 4. Biomarker sources inferred from stable carbon isotope compositions of individual compounds. Organic Geochemistry 21, 713-719.

Strobl, S.A.I., Sachsenhofer, R.F., Bechtel, A., Gratzer, R., Gross, D., Bokhari, N.H., Liu, R., Liu, Z., Meng, Q., Sun, P., 2014. Depositional environment of oil shale within the Eocene Jijuntun Formation in the Fushun Basin (NE China). Marine and Petroleum Geology 56, 166-183.

Su, K., Quan, C., Liu, Y., 2014. Cycas fushunensis sp. nov. (Cycadaceae) from the Eocene of northeast China. Review of Paleobotany and Palynology 204, 43-49.

Sun, P., Sachsenhofer, R.F., Liu, Z., Strobl, S.A.I., Meng, Q., Liu, R., Zhen, Z., 2013. Organic matter accumulation in the oil shale- and coal-bearing Huadian Basin (Eocene; NE China). International Journal of Coal Geology 105, 1-15.

Sweeney, J.J., Burnham, A.K., 1990. Evaluation of a simple model of vitrinite reflectance based on chemical kinetics. AAPG Bulletin 74, 1559-1570.

Sykes, R., Snowdon, L.R., 2002. Guidelines for assessing the petroleum potential of coaly source rocks using Rock-Eval pyrolysis. Organic Geochemistry 33, 1441-1455.

Sýkorová, I., Pickel, W., Christanis, K., Wolf, M., Taylor, G.H., Flores, D., 2005. Classification of huminite – ICCP System 1994. International Journal of Coal Geology 62, 85-106.

Taylor, H., Teichmüller, M., Davis, A., Diessel, C.F.K., Littke, R., Robert, P., 1998. Organic Petrology. Borntraeger. Berlin-Stuttgart.

von der Brelie, G., Wolf, M., 1981. Zur Petrographie und Palynologie heller und dunkler Schichten im rheinischen Hauptbraunkohlenflöz. Fortschr. Geol. Rheinl. Westfalen 29, 95-163.

Wang, Q., Ferguson, D.K., Feng, G., Ablaev, A.G., Wang, Y., Yang, J., Li, Y., Li, C., 2010. Climatic change during the Paleaocene to Eocene based on fossil plants from Fushun, China. Paleogeography, Paleoclimatology, Paleoecology 295, 323-331.

Wu, C., Yuan, Y., Li, S., 1998. The synsedimentary structure framework and its control on the thickness of extra-thick coal bed and oil shale, Fushun Basin, China. Coal Geology and Exploration 6, 2-7.

Wu, C., Yang, Q., Zhu, Z., Liu, G., Li, X., 2000. Thermodynamic analysis and simulation of coal metamorphism in the Fushun Basin, China. International Journal of Coal Geology 44, 149-168.

Wu, C., Wang, X., Liu, G., Li, S., Mao, X., Li, X., 2002. Study on dynamics of tectonic evolution in the Fushun Basin, Northeast China. Science in China 45, 311-324.

Xu, S., Liu, Z., Dong, Q., Liu, S., Liu, R., Meng, Q., 2012. Eocene sedimentary evolution and its control over coal and oil shale development in Fushun Coalfield. Journal of China University of Petroleum 36, 45-67.

9 Deposition of coal and oil shale in NE China: the Eocene Huadian Basin compared to the coeval Fushun Basin

Submitted to Marine and Petroleum Geology

Susanne A.I. Strobl[a], Reinhard F. Sachsenhofer[a], Achim Bechtel[a], Qingtao Meng[b], Pingchang Sun[b]

[a] Department of Applied Geosciences and Geophysics, Montanuniversitaet Leoben, Peter-Tunner-Straße 5, 8700 Leoben, Austria
[b] College of Earth Sciences, Jilin University, Changchun 130061, China

Keywords

Huadian Basin; Fushun Basin; depositional environment; organic geochemistry; coal; oil shale

Abstract

The Huadian and Fushun basins, located along the DunMi fault zone (NE China), are filled with non-marine coal- and oil shale-bearing sediments of Eocene age. Despite similar tectonic setting, the habitat of coal and oil shale differs significantly. During this study the depositional environment of organic-rich sediments in the Huadian Basin and factors controlling differences between both basins were investigated. Early in the history of the Huadian Basin, thin coaly and bituminous mudstones accumulated in shallow lake environments (Pyrite Member). Water depth increased during deposition of the Oil Shale Member, but did not exceed a few tens of meters preventing stable water column stratification. Moreover, deposition of fan delta sediments interrupted accumulation of fine-grained rocks. Nevertheless, algal blooms and oxygen-depleted conditions resulted in accumulation of 13 thin (< 7 m) oil shale layers. Oil shale quality varies between different layers due to variable portions of terrestrial organic matter. Ash-rich coal layers mined in the Huadian Basin developed during the regressive late stage of basin evolution (Carbonaceous Shale Member).

Biomarkers indicate a change from an angiosperm- to a gymnosperm-dominated vegetation. In the Fushun Basin, a single 120-m-thick coal seam formed during early basin subsidence. Subsequently, high subsidence rates established deep lacustrine conditions with photic zone anoxia and a water depth probably exceeding 150 m. Stable, strictly anoxic conditions allowed accumulation of a 300-m-thick oil shale layer. The main factor controlling differences between the Huadian and Fushun basins is tectonic subsidence. High subsidence rates in the Fushun Basin favored deposition of thick coal during the transgressive stage and of oil shale in a deep lake. In contrast minor subsidence in the Huadian Basin resulted in a lake with moderate water depth and deposition of several oil shale layers with varying quality. In this basin economic coal developed only during the regressive stage.

9.1 Introduction

World-class coal and oil shale deposits have been formed during Eocene time along the Dunhua-Mishan ("DunMi") fault zone in northeastern China (Fig. 9.1). The economically most important deposit is located within the Fushun Basin, where a single, up to 120-m-thick coal seam overlain by 300-m-thick oil shale is exploited in a huge openpit mine (Liu et al., 2009; Sun et al., 2013; Strobl et al., 2014; in press). The annual oil shale production is 11 mio. t yielding 330,000 t of shale oil.

Coal and oil shale is also produced in the Huadian Basin, where a high number of coal and oil shale layers, only a few meters thick, is mined underground. Main mining activities in the Huadian Basin are concentrated in its eastern part (Gonglangtou district). Compared to the Fushun Basin, annual oil shale production is minor (about 1.3 mio. t). The produced oil (70,000-80,000 t/a) is used as ship fuel. Both, in the Fushun and Huadian mining districts, oil shale is defined by an oil yield exceeding 3.5 wt.%.

Obviously, major differences in the thickness and distribution of coal and oil shale layers exist between the non-marine Huadian and Fushun basins, although both basins are located at the same strike-slip zone and formed roughly contemporaneously.

Whereas the depositional environment of coal and oil shale in the Fushun Basin has been studied recently (Strobl et al., 2014; in press), only total organic carbon (TOC) contents, hydrogen index (HI) values, oil yield (Sun et al., 2013) and some petrographic data (Xie et al., 2014) are available from the Huadian Basin.

Therefore, the present study has two major aims: to reconstruct the depositional environment of coal and oil shale layers in the Huadian Basin and to compare it with that of coal and oil shale in the coeval Fushun Basin.

To reach the goals, core samples from borehole Hd3 (Fig. 9.1), representing the fill in the Huadian Basin (Huadian Formation) in the eastern part of the basin, have been studied using bulk geochemical proxies, maceral and biomarker data. The borehole was selected because continuous TOC and HI profiles are available (Sun et al., 2013). The depositional environment and the architecture of the coal and oil shale layers are compared with results of a similar study in the Fushun Basin (Strobl et al., 2014; in press).

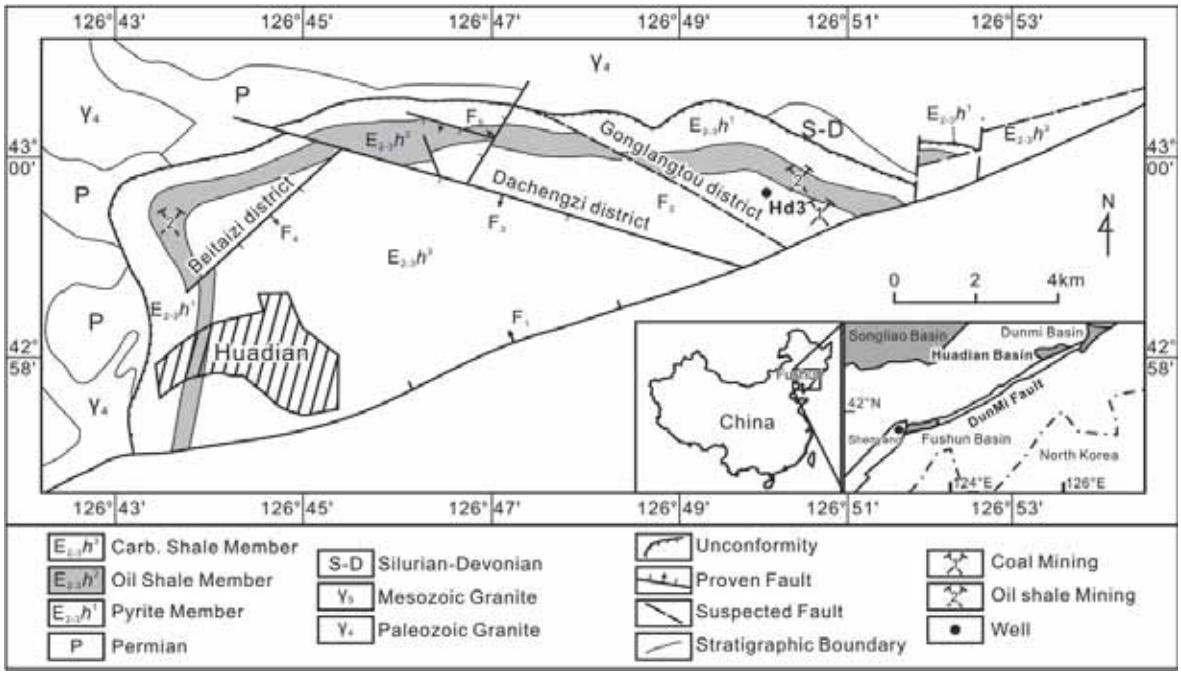

Fig. 9.1: Geological map of the Huadian Basin [modified according to Sun et al. (2013)]. An overview map with special focus on the location of the Huadian and Fushun basins and the DunMi fault zone is shown as inset [modified according to Meng et al. (2012), Strobl et al. (2014; in press)].

9.2 Geological setting of the Huadian Basin

The non-marine Huadian Basin is an E-W trending halfgraben basin located along the DunMi fault zone (Fig. 9.1). The Eocene basin fill (Huadian Formation) is up to 1500 m thick and overlies various basement units including granite, Lower Paleozoic and Permo-Carboniferous sedimentary rocks. Outcrops of the Huadian Formation are rare because of a Quaternary cover up to 15 m thick. The Huadian Formation is subdivided from bottom to top into three members: Pyrite Member, Oil Shale Member, and Carbonaceous Shale Member (Liu et al., 2009; Sun et al., 2011, 2013).

The Pyrite Member represents the early, shallow stages of basin evolution. It comprises conglomerates and red mudstones near its base overlain by varicolored calcarenitic fine-grained sandstones, mudstones and coaly layers deposited in alluvial fan, fan delta, and shallow lake environments. The presence of pyrite crystals in fractures and pore spaces, interpreted to be hydrothermal in origin by Sun (2010), is eponymous for this member.

The Oil Shale Member was deposited during the expansion and deepening of the lake (Sun et al., 2013). It was dated as Middle Eocene based on a mammalian fauna (Zhang et al., 1986; Beard and Wang, 1991; Manchester et al., 2005). The total thickness of this member ranges from 65 to 244 m. The total number of oil shale layers varies from 6 to 26, but only 13 layers (numbered from top to bottom) are suitable for shale oil exploitation (Wang et al., 2005). Note that compared to Sun et al. (2013), the numbering of oil shale layers was modified based on new well correlations. Top and bottom of the Oil Shale Member are set at the top of oil shale layer 1 and the bottom of oil shale layer 13, respectively. Significant differences exist between oil shale deposited in the lower, middle and upper parts of the Oil Shale Member: Oil shale with relative high thickness (up to 7 m), but low to moderate quality occurs in the lower part (layers 13-8), whereas thin (<3 m) oil shales with high quality are found in the middle part (layers 7-4). Low quality oil shale, less than 2 m thick, occurs in the upper part (layers 3-1). The lateral extent of the oil shale layers increases upward within the lower part, reaches a maximum in the middle part and decreases upward in the upper part (Sun et al., 2013). Only layers 7 to 4 are currently mined underground. The average TOC content of the Oil Shale Member is 3.6 wt.%. The

highest TOC value of a 1-m-thick interval occurs in the middle part (30.0 wt.%; Sun et al., 2013; Fig. 9.2, grey solid line).

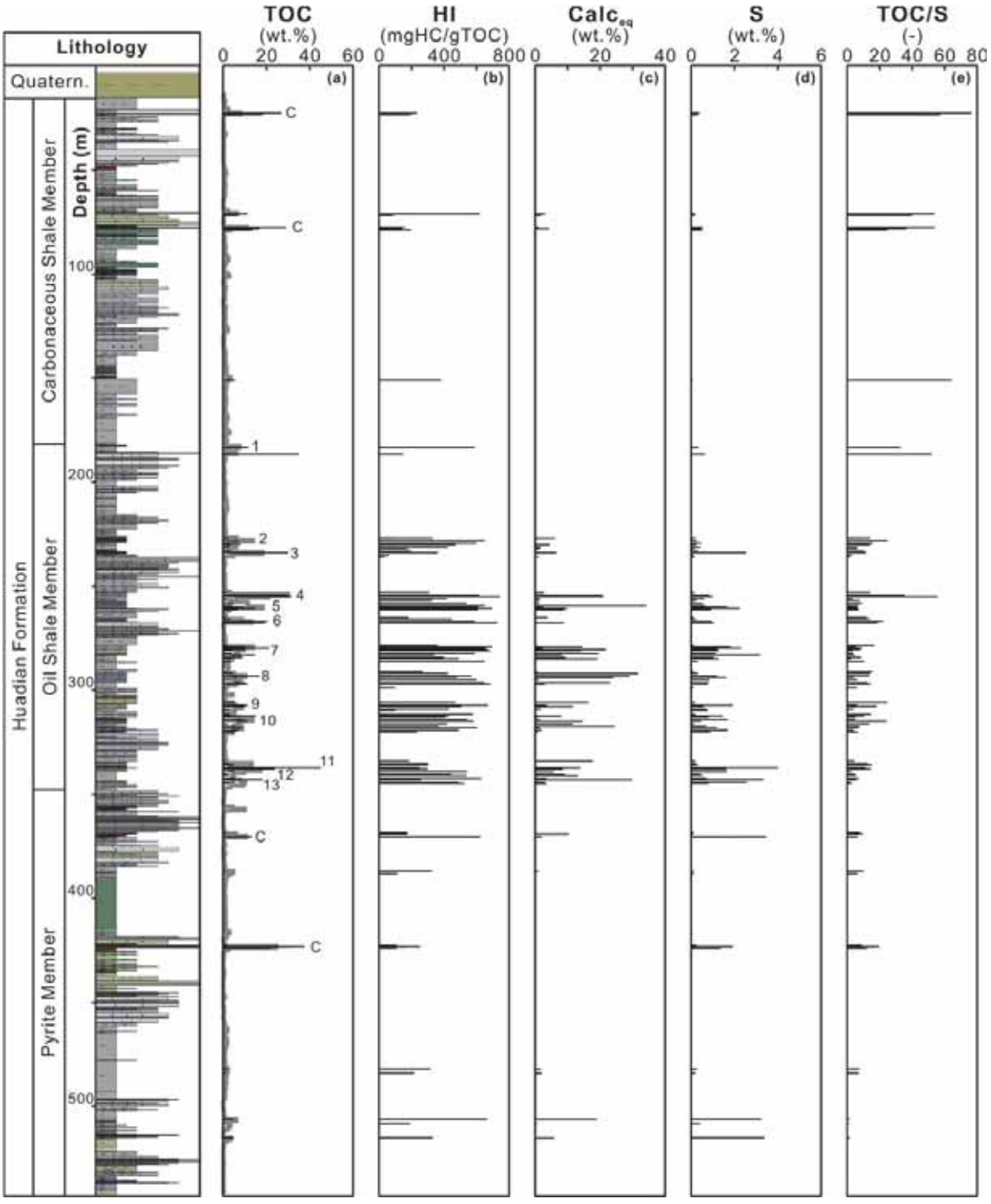

Fig. 9.2: Depth profiles of bulk geochemical proxies of the Huadian Formation. The lithology profile and the average TOC content are taken from Sun et al. (2013). Oil shale layers are numbered from top to bottom. *C, coaly layer.*

Shallow lacustrine conditions prevailed during deposition of the Carbonaceous Shale Member. It represents the final filling stage of basin evolution. Economic coal seams

accumulated along the lake margins are accompanied by bituminous shale (Sun et al., 2013).

9.3 Samples and methods

A total of 96 core samples were taken from borehole Hd3 (Fig. 9.1) within the depth interval of 23.1 to 515.5 m. This interval represents the whole Huadian Formation consisting of Pyrite (14 samples), Oil Shale (73 samples), and Carbonaceous Shale (9 samples) members. Sample selection was based on the average TOC content of 1-m-thick intervals provided by Sun et al. (2013; Fig. 9.2, grey solid line). Special focus has been taken on the oil shale and coaly layers. Bulk geochemical analyses were performed on all 96 samples.

9.3.1 Carbon and sulfur analyses

Total carbon (TC) and sulfur (S) contents of all samples were determined using a Leco CS-230 elemental analyzer. Total organic carbon (TOC) content was determined with the same instrument on samples pre-treated with hydrochloric acid. Total inorganic carbon (TIC) contents were calculated by the difference between TC and TOC. The TIC is used to calculate calcite equivalent percentages ($Calc_{eq}$ = TIC x 8.333) of the samples.

9.3.2 Rock Eval pyrolysis

Pyrolysis analysis was performed using a Rock Eval 2+ analyzer. Depending on the TOC content, 15 mg to 60 mg of each pulverized sample were heated gradually in an inert atmosphere. Within this method, the amount of pyrolyzate released from kerogen was normalized to TOC to give the hydrogen index (HI). The temperature of maximum hydrocarbon generation (T_{max}) is defined at the maximum value of the S_2-peak.

Based on TOC and Rock Eval data, 42 samples were selected for maceral, biomarker and compound-specific isotope analyses.

9.3.3 Organic petrography and vitrinite reflectance measurements

Microscopic analysis was performed using polished blocks of whole-rocks cut perpendicular to bedding planes, a Leica MPV microscope and oil immersion objectives. Maceral analysis was performed using reflected white and fluorescent light and a 50x objective. 500 points per polished block were counted using the single scan method (Taylor et al., 1998). Maceral percentages are given in vol.% on a mineral matter free basis. Vitrinite reflectance was measured on four samples using a 50x objective in non-polarized light at a wavelength of 546 nm (Taylor et al., 1998). 50 points per sample were measured. Results are presented as mean random reflectance values ($\%R_r$).

9.3.4 Organic geochemistry (biomarker analysis)

For organic geochemical analysis, portions of selected samples were extracted for approximately one hour using dichloromethane (DCM) in a Dionex ASE 200 accelerated solvent extractor. Asphaltenes were precipitated from a hexane-DCM solution (80:1) and separated by centrifugation. The hexane-soluble fractions were separated into NSO compounds, saturated and aromatic hydrocarbons using medium pressure liquid chromatography (MPLC) with a Köhnen-Willsch instrument (Radke et al., 1980). The saturated and aromatic hydrocarbon fractions were analyzed using a gas chromatograph equipped with a 30 m DB-5MS fused silica column (i.d. 0.25 mm; 0.25 µm film thickness) and coupled to a Thermo Fisher ISQ quadrupol mass spectrometer (GC-MS system). The oven temperature gradient was programmed from 70°C to 300°C at 4°C min^{-1}, followed by an isothermal period of 15 min. Helium was used as carrier gas. The sample was injected splitless, with the injector temperature at 275°C. The spectrometer was operated in the EI (electron ionization) mode over a scan range from *m/z* 50 to 650 (0.7 s total scan). Data were processed using an Xcalibur data system. Individual compounds were identified on the basis of retention time in the total ion current (TIC) chromatogram and by comparison of the mass spectra with published data. Relative percentages and absolute concentrations of different compound groups in the saturated and aromatic hydrocarbon fractions were calculated using peak areas from the gas chromatograms in relation to that of internal standards (deuteriated *n*-tetracosane and 1,1'binaphthyl, respectively).The concentrations were normalized to the TOC content.

9.3.5 Compound-specific stable isotope geochemistry

Carbon isotope determination of *n*-alkanes and acyclic isoprenoids was performed using a Trace GC instrument attached to a ThermoFisher DELTA-V isotope ratio mass spectrometer via a combustion interface (GC isolink, ThermoFisher). For calibration, CO_2 was injected at the beginning and end of each analysis. The GC column and temperature program are the same as for GC-MS. Stable isotope ratios are reported in delta notation ($\delta^{13}C$; Coplen, 2011) relative to the Vienna-Pee Dee Belemnite (V-PDB) standard ($\delta^{13}C=[(^{13}C/^{12}C)_{sample}/(^{13}C/^{12}C)_{standard}-1]$). Delta notation is expressed in parts per thousand or per mil (‰). The analytical error was better than 0.2‰.

9.4 Results

9.4.1 Bulk geochemical parameters

Bulk geochemical data of studied samples are listed in Tab. 9.1. The vertical distribution of organic-rich layers in borehole Hd3 (Fig. 9.2) is described separately for each member.

9.4.1.1 Pyrite Member

TOC contents of mudstones in the Pyrite Member are generally low (< 1.0 wt.%), but reach higher values in some bituminous beds (< 10.0 wt.%) and in coaly layers (e.g. 24.8 wt.% at 424 m depth) (Sun et al., 2013; Fig. 9.2a). Fourteen samples have been selected for the present study. High TOC values are measured in the coaly layer at 424 m depth (31.6-37.6 wt.%) and in an organic rich layer at 371 m depth (10.4-13.4 wt.%; Fig. 9.2a). HI values ranging from 125 to 251 mgHC/gTOC show that the coaly layer and the lower part of the organic rich layer comprise kerogen type III, whereas the upper part of the organic rich layer includes hydrogen rich kerogen type-I to II (623 mgHC/gTOC; Fig. 9.2b).

The TOC of remaining mudstone samples vary between 0.4 and 5.1 wt.% (Fig. 9.2b). HI values of these range from 108 to 664 mgHC/gTOC (Fig. 9.2b) indicating the presence of kerogen type III, II and I (Fig. 9.3).

T_{max} values vary between 431 and 440°C (Tab. 9.1). Sulfur contents are low (< 0.4 wt.%) in organic lean mudstones, but relative high (1.5-3.5 wt.%) in organic rich mudstones and coaly layers (Fig. 9.2d). TOC/S ratios are very low in the lower part (< 1.5) and increase upward (up to 10.0). The highest TOC/S ratios occur in the coaly layer at 424 m depth (< 19.6; Fig. 9.2e). Carbonate content is generally low (< 6 wt.% $Calc_{eq}$), but is elevated in mudstone samples near the base and the top of the Pyrite Member (Fig. 9.2c).

9.4.1.2 Oil Shale Member

TOC contents vary significantly between oil shale layers and country rocks (Sun et al., 2013; Fig. 9.2a). In the present study, focus was taken on the 13 oil shale layers and their floor and roof rocks. Within these layers TOC contents reach a maximum of 45.4 wt.% (layer 11; Fig. 9.2a). HI values show a general increasing upward trend and reach 744 mgHC/gTOC in layer 4. Most of the samples plot inside the fields characteristic for type I and II kerogen, but samples with type II to III kerogen are also present (e.g. layers 13-11; Fig. 9.3). T_{max} values vary between 425 and 441°C. High T_{max} values are typically measured in samples with high HI values (Tab. 9.1). Sulfur contents range from 0.1 to 4.0 wt.% and show elevated values in the stratigraphically deep oil shale layers 13 and 11 (Fig. 9.2d). High TOC contents result in high TOC/S ratios up to 55.5 (Fig. 9.2e). The carbonate content of oil shale layers varies significantly between 0 and 34 wt.% $Calc_{eq}$ (Fig. 9.2c).

9.4.1.3 Carbonaceous Shale Member

The Carbonaceous Shale Member is characterized by two coaly layers and several layers with bituminous shale. The average TOC content of 1-m-thick intervals comprising coaly layers is relative low (< 11 wt.%) because of low seam thickness and high mineral matter contents (Sun et al., 2013; Fig. 9.2a). Six samples representing the coaly layers and three bituminous shale layers were investigated within the frame of the present study. TOC contents of coaly samples vary between 13.6 and 28.9 wt.% (Fig. 9.2a). Their HI ranges from 141 to 234 mgHC/gTOC (Fig. 9.2b) indicating the presence of kerogen type III (Fig. 9.3). Bituminous shales contain 5.8 to 11.3 wt.% TOC (Fig. 9.2a) and a kerogen type II (HI: 382 – 619 mgHC/gTOC;

Fig. 9.2b, Fig. 9.3). T_{max} values vary between 425 and 437°C (Tab. 9.1). Sulfur contents are low (< 0.6 wt.%; Fig. 9.2d) resulting in high TOC/S ratios (24.6-75.6; Fig. 9.2e). Samples from the Carbonaceous Shale Member are largely carbonate-free (< 4.3 wt.% $Calc_{eq}$; Fig. 9.2c).

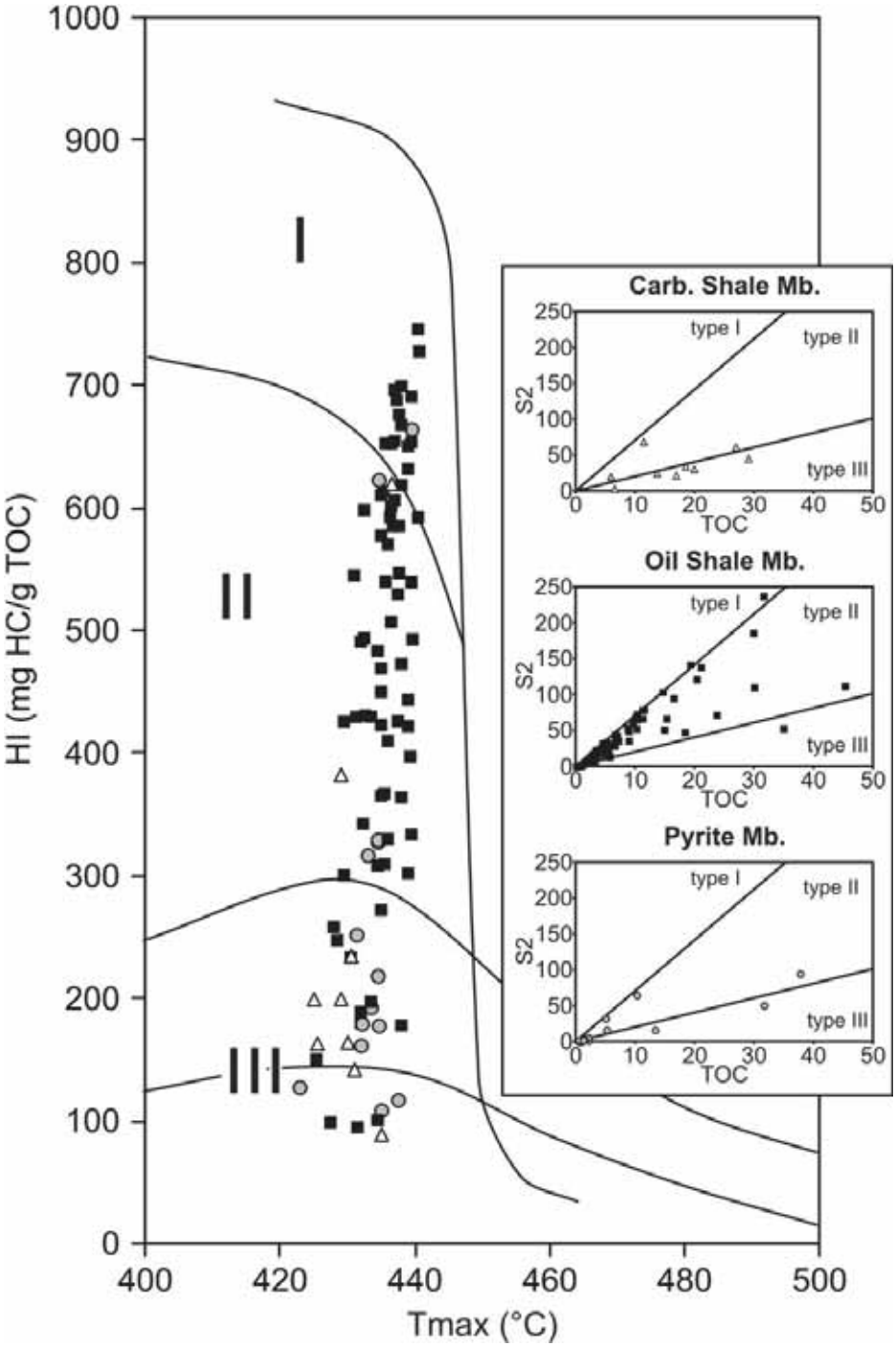

Fig. 9.3: Plot of HI vs. T_{max} [according to Espitalié et al. (1984)] outlining kerogen types of sediments from the Huadian Formation. S_2 vs. TOC correlations for all three members are shown as insets [according to Langford and Blanc-Valleron (1990)].

Tab. 9.1: Data from LECO and Rock Eval measurements (bulk geochemical data), and from organic petrography and vitrinite reflectance measurements.

Sample	Depth (m)	TOC (wt.%)	HI (mgHC/gTOC)	S_2 (mgHC/g)	T_{max} (°C)	S (wt.%)	TOC/S (-)	$Calc_{eq}$ (wt.%)	Terrig. OM (vol.%, mmf)	Algenic (vol.%, mmf)	Vitr. Refl. (%R_r)	SD (-)
Carbonaceous Shale Member												
HD 1	23.1	26.8	234	62.8	431	0.4	75.6	0.0	76	24	0.43	0.017
HD 2	23.3	19.8	164	32.4	430	0.4	50.0	0.0				
HD 3	23.4	18.4	199	36.5	425	0.3	58.2	0.0				
HD 4	71.3	11.3	619	70.1	437	0.2	54.3	3.1	21	79		
HD 5	72.3	6.4	88	5.7	435	0.2	29.0	1.8				
HD 6	78.1	28.9	163	47.1	426	0.5	53.1	0.9	98	2	0.43	0.0135
HD 7	78.7	16.8	141	23.7	431	0.5	36.5	4.3				
HD 8	79.3	13.6	199	27.0	429	0.6	24.6	0.0				
HD 9	151.4	5.8	382	22.1	429	0.1	65.2	0.0				
Oil Shale Member												
HD 10	183.6	11.9	587	70.1	437	0.4	33.3	0.4	24	76		
HD 11	186.8	34.9	150	52.3	425	0.7	52.1	0.0	93	7		
HD 12	227.0	0.9	93	0.9	432	0.1	8.8	1.7				
HD 13	227.5	2.5	332	8.4	440	0.2	14.1	5.9				
HD 14	228.5	6.7	652	43.7	440	0.3	24.9	0.0				
HD 15	229.5	7.1	600	42.4	437	0.4	15.8	0.5	37	63		
HD 16	230.5	3.6	471	17.0	436	0.3	14.4	4.5				
HD 17	231.5	2.3	424	10.8	438	0.4	6.1	1.8				
HD 18	232.5	1.0	176	1.7	438	0.1	6.7	1.6				
HD 19	233.5	3.3	196	6.4	434	0.3	10.4	0.5				
HD 20	234.5	30.1	364	109.6	435	2.5	11.9	6.4	71	29		
HD 21	235.5	0.4	63	0.3	-	0.1	3.2	0.2				
HD 22	236.0	0.2	31	0.1	-	0.1	1.6	1.9				
HD 23	253.5	2.0	308	6.1	436	0.1	13.9	2.8	19	81		
HD 24	254.5	30.0	617	184.8	438	0.8	35.6	20.8	10	90		
HD 25	255.0	31.7	744	235.7	441	0.6	55.5	21.0	5	95		
HD 26	255.5	6.7	428	28.5	431	1.0	6.5	0.9	32	68		
HD 27	256.5	2.1	421	8.9	435	0.6	3.5	1.6	31	69		
HD 28	257.5	1.6	328	5.4	436	0.2	7.4	1.4	30	70		
HD 29	258.5	5.1	538	27.7	436	0.5	9.4	1.3	37	63		
HD 30	259.5	4.7	651	30.6	436	0.7	7.2	34.2	11	89		
HD 31	260.3	9.7	612	59.1	435	1.7	5.9	2.6	15	85		
HD 32	261.0	14.7	698	102.8	438	2.2	6.6	9.9	33	67		
HD 33	261.5	6.8	609	41.1	435	0.9	7.2	8.9	14	86		
HD 34	265.5	1.3	180	2.4	433	0.1	12.5	3.9				
HD 35	266.3	3.5	448	15.5	435	0.2	14.5	0.3				
HD 36	267.5	20.4	591	120.7	436	0.9	22.1	0.3	21	79		
HD 37	268.0	19.4	726	140.8	441	1.0	18.8	8.9				
HD 38	279.0	2.0	362	7.3	438	0.1	17.5	0.5				
HD 39	279.5	10.4	695	72.2	437	1.8	5.7	14.6				
HD 40	280.0	21.1	651	137.7	437	2.3	9.1	2.3	29	71		
HD 41	280.5	10.2	666	67.7	438	1.2	8.3	21.8				
HD 42	281.5	4.7	689	32.2	440	1.3	3.7	14.1				
HD 43	282.5	4.0	591	23.9	441	1.1	3.7	19.4				
HD 44	283.5	15.0	341	51.1	432	3.2	4.7	8.4	79	21		
HD 45	284.5	9.9	396	35.7	439	1.0	8.6	9.4				
HD 46	285.5	5.4	491	16.9	440	1.3	2.7	19.4				
HD 47	286.3	3.5	649	22.8	439	0.3	10.4	0.1				
HD 48	291.5	1.8	270	4.7	435	0.1	16.4	0.7				
HD 49	292.5	4.6	424	19.5	430	0.3	14.3	31.8				
HD 50	293.5	16.6	569	94.1	436	1.2	13.8	29.1	22	78		
HD 51	294.5	6.5	482	31.3	435	1.6	4.0	24.1				
HD 52	295.5	5.2	597	31.0	433	0.8	6.1	1.1				
HD 53	296.5	10.4	653	68.2	437	0.8	12.7	23.0				
HD 54	297.5	11.3	687	77.7	437	0.8	15.0	3.0	20	80		
HD 55	299.0	0.7	98	0.7	435	0.1	5.9	0.2				
HD 56	306.2	5.2	468	24.3	435	0.2	24.8	16.6				
HD 57	307.5	11.6	674	78.1	438	1.9	6.0	3.6	18	82		
HD 58	308.5	10.3	505	52.2	437	0.6	18.2	11.8				
HD 59	309.5	2.9	428	12.3	434	0.7	4.0	1.9				
HD 60	310.0	0.8	97	0.8	428	0.8	1.1	0.0				
HD 61	312.0	2.9	576	16.9	435	0.2	15.0	0.1				
HD 62	312.5	15.4	429	65.9	433	1.4	10.6	8.1	73	27		
HD 63	313.5	4.3	408	17.5	436	0.8	5.2	0.8				
HD 64	314.5	9.0	543	48.8	431	1.7	5.2	1.5				
HD 65	315.5	11.3	584	66.1	438	0.5	24.3	14.6	16	84		
HD 66	316.5	2.2	420	9.3	439	0.2	14.1	11.8				
HD 67	317.5	5.6	365	20.4	436	0.7	7.9	24.5				
HD 68	318.5	8.8	605	53.2	437	1.2	7.3	1.5	22	78		
HD 69	319.5	7.3	489	35.5	432	1.7	4.3	2.0				
HD 70	320.5	5.8	232	13.5	431	0.9	6.5	0.8				
HD 71	334.5	0.8	187	1.6	432	0.2	4.0	17.8	36	64		
HD 72	335.5	2.8	300	8.4	439	0.2	12.5	9.9	17	83		
HD 73	336.5	5.1	307	15.7	435	0.3	15.5	0.2	60	40		
HD 74	337.5	45.4	246	111.5	429	4.0	11.3	13.9	87	13		
HD 75	338.5	23.8	299	71.1	430	1.6	14.6	8.6	84	16		
HD 76	339.5	5.3	545	28.9	438	1.7	3.2	6.0	63	37		
HD 77	340.5	2.3	442	10.0	439	0.4	5.1	9.0	36	64		
HD 78	341.5	3.0	538	16.2	440	0.5	5.7	13.2	25	75		
HD 79	342.5	5.3	630	33.1	439	0.7	7.1	3.7	57	43		
HD 80	343.5	16.4	256	47.3	428	3.4	5.5	30.0	91	9	0.42	0.011
HD 81	344.5	5.6	492	27.4	433	2.6	2.2	3.0	31	69		
HD 82	345.5	2.5	528	13.4	438	0.8	3.1	3.7	45	55		
Pyritic Member												
HD 83	369.0	1.0	178	1.8	432	0.1	7.7	0.4				
HD 84	369.5	0.7	177	1.2	435	0.1	9.7	10.4				
HD 85	370.5	10.4	623	64.8	435	1.5	6.7	1.9	20	80		
HD 86	371.0	13.4	125	16.8	423	3.5	3.9	0.0				
HD 87	387.5	1.2	327	4.0	435	0.1	10.0	1.1				
HD 88	388.5	0.9	116	1.0	438	0.1	6.9	0.3				
HD 89	423.0	2.0	109	2.2	435	0.2	8.9	0.0				
HD 90	423.5	37.6	251	94.5	431	1.9	19.6	0.0	93	7	0.43	0.012
HD 91	424.0	31.6	161	50.7	432	1.9	16.4	0.0				
HD 92	482.5	2.0	316	6.2	433	0.3	7.7	1.8				
HD 93	484.5	1.3	219	2.9	435	0.2	7.4	2.2				
HD 94	506.5	4.9	664	32.4	440	3.2	1.5	18.9	70	30		
HD 95	508.5	0.4	192	0.8	434	0.4	0.9	0.5				
HD 96	515.5	5.1	329	16.7	435	3.8	1.3	3.7				

TOC: total organic carbon; HI: hydrogen index; S_2 hydrocarbons generated during Rock Eval pyrolysis;
T_{max}: temperature with maximum hydrocarbon generation; S: sulfur; $Calc_{eq}$: calcite equivalent; Terrig. OM: terrigenous organic matter;
Vitr. Refl.: vitrinite reflectance; SD: standard deviation.

9.4.2 Organic petrography and vitrinite reflectance

The vertical variability of terrigenous organic matter (OM; sum of vitrinite, inertinite, sporinite, resinite, cutinite, fluorinite, liptodetrinite) and alginite (sum of lamalginite and telalginite; Tab. 9.1) is plotted in Fig. 9.4a, Fig. 9.4b. Representative photomicrographs of samples from the Huadian Formation are shown in Fig. 9.5.

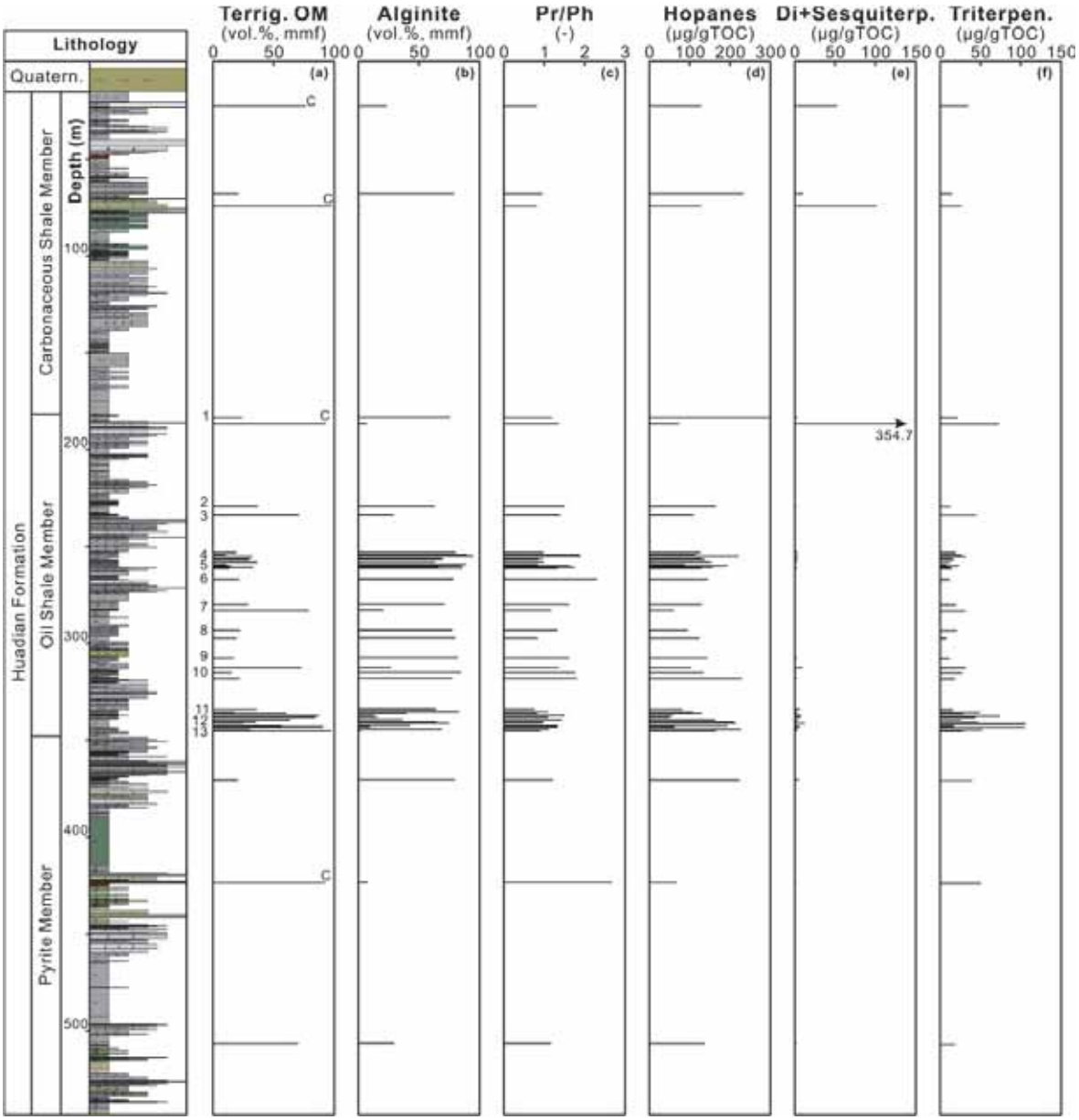

Fig. 9.4: Distribution of (a) macerals – terrigenous organic matter (Terrig. OM), (b) macerals – alginite (lamalginite + telaginite), (c) pristane/phytane ratios, (d) hopane concentrations, (e) diterpenoid+sesquiterpenoid concentrations, and (f) triterpenoid concentrations, within the Huadian Formation. The lithology profile is taken from Sun et al. (2013). Oil shale layers are numbered from top to bottom. *C, coaly layer.*

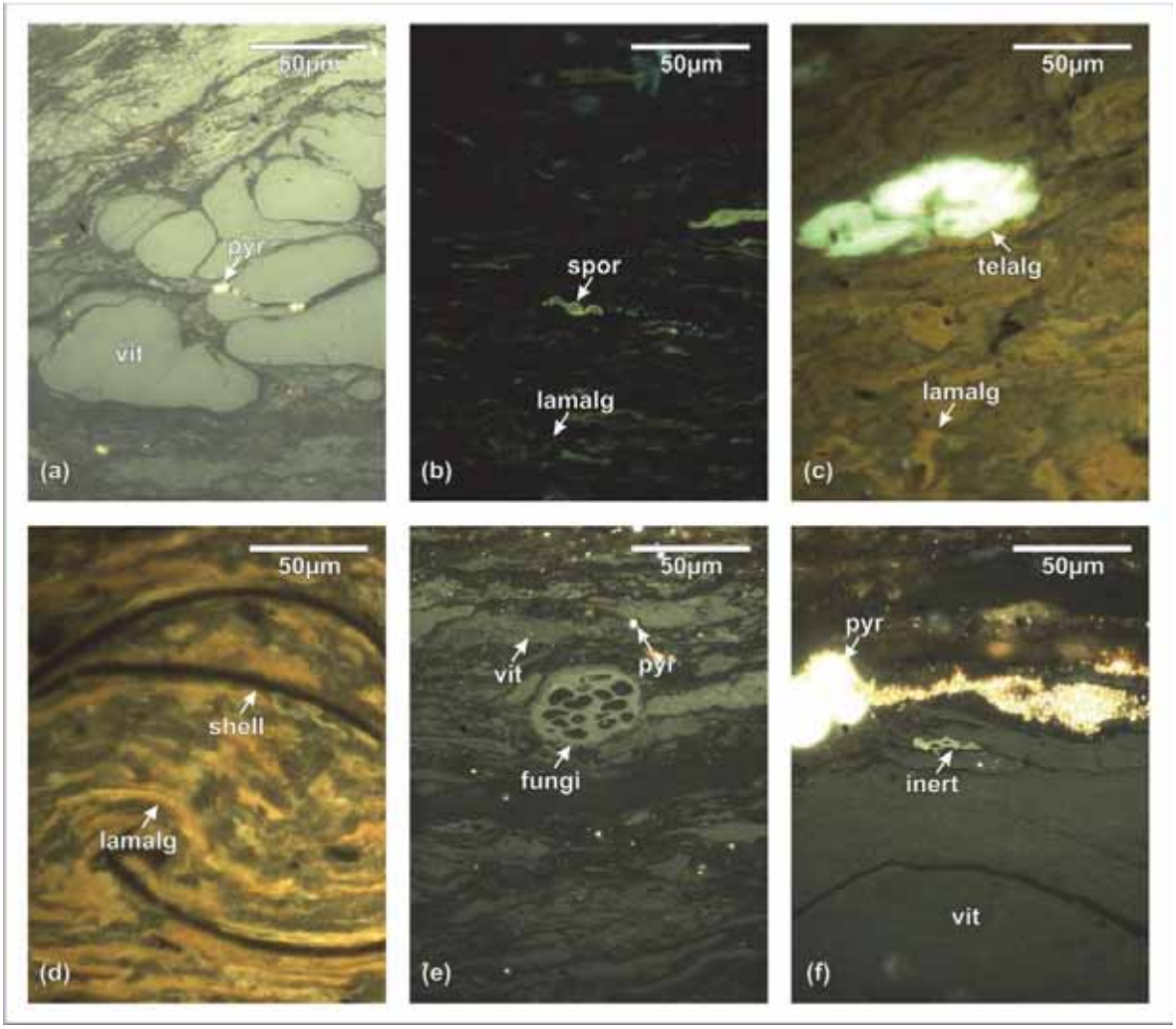

Fig. 9.5: Photomicrographs of the Huadian Formation. (a) HD 6 under white light, (b) HD 20 under UV light, (c) HD 25 under UV light, (d) HD 65 under UV light, (e) HD 80 under white light, and (f) HD 80 under white light. *Abbreviations: vit, vitrinite; pyr, pyrite; spor, sporinite; lamalg, lamalginite; telalg, telaginite; shell, ostracode shell; fungi, funginite; inert, inertinite.*

Coaly and bituminous samples from the Pyrite Member have been selected for maceral analysis. Whereas the coaly sample is characterized by high amounts of terrigenous OM (93 vol.%; Fig. 9.4a) beside minor alginite (7 vol.%; Fig. 9.4b), bituminous samples are enriched in alginite (30 and 80 vol.%; Fig. 9.4b). Vitrinite and sporinite are the predominant landplant-derived macerals. Minor funginite is the main maceral of the inertinite group. Lamalginite predominates over telalginite in all samples. Lamalginite may originate from assemblages of algae and bacteria. Telaginite covers solitary and colonial algae.

The Oil Shale Member is characterized by strongly varying, but often very high, amounts of alginite (2-95 vol.%; average 60 vol.%; Fig. 9.4b). Lamalginite prevails significantly over telaginite. The highest percentage of telalginite occurs in layer 4 (3.5 vol.%; Fig. 9.5c). Terrigenous OM is generally more abundant in the lower (e.g. layers 13-11) than in the upper part (e.g. layers 7-4) of this member (Fig. 9.4a). Vitrinite and sporinite are the prevailing landplant-derived macerals. Shells of ostracodes occur as well (see also Sun et al., 2013).

Coaly shale layers from the Carbonaceous Shale Member contain abundant terrigenous OM (76-98 vol.%; Fig. 9.4a), whereas alginite is abundant in the bituminous shales (79 vol.%; Fig. 9.4b). Lamalginite, vitrinite and sporinite are the prevailing macerals.

Typically, lamalginite is characterized by an orange fluorescence color, whereas telaginite and sporinite display yellow to light greenish colors.

Vitrinite reflectance was measured on four samples at 23.1 m, 75.0 m, 343.5 m, and 423.5 m depths and ranges from 0.42 to 0.43%R_r (Tab. 9.1). These values are consistent with those reported by Xie et al. (2014) and indicate that the Huadian Formation is immature.

9.4.3 Organic geochemistry

Within the Huadian Formation, the amount of extractable organic matter (EOM) varies between 10 and 43 mg/gTOC (average 24 mg/gTOC). The proportion of hydrocarbons ranges between 8 and 46% of EOM. Saturated hydrocarbons (average 21% of EOM) are predominant over aromatic hydrocarbons (average 4% of EOM). The EOM is also composed of NSO compounds (average 37% of EOM) and asphaltenes (average 38% of EOM; Tab. 9.2).

Total ion chromatograms (TICs) of saturated and aromatic hydrocarbon fractions of representative samples from the Huadian Formation (Oil Shale Member) are shown in Fig. 9.6. The concentrations and concentration ratios of compounds and compound groups in hydrocarbon fractions are listed in Tab. 9.2.

Tab. 9.2: Data from biomarker analysis.

Sample	Depth	EOM	Sat. HC	Aro. HC	NSO	Asphalt.	n-C_{15-19}/ n-alk.	n-C_{25-29}/ n-alk.	n-C_{27-31}/ n-alk.	CPI	Pr/Ph	Hopanes	Benzo-hopanes	Diterpenoids	Sesquiterp.	Triterpenoids	Aryl-isoprenoids	MTTC ratio
	(m)	(mg/gTOC)	(%)	(%)	(%)	(%)	(-)	(-)	(-)	(-)	(-)	(µg/gTOC)	(µg/gTOC)	(µg/gTOC)	(µg/gTOC)	(µg/gTOC)	(µg/gTOC)	(-)
Carbonaceous Shale Member																		
HD 1	23.1	32	12	2	36	49	0.04	0.38	0.51	5.96	0.8	127.1	1.3	49.5	3.3	34.7	0.8	0.27
HD 4	68.1	39	9	1	23	67	0.05	0.38	0.47	3.28	0.9	231.7	1.4	9.2	1.0	14.6	0.2	0.37
HD 6	75.0	26	11	4	46	39	0.05	0.44	0.41	4.13	0.8	127.8	1.4	96.2	5.2	26.3	0.9	0.23
Oil Shale Member																		
HD 10	183.6	21	19	4	41	36	0.07	0.38	0.46	3.93	1.2	299.3	2.6	2.6	0.7	21.3	0.3	0.57
HD 11	186.8	17	16	6	45	33	0.05	0.34	0.51	4.70	1.4	74.1	1.7	349.2	5.4	73.0	0.6	0.27
HD 15	229.5	20	24	3	41	32	0.08	0.39	0.44	3.47	1.5	164.8	2.0	1.3	1.1	12.9	0.3	0.48
HD 20	234.5	12	18	8	50	23	0.04	0.29	0.55	4.05	1.4	107.7	1.4	1.3	0.6	44.4	0.0	0.56
HD 23	253.5	22	38	5	34	24	0.07	0.31	0.52	3.32	1.0	126.6	1.3	1.1	2.3	19.7	0.4	0.37
HD 24	254.5	17	9	4	60	27	0.05	0.32	0.53	4.92	1.9	113.6	1.2	1.2	0.2	26.3	0.0	0.41
HD 25	255.0	10	23	9	30	38	0.09	0.40	0.43	4.00	1.9	80.5	1.8	0.4	0.2	12.9	0.0	0.54
HD 26	255.5	26	28	3	43	26	0.11	0.33	0.45	3.65	0.9	221.2	1.6	3.0	1.4	31.2	0.2	0.48
HD 27	256.5	26	32	4	40	24	0.11	0.35	0.45	3.84	1.0	129.9	1.3	0.7	1.5	16.1	0.2	0.32
HD 28	257.5	41	36	3	40	22	0.16	0.36	0.38	3.40	0.9	138.2	1.6	1.3	2.6	16.3	0.3	0.41
HD 29	258.5	24	24	2	37	37	0.10	0.35	0.45	3.28	1.0	153.4	2.5	1.5	1.5	12.4	0.2	0.53
HD 30	259.5	29	18	2	20	59	0.11	0.33	0.45	3.58	0.8	86.5	0.6	0.2	1.4	7.8	0.0	0.33
HD 31	260.3	27	20	2	30	49	0.08	0.37	0.47	5.20	1.6	193.0	1.0	0.7	0.8	23.1	0.2	0.48
HD 32	261.0	23	14	2	29	54	0.06	0.37	0.49	4.29	1.7	157.1	1.7	0.6	0.6	12.3	0.1	0.47
HD 33	261.5	26	25	2	32	41	0.10	0.35	0.46	4.50	1.3	128.9	1.0	1.5	1.2	14.4	0.2	0.50
HD 36	267.5	17	12	4	39	45	0.07	0.34	0.49	3.70	2.3	146.2	1.3	0.3	0.4	11.8	0.1	0.45
HD 40	280.0	39	7	1	20	72	0.05	0.37	0.49	4.51	1.6	130.3	1.6	0.4	0.2	19.0	0.0	0.60
HD 44	283.5	14	19	5	46	30	0.08	0.36	0.47	5.75	1.2	60.4	0.6	0.8	1.0	31.2	0.2	0.66
HD 50	293.5	21	20	4	36	40	0.07	0.35	0.48	4.54	1.3	94.5	1.1	0.5	0.8	19.9	0.1	0.44
HD 54	297.5	21	15	2	23	60	0.07	0.38	0.44	3.34	0.8	124.9	1.3	0.3	0.6	7.7	0.0	0.39
HD 57	307.5	24	26	4	34	36	0.07	0.35	0.49	3.87	1.6	142.6	1.6	2.0	0.7	11.7	0.1	0.51
HD 62	312.5	19	22	5	43	30	0.07	0.35	0.49	4.07	1.4	103.1	0.9	8.9	1.0	31.2	0.1	0.57
HD 65	315.5	14	19	5	37	38	0.08	0.35	0.47	3.67	1.8	133.8	1.6	0.5	0.7	27.6	0.1	0.41
HD 68	318.5	19	20	5	37	38	0.06	0.40	0.42	2.96	1.8	227.7	3.5	2.0	1.0	18.9	0.3	0.34
HD 71	334.5	35	43	3	44	10	0.14	0.34	0.41	3.08	0.8	82.4	1.1	3.8	2.7	15.3	0.2	0.35
HD 72	335.5	26	20	3	25	52	0.08	0.33	0.49	3.63	1.1	106.1	1.6	1.2	1.0	49.8	0.1	0.30
HD 73	336.5	23	33	5	40	23	0.08	0.28	0.54	3.49	0.8	129.3	1.9	1.6	2.2	28.4	0.3	0.26
HD 74	337.5	18	8	5	43	44	0.06	0.33	0.48	3.87	1.5	58.3	3.5	4.6	3.2	73.7	0.3	0.42
HD 75	338.5	12	15	6	50	29	0.05	0.30	0.52	4.57	1.1	51.0	0.8	6.0	1.1	44.1	0.0	0.38
HD 76	339.5	32	27	2	36	35	0.08	0.30	0.54	5.48	1.4	162.4	1.2	2.7	1.7	25.8	0.1	0.50
HD 77	340.5	34	35	2	41	22	0.15	0.34	0.41	3.85	1.0	210.2	2.8	0.6	2.5	46.4	0.2	0.26
HD 78	341.5	30	31	3	40	25	0.11	0.34	0.43	3.29	0.9	215.9	12.9	1.6	10.8	105.1	0.6	0.24
HD 79	342.5	21	28	4	42	26	0.06	0.31	0.53	3.92	1.3	192.9	3.3	1.0	1.3	17.0	0.2	0.39
HD 80	343.5	20	12	5	37	46	0.07	0.33	0.50	4.54	1.3	61.6	3.4	3.0	3.4	104.7	0.6	0.51
HD 81	344.5	43	20	2	32	45	0.06	0.33	0.51	4.46	1.1	227.5	2.5	2.6	1.2	52.5	0.3	0.49
HD 82	345.5	32	27	3	37	32	0.09	0.34	0.47	3.86	0.9	163.9	2.6	0.9	2.3	27.8	0.3	0.34
Pyrite Member																		
HD 85	370.5	25	17	5	31	47	0.06	0.35	0.49	3.84	1.2	223.7	1.8	3.0	2.6	39.4	1.1	0.47
HD 90	423.5	11	13	6	44	37	0.06	0.32	0.50	3.65	2.7	68.3	1.9	1.5	0.9	50.4	0.2	0.34
HD 94	506.5	27	27	3	29	40	0.08	0.30	0.52	3.76	1.2	136.8	2.6	1.0	1.5	18.5	0.1	0.36

EOM: extractable organic matter; Sat. HC: saturated hydrocarbons; Aro. HC: aromatic hydrocarbons; Asphalt.: asphaltenes; CPI: carbon preference index; Pr/Ph: pristane/phytane ratio; Sesquiterp.: sesquiterpenoids.

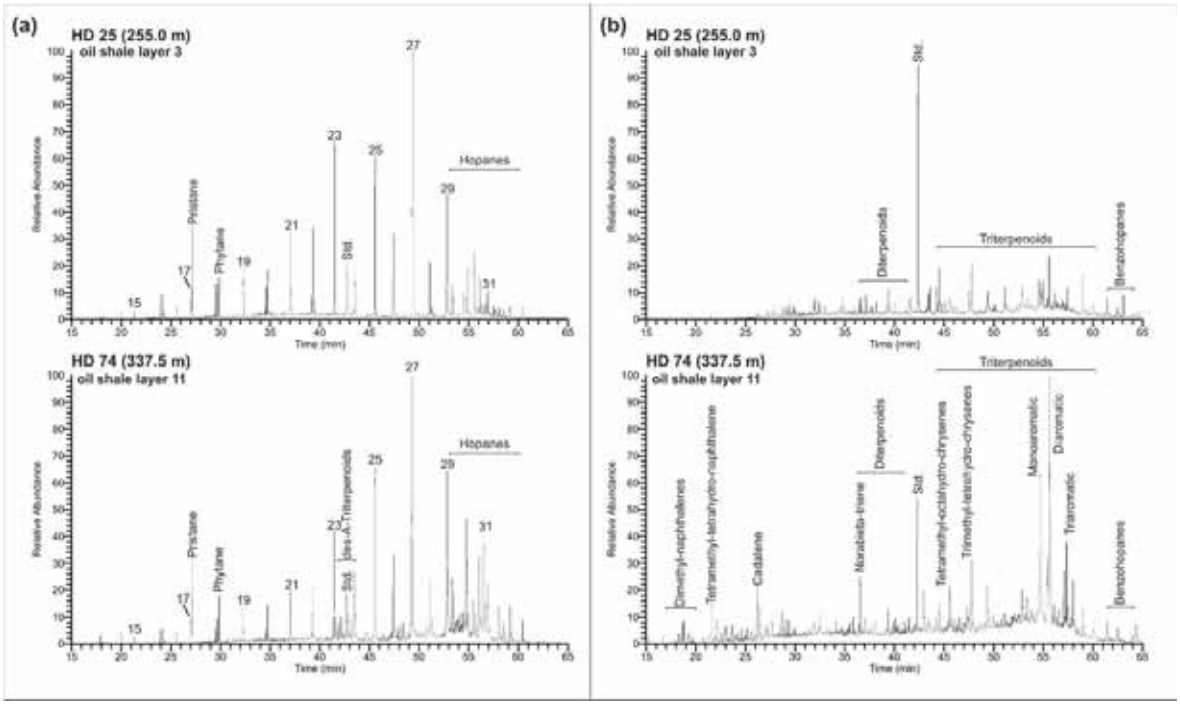

Fig. 9.6: Gas chromatograms (TICs) of (a) saturated and (b) aromatic hydrocarbon fractions of samples from oil shale layer 4 and 11. *n*-Alkanes are labeled according to their carbon number. *Std., standard*.

Sediments of all three members are dominated by *n*-alkanes of intermediate (*n*-C_{21-25}) to long (*n*-C_{27-31}) chain length with an odd to even predominance. Long-chain lipids are characteristic biomarkers for higher terrestrial plants, as they are the main components of plant waxes (Eglinton and Hamilton, 1967). The *n*-alkanes of intermediate molecular weight are reported to have been originated from aquatic macrophytes (Ficken et al., 2000). The low molecular weight members are predominatly found in algae and microorganisms (Cranwell, 1977). The carbon preference index (CPI; Bray and Evans, 1961) varies between 3 and 6 indicating low thermal maturity (Tab. 9.2).

The acyclic isoprenoids pristane (Pr) and phytane (Ph) are present in all samples. Pr/Ph ratios range between 0.8 and 2.7 within the Huadian Formation. The highest value occurs in the coaly layer at 424 m depth from the Pyrite Member. Pr/Ph ratios in the Oil Shale Member show an average value of 1.3, whereat high values occur in the organic-rich layers. Sediments of the Carbonaceous Shale Member are characterized by low Pr/Ph ratios (0.8-0.9; Fig. 9.4c). According to Didyk et al. (1978), Pr/Ph values below 1.0 indicate anaerobic conditions during early diagenesis and values between 1.0 and 3.0 reflect dysaerobic environments. However, Pr/Ph ratios

are known to be also affected by maturation (Tissot and Welte, 1984) and by differences in the precursors for acyclic isoprenoids (i.e. bacterial origin; Goossens et al., 1984; Volkman and Maxwell, 1986; ten Haven et al., 1987).

Within the Huadian Formation, the hopanoid patterns are characterized by 17α, 21β and 17β, 21*b* hopanes from C_{27} to C_{31}, with C_{28} hopanes absent. C_{29} to C_{30} hop-17(21)-enes and oleanenes are also present. Predominant triterpenoids are the C_{29} hop-17(21)-ene, olean-12-ene and 17α, 21β C_{31} (22R) hopane. Benzohopanes occur in all samples and vary between 0.6 and 12.9 µg/gTOC (Tab. 9.2). Hopanes occur in variable amounts (58.3-299.3 µg/gTOC; average 140.8 µg/gTOC; Fig. 9.4d). The occurrence of these biomarkers indicates an input from bacterial biomass (Hussler et al., 1984; Ourisson et al., 1979; Farrimond et al., 2004).

Diterpenoids (e.g. norpimarane, pimarane, phyllocladane, norabieta-riene, simonellite, retene) occur in low amounts in the Pyrite and Oil Shale members (1.0-1.5 µg/gTOC and 0.2-6.0 µg/gTOC, respectively). The uppermost part of the Oil Shale Member and the Carbonaceous Shale Member are characterized by a high amount of diterpenoids (2.6-349.2 µg/gTOC; Tab. 9.2). Sesquiterpenoids (e.g. Cadalene) are present in all samples and vary between 0.2 and 10.8 µg/gTOC (Tab. 9.2). Diterpenoids and sesquiterpenoids indicate a contribution of conifer species (e.g. Otto et al., 1997; Otto and Wilde, 2001). The sum of diterpenoids and sesquiterpenoids (0.6-354.7 µg/gTOC) is plotted versus depth in Fig. 9.4e.

Non-hopanoid triterpenoids (e.g. des-A-oleanenes, des-A-lupane, trimethyl-tetrahydro-chrysenes, olean-12-ene), originating from angiosperms (Karrer et al., 1977; Dev, 1989), occur in relative high amounts (7.7-05.1 µg/gTOC). The highest values occur in the lower and upper part of the Oil Shale Member and in the Pyrite and Carbonaceous Shale members (Fig. 9.4f).

Angiosperm-derived triterpenoids are predominant over di- and sesquiterpenoids in the Pyrite and Oil Shale Member, whereas the opposite distribution occurs within the Carbonaceous Shale Member (Fig. 9.4e, Fig. 9.4f).

C_{14} and C_{16} aryl isoprenoids are present in very low amounts (< 1.1 µg/gTOC) in the Huadian Formation (Tab. 9.2). Aryl isoprenoids originate from photosynthetic green

sulfur bacteria and, therefore, indicate photic zone anoxia (Summons and Powell, 1987).

The MTTC ratio is defined as the concentration of trimethylated MTTC relative to the sum of methylated MTTCs (Sinninghe Damsté et al., 1987) and has been widely used for paleosalinity reconstruction (Sinninghe Damsté et al., 1993; Barakat and Rullkötter, 1997). The MTTC ratio within the Huadian Formation varies in the range between 0.23 and 0.66 (Tab. 9.2) indicating a salinity-stratified, alkaline water column.

9.4.4 Compound-specific stable isotope geochemistry

The carbon isotopic composition of short-chain and long-chain *n*-alkanes, pristane and phytane of eight selected samples from the Huadian Formation is plotted in Fig. 9.7. The measured data from all samples are listed in Tab. 9.3.

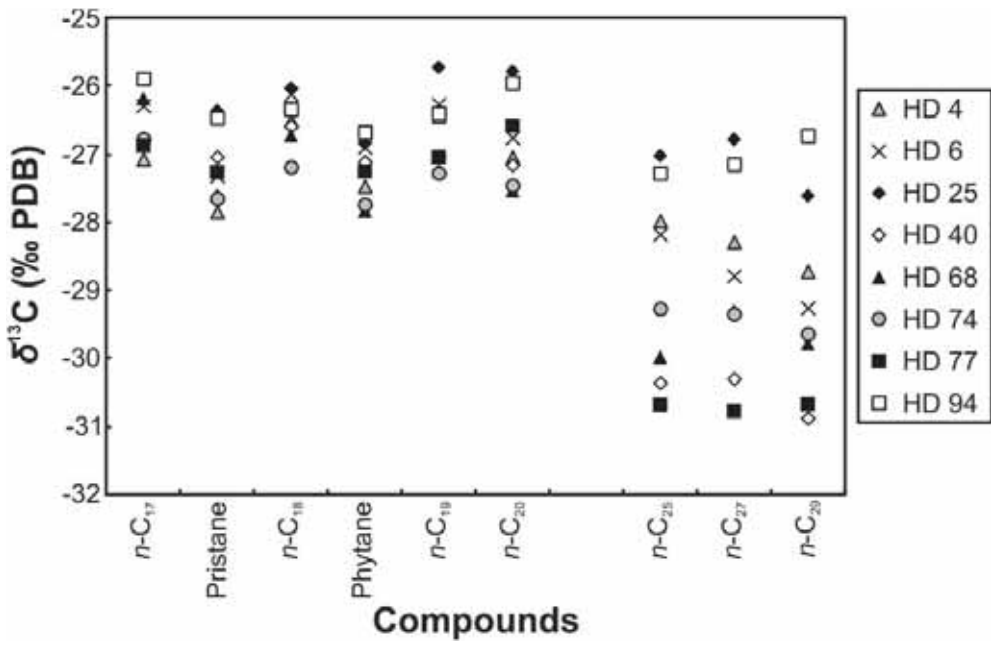

Fig. 9.7: Carbon isotopic composition of selected compounds in saturated hydrocarbon fractions of selected samples from the Huadian Formation.

The $\delta^{13}C$ values for the *n*-C_{17} to *n*-C_{20} alkanes vary between -25.5 to -28.0‰. Short-chain even *n*-alkanes are slightly depleted in ^{13}C compared to the neighboring odd *n*-alkanes. The odd long-chain *n*-alkanes (*n*-C_{25} to *n*-C_{29}) are more depleted in ^{13}C (ca. 2‰) than the short-chain *n*-alkanes. This result argues for a contribution of

terrigenous organic matter (i.e. C_3 plants; O'Leary, 1988; Farquhar et al., 1989; Collister et al., 1994; Murray et al., 1994).

The acyclic isoprenoids pristane and phytane are more depleted in ^{13}C than the short chain *n*-alkanes. Both compounds show nearly equal $\delta^{13}C$ values, which argues for a similar precursor (i.e. chlorophyll; Didyk et al., 1978; Goossens et al., 1984).

Tab. 9.3: Data from compound specific stable isotope geochemistry.

Sample	Depth (m)	*n*-C_{17} ($\delta^{13}C$, ‰, PDB)	Pristane ($\delta^{13}C$, ‰, PDB)	*n*-C_{18} ($\delta^{13}C$, ‰, PDB)	Phytane ($\delta^{13}C$, ‰, PDB)	*n*-C_{19} ($\delta^{13}C$, ‰, PDB)	*n*-C_{20} ($\delta^{13}C$, ‰, PDB)	*n*-C_{25} ($\delta^{13}C$, ‰, PDB)	*n*-C_{27} ($\delta^{13}C$, ‰, PDB)	*n*-C_{29} ($\delta^{13}C$, ‰, PDB)
Carbonaceous Shale Member										
HD 1	23.1	-27.09	-27.63	-26.70	-27.09	-27.38	-27.10	-28.43	-28.42	-29.04
HD 4	68.1	-27.07	-27.85	-26.51	-27.47	-26.45	-27.04	-27.98	-28.29	-28.72
HD 6	75.0	-26.29	-27.32	-26.12	-26.90	-26.27	-26.76	-28.18	-28.79	-29.26
Oil Shale Member										
HD 10	183.6	-25.49	-26.35	-25.93	-26.48	-26.21	-26.02	-27.30	-28.72	-28.53
HD 11	186.8	-26.43	-27.29	-26.67	-26.91	-27.05	-27.30	-28.48	-29.14	-29.63
HD 15	229.5	-26.83	-27.99	-27.30	-28.47	-27.95	-27.89	-29.92	-30.58	-30.42
HD 20	234.5	-26.33	-27.55	-26.87	-28.33	-28.20	-27.98	-28.86	-28.79	-28.48
HD 23	253.5	-25.47	-26.91	-25.94	-27.20	-26.72	-27.13	-28.06	-27.62	-28.34
HD 24	254.5	-26.44	-27.69	-26.51	-27.66	-27.19	-27.80	-28.88	-28.79	-29.42
HD 25	255.0	-25.91	-26.36	-26.03	-26.84	-25.72	-25.78	-27.02	-26.78	-27.61
HD 26	255.5	-25.79	-26.81	-26.32	-27.45	-26.50	-25.83	-28.33	-28.30	-28.42
HD 27	256.5	-25.53	-26.48	-25.41	-27.00	-25.63	-25.75	-27.54	-28.34	-28.16
HD 28	257.5	-26.27	-26.85	-26.56	-27.21	-25.88	-26.59	-28.05	-28.49	-28.99
HD 29	258.5	-26.06	-26.61	-26.48	-26.86	-26.17	-26.03	-28.13	-29.27	-28.88
HD 30	259.5	-26.86	-27.22	-26.49	-27.27	-26.86	-26.57	-29.40	-29.95	-30.28
HD 31	260.3	-26.30	-27.05	-26.33	-26.72	-26.81	-26.40	-27.75	-27.34	-27.37
HD 32	261.0	-25.58	-26.26	-25.84	-26.49	-25.93	-25.65	-28.52	-28.35	-29.16
HD 33	261.5	-25.82	-26.29	-26.16	-26.42	-26.48	-26.06	-27.71	-28.11	-28.28
HD 36	267.5	-25.23	-26.20	-25.15	-25.79	-25.02	-25.58	-27.63	-27.44	-27.62
HD 40	280.0	-26.77	-27.04	-26.59	-27.11	-27.03	-27.16	-30.36	-30.30	-30.88
HD 44	283.5	-26.34	-27.19	-26.73	-27.42	-26.48	-26.60	-30.86	-30.74	-30.69
HD 50	293.5	-25.60	-26.58	-25.72	-26.34	-25.96	-25.75	-28.86	-28.74	-29.13
HD 54	297.5	-25.93	-27.05	-26.38	-27.17	-26.57	-26.50	-28.11	-27.83	-28.05
HD 57	307.5	-25.83	-26.76	-25.99	-26.51	-26.20	-25.84	-28.93	-28.37	-28.54
HD 62	312.5	-25.44	-26.47	-26.12	-26.84	-26.35	-26.16	-28.53	-28.22	-27.99
HD 65	315.5	-26.37	-26.96	-26.44	-27.32	-27.09	-27.11	-28.35	-28.12	-29.04
HD 68	318.5	-26.18	-27.60	-26.72	-27.83	-27.24	-27.53	-29.98	-29.30	-29.78
HD 71	334.5	-25.47	-26.30	-25.91	-26.29	-25.97	-26.62	-28.19	-28.37	-28.80
HD 72	335.5	-27.01	-27.59	-27.07	-27.88	-26.99	-27.61	-29.43	-29.56	-29.47
HD 73	336.5	-26.10	-27.08	-26.51	-26.79	-26.66	-26.30	-28.68	-29.30	-28.67
HD 74	337.5	-26.78	-27.65	-27.19	-27.74	-27.28	-27.46	-29.27	-29.35	-29.64
HD 75	338.5	-26.25	-27.17	-26.00	-26.74	-26.59	-25.92	-28.34	-28.71	-28.78
HD 76	339.5	-26.09	-27.11	-26.27	-26.85	-26.56	-26.14	-30.11	-30.18	-30.05
HD 77	340.5	-26.87	-27.26	-26.33	-27.25	-27.04	-26.58	-30.68	-30.77	-30.67
HD 78	341.5	-26.94	-27.35	-26.93	-27.49	-27.11	-26.37	-30.71	-30.69	-30.66
HD 79	342.5	-25.49	-25.85	-25.91	-26.28	-26.63	-26.49	-28.55	-27.93	-28.21
HD 80	343.5	-26.82	-27.05	-26.30	-27.10	-26.27	-26.63	-29.41	-30.22	-30.06
HD 81	344.5	-26.41	-26.72	-26.68	-26.81	-26.84	-26.63	-29.39	-29.60	-29.15
HD 82	345.5	-26.95	-28.00	-27.22	-28.10	-27.53	-27.17	-31.00	-31.30	-30.73
Pyrite Member										
HD 85	370.5	-24.81	-24.95	-24.96	-25.41	-25.34	-25.28	-27.91	-27.63	-27.47
HD 90	423.5	-26.53	-26.84	-26.65	-26.77	-27.14	-26.91	-29.77	-29.60	-29.43
HD 94	506.5	-25.89	-26.47	-26.34	-26.68	-26.40	-25.95	-27.28	-27.15	-26.73

9.5 Discussion

9.5.1 Depositional environment of the Huadian Basin

Cartoons illustrating the depositional environment during different evolution stages of the Huadian Formation are shown in Fig. 9.8.

Fig. 9.8: Cartoon illustrating the depositional environment of the Huadian Formation.

9.5.1.1 Pyrite Member

The Pyrite Member accumulated in a shallow lake early in the basin's history. Fan deltas and alluvial fans existed along the lake margins. According to Sun et al. (2013), mudstones with low TOC contents, but high HI values prevail. Based on this observation, they suggest that conditions for organic matter preservation were good. Consequently, the low TOC contents might result either from low productivity or high sedimentation rates causing dilution of the accumulated organic matter by detrital minerals.

A shallow lake environment is also supported by the presence of coaly sediments at 424 and 371 m depth. Vitrinite is the main maceral in coaly sediments. The presence of minor alginite is indicative for sub-aquatic accumulation. The lower coaly layer is overlain by grey mudstone with 2 wt.% TOC containing terrestrial organic matter (HI: 108 mgHC/gTOC) and coarse-grained sandstone deposited in a fan delta environment. The upper coaly layer overlies rocks with a crumbly structure interpreted as paleo-soil and is overlain by bituminous mudstone with high TOC (10.4 wt.%) and high HI (623 mgHC/gTOC). Alginite is the prevailing maceral in the bituminous mudstone and indicates drowning of the mire. Red-colored bioturbated sediments follow 30 cm above the bituminous mudstone indicating a major change towards an oxic environment. Mudstones below and above the red layer contain minor amounts of landplant-derived organic matter (TOC < 1 wt.%; HI < 200 mgHC/gTOC).

Lacustrine mudstones unrelated to coaly horizons contain 0.4 to 5.1 wt.% TOC and HI values ranging widely from 116 to 664 mgHC/gTOC. Maceral data show that the organic matter of the hydrogen-rich sample is mainly derived from allochthonous sporinite and autochthonous alginite.

A high amount of landplant-derived macerals (sporinite, vitrinite) is reflected by biomarker and stable isotope composition. The terpenoid hydrocarbon composition shows a predominance of angiosperms in the surrounding vegetation. Minor bacterial activity is reflected by the low contents of hopanes. Relative high Pr/Ph ratios indicate the influence of coaly material within this member. The presence of

hydrothermal pyrite (Sun, 2010) causes relative high sulfur contents and low TOC/S ratios in the lower part of the Pyrite Member.

9.5.1.2 Oil Shale Member

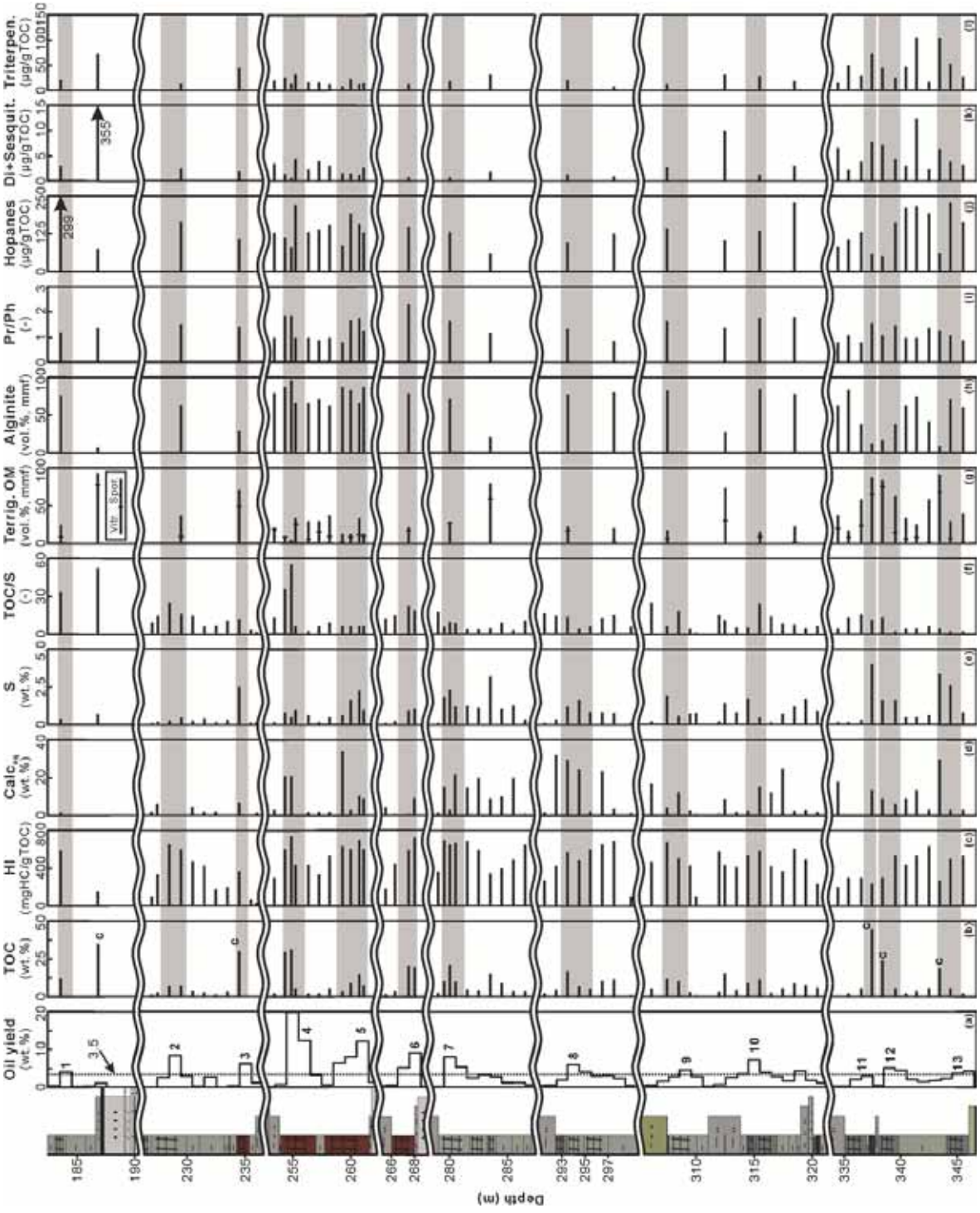

Fig. 9.9: Depth profiles showing important parameters of all 13 oil shale layers. *c, coaly layer.*

The Oil Shale Member is about 160 m thick. Apart from 13 oil shale layers with a total net thickness of 22 m, it includes organic-lean mudstones and thick sandy intervals. Many of the sandy intervals display a coarsening upward trend (Fig. 9.2) and are interpreted as prograding fan deltas.

Petrographical and geochemical data from oil shale layers are summarized in Fig. 9.9 together with average oil yield of 1 m thick intervals (according to Sun et al., 2013). HI of oil shale samples ranges from 246 to 744 mgHC/gTOC indicating that organic matter from variable sources is present in different oil shale layers.

Whereas oil shale with low HI values (kerogen type III) prevail in the lower part of the member (layers 13-11), those with high HI (kerogen type II-I) prevail in its middle and upper part (Fig. 9.9c). Oil shale of different stratigraphic position, therefore, is discussed separately below. Before that, salinity and redox proxies are evaluated because they are similar for oil shale in the entire member.

A freshwater environment is generally accepted for the Oil Shale Member, although the presence of Rhodophyta raises the possibility that the depositional environment of some oil shale layers was influenced by marine flooding (Xie et al., 2014). Although sulfur contents in some oil shale layers are as high as 4 wt.% (e.g. layer 11; Fig. 9.9e), TOC/S ratios are generally above 2.8 (Fig. 9.9f) consistent with the postulated non-marine environment (Berner, 1984). Ratios around 2.8 are restricted to a few samples underlying oil shale layers 13, 12 and 3 (Tab. 9.1). In contrast, relatively low MTTC ratios (0.24 – 0.66, Tab. 9.2) agree with a marine environment. In any case, the absence of gammacerane argues against a highly saline environment.

Stable carbon isotope ratios from pristane and phytane (Tab. 9.3) indicate the same precursor of the acyclic isoprenoids. In addition, maturity variations in the studied succession are negligible. Therefore, Pr/Ph ratios may be used as redox proxies. The determined values vary between 0.8 and 2.3 (Fig. 9.9i) and indicate dysaerobic to anaerobic conditions. Very low amounts of aryl isoprenoids show that permanent photic zone anoxia was not established. Whereas oxygen depleted conditions prevailed during deposition of oil shale layers and mudstones, frequent bioturbation indicates oxic conditions during deposition of sandy units.

Carbonate contents in mudstones and oil shales are often high (up to 35 wt.% $Calc_{eq}$; Fig. 9.9d). This may be a result of abundant ostracode shells (e.g. oil shale layer 8).

Oil shale layers 13 to 11

The stratigraphically deep oil shale layers 13 to 11 are restricted to the eastern part of the basin (Sun et al., 2013). The parting between layers 13 and 12 and the base of both layers is formed by mudstone with relatively low TOC, but high HI values (442-630 mgHC/gTOC; Fig. 9.9b) containing abundant alginite (Fig. 9.9h), whereas the upper part of layers 13 and 12, as well as layer 11 are composed of coaly rocks with high TOC contents (Fig. 9.9b), low HI values (<300 mgHC/gTOC; Fig. 9.9c) and abundant landplant-derived macerals (Fig. 9.9g).

High amounts of terrestrial organic matter are reflected by high amounts of landplant-derived biomarkers. Angiosperm-derived triterpenoids (Fig. 9.9l) predominate over gymnosperm-derived di- and sesquiterpenoids (Fig. 9.9k). Hopanoids, a proxy for bacterial biomass, occur in low amounts, but are abundant in lacustrine samples rich in alginite (Fig. 9.9j).

Abundant coaly material and the coaly upper part of oil shale layers 13 and 12 proves that the lake was shallow during deposition of layers 13 to 11.

Oil shale layers 10 to 8

Layer 10 is separated from layer 11 by a sandy succession, 16 m thick. The oil shale layers 10 to 8 are relatively thick, but the oil yield is low (Fig. 9.9a). This is a consequence of their moderate TOC contents (9-17 wt.%; Fig. 9.9b). HI values of oil shale samples range from 429 to 687 mgHC/gTOC (Fig. 9.9c). Maceral and biomarker data show that the organic matter of oil shale is dominated by algae (Fig. 9.9h) and bacteria (Fig. 9.9j). Terrestrial organic matter, dominated by angiosperms, is abundant only in a thin layer (312.5 m) intercalated between delta front sediments separating oil shale layers 10 and 9 (Fig. 9.9k, Fig. 9.9l). Layer 8 is separated from layer 9 by another interval with delta front sediments, which are bioturbated at 304 m depth (Sun, 2010).

The lateral extension of layers 10 to 8 increases significantly westward (Sun et al., 2013). This together with a general trend towards finer-grained sediments and the absence of coaly layers indicates a pronounced expansion and deepening of the lake.

Oil shale layers 7 to 4

Layers 7 to 4 cover most of the Huadian Basin. Their thickness is relatively low (up to 3 m), but TOC contents are very high and reach a maximum in layer 4 (31.7 wt.%; Fig. 9.9b). High TOC contents together with high HI (up to 744 mgHC/gTOC, Fig. 9.9c) result in very high oil yields, which increase upward and reach 20 wt.% in layer 4 (Fig. 9.9a). High HI values are a result of the presence of well-preserved algal material (Fig. 9.9h). Biomarkers suggest high amounts of bacterial biomass (Fig. 9.9j) and low contents in landplants (Fig. 9.9k, Fig. 9.9l). Similar to underlying layers, the terrestrial organic matter is dominated by angiosperms (Fig. 9.9l).

Layers 6 and 5 overlie coarsening upward sediments deposited in prograding fan deltas with a sharp contact. A 10-cm-thick interval with gastropods occurs 15 cm below layer 6. Sandstones underlying layer 5 are bioturbated. A well preserved 3 cm large gastropode occurs within layer 5 (260 m depth). The upper boundary of oil shale layers 7 to 4 is gradual and forms the base of upward coarsening successions (layers 7, 6, 4). Sediments 1.5 m above layer 4 are bioturbated. Layers 5 and 4 are separated by grey mudstones with moderate TOC contents (1.6-5.1 wt.%; Fig. 9.9b). HI values between 328 and 538 mgHC/gTOC are still high (Fig. 9.9c) and Pr/Ph ratios low (~1; Fig. 9.9i) suggesting that low TOC contents are rather due to low organic productivity than due to poor preservation.

The observed succession reflects three progradations of fan deltas establishing oxic conditions. Each progradation was terminated by a rapid relative sea level rise resulting in oxygen-depleted conditions favoring oil shale deposition. The frequent changes between bioturbated sediments and oil shale layers argues against a deep lacustrine environment, which often produces stable conditions. The thickness of the coarsening upward complexes suggests that water depth was in the order of a few tens of meters and probably reached a maximum during deposition of layer 4.

Oil shale layers 3 to 1

Oil shale layers 3 to 1 are thin, but average TOC (8-10 wt.%) and HI values (740-800 mgHC/gTOC) are very high (Sun et al., 2013). The sample from layer 3 investigated during the present study has a significantly lower HI (364 mgHC/gTOC; Fig. 9.9c) resulting from abundant angiosperm-dominated terrigenous organic matter (Fig. 9.9l). Layer 3 has been deposited after a major fan delta progradation. Thus, the high percentage of landplant material (Fig. 9.9g) reflects a shallow depositional environment. Shallow water depth is also indicated by cross-bedding observed in oil shale layer 2 and a coaly layer at 186.8 m depth. In contrast to underlying rocks, gymnosperm-derived biomarkers prevail over angiosperm-derived biomarkers in the coaly layer (Fig. 9.9k, Fig. 9.9l).

9.5.1.3 Carbonaceous Shale Member

The Carbonaceous Shale Member represents the final filling stage of the Huadian lake. Several high-ash (~30 wt.% TOC) coal seams accumulated along the lake margins. Two of them, each about 2 m thick, are currently mined. The upper seam is overlain by 1-m-thick oil shale reflecting a short-term deepening of the lake during a general regressive trend. No coal seam, but two coaly layers and some bituminous shales with abundant alginite have been drilled in Hd3. Similar to the coaly layer in the uppermost Oil Shale Member (186.8 m depth) gymnosperm-derived biomarkers prevail over angiosperm-derived biomarkers suggesting a major change in paleo-vegetation during deposition of the uppermost part of the Oil Shale Member. Low sulfur contents and high TOC/S ratios argue for a freshwater environment.

9.5.2 Comparison of the Huadian and Fushun basins

Both, the Huadian and Fushun basins have been formed during Eocene time along the DunMi Fault Zone and contain economic sub-bituminous coal and oil shale with similar maturity. Moreover, a freshwater environment prevailed in both basins. Nevertheless, the habitat of the coal and oil shale deposits differs significantly (Liu et al., 2009). In this section, the depositional environment of the coal-bearing Guchengzi Formation and the oil shale-bearing Jijuntun Formation in the Fushun Basin is discussed first, based on data from Strobl et al. (2014; in press; Fig. 9.10). Afterwards

the mechanisms controlling the differences between the Fushun and Huadian basins are investigated.

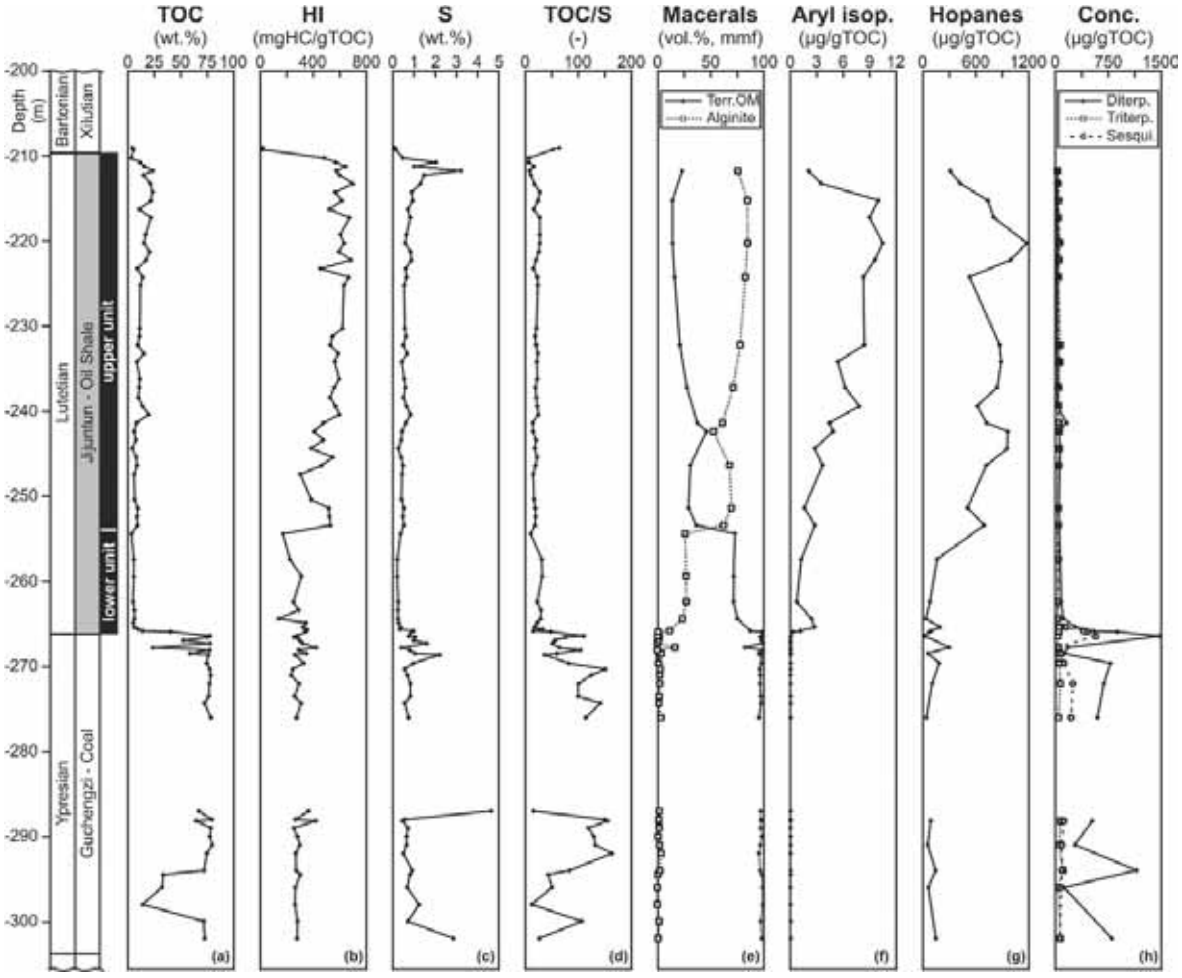

Fig. 9.10: Depth profiles of important parameters of the coal and oil shale bearing formations within the Fushun Basin [modified according to Strobl et al. (2014; in press)].

The Guchengzi Formation contains a single coal seam, several tens of meters thick, which has been deposited close to the lake level. Abundant di- and sesquiterpenoids (Fig. 9.10h) indicate that the vegetation was dominated by gymnosperms. The great seam thickness shows that peat accumulation was in equilibrium with tectonic subsidence for a long time. Finally subsidence rates increased and the mire was replaced by a shallow lake, resulting in the deposition of the ash-rich top of the seam and in accumulation of the lower unit of the oil shale-bearing Jijuntun Formation. The latter contains relative low TOC contents (~5 wt.%; Fig. 9.10a). A mixture of prevailing landplant-derived and algal material (Fig. 9.10e) caused a moderate HI (~400 mgHC/gTOC; Fig. 9.10b). Oil shale of the upper unit of the Jijuntun Formation

containing up to 25 wt.% TOC (Fig. 9.10a) and dominant lacustrine organic matter (HI: ~700 mgHC/gTOC, Fig. 9.10b) has been deposited in a deep lake. Concentrations of aryl isoprenoids, indicative for photic zone anoxia, increase upward (Fig. 9.10f). The absence of gammacerane suggests that water column stratification in the deep lake originated without significant changes in bottom water salinity. Photic zone anoxia in modern Lake Tanganyika occurs beneath ~150 m water depth (De Wever et al., 2005). A similar water depth may be assumed for the upper unit of the Jijuntun Formation. The high water depth was responsible for stable conditions, the lack of coarse grained clastic rocks, and the accumulation of high quality oil shale, several tens of meters thick. Photic zone anoxia vanished during deposition of the uppermost part of the Jijuntun Formation (Fig. 9.10f). At the same time TOC contents decrease drastically. Later the lake in the Fushun Basin was filled by a mixed clastic-carbonate shallow water succession (Xilutian Formation) and clastic shallow water to terrestrial rocks (Gengjiajie Formation).

Thus, the fill of the Fushun Basin reflects a continuous upward deepening trend followed by a shallowing trend, typical for many fault controlled rift and strike-slip basins. Depending on climatic conditions, the stratigraphic succession of these basins often includes from base to top fluvial sediments, a thick coal seam, shallow and deep lacustrine deposits reflecting high subsidence rates during active faulting (Lambiase, 1990; Sachsenhofer, 2000; Sachsenhofer et al., 2003). Later the deep lake is filled by deltaic sediments. Coal may form also during the regressive filling stage of the basin, but this coal is typically of lower thickness than that deposited during the transgressive stage. Within the Fushun Basin, coal deposited during the regressive stage is not known.

The major differences between the depositional environments of the Huadian and Fushun basins are summarized in cartoons shown in Fig. 9.11.

The stratigraphic succession in the Huadian Basin is much more complex and does not show a clear depth trend. The distribution of sandy sediments suggests that a maximum flooding interval exists at about 300 m depth (between oil shale layers 8 and 7; Fig. 9.2) and that the basin remained relatively deep till deposition of oil shale layer 4. However, water depth was generally significantly lower in the Huadian Basin than in the Fushun Basin. This may result either from lower subsidence rates or from

significantly higher clastic input causing a higher accumulation rate. Because the thickness of the Oil Shale Member in the Huadian Basin is similar to that of the Jijuntun Formation in the Fushun Basin, we prefer the first explanation. Probably, the relative low water depth hindered the establishment of a stable stratified water column, caused changes in redox conditions, and favored the frequent progradation of clastic units, all of them preventing deposition of thick oil shale. Shallow water depth also caused relatively high amounts of terrestrial organic matter and, therefore, relative low quality of some oil shale layers. In contrast to the Fushun Basin, the terrestrial organic matter influx was dominated by angiosperms. Hopane concentrations show that bacterial biomass played a subordinate role in Huadian oil shale compared to the Fushun oil shale.

Coaly layers, but no economic seam accumulated during deposition of the Pyrite Member, which represents the early transgressive phase of the Huadian Basin. Sun et al. (2013) speculate that the absence of thick coal is due to a prevailing arid climate during deposition of the Pyrite Member postulated by Meng (2010), which prevented thick peat accumulations. In contrast, a subtropical climate prevailed during deposition of the Fushun coal (Wang et al., 2010). The climatic difference may indicate that the Pyrite Member and the Guchengzi Formation are not strictly coeval.

Economic, but thin high-ash coal (up to 2.1 m in mine areas) accumulated in the Carbonaceous Shale Member. The relative low thickness and its high content in mineral matter are typical for coal deposited during the final filling stage of fault controlled basins. Comparable seams are missing in the Fushun Basin.

Summarizing, the different stratigraphic position, number and thickness of individual coal and oil shale layers in the Huadian and Fushun basins are mainly controlled by different subsidence rates, which have been significantly higher in the Fushun Basin. Climatic factors may have played a secondary role.

Fig. 9.11: Simplified cartoon illustrating the depositional environments of the Huadian and Fushun basins outlining major differences.

9.6 Conclusions

The fill of the Huadian Basin comprises from bottom to top the Pyrite Member, the Oil Shale Member and the Carbonaceous Shale Member. The most important conclusions regarding the depositional environment of the Huadian Basin include:

- Although different salinity proxies yield inconsistent results, a non-marine depositional environment is generally accepted.
- Water depth of the lake in the Huadian Basin reached a maximum during deposition of the middle part of the Oil Shale Member, but did not exceed a few tens of meters. Probably, this is a result of relative low subsidence rates.
- Deposition of fan delta sediments and changes in redox conditions frequently disrupted oil shale accumulation. Consequently, a high number of thin oil shale layers is present in the Huadian Basin.
- Water depth was not high enough to establish a stable stratified water column. Moreover the amount of terrestrial organic matter is significant, especially in oil shale from the lower part of the Oil Shale Member. The oil shale quality, therefore, varies significantly between different layers. Economically most important are layers 7 to 4.
- Coaly layers and bituminous shale occur in all three members, but economic coal, about 2 m thick, is limited to the Carbonaceous Shale Member.

A comparison of the non-marine Fushun and Huadian basins shows that:

- In contrast to the Huadian Basin, the Fushun Basin is characterized by a distinct deepening upward – shallowing upward trend characteristic for many fault controlled basins. This succession reflects high subsidence rates during early basin formation and the filling of a deep lake during late stage basin evolution.
- A single coal seam, up to 120 m thick, formed early in the history of the Fushun Basin. Similar thick transgressive coal is missing in the Huadian Basin, perhaps because of an arid climate.
- Increased subsidence rate caused drowning of the Fushun coal and the development of shallow and deep lacustrine conditions. Photic zone anoxia have been established in the deep lake suggesting a water depth of more than

150 m. Stable, strictly anoxic conditions together with high productivity allowed the accumulation of a world-class oil shale deposit, up to 300 m thick. In contrast, subsidence rates were minor in the Huadian Basin, resulting in moderate water depth and the accumulation of a high number of thin oil shale layers.

- Strong terrestrial input in the lower part of the oil shale unit is recorded in both basins, but gymnosperms prevail in the Fushun Basin, whereas angiosperms prevail in the Huadian Basin.
- Bacterial biomass is more abundant in Fushun oil shale than in Huadian oil shale.
- Economic, but thin and ash rich coal accumulated during the regressive stage in the Huadian Basin. Equivalent coal in the Fushun Basin is missing.
- Differences in stratigraphic position, quantity and quality of coal and oil shale in the Fushun and Huadian basins are mainly controlled by different subsidence rates, which have been significantly higher in the Fushun Basin. Climatic factors may have played a secondary role.

9.7 Acknowledgments

Special thanks to the “Material Centre of Ministry of Land and Resources”, who generously provided core samples from well Hd3 to us. We would like to express our gratitude to Prof. Zhaojun Liu from the Jilin University in Changchun (NE China) for his help to organize the sample material.

9.8 References

Barakat, A.O., Rullkötter, J., 1997. A comparative study of molecular paleosalinity indicators: chromans, tocopherols and C20 isoprenoid thiophenes in Miocene lake sediments (Nördlinger Ries, Southern Germany). Aquatic Geochemistry 3, 169-190.

Beard, K.C., Wang, B., 1991. Phylogenetic and biogeographic significance of the tarsiiform primate Asiomomys changbaicus from the Eocene of Jilin Province, Peoples Republic of China. American Journal of Physical Anthropology 85, 159-166.

Berner, R.A., 1984. Sedimentary pyrite formation: An update. Geochimica et Cosmochimica Acta 48, 605-615.

Bray, E.E., Evans, E.D., 1961. Distribution of *n*-paraffins as a clue to recognition of source beds. Geochimica et Cosmochimca Acta 22, 2-15.

Collister, J.W., Rieley, G., Stern, B., Eglinton, G., Fry, B., 1994. Compound-specific $\delta^{13}C$ analysis of leaf lipids from plants with differing carbon dioxide metabolism. Organic Geochemistry 21, 619-627.

Coplen, T.B., 2011. Guidelines and recommended terms for expression of stable-isotope-ratio and gas-ratio measurement results. Rapid Communications in Mass Spectrometry 25, 2538-2560.

Cranwell, P.A., 1977. Organic geochemistry of CamLoch (Sutherland) sediments. Chemical Geology 20, 205-221.

De Wever, A., Muylaert, K., Van der Gucht, K., Pirlot, S., Cocquyt, C., Descy, J.-P., Plisnier, P.-D, Vyverman, W. 2005. Bacterial Community Composition in Lake Tanganyika: Vertical and Horizontal Heterogeneity. Applied Environmental Microbiology 71, 5029-5037.

Dev, S., 1989. Terpenoids; in: Rowe, J.W. (Ed.), Natural Products of Woody Plants. Springer, Berlin, pp. 691-807.

Didyk, B.M., Simoneit, B.R.T., Brassell, S.C., Eglinton, G., 1978. Organic geochemical indicators of paleoenvironmental conditions of sedimentation. Nature 272, 216-222.

Eglinton, G., Hamilton, R.J., 1967. Leaf epicuticular waxes. Science 156, 1322-1335.

Espitalié, J., Marquis, F., Barsony, I., 1984. Geochemical logging, in: Voorhess, K.J. (Ed.), Analytical Pyrolysis. Butterworths, Boston, pp. 53-79.

Farrimond, P., Talbot, H.M., Watson, D.F., Schulz, L.K., Wilhelms, A., 2004. Methylhopanoids: Molecular indicators of ancient bacteria and a petroleum correlation tool. Geochimica et Cosmochimica Acta 68, 3873-3882.

Farquhar, G.D., Ehleringer, J.R., Hubick, K.T., 1989. Carbon isotope discrimination and photosynthesis. Annual Review of Plant Physiology and Plant Molecular Biology 40, 503-537.

Ficken, K.J., Li, B., Swain, D.L., Eglinton, G., 2000. An *n*-alkane proxy for the sedimentary input of submerged/floating freshwater aquatic macrophytes. Organic Geochemistry 31, 745-749.

Goossens, H., de Leeuw, J.W., Schenck, P.A., Brassel, S.C., 1984. Tocopherols as likely precursors of pristane in ancient sediments and crude oils. Nature 312, 440-442.

Hussler, G., Albrecht, P., Ourisson, G., 1984. Benzohopanes, a novel family of hexacyclic geomarkers in sediments and petroleums. Tetrahedron Letters 25, 1179-1182.

Karrer, W., Cherbuliez, E., Eugster, C.H., 1977. Konstitution und Vorkommen der organischen Pflanzenstoffe – Ergänzungsband 1. Birkhäuser, Basel – Stuttgart.

Lambiase, J.J., 1990. A model for tectonic control of lacustrine stratigraphic sequences in continental rift basins, in: Katz, B.J. (Ed.), Lacustrine basin exploration: case studies and modern analogs. AAPG Memoir 50, 265-276.

Langford, F.F., Blanc-Valleron, M.M., 1990. Interpreting Rock-Eval pyrolysis data using graphs of pyrolyzable hydrocarbons vs. total organic carbon. AAPG Bulletin 74, 799-804

Liu, Z. Dong, Q., Zhu, J., Guo, W., Ye, S., Liu, R., Meng, Q., Zhang, H., Gan, S., 2009. Oil Shale in China. Petroleum Industry Press, Beijing.

Manchester, S.R., Chen, Z., Geng, B., Tao, J., 2005. Middle Eocene flora of Huadian, Jilin Province, Northeastern China. Acta Paleobotanica 45, 3-26.

Meng, Q., 2010. Research on petrologic and geochemical characteristics of Eocene oil shale and its enrichment regularity, Huadian Basin. Thesis Jilin University.

Meng, Q., Liu, Z., Bruch, A.A., Liu, R., Hu, F., 2012. Paleoclimatic evolution during Eocene and its influence on oil shale mineralisation, Fushun basin, China. Journal of Asian Earth Sciences 45, 95-105.

Murray, A.P., Summons, R.E., Boreham, C.J., Dowling, L.M., 1994. Biomarker and *n*-alkane isotope profiles for Tertiary oils: relationship to source rock depositional setting. Organic Geochemistry 22, 521-542.

O'Leary, M.H., 1988. Carbon Isotopes in Photosynthesis – Fractionation techniques may reveal new aspects of carbon dynamics in plants. BioScience 38, 328-336.

Otto, A., Walther, H., Püttmann, W., 1997. Sesqui- and diterpenoid biomarkers in Taxodium-rich Oligocene oxbow lake clays Weisselster basin, Germany. Organic Geochemistry 26, 105-115.

Otto, A., Wilde, V., 2001. Sesqui-, di-, and triterpenoids as chemosystematic markers in extant conifers – a review. Botanical Review 67, 141-238.

Ourisson, G., Albrecht, P., Rohmer, M., 1979. The hopanoids: paleo-chemistry and biochemistry of a group of natural products. Pure and Applied Chemistry 51, 709-729.

Radke, M., Willsch, H., Welte, D.H., 1980. Preparative hydrocarbon group type determination by automated medium pressure liquid chromatography. Analytical Chemistry 52, 406-411.

Rohmer, M., Bouvier-Nave, P., Ourisson, G., 1984. Distribution of hopanoid triterpenes in prokaryotes. Journal of General Microbiology 130, 1137-1150.

Sachsenhofer, R.F., 2000. Geodynamic controls on deposition and maturation of coal in the Eastern Alps, in: Neubauer, F., Höck, V. (Eds.), Aspects of Geology in Austria. Mitteilungen der Österreichischen Geologischen Gesellschaft 92, 185-194.

Sachsenhofer, R.F., Bechtel, A., Reischenbacher, D., Weiss, A., 2003. Evolution of lacustrine systems along the Miocene Mur-Mürz fault system (Eastern Alps, Austria) and implications on source rocks in pull-apart basins. Marine and Petroleum Geology 20, 83-110.

Sinninghe Damsté, J.S., Kock-Van Dalen, A.C., de Leeuw, J.W., Schenk, P.A., Guoying, S., Brassell, S.C., 1987. The identification of mono-, di-, and trimethyl 2-methyl-2-(4,8,12-trimethyltridecyl)chromans and their occurrence in geosphere. Geochimica et Cosmochimica Acta 51, 2393-2400.

Sinninghe Damsté, J.S., Keely, B.J., Betts, S.E., Baas, M., Maxwell, J.R., de Leeuw, J.W., 1993. Variations in abundances and distributions of isoprenoid chromans and long-chain alkylbenzenes in sediments of the Mulhouse Basin: a molecular sedimentary record of paleosalinity. Organic Geochemistry 20, 1201-1215.

Strobl, S.A.I., Sachsenhofer, R.F., Bechtel, A., Gratzer, R., Gross, D., Bokhari, N.H., Liu, R., Liu, Z., Meng, Q., Sun, P., 2014. Depositional environment of oil shale within the Eocene Jijuntun Formation in the Fushun Basin (NE China). Marine and Petroleum Geology 56, 166-183.

Strobl, S.A.I., Sachsenhofer, R.F., Bechtel, A., Meng, Q., in press. Paleoenvironment of the Eocene coal seam in the Fushun Basin (NE China): Implications from petrography and organic geochemistry. International Journal of Coal Geology.

Summons, R.E., Powell, T.G., 1987. Identification of aryl isoprenoids in source rocks and crude oils: biological markers for the green sulphur bacteria. Geochimica et Cosmochimica Acta 51, 557-566.

Sun, P., 2010. Research on Sedimentary Characteristics of Huadian Formation of Paleogene in Huadian Basin. Thesis Jilin University.

Sun, P., Liu, Z., Meng, Q., Liu, R., Jia, J., Hu, X., 2011. Effect of the basin-fill features on oil shale formation in Paleogene, Huadian Basin. Journal of China Coal Society 36, 1110-1116.

Sun, P., Sachsenhofer, R.F., Liu, Z., Strobl, S.A.I., Meng, Q., Liu, R., Zhen, Z., 2013. Organic matter accumulation in the oil shale- and coal-bearing Huadian Basin (Eocene; NE China). International Journal of Coal Geology 105, 1-15.

Taylor, H., Teichmüller, M., Davis, A., Diessel, C.F.K., Littke, R., Robert, P., 1998. Organic Petrology. Borntraeger. Berlin-Stuttgart.

ten Haven, H.L., de Leeuw, J.W., Rullkötter, J., Sinninghe Damsté, J.S., 1987. Restricted utility of the pristane/phytane ratio as a paleoenvironmental indicator. Nature 330, 641-643.

Tissot, B.T., Welte, D.H., 1984. Petroleum Formation and Occurence, 2nd ed., Springer Verlag, Berlin.

Volkman, J.K., Maxwell, J.R., 1986. Acyclic isoprenoids as biological markers, in: Johns, R.B. (Ed.), Biological Markers in the Sedimentary Record. Elsevier, Amsterdam, pp.1-42.

Wang, Q., Bai, J., Sun, B., Sun, J., 2005. Strategy of Huadian oil shale comprehensive utilization. Oil Shale 22, 305-315.

Xie, X., Volkman, J.K., Qin, J., Borjigin, T., Bian, L., Zhen, L., 2014. Petrology and hydrocarbon potential of microalgal and macroalgal dominated oil shales from the Eocene Huadian Formation, NE China. International Journal of Coal Geology 124, 36-47.

Zhang, P.L., Lu, B.C., Li, C.T., Sun, J.R., Liu, A., 1986. Discovery of the Huadian Fauna of the Early Tertiary and its geological significance. Jilin Geology 4, 1-14.

APPENDIX

10 Appendix

10.1 Author contributions on publications included in this thesis

10.1.1 Publication I

Depositional environment of oil shale within the Eocene Jijuntun Formation in the Fushun Basin (NE China)

Marine and Petroleum Geology 56 (2014), 166-183
DOI: 10.1016/j.marpetgeo.2014.04.011

Susanne A.I. Strobl, Reinhard F. Sachsenhofer, Achim Bechtel, Reinhard Gratzer, Doris Gross, Syed N.H. Bokhari, Rong Liu, Zhaojun Liu, Qingtao Meng, Pingchang Sun

Author contributions

Susanne A.I. Strobl did the sampling in China together with Reinhard F. Sachsenhofer and the Chinese colleagues mentioned as co-authors above. Susanne A.I. Strobl did the sample preparation, conducted all measurements, interpreted all data and wrote the manuscript. Reinhard F. Sachsenhofer was helpful during interpretation of the results and proofread the manuscript. Achim Bechtel and Reinhard Gratzer helped with biomarker analyses and isotope geochemistry. Doris Gross was helpful during LECO and Rock Eval measurements, organic petrography, and during interpretation of the results. Syed N.H. Bokhari helped with XRF measurements. Rong Liu, Zhaojun Liu, Qingtao Meng and Pingchang Sun organized the field work in China and contributed with helpful discussions. Approximately 90% of the required work for this publication was conducted by Susanne A.I. Strobl.

10.1.2 Publication II

Paleoenvironment of the Eocene coal seam in the Fushun Basin (NE China): Implications from petrography and organic geochemistry

Accepted for publication in International Journal of Coal Geology
DOI: 10.1016/j.coal.2014.10.001

Susanne A.I. Strobl, Reinhard F. Sachsenhofer, Achim Bechtel, Qingtao Meng

Author contributions

Susanne A.I. Strobl did the sampling in China together with Reinhard F. Sachsenhofer and Qingtao Meng. Susanne A.I. Strobl did the sample preparation, conducted all measurements, interpreted all data and wrote the manuscript. Reinhard F. Sachsenhofer provided fruitful discussions particularly on coal data and proofread the manuscript. Achim Bechtel helped with biomarker analyses and isotope geochemistry and interpretation of these datasets. Qingtao Meng provided translations of Chinese publications and contributed with discussions on coal seam distribution. Approximately 90% of the required work for this publication was conducted by Susanne A.I. Strobl.

10.1.3 Publication III

Deposition of coal and oil shale in China: the Eocene Huadian Basin compared to the coeval Fushun Basin

Submitted to Marine and Petroleum Geology

Susanne A.I. Strobl, Reinhard F. Sachsenhofer, Achim Bechtel, Qingtao Meng, Pingchang Sun

Author contributions

Susanne A.I. Strobl did the sample preparation, conducted all measurements, interpreted all data and wrote the manuscript. Reinhard F. Sachsenhofer helped to outline the manuscript, helped during interpretation of the results and proofread the manuscript. Achim Bechtel helped with biomarker analyses and isotope geochemistry and interpretation of these datasets. Qingtao Meng provided information on oil shale and coal production, organized the sample taking and contributed with discussions on stratigraphy and structural geology. Pingchang Sun took the core samples in China provided by the “Material Centre of Ministry of Land and Resources”, provided translations of Chinese publications and contributed with helpful discussions. Approximately 90% of the required work for this publication was conducted by Susanne A.I. Strobl.

10.2 Posters, oral presentations and publications related to study results (not included in this thesis)

Strobl, S.A.I., Bechtel, A., Sachsenhofer, R.F., Sun, P., Meng, Q., Liu, R., Liu, Z., 2013. Deposition of Oil Shale in the Fushun Basin, Eocene, NE China. 75th EAGE Conference & Exhibition incorporating SPE EUROPEC 2013, London. Poster presentation.

Strobl, S.A.I., Bechtel, A., Liu, Z., Sachsenhofer, R.F., Sun, P., Xu, J., 2014. Deposition of Oil Shale in the Huadian Basin (Eocene, NE China). AAPG International Conference and Exhibition 2014, Istanbul. Oral presentation.

Strobl, S.A.I., Sachsenhofer, R.F., Bechtel, A., 2014. Depositional environment of oil shale and coal deposits – the example of the Fushun and Huadian basins (Eocene, NE China). Jilin University, Changchun. Oral presentation.

Sun, P., Sachsenhofer, R.F., Liu, Z., Strobl, S.A.I., Meng, Q., Liu, R., Zhen, Z., 2013. Organic matter accumulation in the oil shale- and coal-bearing Huadian Basin (Eocene, NE China). International Journal of Coal Geology 105, 1-15.

10.3 Fushun Basin – selected photographs

Overview of the stratigraphic succession and approximate location of study profile within the West Open Pit mine

10.3.1 Guchengzi Formation – Coal

Guchengzi Formation in the West Open Pit mine with gallery from "Japanese" underground mine

Coal with amber (open pit)

Coal (open pit)

Sample FS04 (-296.00 m)

Sample FS24 (-268.60 m)

Sample FS27 (-267.75 m)

Sample FS30a (-266.50 m), coal with amber

10.3.2 Jijuntun Formation – Oil Shale

Jijuntun Formation in the West Open Pit mine

Sample FS64 (-238.35 m)

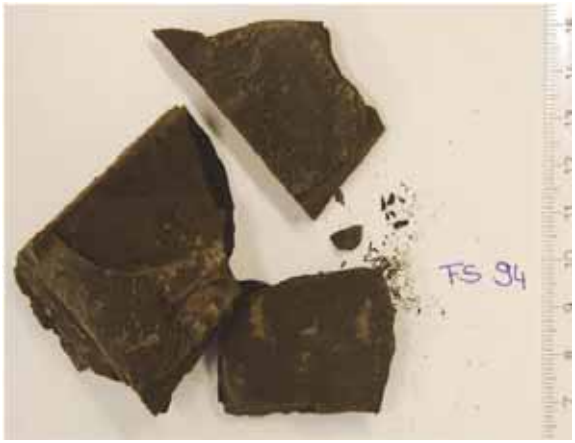

Sample FS94 (-211.65 m)

10.3.3 Xilutian Formation

Jijuntun and Xilutian formations in the West Open Pit mine

Sample FS99(-208.95 m)

10.4 Huadian Basin – selected core photographs

Samples investigated in the present study are labelled.

10.4.1 Carbonaceous Shale Member

10.4.2 Oil Shale Member

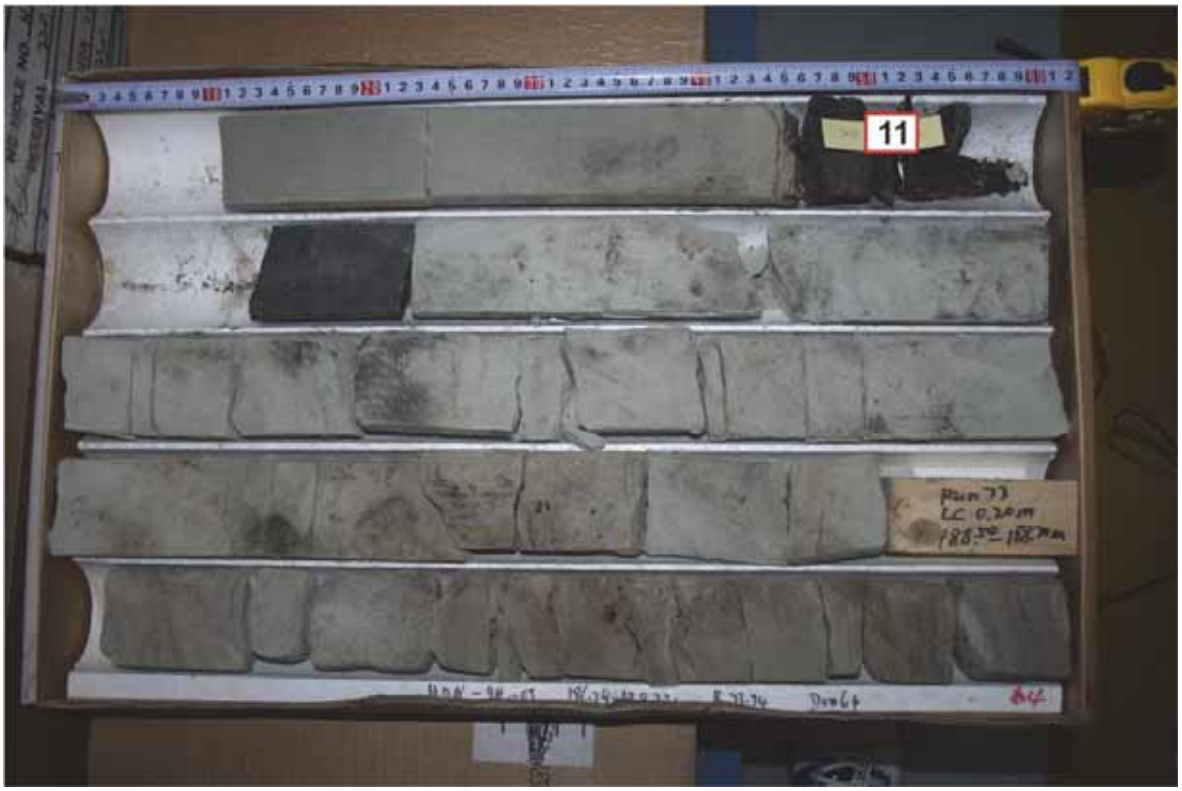
11
Run 77
LC 0.20m

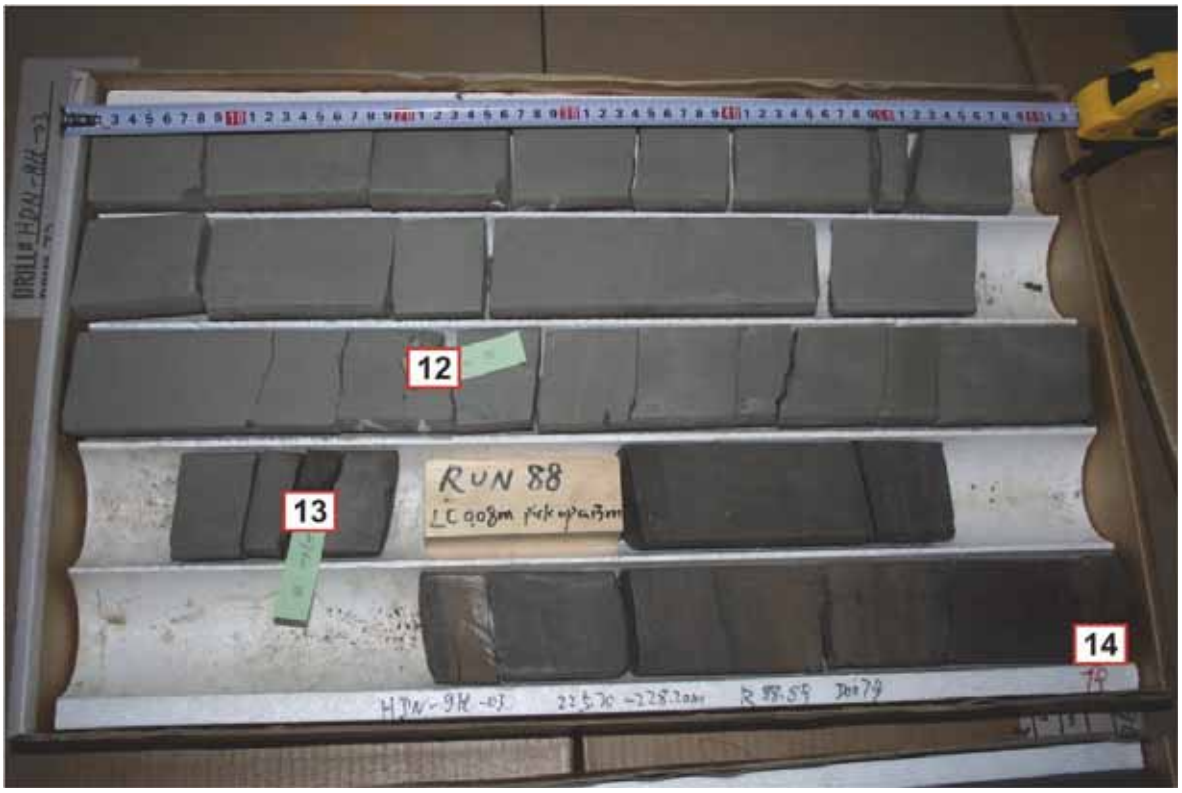
12
RUN 88
13
14


15
16
RUN 89
LC 0.40m


17
RUN 90
18
19


RUN 91
No LC pickup zone
RUN 92
No LC
20
21
22


23
24
Run 99
No LC

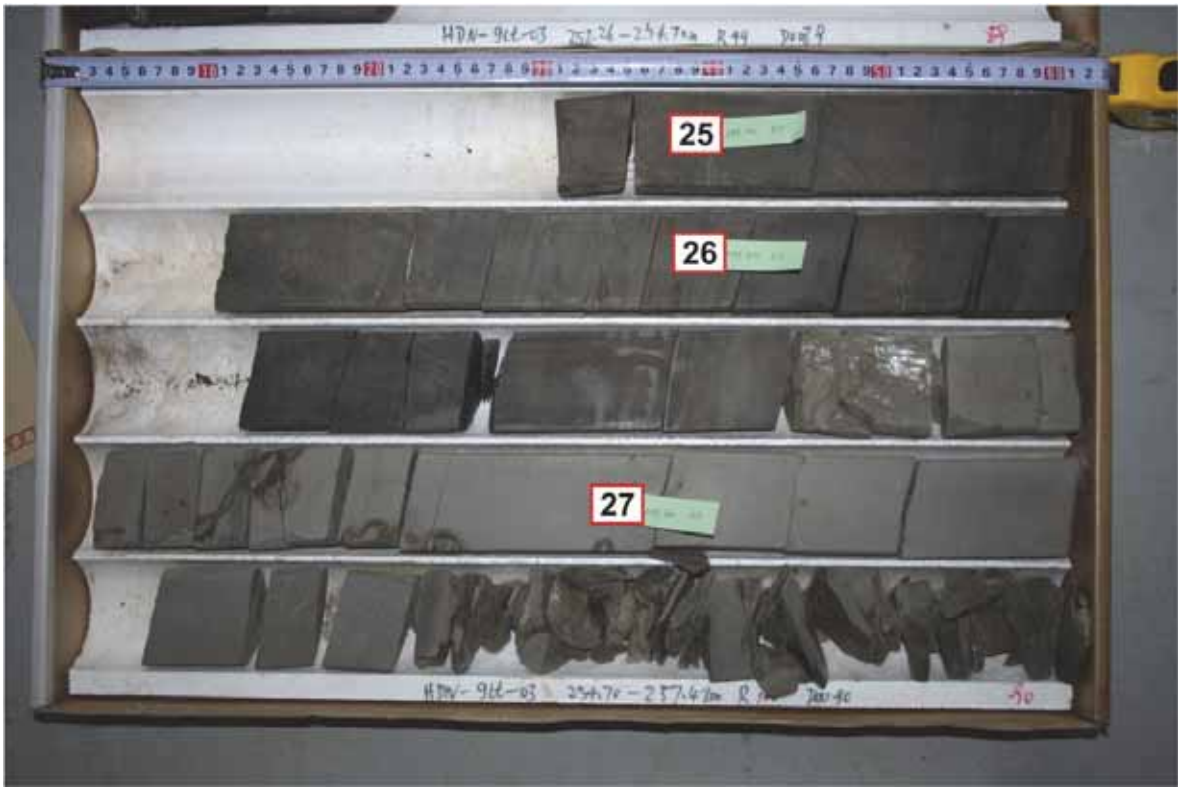
25
26
27


28
29
30
Run 102
No LC

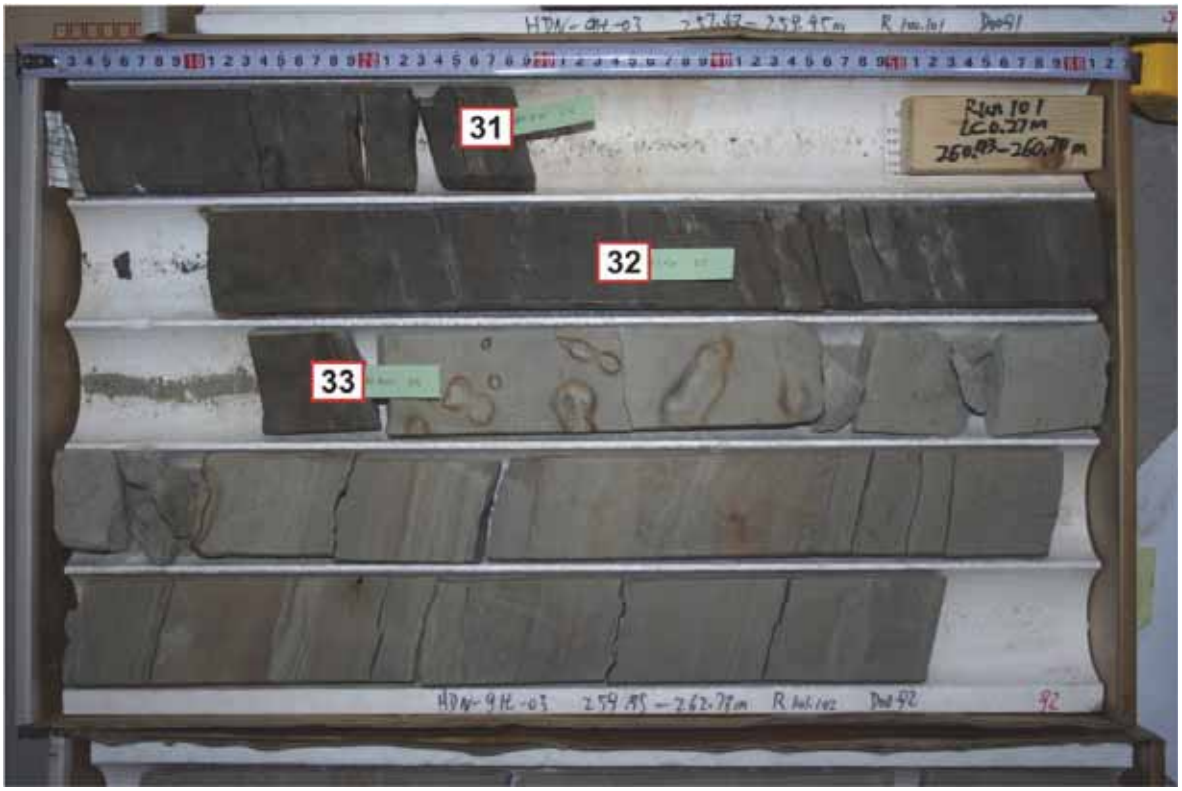
31
32
33

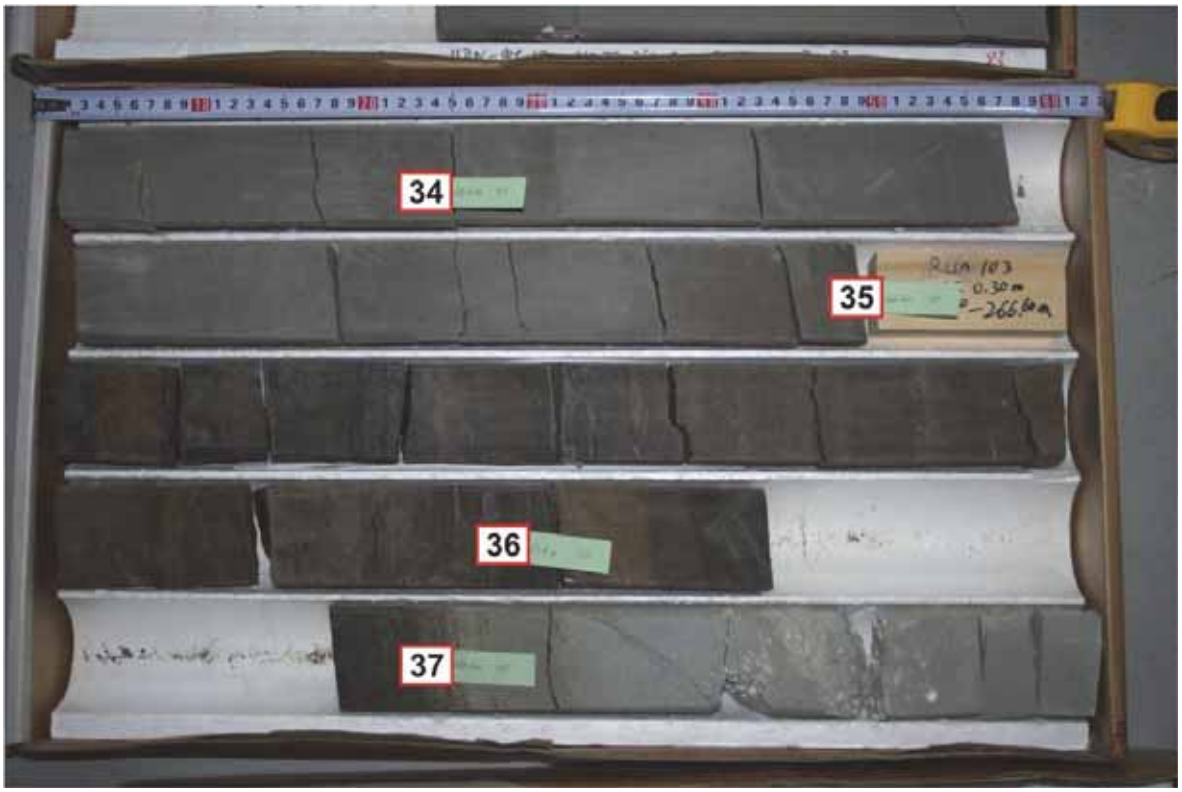
34
35
36
37


RUN 108
No LC pickup
38
39
40
41


42
RUN 109
No LC
43


44
45
RUN 110
NO LC
46


47
RUN 111
LC 0.04m
285.97m-288.40m


48


49
50
51


52
53
54


55


RUN 120
LC 1.41m
56
57
58


RUN 121
pick-up 0.81m
Run 122
NO LC
59
60

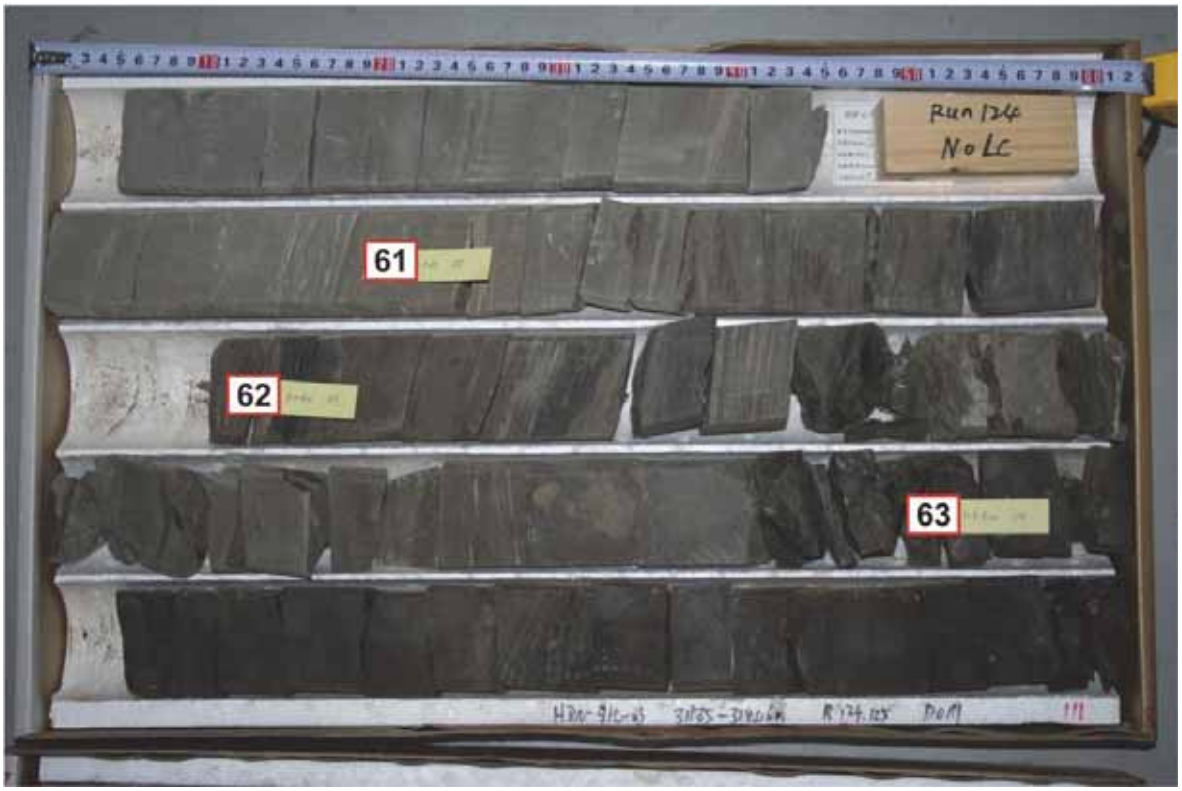
Run 124
No LC
61
62
63


Run 125
No LC
64
65
66


67
68
Run 126
No LC


69
70
Run 127
No LC

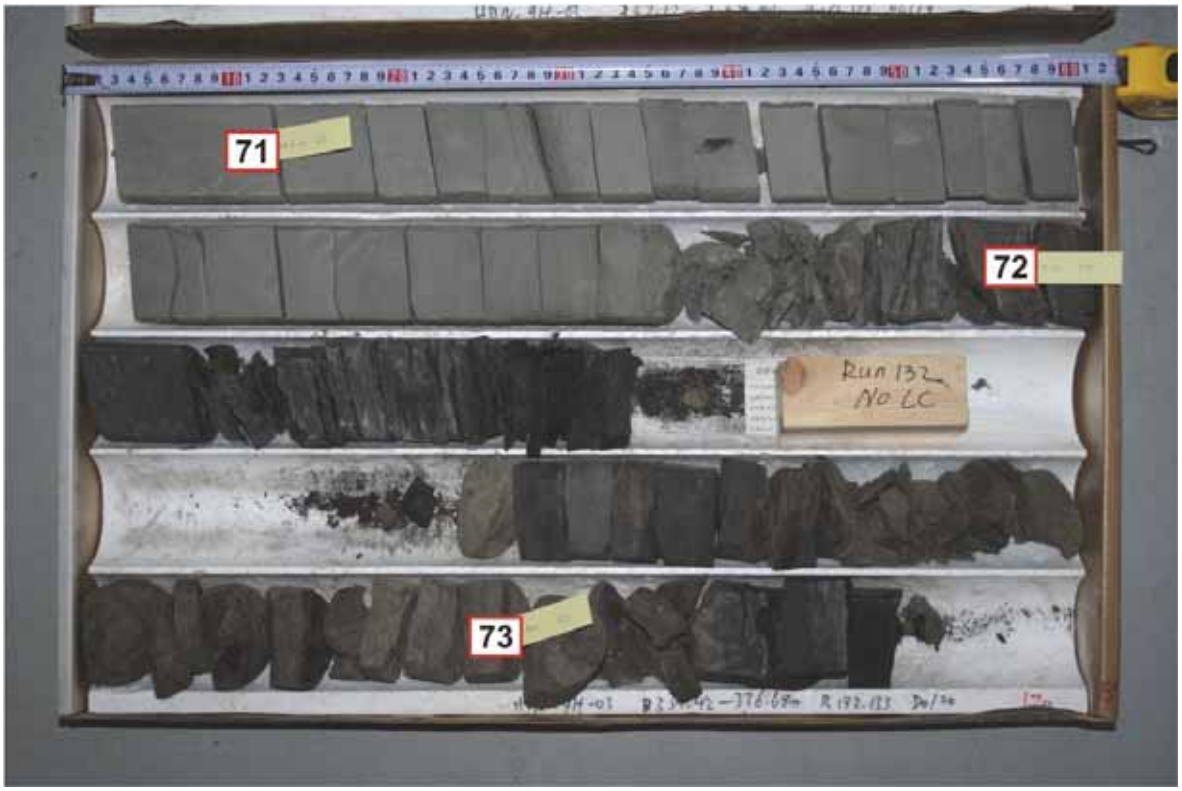
71
72
Run 132
No LC
73


74
Run 133
LC 0.85m
75
HDN-44-03 336.68m – 338.80m R133,134


76
77
78


RUN 135
79
80

10.4.3 Pyrite Member


Run 151
87
HDN-91t-03 384.76m-387.48m R151.52 139


RUN 152
88
RUN 153
HDN-91t-03 387.48m-389.93m R152.153.154 140

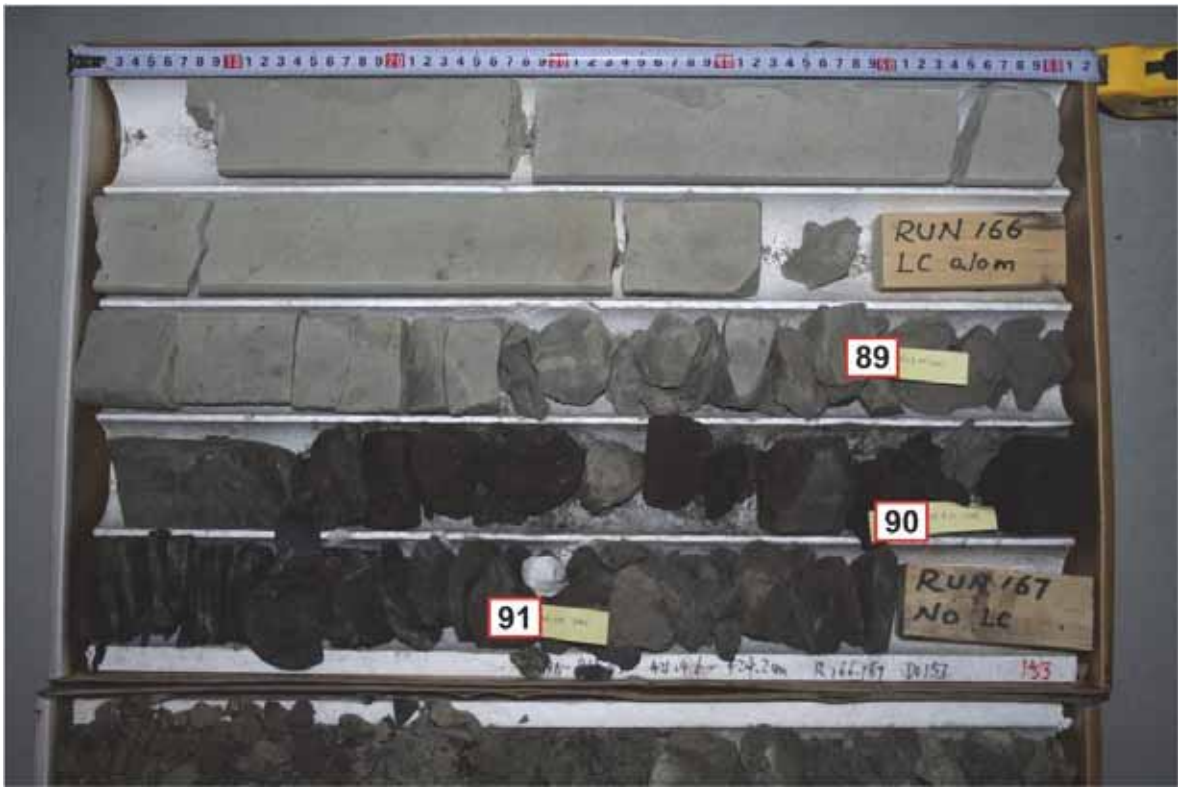
RUN 166
LC a.0m
89
90
RUN 167
NO LC
91


92
Run 191
No LC
93
Run 192
LC a.89m


94
LC 0.30m


95
Run 202
LC 0.60m Pick-up 0.20m


Run 204
LC 1.65m
96
Run 205
LE 0.35m